LOW TEMPERATURE PHYSICS VOLUME 29, NUMBER 4 APRIL 2003

QUANTUM LIQUIDS AND QUANTUM CRYSTALS

Relation between the temperature gradient and concentration gradient in superfluid ^{3}He–^{4}He mixtures

A. A. Zadorozhko, T. V. Kalko, É. Ya. Rudavskii, V. K. Chagovets, and G. A. Sheshin*

B. Verkin Institute for Low Temperature Physics and Engineering, National Academy of Sciences of Ukraine, pr. Lenina 47, 61103 Kharkov, Ukraine

(Submitted October 17, 2002)
Fiz. Nizk. Temp. **29**, 367–374 (April 2003)

The temperature and concentration gradients ∇T and ∇x created by a heat flow in a superfluid ^{3}He–^{4}He mixture with a concentration of 9.8% ^{3}He are measured in the steady state in the temperature range $T=70-500$ mK. It is found that the ratio $\nabla x/\nabla T$ obtained in the experiment can be described on the basis of a dependence of the osmotic pressure on the temperature and concentration. The data are used to find the thermodiffusion ratio and, hence, the thermodiffusion coefficient of this mixture. © *2003 American Institute of Physics.*

[DOI: 10.1063/1.1542466]

1. INTRODUCTION

One of the distinctive features of superfluid mixtures of ^{3}He in ^{4}He in comparison with the properties of pure He II is the possibility of simultaneous creation of temperature and concentration gradients at constant pressure. A steady temperature gradient can exist in pure superfluid ^{4}He only in the presence of a supergap impermeable to the normal component. Then a thermomechanical pressure arises which can be interpreted as an osmotic pressure of the thermal excitations—phonons and rotons.

In superfluid ^{3}He–^{4}He mixtures at normal pressure there are not only the thermal but also impurity excitations, which are ^{3}He quasiparticles. Here the expression for the impurity flux has the form

$$i=-\rho D\left[\nabla c+\frac{k_T}{T}\nabla T+\frac{k_P}{P}\nabla P\right], \tag{1}$$

where ρ is the density of the liquid, D is the diffusion coefficient, $k_T D$ is the thermodiffusion coefficient, $k_P D$ is the barodiffusion coefficient, and c is the mass concentration of ^{3}He in the mixture.

Under steady-state conditions, when the pressure gradient is equal to zero and one can neglect the nondissipative flow of impurities, as was shown by Khalatnikov,[1] one obtains the following relation between the temperature and concentration gradients:

$$\nabla c=-\frac{k_T}{T}\nabla T. \tag{2}$$

This means that steady temperature and concentration gradients can arise in superfluid mixtures even in the absence of a supergap.

The appearance of steady-state conditions in superfluid mixtures of ^{3}He and ^{4}He under different conditions was investigated theoretically in Refs. 2 and 3 with allowance for the interaction between quasiparticles. At low enough temperatures, such that one can neglect the influence of rotons and phonons, the ratio of the temperature and concentration gradients in the mixture is determined solely by the partial pressure P_f of impurity excitations in the mixture:[3]

$$\frac{\nabla x}{\nabla T}=-\frac{(\partial P_f/\partial T)_{xP}}{(\partial P_f/\partial x)_{TP}}, \tag{3}$$

where x, the molar concentration of ^{3}He in the mixture, is related to the mass concentration c by the relation $x=4c/(3+c)$.

Experimental study of the ratio between ∇T and ∇x in ^{3}He–^{4}He mixtures has been done only at high temperatures in highly concentrated mixtures.[4] In the present study we investigate steady-state temperature and concentration gradients under conditions such that the thermodynamic and kinetic properties of the ^{3}He–^{4}He mixture are determined by impuritons (^{3}He quasiparticles).

2. EXPERIMENTAL TECHNIQUE

Simultaneous measurements of the gradients of temperature and concentration were made in the cell shown schematically in Fig. 1. The upper flange *1* is in constant thermal contact with the plate of the mixing chamber, and a silver heat exchanger *2* is used to reduce the boundary thermal resistance with the liquid. The cell has a 0.1-mm thick stainless steel body *3* with a diameter of 2.4 cm and a height of 4.7 cm. The heat flux was created by a planar heater *4* placed in the liquid in the lower part of the cell. The filling capillary *5* passes through the lower flange *6* of the cell.

For measurement of the temperature distribution along the height of the cell we used two thermometers *8* mounted a fixed distance (10 mm) apart in the middle region of the cell. The concentration of the mixture could be determined from the change in its dielectric permittivity (see Refs. 5 and 6), measured by means of two capacitive concentration sensors *9* in the form of cylindrical capacitors (0.5 cm in height) with helically wound electrodes having gaps between turns of 0.1

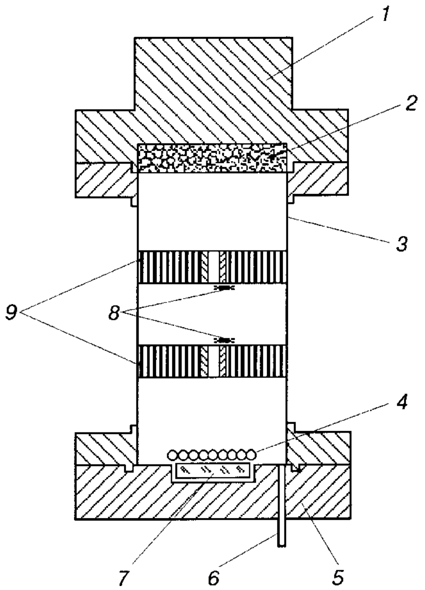

FIG. 1. Diagram of the measurement cell: *1*—top flange, *2*—sintered heat exchanger, *3*—wall of cell, *4*—heater, *5*—bottom flange, *6*—filling capillary, *7*—pressure sensor, *8*—resistance thermometer, *9*—capacitive concentration sensor.

and 0.2 mm for the upper and lower sensors, respectively. The nominal capacitances of the upper and lower sensors were 300 and 750 pF, respectively, corresponding to a capability of determining the ^{3}He concentration to an error of 0.1% for the upper sensor and 0.05% for the lower. The thermometers were identical RuO_2 resistance thermometers with a nominal resistance of 1000 Ω at room temperature. The resistance of the thermometers was measured by means of a bridge (CryoBridge R441), and the error of determination of the temperature was ± 0.2 mK at 230 mK and decreases with decreasing temperature.

The power of the heat flux created by the heater was determined to within less than 1% with the aid of a milliammeter. The cold plate of the dilution refrigerator, which was in plane-to-plane thermal contact with the flange *1*, was equipped with its own heater and resistance thermometer to permit stabilization of its temperature. The surface of the heat exchanger *2*, made from ultradisperse silver powder, had an area of ~ 1.5 m^2. Also mounted on the plate was a ^{3}He melting-curve thermometer, which was used to calibrate the resistance thermometers.

The 9.8% ^{3}He mixture used was prepared by mixing known portions of gaseous helium isotopes. Below 235 mK the liquid mixture separates, but both concentration sensors *9* and both thermometers *8* were located in the lower superfluid phase, the equilibrium concentration of which as a function of temperature is well known. The calibration of the thermometers and concentration sensors was carried out in the absence of heat fluxes, when the temperature and concentration were uniform throughout the cell.

3. PHASE SEPARATION OF SUPERFLUID MIXTURES IN THE PRESENCE OF HEAT FLUX

Measurements of the steady-state temperature gradient ∇T and concentration gradient ∇x were made at various temperatures and heat flux powers $\dot{Q}$. Two types of experiments were done:

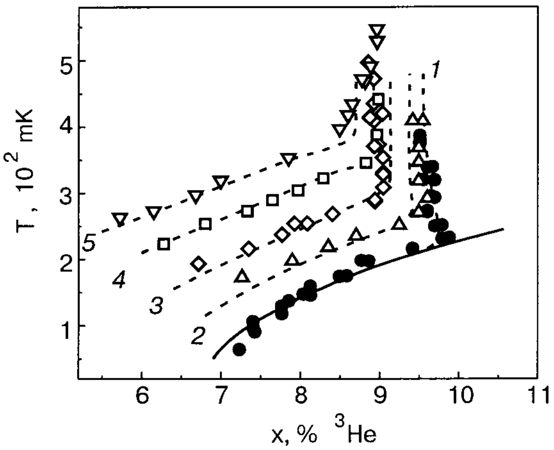

FIG. 2. Temperature dependence of the concentration of the mixture in experiment A at different constant values of the heat flux power $\dot{Q}$ [μW/cm^2]: 0 (*1*), 2.25 (*2*), 4.5 (*3*), 9 (*4*), 13.5 (*5*); the solid curve shows the data of Ref. 7.

— Experiment A: The temperature dependence of ∇T and ∇x in the mixture was measured at a constant power radiated by the heater, while the temperature of the liquid in the cell was varied by changing the temperature of the plate of the dilution refrigerator.

— Experiment B: The temperature of the dilution chamber was held constant while the temperature dependence of the gradients ∇T and ∇x were recorded as the heater power $\dot{Q}$ was varied.

The relative error of measurement of ∇T and ∇x depends on the power deposition; for $\dot{Q}=4.5$ μW/cm^2 it amounts to $\sim 2.5\%$ for ∇T and $\sim 10\%$ for ∇x. This error decreases with increasing $\dot{Q}$.

The typical temperature dependence of the concentration of the mixture as registered by the lower sensor in experiment A is shown in Fig. 2, where the average temperature of the liquid measured by the two thermometers is plotted on the vertical axis. Curve *1* corresponds to zero power, and the kink on it is due to phase separation of the initial mixture. As the temperature is decreased further, the concentration sensors register the concentration of the lower of the separated phases; this is in good accord with the known experimental data concerning the phase separation line,[7,8] as can be seen in Fig. 2.

Curves *2–5* in Fig. 2 were obtained for different constant values of the input power $\dot{Q}$, which produced steady temperature gradients along the length of the cell. According to the two-fluid model of superfluid helium, this initiates a counterflow of the normal and superconducting components, and the ^{3}He atoms taking part in the normal motion will move in the direction of lower temperatures. As a result, a steady concentration gradient which depends on the input power $\dot{Q}$ is established along the length of the cell. If it is assumed that the distributions of the temperature and concentration over the length of the cell are of a linear character, then estimates for $\dot{Q}=4.5$ μW/cm^2 give a value $x_{\text{top}}\sim 11\%$ ^{3}He for the concentration of the mixture in the upper part of the cell and a value $x_{\text{bot}}\sim 9\%$ ^{3}He for the lower part; for $\dot{Q}=13.5$ μW/cm^2 the values are $\chi_{\text{top}}\sim 13.5\%$ ^{3}He and χ_{bot}

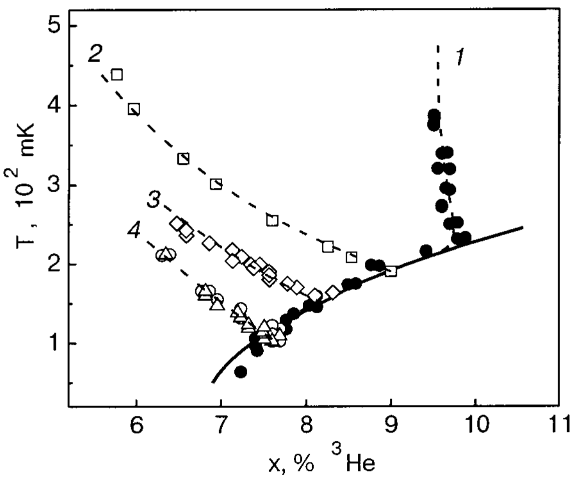

FIG. 3. Temperature dependence of the isotopic concentration registered by the lower sensor in experiment B for the following values of the mixing-chamber temperature T_m [mK]: 195 (*2*), 165 (*3*), 105 (*4*). The data of experiment A for $\dot{Q}=0$ (*1*); the solid curve was plotted according to the results of Ref. 7.

$\sim 8.5\%$ ^{3}He. Since the separation of the mixture begins in the upper, colder part of the cell, the corresponding phase separation temperatures, according to Ref. 7, will be $T_s = 290$ mK for $\dot{Q}=4.5$ μW/cm^2 and $T_s=330$ mK for $\dot{Q} = 13.5$ μW/cm^2. These values correlate well with the position of the kinks on curves *2* and *4* in Fig. 2; similar agreement is also observed for the other values of $\dot{Q}$. We note only that with increasing $\dot{Q}$ the kink corresponding to phase separation becomes less sharp.

Figure 3 shows typical results for experiment B, where the measurements were made at a constant value T_{mc} of the mixing-chamber temperature while the heat flux was varied. As in Fig. 2, here the concentration registered by the lower sensor is given, and the temperature corresponds to the average of the values indicated on the two thermometers. For comparison, Fig. 3 also shows the results obtained in experiment A for the case $\dot{Q}=0$ (curve *1*). Curves *2–4* in Fig. 3 were obtained as follows. The initial point for each curve is the corresponding point lying on the phase separation line for $\dot{Q}=0$. Then the mixture-chamber temperature T_m corresponding to that point was stabilized, and the power $\dot{Q}$ delivered to the heater was gradually increased at a constant value of T_m. The value of $\dot{Q}$ reached 11.2 μW/cm^2 for $T_m = 105$ mK and 18 μW/cm^2 for $T_m=195$ mK. In this case steady temperature and concentration gradients arose in the mixture. A comparison of the experimental curves given in Figs. 2 and 3 showed that for the same average temperature and the same input power, the values of the concentration registered in experiments A and B were in good agreement.

4. STEADY TEMPERATURE AND CONCENTRATION GRADIENTS IN THE MIXTURES. COMPARISON WITH THEORY

From the differences ΔT and Δx of the temperatures and concentrations measured by the sensors at the different sites we determined the gradients ∇T and ∇x. For correct comparison of the values obtained for ∇T and ∇x these gradients were determined at the same site of the cell. Here we took into consideration that the height of a sensor $l=5$ mm is comparable to the distance L between thermometers. In addition, the heat flux propagating in the liquid inside a capacitive concentration sensor was different from the flux between sensors, since an appreciable part of the cross section of a sensor is occupied by the metal electrode. If S is the cross-sectional area of the cell in the absence of a concentration sensor and S_1 is the cross-sectional area of the liquid through which the heat is flowing in the presence of a sensor, then the desired concentration gradient is expressed as follows:

$$\nabla x = \frac{\Delta x}{L\left(1+\dfrac{Sl}{S_l L}\right)}. \tag{4}$$

The difference in the value of S_1 for the two concentration sensors was in the 5% range, and it was not taken into account in deriving formula (4).

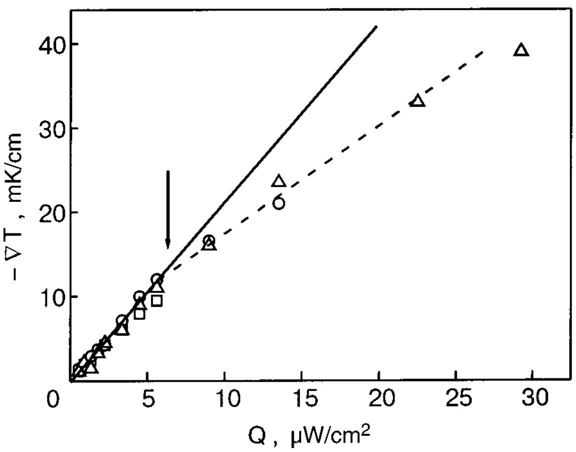

FIG. 4. Temperature gradient versus the power of the heat flux for different average cell temperatures T [mK]: 200 (□), 300 (○), 400 (△).

In calculating the temperature gradients we neglected the size of the thermometers in comparison with the distance between them, and we also neglected the heat released by the resistance thermometers and capacitive concentration sensors during the measurements.

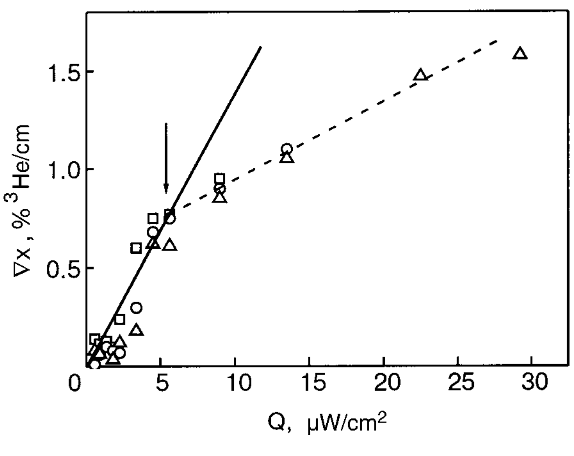

FIG. 5. Dependence of the concentration gradient on the power of the heat flux for different average cell temperatures T [mK]: 200 (□), 300 (○), 400 (△).

Figures 4 and 5 show typical curves of the temperature

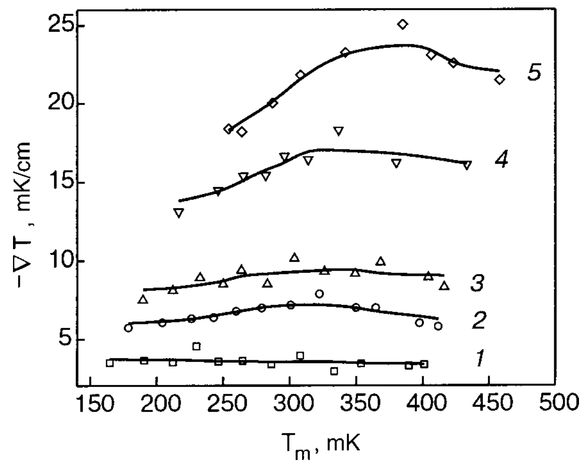

FIG. 6. Temperature dependence of the temperature gradient for different values of the injected power $\dot{Q}$ [μW/cm^2]: 1.8 (*1*), 3.37 (*2*), 4.5 (*3*), 9 (*4*), 13.5 (*5*).

and concentration gradients as functions of the power of the injected heat flux. The errors of determination of ∇T and ∇x are mainly due to the errors of measurement of the difference of the temperatures and concentrations between the sensors and were 0.5 mK and 0.07% ^{3}He. As can be seen in the plots, the gradients ∇T and ∇x depend linearly on $\dot{Q}$ at small values of $\dot{Q}$ and begin to deviate from linearity at $\dot{Q} > 5.6$ μW/cm^2. The deviation from linearity is apparently due to the onset of convection in the mixture under study. The problem of convection under the conditions of this experiment will be discussed in a separate paper.

It is also seen from Figs. 4 and 5 that the temperature and concentration gradients are only weakly temperature dependent. This may be seen most transparently in Figs. 6 and 7, which give the temperature dependence of ∇T and ∇x for different $\dot{Q}$.

For comparison of the experimental data on the steady temperature gradients and concentration gradients in superconducting ^{3}He–^{4}He mixtures with the theory it is convenient to consider the ratio $\nabla x/\nabla T$, which is plotted in Figs. 8 and 9.

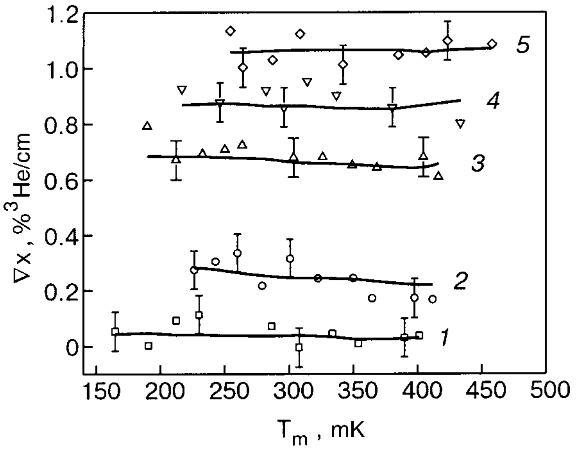

FIG. 7. Temperature dependence of the concentration gradient for different values of the input power $\dot{Q}$ [μW/cm^2]: 1.8 (*1*), 3.37 (*2*), 4.5 (*3*), 9 (*4*), 13.5 (*5*).

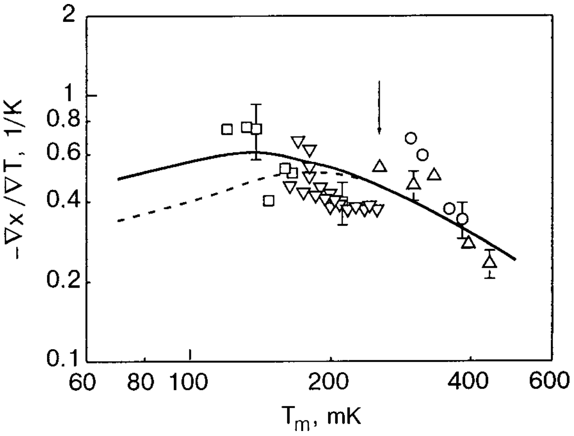

FIG. 8. Temperature dependence of the ratio $\nabla x/\nabla T$ obtained in experiment B for the following values of the temperature of the top flange [mK]: 105 (□), 160 (▽); 195 (△), 260 (○). The solid line is calculated according to formula (12) for a concentration of 9.8% ^{3}He, and the dashed curve is for a variable concentration corresponding to the lower phase of the separated mixture. The arrow corresponds to the phase separation temperature.

According to the theory of Khalatnikov,[1] the ratio between ∇c and ∇T can be obtained by proceeding from expression (2), where the parameter k_T has the general form

$$\rho D k_T = \alpha T \frac{\partial}{\partial T}\left(\frac{Z}{\rho T}\right) + \frac{\beta}{T}. \tag{5}$$

The first term in (4) corresponds to the contribution of impurity excitations, and the second corresponds to the phonon contribution to the weight factors α and β. The potential Z is expressed in terms of the difference of the chemical potentials of ^{3}He and ^{4}He in the mixture:

$$Z = \rho(\mu_3 - \mu_4). \tag{6}$$

If the phonon contribution is neglected, Eqs. (2), (5), and (6) lead to the the following relation for the concentration and temperature gradients:

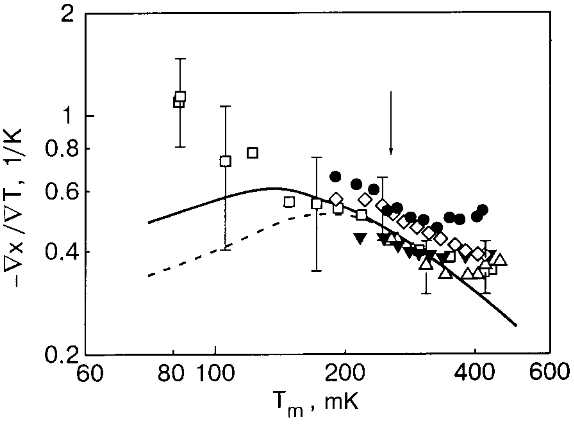

FIG. 9. Temperature dependence of the ratio $\nabla x/\nabla T$ obtained in experiment A for the following values of the input power [μW/cm^2]: 1.35 (□), 4.5 (○), 5.62 (◇), 9 (▽), 13.5 (△). The solid curve is calculated according to formula (12) for a concentration of 9.8% ^{3}He; the dashed curve is calculated for a variable concentration corresponding to the lower phase of the separated mixture. The arrow corresponds to the phase separation temperature.

$$\frac{\nabla c}{\nabla T} = -\frac{\dfrac{\partial}{\partial T}\left(\dfrac{\mu_3-\mu_4}{T}\right)}{\dfrac{\partial}{\partial c}\left(\dfrac{\mu_3-\mu_4}{T}\right)}. \tag{7}$$

To use relation (7) one needs to know the chemical potentials μ_3 and μ_4, which are usually[9,10] calculated from experimental data on the heat capacity and osmotic pressure. Because of the lack of experimental data for them over the entire range of temperatures and concentrations investigated, it was difficult to use Eq. (6) for comparing with the data on ∇T and ∇x.

In this sense it is more convenient for analysis to take the approach developed in Refs. 2 and 3, where the authors obtained a general expression describing the steady states in a ^{3}He–^{4}He superfluid mixture. With it any thermodynamic quantity can be expressed in terms of three other thermodynamic quantities chosen as independent variables: T, x, and μ_4. Then the total pressure of the mixture can be written in the form of a sum:

$$P = P_4(\mu_4,0,0) + P_T(\mu_4,T,0) + P_3(\mu_4,T,x), \tag{8}$$

where $P_4(\mu_4,T,0)$ is the contribution to the pressure from the superfluid background at $T=0$ and $x=0$; $P_T(\mu_4,T,0)$ is the thermodynamic pressure due to thermal excitations, and $P_3(\mu_4,T,0)$ is the osmotic pressure due to impurity excitations.

In the steady state, when $\mu_4=\text{const}$, and in the absence of a supergap ($P=\text{const}$), expression (8) simplifies to

$$P_T(T) + P_3(T,x) = \text{const}. \tag{9}$$

Since $P_T(T) < P_3(T,x)$ under the given experimental conditions, Eq. (9) simplifies further:

$$P_3(T,x) = \text{const}, \tag{10}$$

which means that

$$\left(\frac{\partial P_3(T,x)}{\partial x}\right)_T dx + \left(\frac{\partial P_3(T,x)}{\partial T}\right)_x dT = 0. \tag{11}$$

Hence

$$\frac{\nabla x}{\nabla T} = -\frac{[\partial P_3(T,x)/\partial T]_x}{[\partial P_3(T,x)/\partial x]_T}, \tag{12}$$

i.e., Eq. (12) is the limiting case of Eq. (3) for the low-temperature region, where one can neglect thermal excitations and assume that the ^{3}He partial pressure in the superfluid mixture is the osmotic pressure of impurity excitations, $P_3(T,x)$.

The osmotic pressure of ^{3}He–^{4}He superconducting mixtures was measured previously in Refs. 11–14, and the results of those measurements were analyzed in Ref. 10, where their smoothed values were given. There is what can be considered to be a complete set of experimental data on the osmotic pressure in the temperature range of interest, and the data are mutually consistent within the total error limits.

The ratios of the concentration gradients to the temperature gradients calculated according to formula (12) are given in Fig. 8 along with the experimental data obtained in experiment B. The solid curve in Fig. 8 corresponds to a calculation for the initial concentration of the mixture, and the dashed curve is calculated for the concentration of the lower superfluid phase of the separated mixture, the value of which varies with temperature. The concentration gradient along the height in the lower phase was not taken into account. The deviation of the average temperature T_m between the sensors is plotted along the horizontal axis in Fig. 8. It is seen from the plot that the experimental data obtained here are in satisfactory agreement with a theoretical model based on the osmotic-pressure dependence of the gradients of the temperature and concentration.

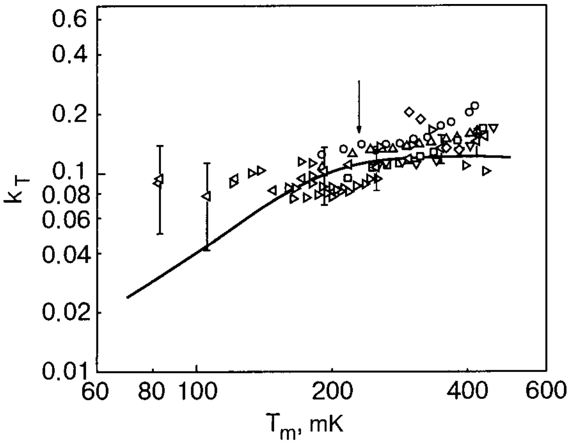

FIG. 10. Temperature dependence of the thermodiffusion ratio for a mixture with an initial concentration of 9.8% ^{3}He. The solid curve was calculated according to formulas (2) and (12) with the use of the osmotic pressure data of Ref. 9. The arrow corresponds to the phase separation temperature.

The analogous results obtained in experiment A are presented in Fig. 9 for different constant values of the injected heat flux. The agreement between experiment and theory is about the same as for experiment B. Here one can notice a decrease in $\nabla x/\nabla T$ with increasing $\dot{Q}$.

The values obtained for the ratios $\nabla x/\nabla T$ can be used to determine an important parameter of the theory of superfluid mixtures—the thermodiffusion ratio k_T, which appears in formulas (1) and (2). The temperature dependence of this parameter is shown in Fig. 10. An appreciable decrease of the calculated value of k_T (the solid curve in Fig. 10) is observed only below 300 mK, where the concentration of the superfluid phase of the separated mixture varies.

CONCLUSION

Simultaneous measurements of the temperature and concentration gradients arising in a ^{3}He–^{4}He superfluid mixture when a heat flux is turned on have been made for the first time in the region below 1 K. Two types of experiments were used: the temperature of the upper flange of the cell was measured at a constant value of the injected power, or the power was measured at a constant temperature of the flange. The two experiments gave mutually consistent values of the steady-state gradients of the temperature and concentration.

A study of the the phase diagram for separation of the mixture in the presence of a heat flux was carried out, and the results of the two experiments were in agreement. The temperature and concentration corresponding to phase separation (the kink on the $T(x)$ curve) agree with the corresponding values obtained in a calculation of the steady-state temperature and concentration distributions along the length of the cell after injection of a heat flux.

We have shown that the ratio of the steady-state concentration and temperature gradients observed in experiment can be explained from the condition of constancy of the partial pressure of ^{3}He impurity quasiparticles in the mixture. In this experiment the role of thermal excitations is negligible, and the ratio $\nabla x/\nabla T$ is determined solely by the behavior of the osmotic pressure of the impuritons. In such an approach one can achieve satisfactory agreement with experiment and determine the thermodiffusion ratio k_T, which in the Khalatnikov theory describes the relation between the diffusion coefficient and the thermodynamic properties of the superfluid mixture and determines the thermodiffusion coefficient.

In closing, let us mention the questions that might be studied under the conditions of this experiment but which have not been discussed in this paper. First among these is the kinetics of the variation of the temperature and concentration when the heat flux is switched on or off, which can be described by the corresponding relaxation times. Another important problem, which was mentioned previously, is the convective stability of ^{3}He–^{4}He superfluid mixtures in the presence of a heat flux. This problem can be described in terms of an effective thermal conductivity of the liquid, which is determined in experiment from both relaxation measurements and the steady temperature gradients. We shall discuss all these interesting question in separate papers.

The authors thank V. N. Grigor'ev, I. N. Adamenko, and K. É. Nemchenko for a helpful discussion of the results of this study.

This study was supported by the the NATO Science Program, Grant PST.CLG.978495.

*E-mail: sheshin@ilt.kharkov.ua

---

[1] I. M. Khalatnikov, *Theory of Superfluidity* [in Russian], Nauka, Moscow (1971).

[2] I. N. Adamenko, K. E. Nemchenko, V. I. Tsyganok, and A. I. Chervanev, Fiz. Nizk. Temp. **20**, 636 (1994) [Low Temp. Phys. **20**, 498 (1994)].

[3] K. É. Nemchenko, Fiz. Nizk. Temp. **23**, 799 (1997) [Low Temp. Phys. **23**, 599 (1997)].

[4] R. P. Behringer and H. Meyer, J. Low Temp. Phys. **46**, 407 (1982); **46**, 435 (1982).

[5] V. A. Mikheev, E. Ya. Rudavskii, V. K. Chagovets, and G. A. Sheshin, Fiz. Nizk. Temp. **20**, 621 (1994) [Low Temp. Phys. **20**, 485 (1994)].

[6] A. A. Zadorozhko, T. V. Kal'ko, E. Ya. Rudavskii, I. A. Usherov-Marshak, V. K. Chagovets, and G. A. Sheshin, Fiz. Nizk. Temp. **28**, 107 (2002) [Low Temp. Phys. **28**, 73 (2002)].

[7] D. O. Edwards, E. M. Ifft, and R. E. Sarwinski, Phys. Rev. **177**, 380 (1969).

[8] G. E. Watson, J. D. Repply, and R. C. Richardson, Phys. Rev. **188**, 384 (1969).

[9] R. Radebough, Nat. Bur. Stand. Tech. Note, No. 362 (1967), p. 137.

[10] J. G. M. Kuerten, C. A. M. Castelijns, A. T. A. M. de Waele, and H. M. Gijsman, Cryogenics **25**, 419 (1985).

[11] J. Landau, J. T. Tough, N. R. Brubaker, and D. O. Edwards, Phys. Rev. A **2**, 2472 (1970).

[12] M. F. Wilson and J. T. Tough, Phys. Rev. A **1**, 914 (1970).

[13] J. Landau and R. L. Rosenbaum, J. Low Temp. Phys. **11**, 483 (1973).

[14] L. J. M. Van der Klundert, M. R. E. Bos, J. A. M. Van der Meij, and H. A. Steffen, Phys. Lett. A **62**, 487 (1977).

Translated by Steve Torstveit

LOW TEMPERATURE PHYSICS VOLUME 29, NUMBER 4 APRIL 2003

LOW-TEMPERATURE MAGNETISM

Magnetoelectric effect in thin films and layered toroidal structures

I. E. Chupis*

B. Verkin Institute for Low Temperature Physics and Engineering, National Academy of Sciences of Ukraine, pr. Lenina 47, 61103 Kharkov, Ukraine

(Submitted July 23, 2002)
Fiz. Nizk. Temp. **29**, 375–379 (April 2003)

A calculation of the magnetoelectric and dielectric susceptibilities is carried out for a layered structure in which thin toroidal layers alternate with dielectric layers not found in a state of spontaneous toroidal ordering. The toroic considered is nickel iodine boracite. It is shown that an anomalous increase of the magnetoelectric and dielectric susceptibilities can occur in the vicinity of the temperature of the induced toroidal phase transition. © *2003 American Institute of Physics.* [DOI: 10.1063/1.1542467]

The magnetoelectric effect, which consists in the induction of an electric polarization **P** by a magnetic field **H** and in the appearance of a magnetization **M** under the influence of an electric field **E**, is characterized by the magnetoelectric susceptibility tensor $\alpha_{ik}=\partial P_i/\partial H_k=\partial M_k/\partial E_i$. A substance in which the linear magnetoelectric (ME) tensor has nonzero antisymmetric components admits the existence of a third (in addition to **P** and **M**) dipole moment **T**, which is called toroidal.[1] A substance having a phase transition at which a spontaneous toroidal moment appears is called a toroic.[2] Toroics include several ferroelectric magnetic compounds, nickel iodine boracite, $Ni_3B_7O_{13}I$, in particular.[3] In that compound the appearance of a toroidal moment at temperatures below $\Theta\approx 64$ K is accompanied by a spontaneous electric polarization and a weak magnetization. The off-diagonal components of the magnetoelectric susceptibility have a value $\alpha_{23}=\alpha_{32}\approx 3\times 10^{-4}$ (Ref. 4). It is known[5] that the value of the magnetoelectric response is proportional to the magnetic and dielectric susceptibilities of the system. Giant values of the dielectric susceptibility have been observed recently in layered structures with thin ferroelectric layers having a weak interlayer interaction in the neighborhood of the so-called thickness-induced ferroelectric phase transition.[6]

It is of interest to study the magnetoelectric effect in films and in systems containing thin toroidal layers in the vicinity of the thickness-induced toroidal phase transition. This is done below for the case of the toroic nickel iodine boracite. It is shown that in the vicinity of the thickness-induced phase transition to the toroidal state, the critical behavior of the magnetoelectric and dielectric susceptibilities can be different from that for a bulk sample, and these susceptibilities can become anomalously large.

We consider a layered structure consisting of toroidal layers A alternating with dielectric layers B which are not found in a state of spontaneous toroidal or any other kind of dipolar ordering. We assume that all the layers are of identical thickness l, so that the period of the structure along the z axis is equal to $2l$ and the thickness of the multilayer structure is $L=2Nl$, where N is the number of periods, and $-L/2\leqslant z\leqslant L/2$. The free energy of the system is written in the form

$$F=\sum_{j=0}^{N-1}(F_{Aj}+F_{Bj}). \qquad (1)$$

In Eq. (1) we have omitted the interaction between layers, since the giant values of the susceptibility in Ref. 6 were observed in the case of a weak interlayer interaction (see also Refs. 7 and 8).

There is no spontaneous toroidal moment in layers B, only the toroidal moment induced by the external electric and magnetic fields. We shall assume below that the electric field is applied perpendicular to the layers, along the z axis ($E=E_z$), and that the magnetic field lies in the plane of the layers, xy.

In a thin toroidal layer the toroidal moment is nonuniform over the thickness of the layer, and therefore

$$F_{Aj}=\frac{1}{l}\int_{Z_1}^{Z_2}F_{Aj}(z)dz,$$

$$Z_1=-\frac{L}{2}+2jl;\quad Z_2=-\frac{L}{2}+(2j+1)l. \qquad (2)$$

Above the toroidal ordering temperature Θ, nickel iodine boracite has cubic symmetry $\overline{4}3m$, and in the ordered phase the electric polarization **P** is directed along the fourfold axis z, while the toroidal moment and magnetization lie in the xy plane. The free energy of nickel iodine boracite is given in Ref. 3 for the case of a uniform distribution of dipoles (a bulk sample). When the gradients along the z axis are taken into account, the free energy density $F_{Aj}(z)=f(z)$ in the toroidal layer $0\leqslant z\leqslant l$ is written

$$f(z)=\alpha(T_x^2+T_y^2)+\beta_1T_x^2T_y^2+\beta_2(T_x^4+T_y^4)-aT_xT_yE_z$$
$$-bT_xT_y(H_xT_y-H_yT_x)-cE_z(H_xT_y-T_xH_y)$$
$$-\frac{1}{2\chi}E_z^2-\frac{1}{2\kappa}(H_x^2+H_y^2)+\lambda\left[\left(\frac{\partial T_x}{\partial z}\right)^2+\left(\frac{\partial T_y}{\partial z}\right)^2\right]$$

$$+\lambda_1\left(H_y\frac{\partial T_x}{\partial z}-H_x\frac{\partial T_y}{\partial z}\right). \tag{3}$$

The components of the electric polarization and magnetization are given by the expressions[3]

$$P_z=aT_xT_y+\frac{1}{\chi}E_z+c(T_yH_x-T_xH_y);$$

$$M_x=bT_x(T_y^2-T_x^2)+\frac{1}{\kappa}H_x+cT_yE_z;$$

$$M_y=bT_y(T_x^2-T_y^2)+\frac{1}{\kappa}H_y-cT_xE_2. \tag{4}$$

The equilibrium values of $T_{x,y}$ are determined by the Euler–Lagrange equations

$$\frac{\partial f}{\partial T_i}-\frac{d}{dz}\frac{\partial f}{\left(\dfrac{\partial T_i}{\partial z}\right)}=0 \quad i=x,y,$$

i.e., by the equations

$$2\alpha T_x+4\beta_2T_x^3+2\beta_1T_xT_y^2-aT_yE_z-b$$
$$\times(H_xT_y^2-2T_xT_yH_y)+cE_zH_y-2\lambda T_x''=0;$$
$$2\alpha T_y+4\beta_2T_y^3+2\beta_1T_yT_x^2-aT_xE_z+b$$
$$\times(H_yT_x^2-2T_xT_yH_x)-cE_zH_x-2\lambda T_y''=0. \tag{5}$$

From Eqs. (5) we see that in a field $H_x=H_y=H$ there exists a solution $T_x=-T_y=T$ satisfying the equation

$$2\alpha T+4\beta T^3-2\lambda T''+aE_zT-3bHT^2+cE_zH=0. \tag{6}$$

where $2\beta=2\beta_2+\beta_1$.

In the absence of external fields, assuming $T=0$ at the boundaries of the toroidal layer, we obtain from (6) the spontaneous toroidal moment T_s:

$$T_s=T_0\sqrt{\frac{2m}{1+m}}\,\mathrm{sn}\left(\frac{z}{l_0\sqrt{1+m}},m\right), \tag{7}$$

where $\mathrm{sn}(u,m)$ is the Jacobi elliptic sine, $m=k^2$ (Ref. 9); $T_0=(-\alpha/2\beta)^{1/2}$ is the spontaneous toroidal moment of a bulk sample, $l_0=(-\lambda/\alpha)^{1/2}$ is the correlation length. The parameter m is given by the relation

$$l=2l_0\sqrt{1+m}K(m), \tag{8}$$

where $K(m)$ is the complete elliptic integral of the first kind, and the parameter m varies from 0 to 1. For $m\to1$ the value of K diverges logarithmically, in which case, as follows from (8), $l\gg l_0$. Consequently, the limit $m=1$ corresponds to the bulk sample (thick layer). On the other hand, for $m\to0$ we have $K\to\pi/2$, and l approaches a minimum (critical) value $l_c=\pi l$, at which the spontaneous toroidal moment equals zero. For values of the thickness $l<l_c$ a spontaneous toroidal moment does not exist. This means that the phase transition from the toroidal state ($T\neq0$) to the paratoroidal ($T=0$) state can occur without a change in temperature through a decrease in the layer thickness (the so-called thickness-induced phase transition[6,7,10]). For $l>l_c$ the phase transition temperature depends on the thickness of the layer. Assuming in (3) a constant $\alpha=\alpha_0(t-\Theta)$ (where t is the temperature and Θ is the transition temperature in a thick layer), from the condition $l=l_c=\pi l_0$ ($t=\Theta_l$) we find

$$\Theta_l=\Theta\left[1-\left(\frac{l_{c0}}{l}\right)^2\right], \quad l_{c0}=\pi\sqrt{\frac{\lambda}{\alpha_0\Theta}}, \tag{9}$$

where l_{c0} is the critical thickness of the layer at zero temperature. For $l\leqslant l_{c0}$ we have $\Theta_l\leqslant0$, i.e., the phase transition to the toroidal state cannot occur at any temperature. We see from (9) that the temperature of the transition to the toroidal state in a layer, Θ_l, is less than the phase transition temperature Θ in a bulk sample.

We are interested in the magnetoelectric susceptibility of the system, i.e., the quantities

$$\alpha_{zx}=\frac{\partial P_z}{\partial H_x}, \quad \alpha_{zy}=\frac{\partial P_z}{\partial H_y}. \tag{10}$$

From Eqs. (4) we obtain

$$\alpha_{zx}=a\frac{\partial}{\partial H_x}(T_xT_y)+cT_y,$$

$$\alpha_{zy}=a\frac{\partial}{\partial H_y}(T_xT_y)-cT_x. \tag{11}$$

For the solution under discussion, $T_y=-T_x=-T$, the magnetoelectric susceptibility of the linear effect in the case $H_x=H_y=H$ is

$$\alpha_{zx}=\alpha_{zy}=\alpha(z)=-cT_s-2aT_s\tau, \quad \tau=\left(\frac{\partial T}{\partial H}\right)_{E,H=0}. \tag{12}$$

Differentiating Eq. (6) with respect to H and making a change of variables to $u=z/l_0\sqrt{1+m}$, we obtain the following equation for determining τ:

$$\tau_u''+(1+m-6m\,\mathrm{sn}^2(u,m))\tau=R\,\mathrm{sn}^2(u,m),$$

$$R=-\frac{3mb}{2\beta}. \tag{13}$$

The magnetoelectric susceptibility of the investigated multilayer structure with noninteracting layers is

$$\bar{\alpha}=\frac{1}{L}\sum_{j=0}^{j=N-1}\int_{Z_1}^{Z_2}[\alpha_{Aj}(z)+\alpha_{Bj}(z)]dz,$$

$$Z_1=-L/2+2jl, \quad Z_2=-L/2+(2j+1)l. \tag{14}$$

Since there is no spontaneous toroidal moment in a B layer, we have:

$$\bar{\alpha}=\frac{1}{l}\int_0^l\alpha(z)dz=\frac{1}{2K}\int_0^{2K}\alpha(u)du. \tag{15}$$

The solution of equation (13) for τ has the form[11]

$$\tau(u)=c_1\tau_1+c_2\tau_2+\tau_3,$$

$$\tau_1=\mathrm{cn}(u,m)\mathrm{dn}(u,m),$$

$$\tau_2=\left(u-\frac{1+m}{1-m}E(amu,m)\right)\mathrm{cn}(u,m)\mathrm{dn}(u,m)+\frac{\mathrm{sn}(u,m)[\mathrm{dn}^2(u,m)+m^2\mathrm{cn}^2(u,m)]}{1-m},$$

$$\tau_3=\frac{R}{3(m-1)^2}[2-(1+m)\mathrm{sn}^2(u,m)],\tag{16}$$

where $E(amu,m)$ is an elliptic integral of the second kind, and $\mathrm{cn}(u,m)$ and $\mathrm{dn}(u,m)$ are the elliptic cosine and delta amplitudes, respectively.

With the aid of the boundary conditions

$$\tau(u=0)=\tau(u=2K)=\tau_s\tag{17}$$

we find the constants c_1 and c_2:

$$c_1=\tau_s-\frac{2R}{3(1-m)^2},$$

$$c_2=\frac{2R-3\tau_s(1-m)^2}{3(1-m)[K(1-m)-E(1+m)]}.\tag{18}$$

Using Eqs. (7), (12), (16), and (18), we obtain the following expression for the susceptibility $\overline{\alpha}$ (15) of the system:

$$\overline{\alpha}=-\frac{T_0}{K\sqrt{2(1+m)}}\left\{\left(c+\frac{ab}{2\beta}\right)\ln\frac{1+\sqrt{m}}{1-\sqrt{m}}+\frac{a\sqrt{m}[b(E-K)-2\tau_s\beta(2E+K(m-1))]}{\beta[K(1-m)-E(1+m)]}\right\}.\tag{19}$$

For a thick film, when $m\to1$, $K\to\infty$, $E\to1$, and $K(1-m)\to0$, we obtain in the limit from (19)

$$\alpha_t=-T_0\left(c+\frac{3ab}{4\beta}\right).\tag{20}$$

This same value for α_t can be obtained by dropping the spatial derivatives in (6).

For a thin film near Θ_l for $m\to0$

$$E-K\cong-\pi m/4,\quad K(0)=E(0)=\pi/2,$$

$$K(1-m)-E(1+m)\cong-3\pi m/4,\ \ \ln\frac{1+\sqrt{m}}{1-\sqrt{m}}\cong2\sqrt{m}.$$

When these relations are taken into account, we obtain the following expression for the magnetoelectric susceptibility of a layered toroidal structure near the thickness-induced phase transition temperature Θ_l:

$$\overline{\alpha}\approx-T_0\frac{2\sqrt{2m}}{\pi}\left[c+\frac{2ab}{3\beta}+\frac{2a\tau_s}{3m}\right].\tag{21}$$

For small values of m Eq. (8) implies the following relation for films having thicknesses close to the critical value l_c:

$$l\cong\pi l_0\left(1+\frac{3}{4}m\right),\ \ m=\frac{4}{3}\left(\frac{l}{l_c}-1\right),\ \ l-l_c\ll l_c.\tag{22}$$

On the other hand, for such films near the temperature temperature Θ_l we use the temperature dependence of l_0 and relation (9) to obtain

$$m\cong\frac{2}{3}\frac{l^2}{l_{c0}^2}\frac{\Theta_l-t}{\Theta}.\tag{23}$$

If $\partial T/\partial H=\tau_s=0$ on the surface of the film, then

$$\overline{\alpha}\propto\sqrt{l-l_c},\quad\overline{\alpha}\propto l\sqrt{\Theta_l-t},\tag{24}$$

i.e., the magnetoelectric susceptibility has the usual (in the framework of Landau theory) square-root temperature dependence, but with a coefficient proportional to the thickness of the film.

On the other hand, if $\tau_s\neq0$ on the surface, then, as can be seen from Eq. (21), the critical dependence of the magnetoelectric susceptibility becomes stronger:

$$\overline{\alpha}\cong\frac{2\sqrt{2}}{\pi\sqrt{3}}\tau_s aT_0\sqrt{\frac{l_c}{l-l_c}},$$

$$\overline{\alpha}\cong-\frac{4a\tau_sT_0}{\pi\sqrt{3}}\frac{l_{c0}}{l}\sqrt{\frac{\Theta}{\Theta_l-t}}.\tag{25}$$

This enhancement of the magnetoelectric effect in thin toroidal films near Θ_l is possible only in the case of a nonzero value of τ_s on the surface. Since there is no spontaneous toroidal moment in the layers, a contribution to τ_s can only come from the induced toroidal moment created by the crossed electric and magnetic fields, $\tau\propto E_zH_{x,y}$. During measurement of the magnetoelectric susceptibility an external magnetic field is applied to the system, while the electric field E_z can be of an external or internal origin. In the absence of external field, there may be a field $E_z\neq0$ at the contacts between layers as a result of the imperfection of the surfaces and depolarization—the contact potential difference. An external electric field also induces a $\tau_s\neq0$, and the corresponding magnetoelectric susceptibility is related to the nonlinear magnetoelectric effect.

In thin-film toroidal structures in the vicinity of the temperature of the thickness-induced toroidal phase transition it is possible also to have anomalous enhancement of the dielectric permittivity in comparison with a bulk sample, in which it has a slight jump at the toroidal transition. Indeed, from Eqs. (4) and (6) we obtain

$$\chi_e=\frac{\partial P_z}{\partial E_z}=\chi^{-1}-2afT_s,\quad f=\frac{\partial\tau}{\partial E_z},$$

$$f''_u+f(1+m-6m\,\mathrm{sn}^2(u,m))=A\,\mathrm{sn}(u,m),$$

$$A=\frac{a(1+m)}{2}\sqrt{-\frac{m}{2\beta}}.\tag{26}$$

Solving Eq. (26) for f in analogy to the previous case with the boundary conditions $f(u=0.2\text{ K})=f_s$, we obtain for the average value of the dielectric susceptibility near Θ_l (for small m)

$$\overline{\chi_e}\cong\chi_t-\frac{4\sqrt{2}af_sT_0}{3\pi\sqrt{m}}\approx-\frac{4af_sT_0}{\pi\sqrt{3}}\frac{l_{c0}}{l}\sqrt{\frac{\Theta}{\Theta_l-t}}.\tag{27}$$

Here χ_t is the dielectric susceptibility of a bulk sample. The value of $f_s=(\partial\tau/\partial E)_s$ on the surface of the film can be nonzero in the presence of a static external magnetic field lying in the plane of the layers.

Thus the thickness-induced phase transition to the toroidal state can be accompanied by anomalous enhancement of both the magnetoelectric susceptibility and the dielectric permittivity.

Since the interaction of the layers was not taken into account, the results obtained here pertain both to multilayer thin-film systems and to individual thin films of toroics under conditions such that there is no spontaneous toroidal moment on the two boundary surfaces of the toroidal layer. In layered structures this condition can be realized owing to the contact of the toroidal layers A with the nontoroidal (or paratoroidal) layers B.

*E-mail: chupis@ilt.kharkov.ua

---

[1] V. M. Dubovik and L. A. Tosunyan, É́lem. Chastits At. Yadra **14**, 1193 (1983) [Sov. J. Part. Nucl. **14**, 504 (1983)].

[2] V. L. Ginzburg, A. A. Gorbatsevich, Yu. V. Kopaev, and B. A. Volkov, Solid State Commun. **50**, 339 (1984).

[3] D. G. Sannikov and I. S. Zheludev, Fiz. Tverd. Tela (Leningrad) **27**, 1369 (1985) [Sov. Phys. Solid State **27**, 826 (1985)].

[4] E. Asher, H. Rieder, H. Schmid, and H. Stossel, J. Appl. Phys. **37**, 1404 (1966).

[5] G. A. Smolenskiĭ and I. E. Chupis, Usp. Fiz. Nauk **137**, 415 (1982) [Sov. Phys. Usp. **25**, 475 (1982)].

[6] Y. Kim, R. A. Gerhardt, and A. Erbil, Phys. Rev. B **55**, 8766 (1997).

[7] M. D. Glinchuk, E. A. Eliseev, V. A. Stephanovich, M. G. Karkut, and R. Farhi, condmat/0004258.

[8] M. D. Glinchuk, E. A. Eliseev, and V. A. Stephanovich, Fiz. Tverd. Tela (St. Petersburg) **44**, 912 (2002) [Phys. Solid State **44**, 953 (2002)].

[9] I. S. Gradshteyn and I. M. Ryzhik, *Tables of Integrals, Series, and Products*, Academic Press, New York (1980), Fizmatgiz, Moscow (1963).

[10] B. D. Qu, W. L. Zhong, and R. H. Prince, Phys. Rev. B **55**, 11218 (1997).

[11] A. Erdélyi (Ed.), *Higher Transcendental Functions (H. Bateman Manuscript Project)*, Vols. 1–3, McGraw-Hill, New York (1953–1955), Nauka, Moscow (1965–1967).

Translated by Steve Torstveit

Anomalous hysteresis in magnetoresistive ceramic and film samples of $(La_{0.8}Sr_{0.2})_{1-x}Mn_{1+x}O_3$ $(0\leqslant x\leqslant 0.4)$

V. T. Dovgij, A. I. Linnik,* V. P. Pashchenko, V. N. Derkachenko, V. K. Prokopenko,
V. A. Turchenko, N. V. Davydeiko, and V. Ya. Sycheva

A. A. Galkin Donetsk Physicotechnical Institute, ul. R. Lyuksemburg 72, 83114 Donetsk, Ukraine;
Institute of Physics of the Polish Academy of Sciences, Al. Lotnikow 32/46, 02-668 Warsaw, Poland

V. P. Dyakonov

A. A. Galkin Donetsk Physicotechnical Institute, ul. R. Lyuksemburg 72, 83114 Donetsk, Ukraine

A. V. Klimov and H. Szymczak

Institute of Physics of the Polish Academy of Sciences, Al. Lotnikow 32/46, 02-668 Warsaw, Poland

(Submitted August 2, 2002)
Fiz. Nizk. Temp. **29**, 380–386 (April 2003)

A study is made of the external structure, magnetization, and magnetoresistive effect in ceramic samples of $(La_{0.8}Sr_{0.2})_{1-x}Mn_{1+x}O_3$ annealed at 1150 and 1500 °C. It is shown that the additional annealing at 1500 °C leads to significant changes in the magnetization and increases the magnetoresistive effect by a factor of 2–3, depending on x. An ''anomalous'' magnetic hysteresis is observed on the initial parts of the magnetization curves in both ceramic and laser-deposited film samples. It is found that the value of the ''anomalous'' magnetic hysteresis depends on the composition of the samples (on x) and their annealing temperature. A mechanism for the appearance of the ''anomalous'' hysteresis is proposed, involving the presence and interaction of ferromagnetic and antiferromagnetic phases. *© 2003 American Institute of Physics.*
[DOI: 10.1063/1.1542468]

INTRODUCTION

In recent years there has been an upsurge in interest in the perovskitelike rare-earth magnets $R_{1-x}A_xMnO_3$ (R $=$La, Pr, Nd, or other rare-earth element, and A is a divalent ion of Ca, Sr, Ba, or Pb) in connection with the colossal magnetoresistive effect observed in them and the promising outlook for their practical application.[1–7] Manganites are solid solutions with a peculiar interrelationship of the electronic, magnetic, and structural properties, which can be regulated by varying the technology of their preparation and their chemical composition, including as a result of doping.[1–7] The question of whether manganites have coexisting ferromagnetic and antiferromagnetic phases, having metallic and insulating (or semiconducting) properties, and the question of the existence of inhomogeneous low-dimensional phases of a phase-separation or planar-cluster type are matters of discussion at the present time.[7–12]

Since the magnetic and transport properties in these materials are determined primarily by the manganese ions, it is of interest to study the magnetic and electric properties of lanthanum-manganite perovskites containing excess superstoichiometric manganese relative to the other cations.[12–15] The main goal of the present study was to compare the magnetic and electrical properties of manganites with an excess of manganese in their composition and to elucidate the possibility of having a coexistence of several magnetic phases and their phase separation with cluster formation.

METHOD OF OBTAINING AND STUDYING THE SAMPLES

The objects of study were samples of strontium-doped lanthanum-manganite perovskites, $(La_{0.8}Sr_{0.2})_{1-x}Mn_{1+x}O_3$ $(0\leqslant x\leqslant 0.4)$. A feature of the compositions was the presence of excess manganese with no change in the ratio La:Sr$=$4. The samples were prepared by the standard ceramic technology. The initial mixtures of powders of definite composition were obtained from ChDA-grade oxides La_2O_3, $SrCO_3$, and Mn_3O_4 after their careful mixing and a synthesizing anneal at at 900 °C for 20 hours. After being ground and pressed into tablets, the samples were baked in two stages: at temperatures of 1150 and 1500 °C for 21 and 2 hours, respectively. After each anneal we carried out a comprehensive investigation of the structural, magnetic, and transport properties of the samples.

An x-ray analysis was done on a DRON-2 diffractometer in FeK_α radiation. The magnetic properties of the samples were measured in a vibration magnetometer and an inductive–frequency apparatus, and the electrical conductivity and magnetoresistance were determined by the standard four-contact method at $H=0$ and 5 kOe.

EXPERIMENTAL RESULTS AND DISCUSSION

According to the x-ray data, the samples of all compositions $(La_{0.8}Sr_{0.2})_{1-x}Mn_{1+x}O_3$ contained a main perovskite-like rhombohedrally distorted $(R\overline{3}c)$ phase with lattice parameters which, depending on x, lay in the ranges: $a=7.784–7.787$ Å, $\alpha=90.41–90.45°$ (annealing at 1150 °C) and $a=7.792–7.782$ Å, $\alpha=90.55–90.48°$ (annealing at

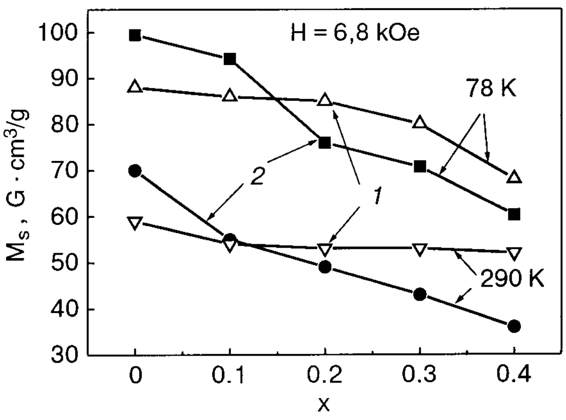

FIG. 1. Influence of the composition on the saturation magnetization of ceramic samples of $(La_{0.8}Sr_{0.2})_{1-x}Mn_{1+x}O_3$ at temperatures of 78 and 290 K for different annealing temperatures: 1150 °C (*1*), 1500 °C (*2*).

1500 °C). For $x=0$ and 0.1 the samples are single-phase, and for $x=0.2$–0.4 they are heterophase: in addition to the main perovskite phase, there are small amounts of a γ-Mn_2O_3 or Mn_3O_4 phase.

According to the magnetic measurements the samples of all compositions $(La_{0.8}Sr_{0.2})_{1-x}Mn_{1+x}O_3$ in the interval $0 \leqslant x \leqslant 0.4$ are magnetically soft ferromagnets, since the magnetic saturation curve obtained on the vibration magnetometer in fields $H=6$ kOe has a characteristic hysteresis loop of width ≈ 30 Oe. Figures 1 and 2 show the values of the saturation magnetization and the Curie temperature T_C, respectively, for ceramic samples obtained at temperatures of 1150 °C (curves *1*) and 1500 °C (curves *2*). For the samples annealed at 1150 °C, the saturation magnetization M_s remains practically unchanged as x increases from 0 to 0.3. If the excess manganese oxide were not dissolved but formed a second phase Mn_3O_4 or Mn_2O_3, then with increasing manganese oxide content the value of M_s should have decreased by approximately 20%, which was not observed in the experiment (curve *1* in Fig. 1). The noticeable decrease of M_s for the sample with $x=0.4$ can be explained by the insolubility of the excess manganese in the main perovskite phase. However, this decrease ($\sim 12\%$) is also less than the calculated value ($\sim 23\%$), especially at a temperature of 290 K.

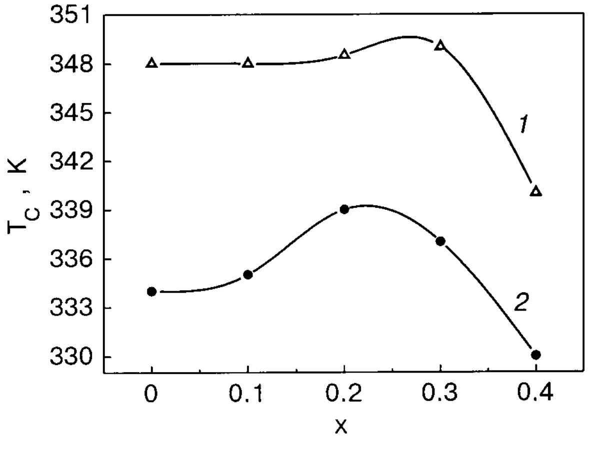

FIG. 2. Dependence of the Curie temperature (T_C) on the composition x for ceramic samples of $(La_{0.8}Sr_{0.2})_{1-x}Mn_{1+x}O_3$ obtained at different annealing temperatures: 1150 °C (*1*), 1500 °C (*2*).

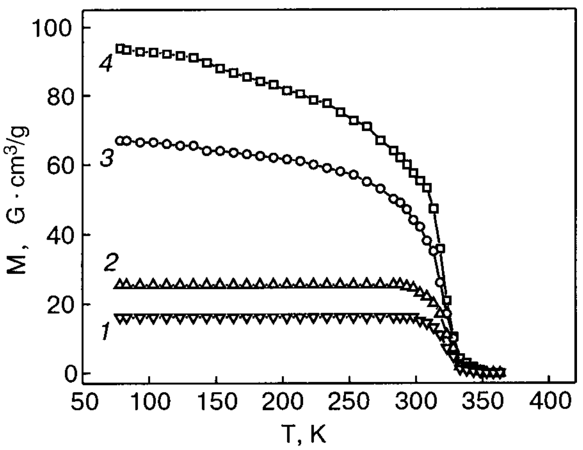

FIG. 3. Temperature dependence of the magnetization of a ceramic sample of $La_{0.8}Sr_{0.2}MnO_3$ in various magnetic fields: 80 Oe (*1*), 150 Oe (*2*), 500 Oe (*3*), 4 kOe (*4*).

For samples annealed at 1500 °C there is a noticeable decrease of M_s with increasing x at both 78 K and 290 K. One notices that only for $x=0$ are the values of M_s larger for the samples annealed at 1500 °C (for $x=0.1$ the values of M_s are close for samples annealed at 1150 and 1500 °C). For the remaining compositions M_s is larger in the samples obtained at 1150 °C. This is apparently evidence of an increase in the number of oxygen vacancies and a change in the composition and density of lattice defects in the manganite phase of the lanthanum-manganite perovskite, with possible phase separation and formation of planar clusters with different composition, structural, magnetic, and transport properties. We note the correlation of the decrease of the magnetization and Curie temperature for the samples with $x=0.4$ annealed at 1150 and 1500 °C.

Studies of the temperature dependence of the magnetization in low (less than 150 Oe) and high (4 kOe) magnetic fields for samples of $(La_{0.8}Sr_{0.2})_{1-x}Mn_{1+x}O_3$ with compositions in the interval $0 \leqslant x \leqslant 0.4$ and sintered at temperatures of 1150 and 1500 °C showed different behavior of M_s: a weak variation of the magnetization over a wide temperature interval in low fields, and a rather significant dependence of the magnetization throughout the entire temperature interval in high fields. As an example, Fig. 3 shows the temperature dependence of the magnetization for a $La_{0.8}Sr_{0.2}MnO_3$ sample ($x=0$, sintering temperature 1500 °C) in different magnetic fields. This difference is possibly due to the presence of magnetic nonuniformities—phases[16–22] or clusters.[12–14] In low fields a more uniform ordered (ferromagnetic) phase apparently forms, and in high fields other, less uniform and ordered, magnetic phases (the boundary region between ferromagnetic and antiferromagnetic phases) or clusters appear. According to x-ray structural studies, the excess manganese oxide is found in the form of a phase or cluster with a composition close to Mn_3O_4 (for $x=0$) or Mn_2O_3 (for $x>0$). When the valence states of the manganese ions and their superposition are taken into account, the compositions of the clustered solid solutions is most probably of the following form:

$$Mn_3O_4 \rightarrow Mn_1^{2+}Mn_2^{3+}O_4^{2-} \rightarrow Mn_{1.5}^{2+}Mn_1^{3+}Mn_{0.5}^{4+}O_4^{2-};$$

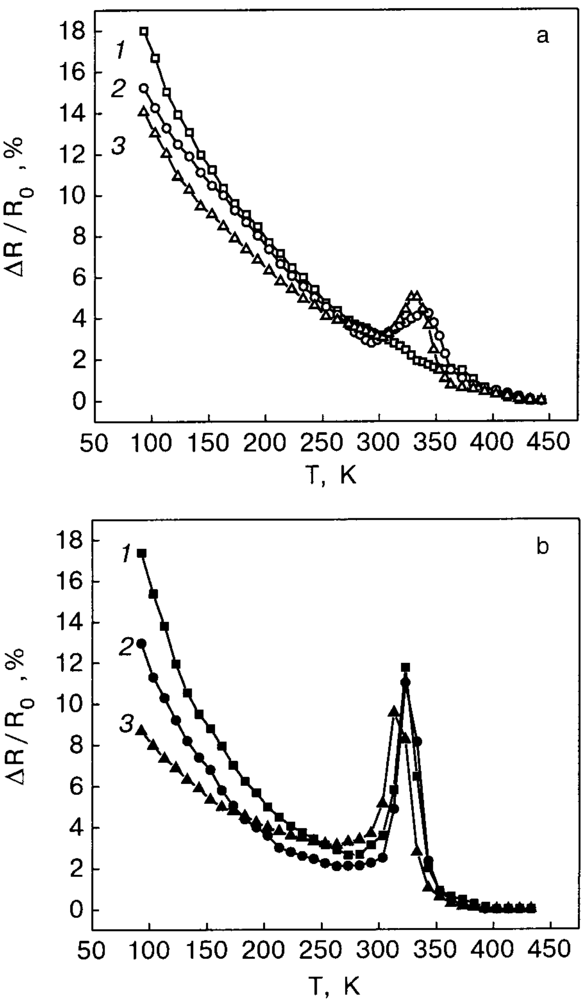

FIG. 4. Temperature dependence of the magnetoresistive effect in samples of the lanthanum-manganite ceramic $(La_{0.8}Sr_{0.2})_{1-x}Mn_{1+x}O_3$ annealed at 1150 °C (a) and 1500 °C (b) for $x=0$ (*1*), 0.2 (*2*), and 0.4 (*3*).

$$Mn_2O_3 \rightarrow Mn_2^{3+}O_3^{2-} \rightarrow Mn_{0.5}^{2+}Mn_1^{3+}Mn_{0.5}^{4+}O_3^{2-} .$$

The temperature dependence of the transport properties of the manganites are presented in Fig. 4 for annealing temperatures of 1150 and 1500 °C. The value of the magnetoresistive effect $\Delta R/R_0=(R_0-R_H)/R_0$, where R_0 and R_H are the resistance of the samples at $H=0$ and 5 kOe, respectively, is 4–6% for the samples annealed at 1150 °C, and the magnetoresistance peak is observed at a temperature 13–14 K below the Curie temperature (Fig. 4a). The curves of the temperature dependence of the resistance for all values of x have a resistance peak (T_{ms}) near T_C. The low-temperature side of the peak corresponds to a "metallic" type of conduction, and the high-temperature side to a semiconductor type. After annealing of the samples at 1500 °C the magnetoresistive effect increased to 10–13% for the different values of x, and the maximum of the magnetoresistance was shifted to a temperature 7–15 K below T_C (Fig. 4b). We note that for $x=0$ the magnetoresistive effect is essentially not observed in the case of annealing at 1150 °C (Fig. 4a), whereas after annealing at 1500 °C for $x=0$ it has a value of 12.5% (Fig. 4b). Analysis of Fig. 4 shows that after annealing at 1500 °C the magnetoresistive effect increases by a factor of 2–3 for the different x. The resistivity of the samples increased by a factor of 2–3, and the temperature dependence of the resistivity for $T\leqslant T_C$ also exhibits a "metallic" type of conduction (against a semiconducting background). However, the resistivity maximum is not clearly manifested, since the semiconducting branch has a weak temperature dependence. Annealing of the samples at 1500 °C lead to a decrease of the Curie temperature by ≈12 K and to a shift of the magnetoresistance maximum T_r by ≈10 K (the average value for the different x). We note that the maximum differences of T_C and T_r are observed for samples with $x=0.4$.

The decrease of the spontaneous magnetization and the Curie temperature and the increase of the resistance and the value of the magnetoresistive effect after annealing at 1500 °C can be explained by an increase in the number of oxygen vacancies[23,24] and by cluster formation and the appearance of a γ-Mn_2O_3 or Mn_3O_4 phase.[12–14]

The magnetization curves and the magnetic hysteresis of ceramic and film samples were investigated on an inductive–frequency apparatus.[25] The manganite sample was placed in an external inductor of a measuring oscillator, the natural frequency of which was $f=5$ MHz. The application of an external magnetic field of various orientations caused a change in the magnetic state of the manganite film or ceramic sample, which led to an inductance change ΔL of the measuring coil and, as a consequence, to a change Δf in the resonance frequency of the oscillator.

Investigation of the magnetic properties of these compounds on the inductive–frequency apparatus revealed an "anomalous" trend of the magnetization curves for ceramic and film samples under the influence of an external quasistatic magnetic field perpendicular ($H_\perp$) or parallel ($H_\parallel$) to the plane of the sample. Figures 5 and 6 show the change in the frequency of the measuring oscillator circuit with the manganite ceramic or film sample in place. The trend of the $\Delta f=f(H)$ and $M(H)$ curves are equivalent, since the frequency shift is proportional to the value of the magnetization of the sample or to the change in energy of the magnet in a magnetic field. The direction of change of the magnetic field in the sample is indicated by arrows in Figs. 5 and 6. Figure 5 shows the initial parts of the magnetization curves of $(La_{0.8}Sr_{0.2})_{1-x}Mn_{1+x}O_3$ ceramic samples in a magnetic field perpendicular to the plane of the sample for $x=0$, 0.2, and 0.4 after annealing at temperatures of 1150 °C (a) and 1500 °C (b). The curves for $x=0.1$ and 0.3 are approximately the same as the curve for $x=0.2$. In a magnetic field parallel to the plane of the ceramic samples ($H_\parallel$) the magnetization curves are less graphic and are not shown in Fig. 5. The upper part of the $\Delta f=f(H)$ curves demonstrates the presence of the "normal" hysteresis typical of magnetically soft materials: the magnetizing curve passes below the demagnetizing curve. The lower part of the $\Delta f=f(H)$ curve (in low fields) manifests an "anomalous" hysteresis wherein the demagnetizing curve passes below the magnetizing curve, and the minimum of the energy of the magnet is reached in a magnetic field of this sign. The value of the "anomalous" magnetic hysteresis of the manganites studied depends on the manganese excess ($0\leqslant x\leqslant 0.4$). The maximum values of the hysteresis are observed for $x=0.1$, 0.2, and 0.3.

The influence of high-temperature annealing (1500 °C) on the value of the "anomalous" magnetic hysteresis is il-

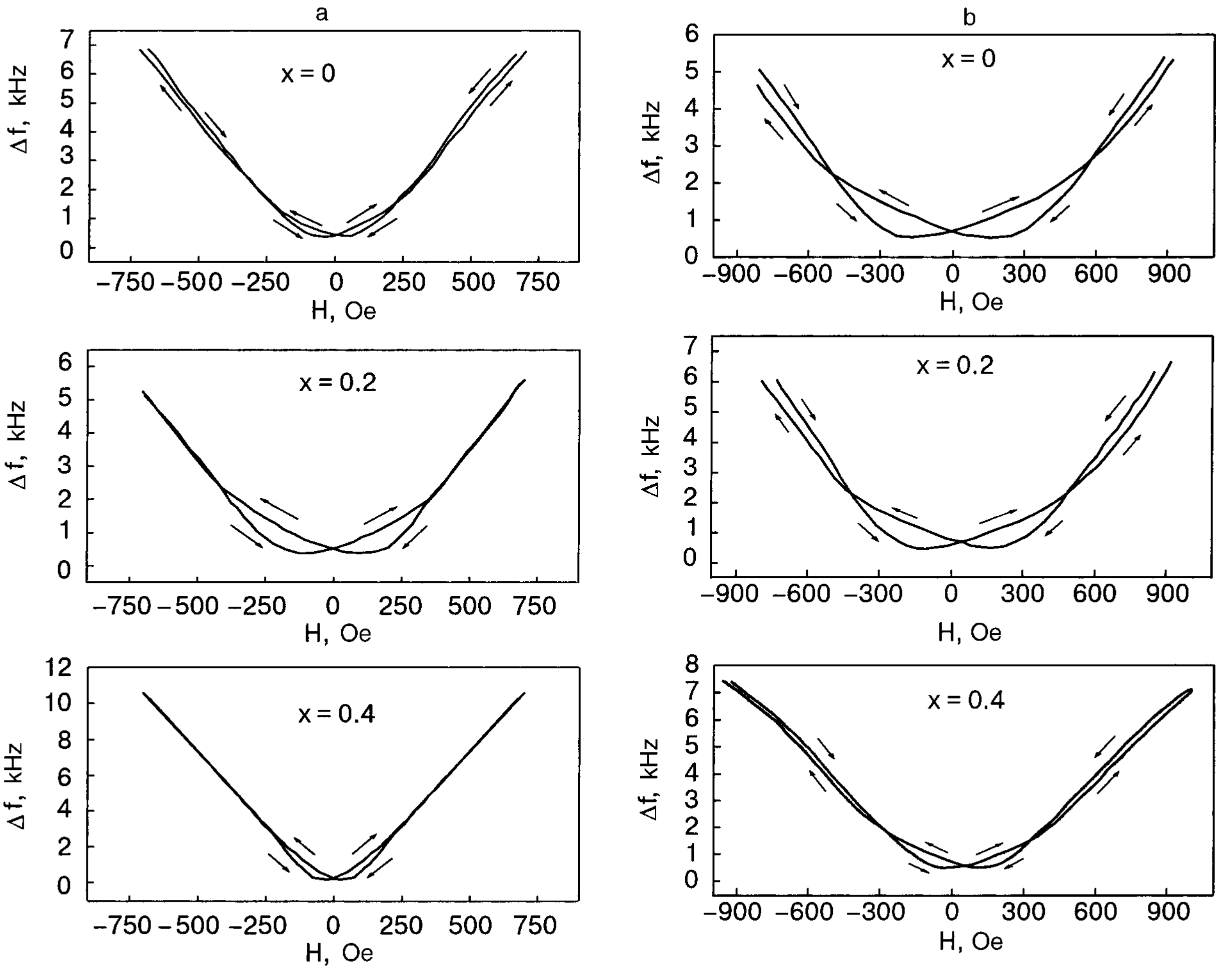

FIG. 5. Shift of the resonance frequency ($\Delta f \propto \Delta M$) of the measuring circuit with a ceramic sample of the manganite $(La_{0.8}Sr_{0.2})_{1-x}Mn_{1+x}O_3$ ($x=0$, 0.2, 0.4) after annealing at 1150 °C (a) and 1500 °C (b) upon variation of the magnetic field $H_\perp$ perpendicular to the plane of the sample.

lustrated in Fig. 5b. It is seen that for the $x=0$ case the "anomalous" magnetic hysteresis has grown considerably and is practically the same as for $x=0.1$, 0.2, and 0.3, while for the $x=0.4$ case it has changed insignificantly. We also note a slight increase in the "normal" magnetic hysteresis of the $(La_{0.8}Sr_{0.2})_{1-x}Mn_{1+x}O_3$ samples after the high-temperature annealing at 1500 °C.

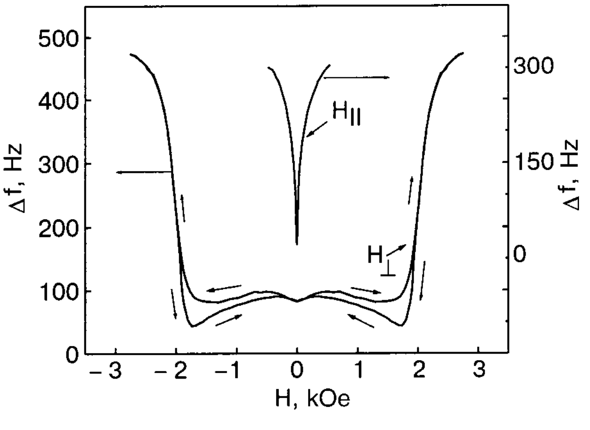

FIG. 6. Shift of the resonance frequency ($\Delta f \propto \Delta M$) of the measuring circuit with a single-crystal sample of $La_{0.6}Sr_{0.2}Mn_{1.2}O_3$ upon variation of the magnetic field parallel ($H_\parallel$) and perpendicular ($H_\perp$) to the film plane.

It is of interest to establish whether the "anomalous" magnetic hysteresis appears in thin-film single-crystal samples. Figure 6 shows the analogous magnetization curves for a $La_{0.6}Sr_{0.2}Mn_{1.2}O_3$ film sample obtained by laser deposition on a substrate. It is seen in the figure that the magnetization of the film is significantly different for fields parallel and perpendicular to the plane. When the external magnetic field is applied parallel to the film plane ($H_\parallel$) a rapid saturation in low magnetic fields (500 Oe) occurs, and hysteresis is not observed. When the film is magnetized in a magnetic field perpendicular to its surface ($H_\perp$) the magnetization remains nearly unchanged up to values $H=1500$ Oe (see Fig. 6) and then changes sharply (by rotation of the magnetic moments) and goes to saturation. In the magnetizing and demagnetizing of the film only "anomalous" hysteresis is observed: the demagnetizing curve passes below the magnetizing curve and reaches a minimum value for this sign of the magnetic field.

We note that after synthesis of the ceramic samples at a temperature of 900 °C (before annealing at 1150 and 1500 °C) only "normal" magnetic hysteresis is observed. The maximum change (shift) of the frequency (upon complete magnetization reversal) for the ceramic samples is approximately 25 kHz, while for the film sample it is 0.5 kHz. The "anomalous" hysteresis (frequency shift Δf) is a relatively small part of the total change in frequency and is approximately 2.5–6% for the ceramic and 8.5–16% for the film samples.

In analyzing the experimental data it can be conjectured that the manganite samples contain magnetic nonuniformities in the form of magnetic phases with different magnetization directions, corresponding to the ''normal'' and ''anomalous'' magnetic hysteresis. A possible mechanism for this sort of behavior is apparently an interaction between two phases characterizing the state of the manganites—a ferromagnetic and an antiferromagnetic phase.[7,16–22]

The coexistence of these phases and their interaction (exchange anisotropy) in the boundary region separating the two phases leads to a shift of the hysteresis loop in the magnetization of these materials.[21,26] We assume that it is this sort of interaction that is responsible for the ''anomalous'' hysteresis and its observation at room temperature (300 K) in magnetic fields of different polarity. This effect is apparently a manifestation of the different magnetic susceptibility of the ferromagnetic and ''canted'' (the boundary zone separating the two phases in the external magnetic field) magnetic phases. This may be confirmed by the following experimental facts:

— The value of the ''anomalous'' hysteresis increases with increasing value of the quasistatic magnetizing field; the experimental curves are symmetric only when the saturating fields of different polarity have the same value.

— For a number of samples, including the ceramic samples synthesized at a temperature of 900 °C, one observes only normal hysteresis; this is evidently due to the absence of ordering in the antiferromagnetic phase ($T_N < T = 300$ K).

The antiferromagnetic phase may be in the form of clusters in the crystallites and in the interlayers between them.

All of what we have said above applies also to the film samples: the presence of magnetically and electrically ''dead'' layers of various thicknesses in manganite thin films was revealed in Ref. 27, and it was shown in Ref. 28 that films of this type can have a ''block'' structure.

CONCLUSION

1. The main phase of the investigated ceramic samples of the lanthanum-manganite system $(\mathrm{La}_{0.8}\mathrm{Sr}_{0.2})_{1-x}\mathrm{Mn}_{1+x}\mathrm{O}_3$ with ''excess'' superstoichiometric manganese ($0 < x < 0.4$), annealed at 1150 and 1500 °C, is a perovskitelike rhombohedrally distorted ($R\bar{3}c$) phase.

2. Additional annealing of the samples at 1500 °C leads to significant changes in the saturation magnetization, to an increase in the magnetoresistive effect by a factor of 2–3, and to a decrease of the Curie temperature and temperature of the magnetoresistance peak for different values of x.

3. An ''anomalous'' magnetic hysteresis is observed in the initial parts of the magnetization curves for the ceramic and film samples. It was shown that the value of the ''anomalous'' magnetic hysteresis depends on x and on the annealing temperature. A mechanism for the ''anomalous'' hysteresis is proposed, involving the presence and interaction of a ferromagnetic phase and an antiferromagnetic phase or cluster having a different composition and defect structure.

4. The changes of the saturation magnetization, magnetoresistive effect, and value of the ''anomalous'' hysteresis are due to changes in the concentration of manganese ions of different valence, Mn^{3+}, Mn^{4+}, and Mn^{2+}, cation and anion vacancies, and mesoscopic inhomogeneities of the cluster type, which depend on x and the annealing temperature.

[*] E-mail: linnik@host.dipt.donetsk.ua

[1] R. M. Kusters, J. Singleton, D. A. Keen, R. McGreevy, and W. Hayes, Physica B **155**, 362 (1989).

[2] R. von Helmont, J. Wecker, B. Holzapfel, M. Schultz, and K. Samwer, Phys. Rev. Lett. **71**, 2331 (1993).

[3] K. Chahara, T. Ohno, M. Kasai, and Y. Kozono, Appl. Phys. Lett. **63**, 1990 (1993).

[4] S. Jin, T. H. Tiefel, M. McCormack, R. A. Fastnacht, R. Ramesh, and L. H. Chen, Science (Washington, DC, U.S.) **264**, 413 (1994).

[5] A. Vrushibara, Y. Moritomo, T. Arima, A. Asamitsu, G. Kido, and V. Tokura, Phys. Rev. B **51**, 14103 (1995).

[6] A. P. Ramires, J. Phys.: Condens. Matter **9**, 8171 (1997).

[7] É. L. Nagaev, Usp. Fiz. Nauk **166**, 833 (1996).

[8] L. P. Gor'kov, Usp. Fiz. Nauk **168**, 665 (1998).

[9] V. M. Loktev and Yu. G. Pogorelov, Fiz. Nizk. Temp. **26**, 231 (2000) [Low Temp. Phys. **26**, 171 (2000)].

[10] Yu. A. Izyumov and Yu. N. Skryabin, Usp. Fiz. Nauk **171**, 121 (2001).

[11] M. Yu. Kagan and K. I. Kugel', Usp. Fiz. Nauk **171**, 577 (2001).

[12] V. P. Pashchenko, S. I. Khartsev, O. P. Cherenkov, A. A. Shemyakov, Z. A. Samoĭlenko, A. D. Loĭko, and V. I. Kamenev, Neorg. Mater. **35**, 1509 (1999).

[13] V. P. Pashchenko, A. A. Shemyakov, V. K. Prokopenko, V. N. Derkachenko, O. P. Cherenkov, V. I. Mihajlov, V. N. Varyukhin, V. P. Dyakonov, and H. Szymczak, J. Magn. Magn. Mater. **220**, 52 (2000).

[14] V. P. Pashchenko, V. K. Prokopenko, A. A. Shemyakov, V. N. Varyukhin, V. N. Derkachenko, A. D. Loĭko, V. P. D'yakonov, Kh. Shimchak, and A. Gladchuk, Metallofiz. Noveĭshie Tekhnol. **22**, 18 (2000).

[15] S. S. Kucherenko, V. P. Pashchenko, P. I. Polyakov, V. A. Shtaba, and A. A. Shemyakov, Fiz. Nizk. Temp. **27**, 761 (2001) [Low Temp. Phys. **27**, 559 (2001)].

[16] T. I. Arbuzova, I. B. Smolyak, S. V. Naumov, A. A. Samokhvalov, A. V. Mostovshchikov, and N. I. Solin, Zh. Éksp. Teor. Fiz. **116**, 1664 (1999) [JETP **89**, 899 (1999)].

[17] K. N. Mikhalev, S. A. Lekomtsev, A. P. Gerashchenko, V. E. Arkhipov, A. V. Korolev, Ya. M. Mukovskiĭ, and A. A. Arsenov, JETP Lett. **72**, 599 (2000).

[18] K. N. Mikhalev, S. A. Lekomtsev, A. P. Gerashchenko, V. V. Serikov, I. A. Fogel', and A. R. Kaul', Fiz. Met. Metalloved. **93**, 32 (2002).

[19] L. I. Koroleva, R. V. Demin, and A. M. Balbashov, JETP Lett. **65**, 474 (1997).

[20] O. Yu. Gorbenko, R. V. Demin, A. R. Kaul', L. I. Koroleva, and R. Szymczak, Fiz. Tverd. Tela (St. Petersburg) **40**, 290 (1998) [Phys. Solid State **40**, 263 (1998)].

[21] R. V. Demin, L. I. Koroleva, R. Szymczak, and H. Szymczak, JETP Lett. **75**, 331 (2002).

[22] A. P. Nosov and P. Strobel', Fiz. Met. Metalloved. **93**, 50 (2002).

[23] I. O. Troyanchuk, D. D. Khalyavin, S. V. Trukhanov, G. N. Chobot, and H. Szymczak, JETP Lett. **70**, 590 (1999).

[24] I. O. Troyanchuk, S. V. Trukhanov, H. Szymczak, J. Przewoznik, and K. Bärner, Zh. Éksp. Teor. Fiz. **120**, 183 (2001) [JETP **93**, 161 (2001)].

[25] J. Maartense, J. Appl. Phys. **53**, 2466 (1982).

[26] W. H. Meiklejohn and C. P. Bean, Phys. Rev. **105**, 904 (1957).

[27] R. P. Borges, W. Guichard, J. G. Lunney, J. M. D. Coey, and F. Ott, J. Appl. Phys. **89**, 3868 (2001).

[28] Yu. A. Boĭkov, T. Klaeson, and A. Yu. Boĭkov, Zh. Tekh. Fiz. **71**, 54 (2001) [Tech. Phys. **46**, 1260 (2001)].

Translated by Steve Torstveit

LOW TEMPERATURE PHYSICS VOLUME 29, NUMBER 4 APRIL 2003

Eigenmodes of the electromagnetic field in the presence of a magnetic domain structure

V. G. Peschansky*

B. Verkin Institute for Low Temperature Physics and Engineering, National Academy of Sciences of Ukraine, pr. Lenina 47, 61103 Kharkov, Ukraine; V. I. Karazin Kharkov National University, pl. Svobody 4, 61077 Kharkov, Ukraine

D. I. Stepanenko

V. I. Karazin Kharkov National University, pl. Svobody 4, 61077 Kharkov, Ukraine

(Submitted August 2, 2002)
Fiz. Nizk. Temp. **29**, 387–391 (April 2003)

The spectrum of weakly damped eigenmodes of the electromagnetic field in metals in a quantizing magnetic field are determined under conditions such that a magnetic domain structure exists. © *2003 American Institute of Physics.* [DOI: 10.1063/1.1542469]

At low temperatures the thermodynamic and kinetic characteristics of a metal placed in a quantizing magnetic field $\mathbf{H}=(0,0,H_0)$ have an oscillatory dependence on the inverse magnetic field. The cause of these oscillations is the presence of features of the density of states of the charge carriers due to the energy quantization in the magnetic field. Here the charges are actually acted upon by a field averaged over regions of the order of the Larmor radius, i.e., a magnetic induction **B**. As long as the magnetic susceptibility χ is small, the difference between **B** and **H** can be neglected. If the distance between energy levels $\Delta\varepsilon\cong\hbar\Omega$ of the charge carriers in the magnetic field is much larger than the carrier temperature T and the level width $\hbar/\tau$ but much smaller than the Fermi energy ε_F, i.e., $\hbar/\tau$, $T\ll\hbar\Omega\ll\varepsilon_F$, the oscillatory part of the magnetic susceptibility can reach values of the order of unity, and the magnetization $\mathbf{M}(\mathbf{B})$ and the magnetic field $\mathbf{H}=\mathbf{B}-4\pi\mathbf{M}(\mathbf{B})$ become functions of the magnetic induction. Here $\hbar$, Ω, and τ are Planck's constant, the cyclotron frequency, and the mean free time of the conduction electrons, respectively. In this case the problem of taking the magnetism of the medium into account is a self-consistent problem even in conductors that do not have magnetic ordering. If $\chi>1/4\pi$ the state of the system becomes unstable, and the sample separates into alternating domains with different values of the magnetic induction.[1,2]

In this paper we investigate the weakly damped eigenmodes of the electromagnetic field in uncompensated metals under conditions such that the distribution of the magnetic induction has a stationary domain structure. The alternating electromagnetic field in the metal is determined by the system of Maxwell's equations

$$\text{curl }\mathbf{B}=\frac{4\pi}{c}\mathbf{J},\quad \text{curl }\mathbf{E}=-\frac{1}{c}\frac{\partial\mathbf{B}}{\partial t},\quad \text{div}\,\mathbf{B}=0, \tag{1}$$

where c is the speed of light in vacuum, $\mathbf{J}=\mathbf{j}+\mathbf{j}'$ is the total current density, consisting of the conduction current density **j** due to the electric field **E** and the magnetization current density $\mathbf{j}'=c\ \text{curl}\,\mathbf{M}$ induced by the magnetic field.

In the case of weak temporal and spatial dispersion

$$\omega\ll\Omega,\quad kr_0\ll1,\quad k_zv_F\tau\ll1,$$

$$\kappa^2\equiv|1-4\pi\chi(\mathbf{B}_0)|\ll1, \tag{2}$$

where r_0 is the radius of curvature of the orbit of the charge carriers in the uniform field $\mathbf{B}_0=(0,0,B_0)$, v_F is their Fermi velocity, and ω and **k** are the frequency and wave vector of the alternating field $\mathbf{B}(y,z,t)$. The integral expressions for the current density and magnetization can be reduced to local form, i.e., they can be written in the form of an expansion in powers of the alternating electric and magnetic fields and their derivatives. For $\kappa^2\equiv|1-4\pi\chi(\mathbf{B}_0)|\ll1$ the linear term of the expansion of the magnetic field **H** in powers of $\mathbf{B}(\mathbf{r},t)$ can turn out to be of the same order of magnitude as the nonlinear terms, and the wave processes become substantially nonlinear. For small-amplitude waves it is sufficient to take into account only the nonlinear correction to the magnetization, which is proportional to the third power of **B**.[3,4] In the expression for the current density one can stop at the linear approximation in the electric field **E** and neglect the gradient terms, which are proportional to powers of the small parameter $(kr_0)^2$, and the quantum oscillatory correction, which is proportional to $(\hbar\Omega/\varepsilon_F)^{1/2}$. The current density $\mathbf{j}'$ induced by the magnetic field is determined by the magnetization component M_z, since the vector **M** is directed predominantly along $\mathbf{B}_0$. The expression for $\mathbf{j}'=(j_x',0,0)$ can be written in the form[3–5]

$$j_x'=c(\text{curl }\mathbf{M})_x=c\frac{\partial M_z}{\partial y}=c\chi(\mathbf{B}_0)\frac{\partial B_z}{\partial y}-4\pi c\beta\frac{\partial B_z^3}{\partial y}+4\pi\alpha c r_0^2\frac{\partial^3 B_z}{\partial y^3}, \tag{3}$$

where $\beta=\zeta(\varepsilon_F/\hbar\Omega B_0)^2$, and α and ζ are numerical coefficients of the order of unity which depend on the concrete form of the dispersion relation for the charge carriers.

In the stationary case in the absence of electric field the solution of system (1) for $\chi(B_0)>1/4\pi$ has the form

$$B_1(y)=b_0\frac{\mu}{\sqrt{1+\mu^2}}\,\text{sn}\left(\frac{y}{\delta\sqrt{1+\mu^2}},\mu\right) \tag{4}$$

and describes a periodic domain structure with period $Y = 4\delta\sqrt{1+\mu^2}K(\mu)$ and domain-wall thickness $\delta = \sqrt{4\pi\alpha r_0/\kappa}$. Here

$$b_0=(\kappa^2/2\pi\beta)^{1/2}\approx\kappa B_0(\hbar\Omega/\varepsilon_F),$$

$$K(\mu)=\int_0^1 dt[(1-t^2)(1-\mu^2t^2)]^{-1/2}\equiv K$$

is a complete elliptic integral of the first kind. The modulus μ of the Jacobi elliptic function sn determines the period Y and is found from the condition that the total thermodynamic potential, including the surface energy at the boundaries of the domains, be minimized with respect to Y. In a case of more practical importance, when the linear dimensions L of the sample are significantly larger than the Larmor radius of the electron, the estimate $Y\sim\sqrt{\kappa^2 r_0 L}$ is valid.[6] Without loss of generality one can assume that the domain sizes are large compared to δ, i.e., $Y\gg\delta$, or

$$K\gg\pi. \tag{5}$$

Then it is easily noted that μ is close to unity, since the asymptotic expression $K\approx-2\ln(1-\mu^2)$ holds for $K\gg1$.

We set $B_z(y,z,t)=B_1(y)+B^{\sim}(y,z,t)$, where $B^{\sim}(y,z,t)=b(y)\mathrm{e}^{-i\omega t+ik_z z}$ is a small space–time perturbation. Linearizing the system of Maxwell's equations (1) with respect to $\mathbf{B}^{\sim}(y,z,t)$ and eliminating the electric field $\mathbf{E}$, we obtain the following equation for the time-dependent field $\mathbf{B}^{\sim}(y,z,t)$:

$$\frac{\partial\mathbf{B}^{\sim}}{\partial t}=-\frac{c^2}{4\pi}\mathrm{curl}\ (\hat{\rho}\ \ \mathrm{curl}\ \ \mathbf{H}^{\sim}). \tag{6}$$

Here

$$(\hat{\rho}\ \ \mathrm{curl}\ \ \mathbf{H}^{\sim})_i=\rho_{ij}(\mathrm{curl}\ \ \mathbf{H}^{\sim})_j,\ \ H_x^{\sim}=B_x^{\sim},\ \ H_y^{\sim}=B_y^{\sim},$$

$$H_z^{\sim}=-\kappa^2 B_z^{\sim}+12\pi\beta B_1^2(y)B_z^{\sim}-4\pi\alpha r_0^2\frac{\partial^2 B_z^{\sim}}{\partial y^2}.$$

The resistivity tensor can be written in the form of a sum of symmetric and antisymmetric parts: $\rho_{ij}\equiv\rho_{ij}^{(s)}+\rho_{ij}^{(a)}$. The components $\rho_{ij}^{(s)}$ are of the same order of magnitude and tend toward constant values for $B_0\to\infty$. We shall assume that the tensor $\rho_{ij}^{(s)}$ is reduced to its principal axes. Generally speaking, this is valid only in the case when the magnetic field is directed along an axis of symmetry of the crystal. However, taking the off-diagonal components of the resistivity tensor into account does not lead to a qualitative change in the wave spectrum but only gives rise to additional terms in the wave damping decrement which do not alter its order of magnitude.

In the leading approximation in powers of the small parameter $(\Omega\tau)^{-1}$ the diagonal components of the resistivity tensor have the values $\rho_{xx}=\beta_1\rho_0(1-i\omega\tau)$, $\rho_{yy}=\beta_2\rho_0(1-i\omega\tau)$, and $\rho_{zz}=\beta_3\rho_0$. Here $\rho_0=\sigma_0^{-1}$, $\sigma_0\cong\omega_p^2\tau/4\pi$ is the static electrical conductivity of the metal in the absence of magnetic field, ω_p is the frequency of plasma oscillations of the charge carriers, and β_1, β_2, and β_3 are dimensionless coefficients of the order of unity which depend on the concrete form of the dispersion relation of the charge carriers and for simplicity will be assumed equal to unity. In the expression for the antisymmetric part of the resistivity tensor $\rho_{ij}^{(a)}$ it is sufficient to keep only the leading, Hall components $\rho_{xy}=-\rho_{yx}=B_0/ce(n_e-n_h)$, where n_e and n_h are the electron and hole densities, and e is the absolute value of the electron charge.

Under these conditions the system of equations (6) takes the form

$$\frac{\partial B_x^{\sim}}{\partial t}=-\frac{c^2\rho_{xy}}{4\pi}\frac{\partial}{\partial z}\left(\frac{\partial H_z^{\sim}}{\partial y}-\frac{\partial B_y^{\sim}}{\partial z}\right)+\frac{c^2\rho_0}{4\pi}\left(\frac{\partial^2}{\partial y^2}+(1-i\omega\tau)\frac{\partial^2}{\partial z^2}\right)B_x^{\sim},$$

$$\frac{\partial B_y^{\sim}}{\partial t}=-\frac{c^2\rho_{xy}}{4\pi}\frac{\partial^2 B_x^{\sim}}{\partial z^2}-\frac{c^2\rho_0}{4\pi}(1-i\omega\tau)\frac{\partial}{\partial z}\left(\frac{\partial H_z^{\sim}}{\partial y}-\frac{\partial B_y^{\sim}}{\partial z}\right),$$

$$\frac{\partial B_z^{\sim}}{\partial t}=\frac{c^2\rho_{xy}}{4\pi}\frac{\partial^2 B_x^{\sim}}{\partial z\partial y}+\frac{c^2\rho_0}{4\pi}(1-i\omega\tau)\frac{\partial}{\partial y}\left(\frac{\partial H_z^{\sim}}{\partial y}-\frac{\partial B_y^{\sim}}{\partial z}\right). \tag{7}$$

Eliminating $B_x^{\sim}$ and $B_y^{\sim}$ from these equations and neglecting terms proportional to $(\Omega\tau)^{-2}$, we obtain the following equation for $b(y)$:

$$\left[k_z^2-i\gamma(1-i\omega\tau)\omega\left(\frac{4\pi}{c^2|\rho_{xy}|}\right)\right]\left[\kappa^2\frac{\partial^2 b(y)}{\partial y^2}-12\pi\beta\frac{\partial^2}{\partial y^2}(b(y)B_1^2(y))+4\pi\alpha r_0^2\frac{\partial^4 b(y)}{\partial y^4}\right]$$
$$=-i\gamma\omega\left(\frac{4\pi}{c^2|\rho_{xy}|}\right)\frac{\partial^2 b(y)}{\partial y^2}+\left[\left(\frac{4\pi}{c^2|\rho_{xy}|}\right)^2\omega^2-k_z^4+2i\gamma(1-i\omega\tau)\omega k_z^2\left(\frac{4\pi}{c^2|\rho_{xy}|}\right)\right]b(y). \tag{8}$$

Here

$$\gamma=(\sigma_0|\rho_{xy}|)^{-1}\approx\left|\frac{n_e-n_h}{n_e+n_h}\right|(\Omega\tau)^{-1}\sim(\Omega\tau)^{-1}\ll1.$$

This equation determines the amplitude and frequency of the eigenmodes of the electromagnetic field in the presence of a periodic domain structure.

The case when the expression in square brackets on the right-hand side of Eq. (8) equals zero corresponds to a wave with frequency

$$\omega=\frac{k^2cB_0}{4\pi e|n_e-n_h|}(1-i\gamma), \tag{9}$$

propagating along the direction of the external magnetic field. In this case Eq. (8) goes over to a Lamé equation, and its solution is expressed in theta functions.[7]

In the limiting case $\gamma\ll\kappa^2$ the solution of this equation has the form

$$b(y)=\Lambda\ \ \mathrm{cn}\left(\frac{y}{\delta\sqrt{1+\mu^2}},\mu\right)\mathrm{dn}\left(\frac{y}{\delta\sqrt{1+\mu^2}},\mu\right), \tag{10}$$

where cn and dn are Jacobi elliptic functions. By virtue of inequality (5) the function $b(y)$ is substantially nonzero only in the region of a domain wall, i.e., in the vicinity of the points $y_n=2nK\delta\sqrt{1+\mu^2}$, where n is an integer. In the region $|y=y_n|\gg\delta$ the time-dependent field $\mathbf{B}^{\sim}(\mathbf{r},t)$ is a helicoid wave propagating along the direction of $\mathbf{B}_0$. If dissipative effects are neglected, the remaining components of the magnetic field have the values

$$\begin{pmatrix} B_x^{\sim} \\ B_y^{\sim} \end{pmatrix} = -k\delta A(1+\mu^2)\begin{pmatrix} 1 \\ i \end{pmatrix}\mathrm{sn}\left(\frac{y}{\delta\sqrt{1+\mu^2}},\mu\right)e^{-i\omega t+ikz}. \tag{11}$$

We consider the case of arbitrary propagation direction of the wave. We introduce a new unknown function $u(y)$ such that $b(y)=d^2u(y)/dy^2$. The equation for this function can be written as

$$u^{(4)}(\xi)+\left[-6\mu^2\mathrm{sn}^2(\xi,\mu)+(1+\mu^2)\left(1+i\frac{\gamma}{\kappa^2}\frac{V}{\eta_z^2}\right)\right] \times u''(\xi)=(1+\mu^2)^2Wu(\xi), \tag{12}$$

where

$$W=\left\{\frac{V^2-\eta_z^4}{\eta_z^2}\left[1+i\gamma(1-i\omega_0\tau V)\frac{V}{\eta_z^2}\right] +2i\gamma(1-i\omega_0\tau V)V\right\},$$

$$\eta_z=\frac{k_z\delta}{\kappa},\quad V=\frac{\omega}{\omega_0},\quad \omega_0=\frac{cB_0\kappa^2}{4\pi e|n_e-n_h|\delta^2}\sim\frac{c^2\Omega\kappa^2}{\omega_p^2\delta^2}.$$

When condition (5) holds and the variable ξ lies in the interval

$$(2m-1)K\leqslant\xi\leqslant(2m+1)K$$

the elliptic sine can be replaced by the hyperbolic tangent: $\mathrm{sn}(\xi,1)=\tanh\xi$. Assuming $\mu=1$ in Eq. (12), we obtain

$$u_m^{(4)}(\xi_m)+\left(\frac{6}{\cosh^2\xi_m}-4+2i\nu\right)u_m''(\xi_m)=4Wu_m(\xi_m). \tag{13}$$

Here $\xi_m\equiv\xi-2mK$, where m is an integer, $-K\leqslant\xi_m\leqslant K$, and $\nu=(\gamma/\kappa^2)(V/\eta_z^2)$.

In the region $-K\leqslant\xi_m\leqslant 0$ the solution of this equation can be sought in the form of a series in powers of $e^{2\xi_m}$:

$$u_m^{(-)}(\xi_m,\lambda)=e^{2\lambda\xi_m}\sum_{n=0}^{\infty}a_n(\lambda)e^{2n\xi_m}, \tag{14}$$

where λ is a parameter which is not a negative integer.

Substituting expression (14) into Eq. (13) and collecting the coefficients of equal powers of $e^{2\xi_m}$, we obtain an infinite system of linear equations for the unknowns $a_n(\lambda)$:

$$\begin{aligned}
&\Phi(0)a_0=0,\\
&2\Psi(0)a_0+\Phi(1)a_1=0,\\
&\Phi(0)a_0+2\Psi(1)a_1+\Phi(2)a_2=0,\\
&\Phi(n-2)a_{n-2}+2\Psi(n-1)a_{n-1}+\Phi(n)a_n=0,\quad n\geqslant 2,
\end{aligned} \tag{15}$$

where

$$\Phi(n)\equiv(n+\lambda)^4-\left(1-\frac{i\nu}{2}\right)(n+\lambda)^2-\frac{W}{4},$$

$$\Psi(n)\equiv(n+\lambda)^4+2\left(1-\frac{i\nu}{4}\right)(n+\lambda)^2-\frac{W}{4}.$$

In the case $0\leqslant\xi_m\leqslant K$ the solution of equation (13) can be written in the form of a series in powers of $e^{2\xi_m}$:

$$u_m^{(+)}(\xi_m,\lambda)=e^{-2\lambda\xi_m}\sum_{n=0}^{\infty}a_n(\lambda)e^{-2n\xi_m} \tag{16}$$

with the same coefficients $a_n(\lambda)$ that satisfy the system of equations (15), where a_0 can be specified arbitrarily and the remaining coefficients are found from the recursion relations

$$a_1=-2a_0\frac{\Psi(0)}{\Phi(1)},\quad a_2=-2a_1\frac{\Psi(1)}{\Phi(2)},\ldots$$

$$a_n=-\frac{a_{n-2}\Phi(n-2)+2a_{n-1}\Psi(n-1)}{\Phi(n)}. \tag{17}$$

A simple numerical analysis shows that for $n\rightarrow\infty$ the coefficients a_n have the following properties:

$$a_n\rightarrow 0,\left|\frac{a_{n+1}}{a_n}\right|\rightarrow 1-0,\ \ \mathrm{sgn}\,\mathrm{Re}\frac{a_{n+1}}{a_n}=-1,$$

$$\mathrm{sgn}\,\mathrm{Im}\frac{a_{n+1}}{a_n}=-1.$$

The first equation of system (15) implies a discrete relation between λ and V and η_z:

$$\Phi(0)\equiv\lambda^4-\left(1-\frac{i\nu}{2}\right)\lambda^2-\frac{W}{4}=0. \tag{18}$$

The four roots of this equation,

$$\begin{aligned}
\lambda_{1,2}&=\pm\sqrt{\frac{1}{2}}\left(1-\frac{i\nu}{2}-\sqrt{\left(1-\frac{i\nu}{2}\right)^2+W}\right)^{1/2},\\
\lambda_{3,4}&=\pm\sqrt{\frac{1}{2}}\left(1-\frac{i\nu}{2}+\sqrt{\left(1-\frac{i\nu}{2}\right)^2+W}\right)^{1/2}
\end{aligned} \tag{19}$$

together with expressions (14) and (16) determine the four linearly independent solutions of equation (13):

$$u_m(\xi_m)=\begin{cases}\displaystyle\sum_{i=1}^{4}A_iu_m^{(-)}(\xi_m,\lambda_i), & -K\leqslant\xi_m\leqslant 0,\\ \displaystyle\sum_{i=1}^{4}C_iu_m^{(+)}(\xi_m,\lambda_i), & 0\leqslant\xi_m\leqslant K,\end{cases} \tag{20}$$

where

$$\begin{aligned}
u_m^{(-)}(\xi_m,\lambda_i)&=e^{2\lambda_i\xi_m}\left(1+\sum_{n=1}^{\infty}a_n(\lambda_i)e^{2n\xi_m}\right),\\
u_m^{(+)}(\xi_m,\lambda_i)&=e^{-2\lambda_i\xi_m}\left(1+\sum_{n=1}^{\infty}a_n(\lambda_i)e^{-2n\xi_m}\right),
\end{aligned} \tag{21}$$

$a_0(\lambda_i)=1$, and A_i and C_i are constants. Series (21) converges absolutely in the entire domain of definition except at the point $\xi_m=0$, where it converges conditionally. It follows from formulas (21) that $u_m^{(+)}(0,\lambda_i)=u_m^{(-)}(0,\lambda_i)$.

The functions (20) form a fundamental system of solutions of the differential equation (13). In the interval $(2m+1)K\leqslant\xi\leqslant(2m+3)K$ (or $-K\leqslant\xi_{m+1}\leqslant K$) the solution of equation (13) should be sought in the form

$$u_{m+1}(\xi_{m+1},\lambda_i)=Cu_m(\xi_m-2K,\lambda_i), \tag{22}$$

where C is a constant.

If dissipative effects are neglected completely, i.e., for $\gamma\to 0$, the real values $W>0$ correspond to imaginary λ_1, λ_2 and real λ_3, λ_4. The wave processes correspond to the solutions $u(\xi_m,\lambda_1)$ and $u(\xi_m,\lambda_2)$. Assuming $\lambda_{1,2}=\pm i\eta_y/2$, where η_y is real, we find from Eq. (21) in the limit $\gamma\to 0$ that the frequency of the eigenmodes of the electromagnetic field has the value

$$\omega=\omega_0\eta_z\sqrt{\eta_z^2+\eta_y^2+\frac{\eta_y^4}{4}}. \tag{23}$$

Let us construct a solution of equation (12) in the interval $0\leqslant\xi_m\leqslant 2K$ in the form a traveling wave. In a neighborhood of the point $\xi_m=K$ the sum in expressions (21) has order of magnitude $O(\mathrm{e}^{-2K})$. Splicing the asymptotic expressions $u_m^{(+)}(\xi_m,-i\eta_y)$ and $u_{m+1}^{(-)}(\xi_{m+1},i\eta_y)$ for $\xi_m\to K$ and using relation (22), we obtain

$$\begin{aligned} u(\xi_m)&=u_m^{(+)}(\xi_m,-i\eta_y)=C_2\mathrm{e}^{i\eta_y\xi_m}=u_{m+1}^{(-)}(\xi_{m+1},i\eta_y)\\ &=Cu_m^{(-)}(\xi_m-2K,i\eta_y)=CA_1\mathrm{e}^{i\eta_y(\xi_m-2K)}. \end{aligned} \tag{24}$$

Equating the coefficients of $\mathrm{e}^{i\eta_y\xi_m}$, we find $C_2=CA_1\mathrm{e}^{-2i\eta_yK}$. Summing the two asymptotic expressions $u_m^{(+)}(\xi_m)$ and $u_{m+1}^{(-)}(\xi_{m+1})$ and then subtracting off their common part (24), we obtain a solution of equation (12) which is valid on the interval $0\leqslant\xi_m\leqslant 2K$:

$$\begin{aligned} u(\xi_m)=C_2\mathrm{e}^{i\eta_y\xi_m}\Bigg(&1+\sum_{n=1}^{\infty}a_n(-i\eta_y)\mathrm{e}^{-2n\xi_m}\\ &+\sum_{n=1}^{\infty}a_n(i\eta_y)\mathrm{e}^{2n(\xi_m-2K)}\Bigg). \end{aligned} \tag{25}$$

It follows from relation (22) that the multiplicative factor C has the value

$$C=\frac{u(2K)}{u(0)}=\exp\left[2i\arg\left(1+\sum_{n=1}^{\infty}a_n(i\eta_y)\right)+2i\eta_yK\right]\equiv\mathrm{e}^{2iKs}. \tag{26}$$

The solution of equation (12) can be written in the form

$$u(\xi)=\mathrm{e}^{is\xi}F(\xi), \tag{27}$$

where $F(\xi)$ is a periodic function with period $2K$, and the dimensionless wave number $s\equiv\sqrt{2}k_y\delta$ has the value

$$s=\eta_y+\frac{\arg(1+\Sigma_{n=1}^{\infty}a_n(i\eta_y))}{K}. \tag{28}$$

The complex conjugate of function (25) is also a solution of equation (12).

Relation (23) implies the folowing dispersion relation of the traveling wave:

$$\omega=\frac{cB_0}{4\pi e|n_e-n_h|}\left[k_z\sqrt{k_z^2+\frac{\kappa^2\eta_y^2(k_y)}{\delta^2}\left(1+\frac{\eta_y^2(k_y)}{4}\right)}\right], \tag{29}$$

where η_y is determined as a function of k_y by expression (28).

In the case of weak spatial dispersion $k_zv_F\ll\tau^{-1}$, the damping is due solely to the scattering of electrons, $\mathrm{Im}\,\omega\sim\gamma\omega$. When the opposite inequality holds, $\tau^{-1}\ll k_zv_F\ll\Omega$, the eigenmode spectrum remains the same, while the expression for the damping decrement acquires additional terms due to Čerenkov absorption of the electromagnetic field by electrons moving in-phase with the wave. In that case the quantization of the energy levels of the electrons has a substantial influence on the damping of the wave.[8]

One of the authors (V.G.P.) would like to thank the INTAS Foundation (Grant 01-0791) for support of this study.

---

[*] E-mail: vpeschansky@ilt.kharkov.ua

[1] D. Shoenberg, Philos. Trans. R. Soc. London, Ser. A **255**, 85 (1962).
[2] J. Condon, Phys. Rev. **145**, 526 (1966).
[3] V. G. Peschanskiĭ (Peschansky) and D. I. Stepanenko, Zh. Éksp. Teor. Fiz. **112**, 1841 (1997) [JETP **85**, 1007 (1997)].
[4] V. G. Peschanskiĭ (Peschansky) and D. I. Stepanenko, Fiz. Nizk. Temp. **25**, 277 (1999) [Low Temp. Phys. **25**, 203 (1999)].
[5] V. G. Peschansky and D. I. Stepanenko, Fiz. Nizk. Temp. **25**, 889 (1999) [Low Temp. Phys. **25**, 666 (1999)].
[6] I. P. Privorotskiĭ and M. Ya. Azbel', Zh. Éksp. Teor. Fiz. **56**, 388 (1969) [Sov. Phys. JETP **29**, 214 (1969)].
[7] V. G. Peschansky and D. I. Stepanenko, Visnik KhNU im. V. N. Karazina, Seriya "Fizika" **516**, 34 (2001).
[8] V. G. Skobov and É. A. Kaner, Zh. Éksp. Teor. Fiz. **47**, 1806 (1964) [Sov. Phys. JETP **19**, 1217 (1964)].

Translated by Steve Torstveit

LOW TEMPERATURE PHYSICS VOLUME 29, NUMBER 4 APRIL 2003

Antiferromagnetic resonance spectrum in $LaMnO_3$

V. N. Krivoruchko* and T. E. Prymak

A. A. Galkin Donetsk Physicotechnical Institute, ul. R. Lyuksemburg 72, 83114 Donetsk, Ukraine

(Submitted August 16, 2002)
Fiz. Nizk. Temp. **29**, 392–395 (April 2003)

The substantially noncollinear magnetic structure realized in $LaMnO_3$ in an external magnetic field is investigated, and the frequency–field diagram of the magnetic eigenmodes of the system is obtained. It is shown that neglect of the Dzyaloshinskii interaction, a measure which a number of authors contend is justified because the corresponding constants of the spin Hamiltonian are small compared to the anisotropy, leads to an incorrect description of the dynamics of the system. © *2003 American Institute of Physics.* [DOI: 10.1063/1.1542470]

Neutron diffraction studies[1,2] have laid the groundwork for the study of the magnetic structure of lanthanum manganite. It was found that $LaMnO_3$ is a type-A layered antiferromagnet with a weak ferromagnetic moment. This weak ferromagnetism has since been studied in detail and is attributed to the presence of a Dzyaloshinskii interaction in the crystal.[3] This substance has seen a recent upsurge in interest in connection with the discovery of colossal magnetoresistance and the growing prospects for its practical application. The complex interplay of the magnetic, charge, orbital, and structural ordering in this substance requires a comprehensive study of its properties—in particular, its fundamental magnetic properties—in order to understand the behavior of this crystal.

One of the most powerful modern tools for studying the dynamic properties of magnetically ordered substances is the magnetic resonance method. The study of the resonance properties of lanthanum manganite[4–9] is complicated by the presence of a large energy gap in its spectrum. The large gap in the antiferromagnetic resonance (AFMR) spectrum, the presence of which is confirmed by neutron scattering experiments,[10] is due to the large value of the uniaxial anisotropy of this substance, as a result of which the relationship between the constants of its spin Hamiltonian is unusual for a multisublattice antiferromagnet: $H_a \gg H_D$, where H_D is the field of the Dzyaloshinskii interaction and H_a is the uniaxial anisotropy field.

$LaMnO_3$ was studied in a four-sublattice model in Refs. 7 and 8 from the standpoint of the interaction of the orbital and magnetic structures, but the antisymmetric exchange H_D was excluded from consideration in those studies. The neglect of this interaction is contrary to general symmetry principles and, as will be shown below, distorts the behavior of the magnetic structure of the crystal in an external magnetic field.

In this paper the noncollinear magnetic structure realized in $LaMnO_3$ in a magnetic field parallel both to the axis of its weak ferromagnetism and to the easy axis of the crystal is studied in the framework of a four-sublattice model. The ground state of $LaMnO_3$ is analyzed, and the field dependence of the frequencies of the magnetic eigenmodes of the system is determined.

1. The $LaMnO_3$ crystal is known[1–3,11] (see also the works cited in Refs. 12 and 13) to have a distorted perovskite structure with the crystallographic group $Pmna$ (D_{2h}^{16}). At $T_N \sim 140$ K there is a phase transition from the paramagnetic to an antiferromagnetic (AFM) phase with type-A ordering, where the magnetic moments within a layer are ordered ferromagnetically while the magnetic ordering between layers is of an antiferromagnetic character. The unit cell of $LaMnO_3$ contains four Mn^{3+} ions, located at the sites 1 (0,0,0), 2 (1/2, 0, 1/2), 3 (0, 1/2, 0), and 4 (1/2, 1/2, 1/2). We associate a magnetic moment with each ion and introduce linear combinations of sublattice magnetizations (in the notation of Ref. 14):

$$\begin{aligned}
M &= 4sm = \mu_1 + \mu_2 + \mu_3 + \mu_4, \\
L_1 &= 4sl_1 = \mu_1 - \mu_2 + \mu_3 - \mu_4, \\
L_2 &= 4sl_2 = \mu_1 + \mu_2 - \mu_3 - \mu_4, \\
L_3 &= 4sl_3 = \mu_1 - \mu_2 - \mu_3 + \mu_4,
\end{aligned}$$

which, respectively, represent the total magnetization and the three possible collinear types of AFM ordering: C, A, and G. A classification of the vectors with respect to irreducible representations of the group D_{2h}^{16} can be found in Refs. 14 and 15, for example.

Proceeding from symmetry considerations, we can write an invariant expansion of the Hamiltonian in irreducible spin operators of the magnetic group. We have

$$\begin{aligned}
\frac{1}{4M_0}\mathcal{H} = {} & -\frac{1}{2}H_{e2}\mathbf{l}_2^2 + \frac{1}{2}H_{e0}\mathbf{m}^2 + \frac{1}{2}H_{e1}\mathbf{l}_1^2 + \frac{1}{2}H_{e3}\mathbf{l}_3^2 \\
& + \frac{1}{2}\sum_i H_{ayi} l_{iy}^2 + \frac{1}{2}\sum_i H_{azi} l_{iz}^2 + H_{Dy}(m_x l_{1z} \\
& - m_z l_{1x}) + H_{Dz}(m_x l_{2y} - m_y l_{2x}) + H_{Dx}(m_y l_{3z} \\
& - m_z l_{3y}) - \mathbf{H}\cdot\mathbf{m},
\end{aligned} \tag{1}$$

where H_{ei} is the effective exchange interaction field, H_{ai} is the anisotropy field, H_D is the Dzyaloshinskii field, and H is the external magnetic field, $i = 1, 2, 3$.

It has been established experimentally[3,10] that in the absence of an external magnetic field the magnetic moments are directed along the **a** (x) axis. In accordance with the type-A AFM ordering this leads to a ground state characterized by vectors (m_y, l_{2x}, l_{3z}). By minimizing the magnetic energy in model (1), one can determine the ground-state vector:

$$l_{2x}\approx 1,\ \ m_y\approx\frac{H_{Dx}}{(H_{e2}+H_{e0})},$$
$$l_{3z}\approx\frac{-H_{Dx}H_{Dz}}{(H_{e2}+H_{e0})(H_{e3}+H_{e2})}. \tag{2}$$

In accordance with Refs. 3 and 10, the magnetic structure is a four-sublattice type-A structure with weak ferromagnetism $(m_y\sim H_D/H_e)$ and G-type antiferromagnetism. In view of the smallness of the components l_{3z} $(l_{3z}\sim(H_D/H_e)^2)$, the ground state obtained from symmetry considerations is in good agreement with experiment.[1,3,12,13]

2. Let us consider the case when the external magnetic field is directed along the **b** (y) axis, i.e., parallel to the weak ferromagnetic (FM) moment and perpendicular to the FM layers. Here the ground state is contained by the same set of principal vectors (l_{2x}, m_y, l_{3z}) as in the absence of external magnetic field, and their field dependence for $H\ll H_e$ is described by the expressions

$$l_{2x}\approx 1,\ \ m_y\approx\frac{H_{Dz}+H_y}{(H_{e2}+H_{e0})},$$
$$l_{3z}\approx\frac{-H_{Dx}(H_{Dz}+H_y)}{(H_{e2}+H_{e0})(H_{e3}+H_{e2})}. \tag{3}$$

With increasing external magnetic field the magnetic moments rotate smoothly along along the field.

The dynamic properties of the system are described by the Landau–Lifshitz equations for the irreducible vectors.[16] Linearizing them, we find the eigenfrequencies of the magnetic excitations of four-sublattice $LaMnO_3$ in an external magnetic field parallel to the axis of weak ferromagnetism. With accuracy to terms of order H_D^2 we have

$$\omega_{\mathrm{ak1}}^2\gamma^{-2}\approx(H_{e0}+H_{e2})H_{a2y}+H_y(H_{Dz}+H_y);$$
$$\omega_{\mathrm{ak2}}^2\gamma^{-2}\approx(H_{e0}+H_{e2})(H_{a2z}+H_{Dz}m_y); \tag{4}$$
$$\omega_{\mathrm{opt1}}^2\gamma^{-2}\approx[(H_{e1}+H_{e2}+H_{a1z}+H_{Dz}m_y)(H_{e3}+H_{e2}+H_{a3y}+H_{Dz}m_y)+m_y^2(H_{e1}+H_{e2})^2];$$
$$\omega_{\mathrm{opt2}}^2\gamma^{-2}\approx[(H_{e1}+H_{e2}+H_{a1y}+H_{Dz}m_y)(H_{e3}+H_{e2}+H_{a3z}+H_{Dz}m_y)+m_y^2(H_{e3}+H_{e2})^2].$$

In accordance with the accepted classification (see, e.g., Ref. 17), two of the AFMR frequencies are acoustic $(\omega_{\mathrm{ak1}}, \omega_{ak2})$ and the other two $(\omega_{\mathrm{opt1}}, \omega_{\mathrm{opt2}})$ are exchange modes. We note that the frequencies ω_{ak1} and ω_{opt1} are excited by a magnetic field parallel to the axes of weak magnetization and weak ferromagnetism ($\mathbf{H}\|\mathbf{a}$ (x axis) and $\mathbf{H}\|\mathbf{b}$ (y axis)), and the frequencies ω_{ak2} and ω_{opt2} by a field perpendicular to these two axes [$\mathbf{H}\|\mathbf{c}$ (z axis)].

For a quantitative description of the resonance properties we adopt the following values for the parameters of the spin Hamiltonian:[4] $H_{ei}\approx H_e=33.9$ T, $H_{ai}\approx H_a=5.3$ T, $H_{Dx}\approx H_{Dy}\approx H_{Dz}\approx H_D=0.2$ T. Using these constants of the Hamiltonian, we constructed the dependence of the AFMR frequencies on an external magnetic field directed along the axis of weak ferromagnetism. The results are presented in Fig. 1. The two lower branches are acoustic frequencies, and the upper curve shows the dependence on the external magnetic field for the two optical branches, which coincide with each other in the approximation used for the parameters of the Hamiltonian.

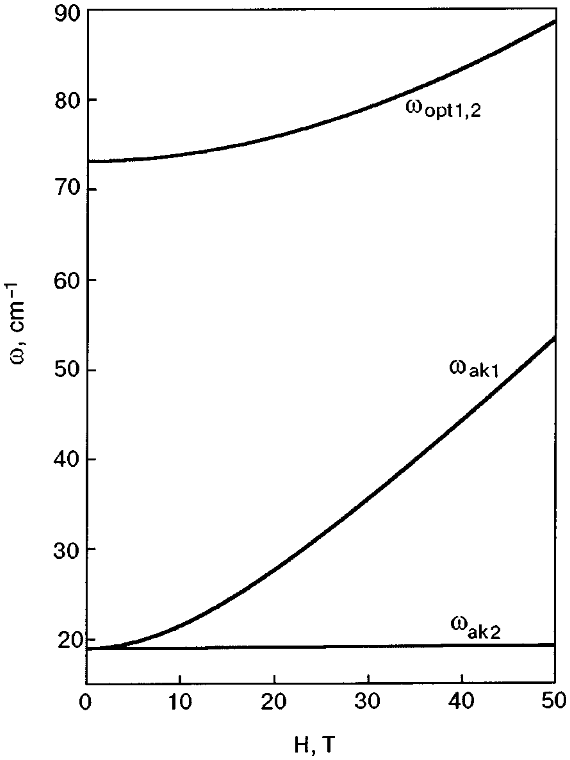

FIG. 1. Frequency–field diagram of $LaMnO_3$ in an external magnetic field along the axis of weak ferromagnetism.

3. A more complex ground state is obtained in the case when the external magnetic field is directed along the easy axis **a** of the crystal (the x axis). Now the field induces a component of the ferromagnetism vector parallel to the field direction. As a result, the ground state of the crystal is characterized by a set of six principal vectors $(m_y, l_{2x}, l_{3z}, l_{2y}, m_x, l_{1z})$. Minimization of the magnetic energy gives the following values for the ground-state vectors:

$$l_{2x}\approx 1,\ \ m_y\approx\frac{H_{Dz}H_{a2y}}{H_{a2y}(H_{e2}+H_{e0})-H_x^2};$$
$$l_{3z}\approx\frac{-H_{Dx}H_{Dz}H_{a2y}}{[H_{a2y}(H_{e2}+H_{e0})-H_x^2](H_{e3}+H_{e2})};$$
$$l_{2y}\approx\frac{-H_{Dz}H_x}{H_{a2y}(H_{e2}+H_{e0})-H_x^2};$$
$$m_x\approx\frac{-H_xH_{Dz}^2}{[H_{a2y}(H_{e2}+H_{e0})-H_x^2](H_{e0}+H_{e2})};$$
$$l_{1z}\approx\frac{-H_xH_{Dz}^2H_{Dy}}{[H_{a2y}(H_{e2}+H_{e0})-H_x^2](H_{e1}+H_{e2})(H_{e3}+H_{e2})}. \tag{5}$$

The moduli of the ground-state vectors satisfy the relations $l_{2x}\gg m_y\gg l_{3z}$ and $l_{2y}\gg m_x\gg l_{1z}$. The components of the ground-state vectors (5) remain practically unchanged up to a certain critical field H_{sf}, at which the magnetic sublattices topple over to an orientation perpendicular to the magnetic field—the so-called spin-flop transition. The field $H_C > H_{sf}$ at which the antiferromagnetic phase becomes absolutely unstable is given by the expression

$$H_C = \frac{1}{2}\left[H_{Dz} + \sqrt{H_{Dz}^2 + 4(H_{e0} + H_{e1})H_{a2y}}\right]. \qquad (6)$$

A numerical analysis of the behavior of the ground-state vectors (5) in an external magnetic field shows that the principal antiferromagnetic vector $\mathbf{l}_2$ is directed along the x axis up to fields close to the spin-flop transition. In the vicinity of the first-order transition the component $l_{2x} \to 0$ and the principal antiferromagnetic vector is reoriented in the direction of the y axis $(l_{2y} \to 1)$. In the field H_C one of the acoustic frequencies should go to zero (see below).

The substantially noncollinear magnetic structure described by the six components of the irreducible vectors (5) leads to nontrivial dynamics of the system, in which all four branches of the AFMR are coupled and are excited by an alternating magnetic field along all the principal directions in the crystal. The expressions for the AFMR frequencies in this case have the form

$$\omega_{\text{ak1}}^2 \gamma^{-2} \approx [(H_{e0} + H_{e2})H_{a2y} + H_x^2](1 - l_{2y}^2);$$

$$\omega_{\text{ak2}}^2 \gamma^{-2} \approx (H_{e1} + H_{e0})H_{a2z} + H_x^2 + H_{Dz}^2(1 + l_{2y}^2);$$

$$\begin{aligned}\omega_{\text{opt1}}^2 \gamma^{-2} \approx [&(H_{e1} + H_{e2} + H_{a1z})(H_{e3} + H_{e2} + H_{a3y}) \\ &+ H_x^2 + (H_{e1} + H_{e2} - H_{a2y} + H_{a1z})(H_{e3} + H_{e2} \\ &- H_{a2y})l_{2y}^2]; \qquad (7)\end{aligned}$$

$$\begin{aligned}\omega_{\text{opt2}}^2 \gamma^{-2} \approx [&(H_{e1} + H_{e2} + H_{a1y})(H_{e3} + H_{e2} + H_{a3z}) \\ &+ H_x^2 + (H_{e1} + H_{e2} - H_{a2y})(H_{e3} + H_{e2} - H_{a2y} \\ &+ H_{a3z})I_{2y}^2].\end{aligned}$$

We see from expressions (5) and (6) that for $H \to H_C$ the component $l_{2y} \to 1$, and the magnetic eigenmode frequency ω_{ak1} (7) goes to zero. Using the same values of the parameters of the system as were used in constructing Fig. 1, we constructed the dependence of the AFMR frequencies of LaMnO_3 on an external magnetic field parallel to the easy axis of the crystal (see Fig. 2). The upper curve is the frequency–field dependence of two nearby optical branches [see Eq. (7)], and the two lower branches reflect the behavior of acoustic frequencies as a function of an external magnetic field along the easy axis of the crystal. As can be seen in this figure, as the field approaches the value H_C a sharp decrease in the mode frequency ω_{ak1} is observed, due to the approach to the boundary of absolute instability of the AFM phase.

The main result of the foregoing analysis is that a loss of stability of the AFM phase $(\omega_{\text{ak1}} \to 0)$ does not occur if the Dzyaloshinskii interaction is neglected. In that case the AFMR frequency increases monotonically with increasing external magnetic field, and the features characteristic for the spin-flop transition are not reflected in the frequency–field diagram. Thus, neglect of the Dzyaloshinskii interaction, which some authors argue is justified by the fact that the constants of the spin Hamiltonian are small compared to the anisotropy constants, may lead to incorrect results in an analysis of the dynamics of lanthanum manganite.

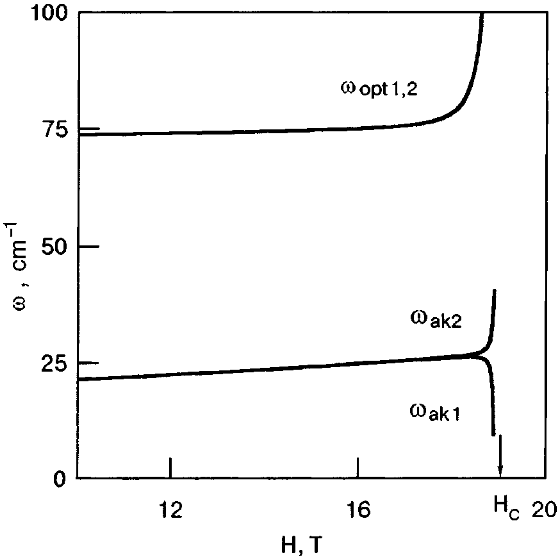

FIG. 2. Dependence of the resonance frequencies of four-sublattice lanthanum manganite on an external magnetic field along the easy axis of the crystal. The arrow indicates the field value $H_C = 19$ T.

The authors thank Yu. G. Pashkevich for a helpful discussion of this study.

*E-mail: krivoruc@host.dipt.donetsk.ua

---

[1] E. O. Wollan and W. C. Koehler, Phys. Rev. **100**, 545 (1955).
[2] J. B. Goodenough, Phys. Rev. **100**, 564 (1955).
[3] G. Matsumoto, J. Phys. Soc. Jpn. **29**, 606 (1970).
[4] V. Yu. Ivanov, V. D. Travkin, A. A. Mukhin, S. P. Lebedev, and A. A. Volkov, J. Appl. Phys. **83**, 7180 (1998).
[5] S. Mitsudo, K. Hirano, H. Nogiri, M. Motokawa, K. Hirota, A. Nishizawa, N. Kaneko, and Y. Endoh, J. Magn. Magn. Mater. **177–181**, 877 (1998).
[6] A. Pimenov, M. Biberacher, D. Ivannikov, A. Loidl, V. Yu. Ivanov, A. A. Mukhin, and A. M. Balbashov, Phys. Rev. **69**, 5685 (2000).
[7] L. E. Gonchar', A. E. Nikiforov, and S. E. Popov, Zh. Éksp. Teor. Fiz. **118**, 1411 (2000) [JETP **91**, 1221 (2000)].
[8] L. E. Gonchar', A. E. Nikiforov, S. E. Popov, and Yu. V. Leskova, Fiz. Tverd. Tela (St. Petersburg) **42**, 1038 (2000) [Phys. Solid State **42**, 1070 (2000)].
[9] A. M. Balbashov, M. K. Gubkin, V. V. Kireev, O. K. Mel'nikov, T. M. Perkalina, S. V. Pushko, L. E. Svistov, and A. Ya. Shapiro, Zh. Éksp. Teor. Fiz. **117**, 542 (2000) [JETP **90**, 474 (2000)].
[10] F. Moussa, M. Hennion, J. Rodriguez-Carvajal, and H. Moudden, Phys. Rev. B **54**, 15149 (1996).
[11] I. Solovyov, N. Hamada, and K. Terakura, Phys. Rev. Lett. **76**, 4825 (1996).
[12] É. L. Nagaev, Usp. Fiz. Nauk **166**, 833 (1996).
[13] V. M. Loktev and Yu. G. Pogorelov, Fiz. Nizk. Temp. **26**, 231 (2000) [Low Temp. Phys. **26**, 171 (2000)].
[14] Fan Zhong and Z. D. Wang, Phys. Rev. B **60**, 11883 (1999).
[15] E. A. Turov, *Physical Properties of Magnetically Ordered Crystals*, Academic Press, New York (1964), Izd. Akad. Nauk SSSR, Moscow (1963).
[16] V. G. Bar'yakhtar, I. M. Vitebskiĭ, and D. A. Yablonskiĭ, Zh. Éksp. Teor. Fiz. **76**, 1381 (1979) [Sov. Phys. JETP **49**, 703 (1979)].
[17] A. I. Zvyagin, M. I. Kobets, V. N. Krivoruchko, A. A. Stepanov, and D. A. Yablonskiĭ, Zh. Éksp. Teor. Fiz. **89**, 2298 (1985) [Sov. Phys. JETP **62**, 1328 (1985)].

Translated by Steve Torstveit

Anisotropy of the magnetoresistance in the case of trapping of magnetic fields in granular bismuth-containing high-T_c superconductors

A. A. Sukhanov* and V. I. Omelchenko

Institute of Radio Engineering and Electronics, Russian Academy of Sciences, pl. Vvedenskogo d. 1, 141190 Fryazino, Moscow District, Russia

(Submitted September 3, 2002)
Fiz. Nizk. Temp. **29**, 396–399 (April 2003)

A study is made of the features of the magnetoresistance in ceramic Bi(Pb)-HTSCs containing trapped magnetic fields. It is found that upon trapping of magnetic flux in these granular HTSCs their magnetoresistance becomes anisotropic. For magnetic fields **H** parallel to the field $\mathbf{H}_i$ that has initiated the trapping and for currents perpendicular to $\mathbf{H}_i$, the field dependence of the magnetoresistance $\Delta R(H)$ is nonmonotonic, and the magnetoresistance at low magnetic fields $H<H_{\text{inv}}$ is negative. The influence on $\Delta R(H)$ of the values and orientation of the trapped field and the transport current is investigated. In particular, it is found that the field H_{inv} at which inversion of the sign of the magnetoresistance occurs increases in a practically linear manner with increasing effective trapped magnetic fields, decreases to zero as the angle between the directions of the fields **H** and $\mathbf{H}_i$ increases to $\pi/2$, and decreases weakly with increasing transport current. The results are explained in the framework of a model of magnetic flux trapping in superconducting granules or superconducting ‘‘rings’’ embedded in a matrix of weak links. © *2003 American Institute of Physics.* [DOI: 10.1063/1.1542471]

1. INTRODUCTION

Magnetic flux trapping affects not only the magnetic properties of a high-T_c superconductor (HTSC), altering, for example, the characteristics of the penetration and screening of the magnetic field, the magnetic susceptibility, and the magnetic moment,[1,2] but also the transport properties, giving rise, in particular, to an excess (frozen) resistance in the region of the resistive superconducting transition.[3,4] Therefore, the study of the properties of HTSCs with trapped magnetic fields not only holds independent interest but can also provide useful information about the nature of the magnetic flux trapping in granular HTSCs, in particular.

In the present study we have investigated the magnetoresistance in granular Bi-HTSCs with trapped magnetic fields and have for the first time observed a negative magnetoresistance effect in such systems.

2. EXPERIMENT

We have investigated samples of ceramic HTSCs of nominal composition $Pb_{0.5}Bi_2Sr_3Ca_4Cu_5O_{16}$ with a temperature of the start of the transition to the superconducting state $T_c=107-110$ K and a width of the resistive transition $\Delta T_c \approx 8-12$ K.

The value of ΔT_c of the ceramics studied depends strongly on the current and magnetic field, increasing to 20–30 K at a current density $j=0.1$ A/cm^2 and field $H=20$ Oe.

The width of the resistive transition also increases substantially as a result of magnetic flux trapping and the appearance of an additional resistance—the so-called frozen magnetoresistance. The value of the frozen magnetoresistance here reaches the values of the magnetoresistance in magnetic fields $H=20-30$ Oe. At the same time, the average trapped magnetic fields measured by Hall sensors is less than 0.1 Oe. This means that in the temperature region near T_c the trapped fields are highly nonuniform and sign-varying.[4]

After the trapping of a magnetic flux, which was usually initiated by a field pulse with a duration of 30 s and a height of $H_i=30-200$ Oe, we measured the field dependence of the magnetoresistance for different values and mutual orientations of the static field H, the initiating field H_i, and the transport current J.

3. RESULTS

It was found that, despite the absence of average trapped magnetic fields, the magnetoresistance of the ceramics becomes highly anisotropic after the trapping of a magnetic flux.

In the case $\mathbf{H}\parallel\mathbf{H}_i\perp\mathbf{J}$ the field dependence of the magnetoresistance $\Delta R(H)=R(H)-R(0)$ of granular HTSC samples containing trapped magnetic fields turns out to be nonmonotonic: the value of ΔR is negative at low fields $H<H_{\text{inv}}$ and changes to positive at $H>H_{\text{inv}}$.

Figure 1 shows the normalized field dependence of the magnetoresistance for $\mathbf{H}\parallel\mathbf{H}_i$, measured for different values of the pulsed field H_i which initiates trapping. It is seen that the negative magnetoresistance effect become more pronounced as the initiating field and, hence, the trapped magnetic field increase.

In the region of the resistive transition of granular HTSCs the magnetic fields trapped in the superconducting regions are closed through the normal regions of the HTSC. As a result of this, they are sign-varying in the plane of the sample. These sign-varying trapped fields can be characterized by their effective value $H_{t\,\text{eff}}$, which is equal to the

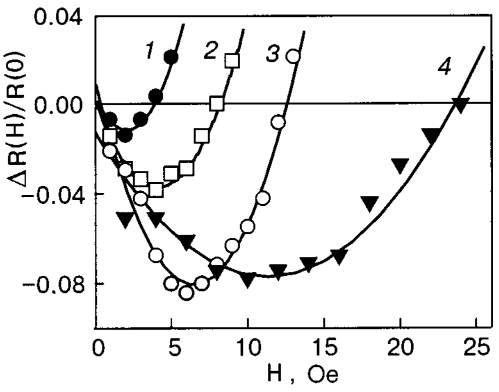

FIG. 1. Normalized field dependence of the magnetoresistance at $T=77.4$ K for different initiating fields H_i [Oe]: 80 (*1*), 100 (*2*), 130 (*3*), 200 (*4*).

external magnetic field that would lead to the same resistance as the trapped field.[4]

It was found that the field H_{inv} at which the inversion of the sign of the magnetoresistance occurs is a practically linear increasing function of the effective value of the trapped magnetic field $H_{t\,\mathrm{eff}}$ (Fig. 2). With increasing $H_{t\,\mathrm{eff}}$ the minimum on the $\Delta R(H)$ curve is shifted to higher fields and becomes deeper.

The field curves of the magnetoresistance of Bi(Pb) ceramics, measured for different orientations of the static field **H** relative to the pulsed field $\mathbf{H}_i$ initiating the trapping, are shown in Fig. 3.

It is important that the field H_{inv} at which inversion of the sign of the magnetoresistance occurs and the maximum absolute value of the negative magnetoresistance decrease with increasing angle α between the directions of the fields **H** and $\mathbf{H}_i$, and the negative magnetoresistance effect vanishes for $\alpha \rightarrow \pi/2$.

Figure 4 shows the angular dependence of the magnetoresistance for magnetic fields of different magnitude H. It is seen that increasing H leads to a decrease of the critical angle at which the magnetoresistance changes sign.

We note that negative magnetoresistance is absent for $\mathbf{H} \| \mathbf{H}_i \| \mathbf{J}$.

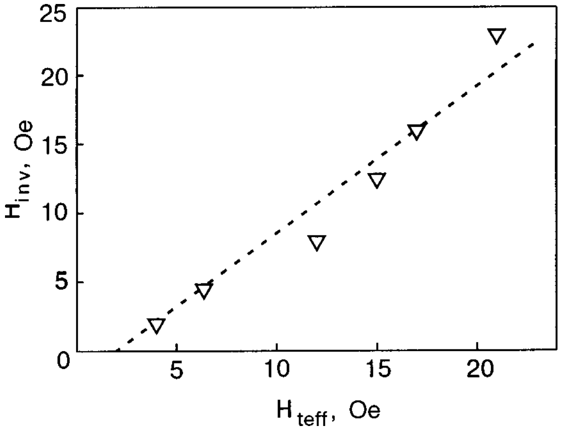

FIG. 2. Field at which the magnetoresistance changes sign versus the effective value of the trapped field.

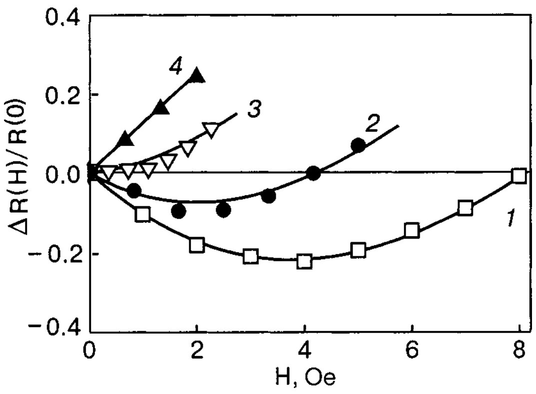

FIG. 3. Normalized field dependence of the magnetoresistance of a HTSC ceramic with trapped magnetic fields for different angles α between the field **H** and the initiating field $\mathbf{H}_i$ ($T=77.4$ K): $\alpha=0$ (*1*), $\pi/4$ (*2*), $\pi/2$ (*3*), π (*4*).

The field H_{inv} at which inversion of the sign of the magnetoresistance occurs and the maximum absolute value of the negative magnetoresistance decrease weakly with increasing transport current (by approximately 15% for $j=0.3$ A/cm^2).

We emphasize the following:

1) Because the magnetoresistance measurements were made using comparatively low fields, $H<H_i$, which had practically no effect on the trapped magnetic fields, the results were reproducible and the functions $R(H,\alpha)$ invertible.

2) We also observed the negative magnetoresistance effect in magnetron films of Bi-HTSC, and it appears to be a characteristic property of all granular HTSCs.

4. DISCUSSION

It is well known that HTSC ceramics have a highly nonuniform granular structure in which the individual superconducting granules are connected by weak links. The concept of such a system as a Josephson medium with a wide scatter of the parameters of the weak links is now generally accepted.[5]

The resistive properties of such a medium are determined by the weak links of the conducting channels; in particular, the magnetoresistance is due to the destruction of the superconductivity of the weak links by the external magnetic field.

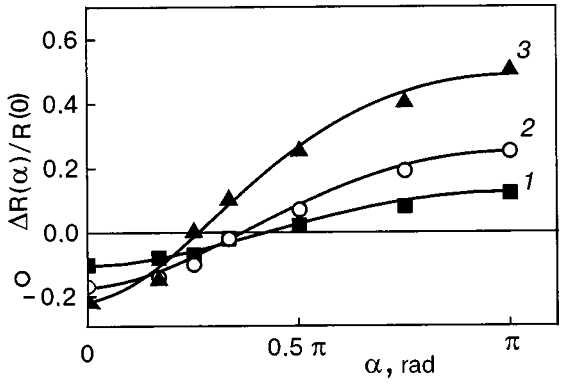

FIG. 4. Normalized angular dependence of the magnetoresistance of a HTSC sample with trapped magnetic fields for $H_{t\,\mathrm{eff}}=6$ Oe and $T=77.4$ K for different fields H [Oe]: 1 (*1*), 2 (*2*), 4 (*3*).

The trapping of magnetic flux in the resistive state of such a Josephson medium occurs in the grains (granules) or in the closed superconducting loops made up of the granules and the weak links between them. The local trapped magnetic fields that arise in this case are highly nonuniform and sign-varying,[4] and so they cannot be observed by the usual methods (Hall sensors, Josephson interferometers). At the same time, these sign-varying trapped magnetic fields destroy the superconductivity of the weak links of the conducting channels and thus give rise to the well-known frozen magnetoresistance effect.

Near the weak links of the current channels the trapped fields are mainly directed counter to the fields in the trapping regions (granules, loops) and are consequently antiparallel to the field $\mathbf{H}_i$ that initiates the trapping. Therefore, the application of an external field $\mathbf{H}\|\mathbf{H}_i$ leads, on the one hand, to a decrease of the local resultant magnetic fields $H_r=|\mathbf{H}_t-\mathbf{H}|$ in the regions with strong trapped fields H_t ($H_r=H_t-H$ for $H_t>H$) and, on the other, to an increase of H_r in regions with weak trapped fields ($H_r=H-H_t$ for $H_t<H$). With increasing H the first factor leads to a transition of the weak links having critical fields $H_c>H_t-H$ to the superconducting state, while the second factor causes a transition of the weak links with $H_c<H-H_t$ to the normal state.

When the effective trapped fields are large, the first is the determining factor at low fields H, and it leads to a drop in the resistance of the network of weak links and to the onset of negative magnetoresistance, while at high fields H the second factor becomes dominant and leads to an increase in resistance and to a change in sign of the magnetoresistance at $H\sim H_{t\,\mathrm{eff}}$. The combination of these two tendencies for $\mathbf{H}\|\mathbf{H}_i$, in accordance with the experimental results, leads to the appearance of negative magnetoresistance and to a nonmonotonic field dependence of the magnetoresistance.

The arguments given above are confirmed by a model calculation. Indeed, it is clear that the resistance of the current channels is determined by the distribution function of the weak links with respect to critical fields, $g(H_c)$, and by the distribution function of the trapped fields near the weak links, $f(H_t)$. Since the weak links pass into the normal state when their critical fields H_c become less than the local resultant fields $H_r=|\mathbf{H}_t-\mathbf{H}|$ ($\mathbf{J}\perp\mathbf{H}$ and $\mathbf{J}\perp\mathbf{H}_t$), we write the magnetoresistance of the medium in the form

$$\Delta R(H)=R(H)-R(0), \tag{1}$$

where

$$R(H)=\int_0^{H_i} f(H_t)\int_0^{H_r} g(H_c)\,dH_c\,dH_t\,.$$

For comparison with the experimental data in a numerical calculation we used a normal distribution of weak links over critical fields and an exponential distribution of the trapped fields:

$$g(H_c)\sim\exp\left[-\left(\frac{H_c-H_{cm}}{\sqrt{2}\Delta H_c}\right)^2\right],$$

$$f(H_t)\sim\exp\left(-\frac{H_t}{H_{t\,\mathrm{eff}}}\right),$$

where H_{cm} is the mean critical field, and ΔH_c is the halfwidth of the distribution function.

The solid curves in Figs. 3 and 4 show the results of a model calculation of the field dependence and angular dependence of the magnetoresistance of a sample containing trapped magnetic fields with the use of Eq. (1). The parameter values used, $H_{t\,\mathrm{eff}}=6.1$ Oe, $H_{cm}=5$ Oe, and $\Delta H_c=4$ Oe, were close to those found from measurements of the frozen magnetoresistance and the field dependence of the magnetoresistance in the absence of trapped magnetic fields.

The results of the calculation are in reasonable agreement with the experimental data.

Thus we have found that magnetic flux trapping in granular HTSCs leads to anisotropy and nonmonotonic field and angular dependence of the magnetoresistance. These results can be explained consistently in a Josephson medium model in which the magnetic flux trapping occurs in granules or superconducting loops, and the trapped magnetic fields are highly nonuniform and sign-varying.

*E-mail: sukh@ms.ire.rssi.ru

---

[1] D. M. Ginsberg (Ed.), *Physical Properties of High Temperature Superconductors*, Vols. 1–4, World Scientific, Singapore-Teaneck, NJ (1989, 1990, 1992, 1994), Mir, Moscow (1990).

[2] K. A. Muller, M. Takashige, and J. G. Bednorz, Phys. Rev. Lett. **58**, 1143 (1987).

[3] K. Y. Chen and Y. J. Qian, Physica C **159**, 131 (1989).

[4] A. A. Sukhanov and V. I. Omel'chenko, Fiz. Nizk. Temp. **27**, 826 (2001) [Low Temp. Phys. **27**, 609 (2001)].

[5] E. Z. Meĭlikhov, Usp. Fiz. Nauk **163**, 27 (1993) [Phys. Usp. **36**, 129 (1993)].

Translated by Steve Torstveit

LOW TEMPERATURE PHYSICS VOLUME 29, NUMBER 4 APRIL 2003

Anisotropy of the hopping magnetoresistance of antiferromagnetic $La_2CuO_{4+\delta}$ single crystals

B. I. Belevtsev,* N. V. Dalakova, A. S. Panfilov, and I. S. Braude

B. Verkin Institute for Low Temperature Physics and Engineering, National Academy of Sciences of Ukraine, pr. Lenina 47, 61103 Kharkov, Ukraine

A. V. Bondarenko

V. N. Karazin Kharkov National University, pl. Svobody 4, 61077 Kharkov, Ukraine

(Submitted October 4, 2002)
Fiz. Nizk. Temp. **29**, 400–405 (April 2002)

The anisotropy of the hopping conductivity of antiferromagnetic $La_2CuO_{4+\delta}$ single crystals with $T_N \approx 188$ K is investigated in the temperature range 5–295 K and the anisotropy of their magnetoresistance, in the temperature range 5–55 K. The resistance is measured by the Montgomery method for different combinations of directions of the transport current and magnetic field relative to the crystallographic axes. For the case when the field and transport current are directed parallel to the CuO_2 layers, a transition from negative to positive magnetoresistance is observed when the temperature is raised to $T \approx 20$ K. For fields perpendicular to the CuO_2 layers, only negative magnetoresistance is observed. The nature of the positive magnetoresistance is discussed. It is shown that the effect is most likely due not to the interaction of the spin of the charge carriers with the surrounding magnetic medium but to the orbital motion of these carriers. The corresponding values of the positive magnetoresistance and its behavior as a function of magnetic field and temperature are found using the well-known model of Shklovskii and Efros, which is based on taking into account the compression of the impurity wave functions of the charge carriers in the magnetic field. © *2003 American Institute of Physics.* [DOI: 10.1063/1.1542472]

1. INTRODUCTION

The unique magnetic and conducting properties of $La_2CuO_{4+\delta}$ oxides with an excess of oxygen have been attracting considerable attention in the last 15 years, since the discovery of high-temperature superconductivity in perovskite copper oxides. The stoichiometric oxide La_2CuO_4 ($\delta = 0$) is an antiferromagnetic (AF) insulator with a Néel temperature T_N of around 300–320 K.[1–3] Saturation with excess oxygen ($\delta > 0$) gives rise to charge carriers (oxygen holes) and leads to suppression of the AF order (lowering of T_N). At a sufficiently high value of δ (>0.05) the system becomes a metal and, below 35–40 K, a superconductor. The crystal lattice of $La_2CuO_{4+\delta}$ belongs to the family of layered perovskite lattices. For $T < 530$ K the lattice is orthorhombic. In the symmetry group $Bmab$ the **c** axis is perpendicular to the CuO_2 layers, while the **a** and **b** axes are parallel to them.[3] The excess oxygen is found in the interstices between CuO_2 layers. The conductivity of the system is governed by holes in the CuO_2 layers, and the magnetic state is determined by the spin of the copper ions Cu^{2+} ($S = 1/2$). At a sufficiently low value of δ (i.e., in the insulating state) antiferromagnetic ordering is observed within the CuO_2 layers. The magnetic interaction between layers is extremely weak. It has been established that all of the spins in the CuO_2 layers are rotated by a small angle from the plane of the layer ($\approx 0.17°$).[1] The CuO_2 layers therefore have small ferromagnetic moments, which undergo AF ordering in the direction perpendicular to the layers for $T < T_N$ (Ref. 1).

For layered perovskite compounds one might expect: 1) quasi-two-dimensional behavior of the conductivity (including the hopping conductivity); 2) substantial anisotropy of the conductivity for directions perpendicular to and parallel to the CuO_2 planes. The first of these expectations is not confirmed by experiment. It has been found[4,5] that for insulating $La_2CuO_{4+\delta}$ crystals at sufficiently low temperatures the resistance has a temperature dependence of the form

$$R(T) \propto \exp[(T_0/T)^{1/4}], \tag{1}$$

corresponding to the case of three-dimensional hopping conductivity with a variable hopping length (VHLC). This means that the charge carriers execute hops not only within the CuO_2 layers but also between them. In addition, a significant anisotropy of the hopping conductivity has been observed in high-quality samples:[2,6] the conductivity σ_{ab} in the direction parallel to the CuO_2 layers is one to two orders of magnitude higher than the conductivity σ_c in the direction perpendicular to the layers.

The known studies of the magnetoresistance of $La_2CuO_{4+\delta}$ in the hopping conductivity regime cannot be considered exhaustive.[1,7,8] A positive magnetoresistance should be expected for VHLC.[9] However, only negative magnetoresistance has been observed for $La_2CuO_{4+\delta}$. The case when the magnetic field **H** and transport current **J** are perpendicular to the CuO_2 layers (i.e., $\mathbf{H}\parallel\mathbf{c}$ and $\mathbf{J}\parallel\mathbf{c}$) has been studied in detail. Under such conditions one observes a rather sharp decrease of the resistance in the vicinity of certain characteristic fields H_c, which depend on the temperature.[1,7,8] For fields far from the value H_c the magnetoresistance is negligible (for $H \ll H_c$) or has a quite large constant value (for $H \gg H_c$). The value of H_c is maximum (around 50 kOe) for $T \to 0$. With increasing temperature the value of H_c decreases, and the decrease is especially rapid near T_N. This effect is absent above T_N. All of this indicates that the magnetoresistive effect in this case is due to changes of the magnetic state of $La_2CuO_{4+\delta}$ under the influence of the external field. Indeed, it has been shown[1,10] that a sufficiently high magnetic field leads to a transition of $La_2CuO_{4+\delta}$ from the AF to a weak ferromagnetic (WF) state, in which the ferromagnetic moments of the CuO_2 layers are parallel. Possible magnetoresistance models involving this transition are considered in Refs. 7 and 10.

The information available on the behavior of the magnetoresistance for other combinations of magnetic-field and transport-current directions is extremely spotty and often contradictory. It was found in Ref. 1 that the magnetoresistance is close to zero for fields parallel to the CuO_2 layers (i.e., for $\mathbf{H} \perp \mathbf{c}$) for $T > 20$ K (for transport currents both parallel and perpendicular to the CuO_2 layers). At the same time, in Ref. 7 a rather significant negative magnetoresistance was observed for $\mathbf{H} \perp \mathbf{c}$ (for currents perpendicular to the CuO_2 layers), which can be attributed to a spin-flop (SF) transition at sufficiently high fields ($H > 100$ kOe).[7,10] Since the spin-flop transition that occurs with increasing field parallel to the CuO_2 layers is continuous (with no jump in magnetoresistance at the transition), it can have a noticeable influence on the magnetoresistance even in fields below 50 kOe.[7] We note that in the published studies known to us only a negative magnetoresistance is observed, and only spin mechanisms of hopping magnetoresistance have been invoked to explain it.[10] On the whole it can be stated that the features and mechanisms of the magnetoresistance in $La_2CuO_{4+\delta}$ crystals in the hopping conductivity region have not been studied in sufficient detail, and it therefore seems that further studies are urgently needed.

In this paper we present the results of a study of the anisotropy of the hopping conductivity and magnetoresistance of $La_2CuO_{4+\delta}$ single crystals. The samples were antiferromagnetic, with $T_N \approx 188$ K. The conductivity in zero magnetic field was measured in the interval 5–295 K, and the magnetoresistance was measured in the interval 5–55 K. The magnetoresistance was measured for different combinations of directions of the magnetic field and transport current relative to the principal crystallographic axes. For the case when both the field and the transport current are directed parallel to the CuO_2 layers, one observes a transition from negative to positive magnetoresistance with increasing temperature. For fields perpendicular to the CuO_2 layers one observes only negative magnetoresistance. We know of no previous published reports of positive magnetoresistance of $La_2CuO_{4+\delta}$ crystals in the AF state. These results suggest that this effect is due not to spin but to orbital processes (compression of the wave functions of the charge carriers in a magnetic field, in accordance with the model of Ref. 9).

2. SAMPLES AND EXPERIMENTAL TECHNIQUES

The initial material for preparing the samples was a $La_2CuO_{4+\delta}$ single crystal (with $T_N \approx 230$ K), the conducting properties of which are described in Ref. 5. Two samples in the form of parallelepipeds with dimensions of $1.3 \times 0.3 \times 0.39$ mm (sample No. 1) and $0.75 \times 0.3 \times 0.29$ mm (sample No. 2) were cut from it. The crystallographic orientation of the samples was determined by an x-ray method. The samples were subjected to a prolonged homogenizing anneal in an oxygen atmosphere (400 °C, 7 days). As a result of the annealing the oxygen content increased somewhat, so that the resistivity ρ of the samples decreased by approximately two orders of magnitude, and the Néel temperature T_N (determined from measurements of the temperature dependence of the magnetic susceptibility) decreased to 188 K. Here the samples remained in an insulating state and possessed hopping conductivity. Measurements showed that the two samples had essentially the same resistive and magnetoresistive characteristics. The resistivity was measured by the Montgomery method,[11] which permits a more reliable study of the anisotropy of the conductivity than does to usual four-contact method. Contacts between the measuring wires and samples were made using a conducting silver paste with a subsequent high-temperature annealing of the samples with the contacts. The following directions of the measuring current were used: $\mathbf{J} \| \mathbf{a}$ and $\mathbf{J} \| \mathbf{c}$ (sample No. 1) and $\mathbf{J} \| \mathbf{a}$ and $\mathbf{J} \| \mathbf{b}$ (sample No. 2). The magnetic fields were directed parallel to the $\mathbf{b}$ or $\mathbf{c}$ axis and always perpendicular to the current.

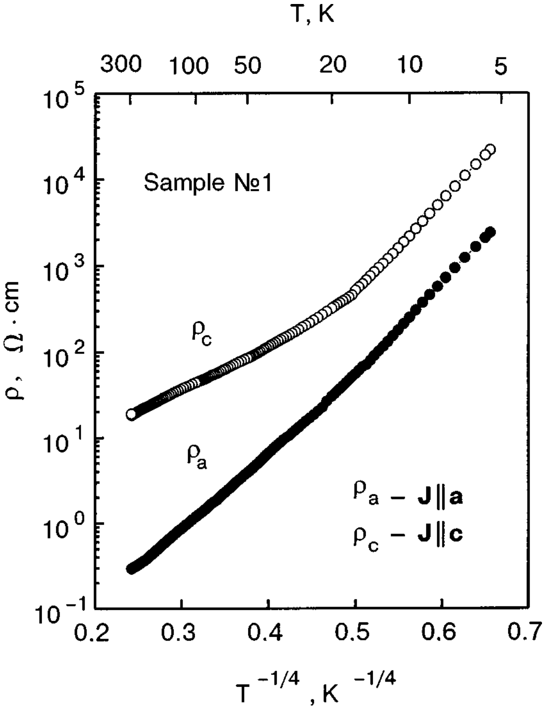

FIG. 1. Anisotropy of the hopping conductivity of the $La_2CuO_{4+\delta}$ crystal. The measurements of the resistivities ρ_a and ρ_c were done for directions of the measuring current (100 μA) along the crystallographic axes **a** and **c**.

3. RESULTS AND DISCUSSION

The temperature dependence $\rho(T)$ for sample No. 1 (under conditions such that Ohm's law holds) is shown in Fig. 1 for different directions of the measuring currents relative to the crystallographic axes. It is seen that Mott's law for VHLC, i.e., Eq. (1), holds for $T \geq 20$ K. No noticeable change in the behavior of $\rho(T)$ near the Néel temperature

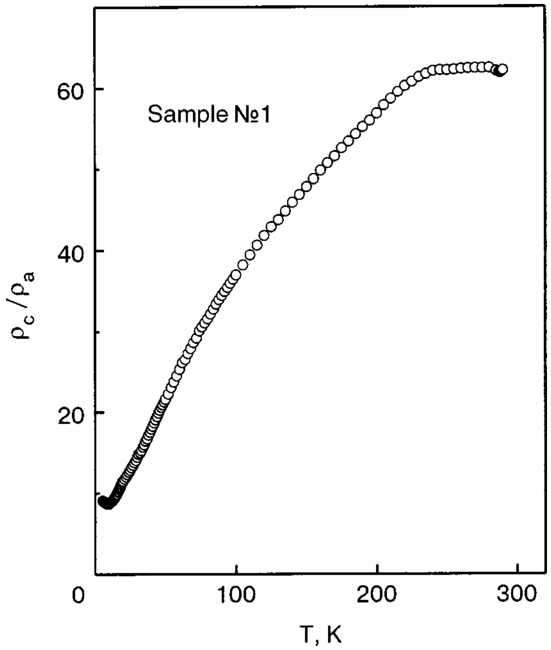

FIG. 2. Temperature dependence of the ratio of the resistivities ρ_a and ρ_c obtained for measuring currents directed along the crystallographic axes **a** and **c**.

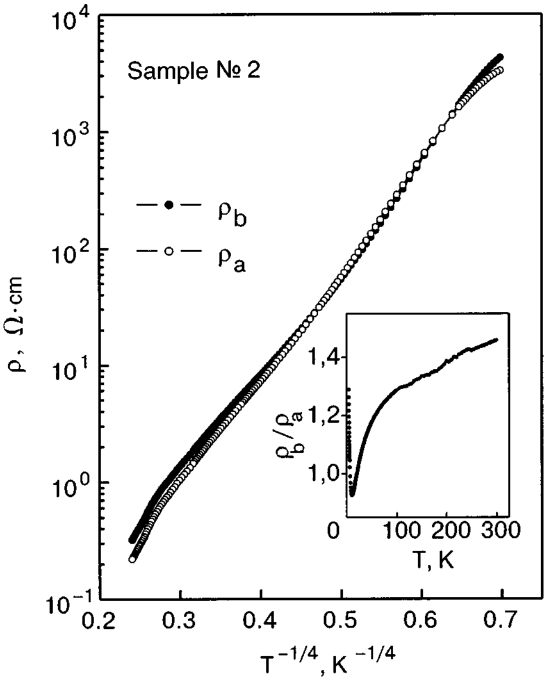

FIG. 3. Temperature dependence of the resistivities ρ_a and ρ_b measured along the crystallographic axes **a** and **b**, which lie in the CuO_2 planes. The inset shows the temperature dependence of the ratio of these resistivities.

(188 K) was observed. The $\rho(T)$ curves, as expected, are highly anisotropic, i.e., the values of ρ_c in the direction perpendicular to the CuO_2 layers is much greater than the value ρ_a in a direction parallel to these layers (Fig. 1). In the investigated temperature interval (5–295 K) the anisotropy of the resistivity is minimum in the region of helium temperatures, where $\rho_c/\rho_a \approx 10$ (Fig. 2). With increasing temperature the ratio ρ_c/ρ_a increases, reaching a value of ≈ 62 at $T \approx 20$ K. Further warming all the way up to room temperature did not lead to any substantial change in ρ_c/ρ_a (Fig. 2). The large values of ρ_c/ρ_a attest to the high crystalline perfection of the samples. In our studies we did not observe strong anisotropy of ρ in the crystal planes parallel to the CuO_2 layers (Fig. 3), primarily because of the unavoidable presence of twins in $La_2CuO_{4+\delta}$ crystals.

For $T < 20$ K we observed a deviation from Mott's law. This effect was investigated earlier[5] and has been attributed to the phenomenon of phase separation in $La_2CuO_{4+\delta}$ crystals.[12] At sufficiently low temperatures, phase separation leads to the presence of small superconducting inclusions in the insulating matrix. This causes a deviation from Mott's law and leads to a negative magnetoresistance which increases with decreasing temperature (see Ref. 5).

Measurements showed that not only the magnitude but even the sign of the magnetoresistance depend on the direction of the transport current relative to the CuO_2 layers. Figures 4–6 show data on the behavior of the magnetoresistance in fields parallel to the CuO_2 layers. In the case when the current is parallel to the CuO_2 layers one observes a transition from negative to positive magnetoresistance with increasing temperature. The transition occurs near $T \approx 18$ K (Fig. 5). At the same time, when the current is perpendicular to the CuO_2 layers one observes only negative magnetoresistance, the value of which increases monotonically with decreasing temperature (Fig. 6). In the case when both the current and field are perpendicular to the CuO_2 layers, one observes the expected behavior of the magnetoresistance, due to the AF–SF transition.[1,7,8]

The $R(H,T)$ curves shown in Figs. 4–6 demonstrate the dependence of the absolute value and sign of the magnetoresistance on the direction of the transport current for the same direction of the magnetic field (along the CuO_2 layers). These results are new. In particular, the positive magnetoresistance of $La_2CuO_{4+\delta}$ crystals in the VHLC regime has

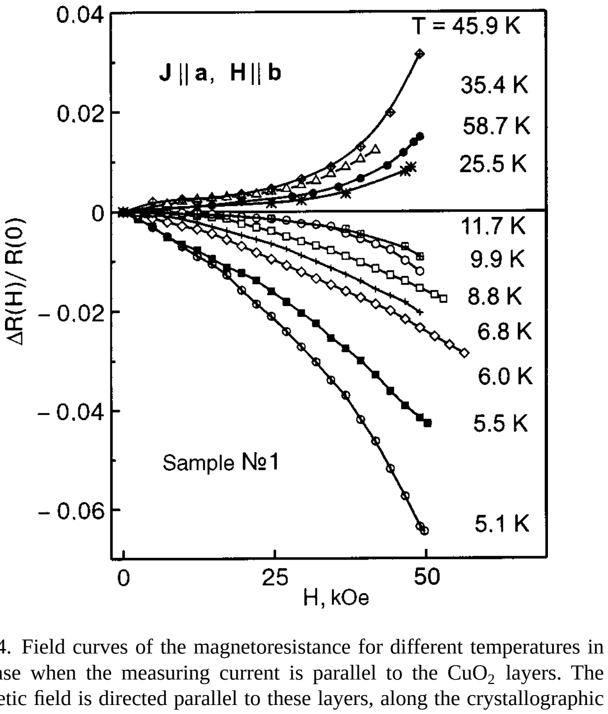

FIG. 4. Field curves of the magnetoresistance for different temperatures in the case when the measuring current is parallel to the CuO_2 layers. The magnetic field is directed parallel to these layers, along the crystallographic axis **b**.

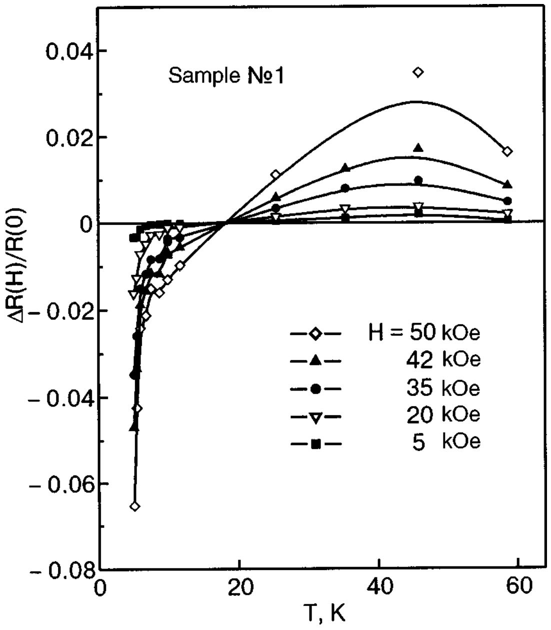

FIG. 5. Change in sign of the magnetoresistance upon an increase in temperature for the case of a measuring current parallel to the CuO_2 layers. The magnetic field is directed parallel to these layers, along the crystallographic axis **b**.

been observed for the first time. The curves in Fig. 4 reflect the competition of at least two mechanisms for the magnetoresistances of different sign. Below $T \approx 20$ K the predominant contribution is the negative magnetoresistance due to the phase separation effect inherent to $La_2CuO_{4+\delta}$, i.e., the separation of the system into regions enriched with and depleted of charge carriers (holes).[12] At a small value of δ the hole-enriched regions are of the nature of isolated metallic inclusions in an insulating matrix. At high temperatures the presence of these inclusions has a weak effect on the hopping conductivity of the system. The transition of these inclusions to the superconducting state leads to a deviation of the $\rho(T)$ curve from Mott's law (1) and to the appearance of a rather strong negative magnetoresistance (see the detailed discussion in Ref. 5).

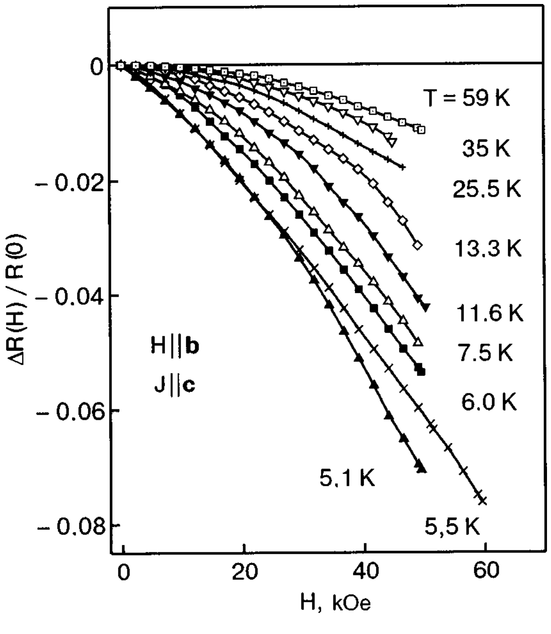

FIG. 6. Field dependence of the magnetoresistance at different temperatures in the case of a measuring current perpendicular to the CuO_2 layers. The magnetic field is directed parallel to these layers, along the crystallographic axis **b**.

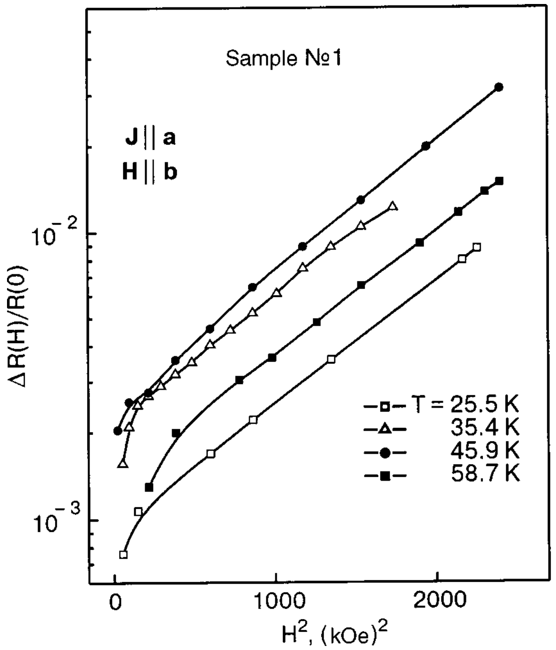

FIG. 7. Plot of $\ln[R(H)/R(0)]$ versus H^2 at different temperatures. The measuring current and magnetic field are parallel to the CuO_2 layers.

An extremely probable cause of the positive magnetoresistance in the case of VHLC is the mechanism[9] based on compression of the impurity wave functions in a magnetic field. For the case of a weak magnetic field ($L_H \gg L_c$, where $L_H=(\hbar/2H)^{1/2}$ is the magnetic length and L_c is the localization length) the value of the magnetoresistance according to this mechanism is given by the expression[9]

$$\ln\frac{R(H)}{R(0)}=t_1\left(\frac{L_c}{L_H}\right)^4\left(\frac{T_0}{T}\right)^{3/4}, \tag{2}$$

where $t_1=5/2016$, and T_0 is the quantity that appears in Eq. (1) for $R(T)$ in the case of VHLC. Analysis of the data has shown that this mechanism is in qualitative (and even semiquantitative) agreement with the experimental results. Indeed, we have found that the field dependence of the positive magnetoresistance is quadratic ($\ln[R(H)/R(0)] \propto H^2$; see Fig. 7), in accordance with with formula (2). The decrease of the magnetoresistance at high temperatures (Fig. 5) also agrees with this mechanism. Moreover, the measured values of $\Delta R(H)/R(0)$ correspond to formula (2) for $L_c \approx 2$ nm. Estimates of L_c in previous papers[4,5] gave a value of around 1 nm. It should be noted, however, that the samples investigated in the present study were much less resistive than the samples in Ref. 5, for example. Therefore, the localization length in them may be somewhat larger. It is apparently this circumstance (i.e., the rather large localization length in the samples studied here) that has made it possible for us to observe the positive magnetoresistance of $La_2CuO_{4+\delta}$ crystals in the insulating state.

Thus the positive magnetoresistance observed in the present study corresponds in a number of respects to the mechanism proposed in Ref. 9. On the other hand, the competition between the two magnetoresistance mechanisms of different sign in the samples studied here precludes a completely reliable comparison of the results with the theory of the positive magnetoresistance in the case of VHLC.[9] It also cannot be ruled out that the positive magnetoresistance may be due to features of the magnetic structure of $La_2CuO_{4+\delta}$, e.g., to AF domains and stripes.[13] These possibilities are considered in Ref. 14 for the AF crystal $YBa_2Cu_3O_{6.32}$, where for fields and currents parallel to the CuO_2 layers a positive magnetoresistance is observed for $\mathbf{H}\perp\mathbf{J}$ and a negative magnetoresistance for $\mathbf{H}\|\mathbf{J}$. Behavior of this sort can be explained if it is assumed that the stripes are aligned along the applied magnetic field. Such an orientation of the stripes in the field is possible if they have a local ferromagnetic moment.[14] Of course, this explanation cannot be regarded as conclusive, and it must be verified by further experimental checks. It follows from Ref. 14 that the AF cuprates can have anisotropy of the magnetoresistance related to the mutual orientation of the current and magnetic field. For the CuO_2 layers this form of anisotropy can depend weakly on the crystallographic anisotropy within the layers. In the studies described in the present paper, for $La_2CuO_{4+\delta}$ single crystals, the magnetic field was always directed perpendicular to the current. We plan further investigations of $La_2CuO_{4+\delta}$ crystals in which we intend to use other mutual orientations of the current and magnetic-field directions to elucidate the nature of the positive magnetoresistance in fields parallel to the CuO_2 layers.

[*] E-mail: belevtsev@ilt.kharkov.ua

---

[1] Tineke Thio, T. R. Thurston, N. W. Preyer, P. J. Picone, M. A. Kastner, H. P. Jenssen, D. R. Gabbe, C. Y. Chen, R. J. Birgeneau, and Amnon Aharony, Phys. Rev. B **38**, 905 (1988).

[2] N. W. Preyer, R. J. Birgeneau, C. Y. Chen, D. R. Gabbe, H. P. Jenssen, M. A. Kastner, P. J. Picone, and Tineke Thio, Phys. Rev. B **39**, 11563 (1989).

[3] M. A. Kastner, R. J. Birgeneau, G. Shirane, and Y. Endoh, Rev. Mod. Phys. **70**, 797 (1998).

[4] M. A. Kastner, R. J. Birgeneau, C. Y. Chen, Y. M. Chiang, D. R. Gabbe, H. P. Jenssen, T. Junk, C. J. Peters, P. J. Picone, Tineke Thio, T. R. Thurston, and H. L. Tuller, Phys. Rev. B **37**, 111 (1988).

[5] B. I. Belevtsev, N. V. Dalakova, and A. S. Panfilov, Fiz. Nizk. Temp. **23**, 375 (1997) [Low Temp. Phys. **23**, 274 (1997)].

[6] M. F. Hundley, R. S. Kwok, S.-W. Cheong, J. D. Thompson, and Z. Fisk, Physica C **172**, 445 (1991).

[7] Tineke Thio, C. Y. Chen, B. S. Freer, D. R. Gabbe, H. P. Jenssen, M. A. Kastner, P. J. Picone, N. W. Preyer, and R. J. Birgeneau, Phys. Rev. B **41**, 231 (1990).

[8] S.-W. Cheong, Z. Fisk, J. O. Willis, S. E. Brown, J. D. Thompson, J. P. Remeika, A. S. Cooper, R. M. Aikin, D. Schiferl, and G. Gruner, Solid State Commun. **65**, 111 (1988).

[9] B. I. Shklovskiĭ and A. L. Efros, *Electronic Properties of Doped Semiconductors*, Springer-Verlag, New York (1984), Nauka, Moscow (1979).

[10] A. O. Gogolin and A. S. Ioselevich, Zh. Éksp. Teor. Fiz. **98**, 681 (1990) [Sov. Phys. JETP **71**, 380 (1990)].

[11] H. C. Montgomery, J. Appl. Phys. **42**, 2971 (1971).

[12] E. Sigmund and K. A. Muller (Eds.), *Phase Separation in Cuprate Superconductors*, Springer-Verlag, Heidelberg (1994).

[13] E. W. Carlson, V. J. Emery, S. A. Kivelson, and D. Orgad, Preprint cond-mat/0206217 (2002).

[14] Yoichi Ando, A. N. Lavrov, and Kouji Segawa, Phys. Rev. Lett. **83**, 2813 (1999).

Translated by Steve Torstveit

LOW TEMPERATURE PHYSICS VOLUME 29, NUMBER 4 APRIL 2003

Low-temperature specific heat of frustrated ferrimagnets $BaFe_{12-x}In_xO_{19}$ with $x=3.0$ and $x=3.6$

A. G. Anders, N. N. Efimova, V. B. Valiev, and S. R. Kufterina

*V. N. Karazin Kharkov National University, pl. Svobody 4, 61107 Kharkov, Ukraine**

A. M. Gurevich, A. I. Krivchikov, A. V. Terechkov, and T. V. Chagovets

B. Verkin Institute for Low Temperature Physics and Engineering, National Academy of Sciences of Ukraine, pr. Lenina 47, 61103 Kharkov, Ukraine

(Submitted October 4, 2002; revised November 1, 2002)
Fiz. Nizk. Temp. **29**, 406–412 (April 2003)

Studies of the temperature dependence of the specific heat C in the temperature range 4.2–16 K and of the magnetization polytherms $\sigma_H(T)$ in the ZFC and FC regimes for $H=(1-25)\times 10^2$ Oe in the temperature range $4.2\text{ K}<T\leqslant 180$ K are carried out for two dilute frustrated ferrimagnetic oxides $BaFe_{12-x}In_xO_{19}$ ($x=3.0$ and 3.6), in which the transition to disordered states of the spin-glass type at $T<90$ K can be caused by destruction of a helicoidal structure. For the sample with $x=3.6$ it is found that $C(T)\propto T$, while for $x=3.0$ a dependence $C(T)\propto T^{3/2}$ is found. Taken together with the results of a study of the magnetic properties, this behavior allows one to identify the low-temperature state in the sample with $x=3.6$ as a spin glass. For the sample with $x=3.0$, in which clearly expressed spin-glass properties are seen in combination with a temperature dependence $C(T)\propto T^{3/2}$, the low-temperature state requires further study. [DOI: 10.1063/1.1542473]

The goal of this study was to investigate the temperature dependence of the low-temperature specific heat $C(T)$ in the range $4.2\text{ K}<T\leqslant 16$ K for two dilute frustrated ferrimagnetic oxides $BaFe_{12-x}In_xO_{19}$ ($x=3.0$ and 3.6), which have a hexagonal crystal structure of the magnetoplumbite type. These compounds exhibit typical spin-glass (SG) properties in the temperature region $T<90$ K: the trend of the magnetization polytherms $\sigma_H(T)$ depends on the prehistory of the samples, and the long-time relaxation of the nonequilibrium magnetization $\sigma_{ZFC}(T,H)$ has a logarithmic character — magnetic irreversibility and magnetic viscosity.[1–4]

In addition, judging from the results on the magnetic properties, the low-temperature state is different for the samples with $x=3.0$ and $x=3.6$. At a concentration of the nonmagnetic In^{3+} ions $x=3.0$ there exists a long-range ferrimagnetic (FiM) order, with a Curie temperature $T_C=213\pm 3$ K, the value of which is reliably determined both from the temperature dependence of the susceptibility $\chi(T)$ at low fields and from analysis of the magnetization isotherms $\sigma_T(H)$ in the framework of mean field theory.[5] This is done by a standard procedure (see, e.g., Ref. 6) in which, in accordance with the mean-field magnetic equation of state $H/\sigma=\alpha(T-T_C)+\beta\sigma^2$, the experimental $\sigma_T(H)$ curves are plotted in the coordinates H/σ versus σ^2. In this way one can determine both T_C and the spontaneous magnetization σ_S. For the sample with $x=3.0$ a nonzero spontaneous magnetization $\sigma_S\neq 0$ exists in the temperature interval from T_C to 4.2 K. In the standard terminology,[1,2] states for which a spontaneous magnetization $\sigma_S\neq 0$ coexists with the spin-glass properties listed above are called mixed states or ferro/ferrimagnetic spin-glass (FSG) states, and the region corresponding to them on the concentration $x-T$ diagram is reentrant. For the sample with $x=3.6$ the $\chi(T)$ curves in low fields have the form of smeared bell-shaped curves, and an analysis of the magnetization isotherms carried out not only in the framework of mean field theory but also with the use of the scaling magnetic equation of state in the form $(H/\sigma)^{0.75}=\alpha(T-T_C)+\beta\sigma^{2.5}$ shows the absence of spontaneous magnetization ($\sigma_S=0$) at all temperatures above 4.2 K.[3] We note in this regard that such an approach, i.e., analysis of the experimental $\sigma_T(H)$ curves with the use of the magnetic equations of state given above has turned out to be very fruitful in the study of the Ga-substituted spinel spin-glass system $Li_{0.5}Fe_{2.5-x}Ga_xO_4$ in the vicinity of the multicritical point x_0 on the $x-T$ diagram, where for $x\geqslant x_0=1.5$ the long-range FiM order is destroyed, and $\sigma_S=0$ at all temperatures above 0 K.[6]

In recent years increasing attention has been devoted to systems in which the SG properties listed above arise as a result of disordering of long-period structures of the helicoidal type.[7,8] Here the structural units are no longer individual spins but regions of mesoscopic size, extending from tens to hundreds of ångstroms, within which the initial ordering is preserved.[7] The study of the properties of frustrated disordered magnets of this kind is only beginning: essentially there are data only for itinerant magnets.[7,8]

The objects of study in this paper belong to the class of Heisenberg systems with a short-range exchange interaction and, according to neutron diffraction studies, have ordering of the helicoidal type at $T<120$ K.[9] The study of these objects is undoubtedly of interest from the standpoint of elucidating the nature and mechanisms of formation of the disordered long-period structures. Among the questions having fundamental significance for identification of magnetic states, an important place is held by the question of the character of the spectrum of magnetic excitations. As a first step it is natural to turn to investigations of the specific heat $C(T)$, a linear or quasilinear temperature dependence of which is regarded as one of the canonical hallmarks of states of the spin-glass type.[1,2] As compared to itinerant magnets, the use of ferrimagnetic oxides for this sort of research is more convenient, since the latter are insulators and, hence, their specific heat does not contain an electronic contribution linear in the temperature.

The specific heat measurements were made on single-crystal $(x=3.0)$ and polycrystalline $(x=3.6)$ samples synthesized by the same technique as in Refs. 3 and 5. The single-phase state of the samples was monitored by x-ray and, for the polycrystalline samples, metallographic methods. The concentration of nonmagnetic ions in the single-phase polycrystals corresponded to the concentrations of the components involved in the solid-phase reaction of ferritization in the temperature interval 1520–1570 K. Attestation of the cation composition of the single crystals was done by means of a comparison of their structural properties (the lattice parameters) with the corresponding properties of single-phase polycrystals.

Measurements of $C(T)$ on the single crystal $(x=3.0)$ were made by a pulsed quasistatic method with the use of the calorimeter described in Ref. 10, at the Institute of Low Temperatures and Structural Research of the Polish Academy of Sciences in Wroclaw, Poland. The measurements of $C(T)$ on the polycrystalline samples $(x=3.6)$ were made by the method of absolute calorimetry[11] at the B. Verkin Institute for Low Temperature Physics and Engineering, National Academy of Sciences of Ukraine in Kharkov. The measurement error is 1% or less in both cases.

In addition to the main results, i.e., the functions $C(T)$, for illustration of the spin-glass behavior of the objects of study we present the magnetization polytherms $\sigma_H(T)$ for different prehistories—$\sigma_{ZFC}(T)$ and $\sigma_{FC}(T)$. Measurements were made on a ballistic magnetometer with a sensitivity of 10^{-3} G·cm/g in the temperature range 4.2–180 K and magnetic fields from 10^2 to 2.5×10^3 Oe. The experiments were done under identical conditions in the two cases (ZFC and FC): on heating at identical rates of temperature increase. The ZFC and FC regimes correspond to a pre-cooling of the samples to some temperature $T<T_f$ (in our case 4.2 K) in the absence of field (ZFC) or in a field of specified strength (FC). T_f is the temperature below which magnetic irreversibility and magnetic viscosity exist. For spin glasses T_f is the freezing temperature of the SG state and depends on the value of the magnetic field H.[1–4,12] According to the results of a study of the lines of critical behavior of $T_f(H)$, which are determined in two ways, from the appearance of irreversibility $(\sigma_{ZFC}(T,H)\neq\sigma_{FC}(T,H))$ and magnetic viscosity $(\sigma_{ZFC}(T,H)\sim S\ln t$, where t is the time, S is the coefficient of viscosity), the value of $T_f(0)$ for the sample with $x=3.6$ is equal to 85 ± 3 K.[3,4] As we see from the data in Fig. 1, close to the same value of $T_f(0)$ is obtained for the single-crystal sample $(x=3.0)$.

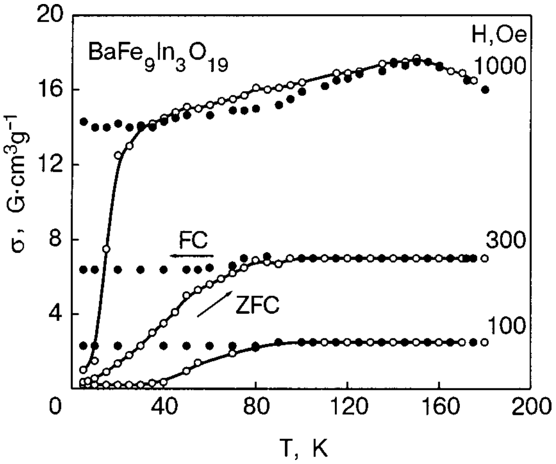

FIG. 1. The magnetization polytherms $\sigma_H(T)$ of the BaFe$_9$In$_3$O$_{19}$ single crystal in the ZFC and FC regimes (see text).

Figures 1 and 2 show the magnetization polytherms $\sigma_H(T)$ in the ZFC and FC regimes for the samples with $x=3.0$ and 3.6, respectively. We note that these were the same samples as in the $C(T)$ measurements in Fig. 3. As we see from the data in Fig. 1, for the sample with $x=3.0$ the $\sigma_H(T)$ curves for fields $H=100$ and 300 Oe have the typical form for the reentrant region of the $x-T$ diagram.[1,2,12] At sufficiently high temperatures there is a plateau, and for $T\leqslant T_f(H)$ irreversibility appears: the nonequilibrium magnetization $\sigma_{ZFC}(T)$ decreases, tending to zero for $T\rightarrow0$ K, while $\sigma_{FC}(T)$, as before, is independent of temperature.

In a field $H=10^3$ Oe the trend of the $\sigma_H(t)$ polytherms changes, and a maximum is formed at $T\sim150$ K. This maximum is most pronounced for $\sigma_{FC}(T)$, which in a first approximation is usually assumed[1,2] to be the equilibrium magnetization. Moreover, in addition to the "spin-glass irreversibility" for $T\rightarrow0$ K (the region $T<40$ K), where $\sigma_{FC}(T)>\sigma_{ZFC}(T)$, there exists a temperature hysteresis of the magnetization at higher temperatures $(40\ \mathrm{K}<T<150\ \mathrm{K})$, where the curves are situated in the opposite order: $\sigma_{ZFC}(T)>\sigma_{FC}(T)$. It is necessary to note that, owing to

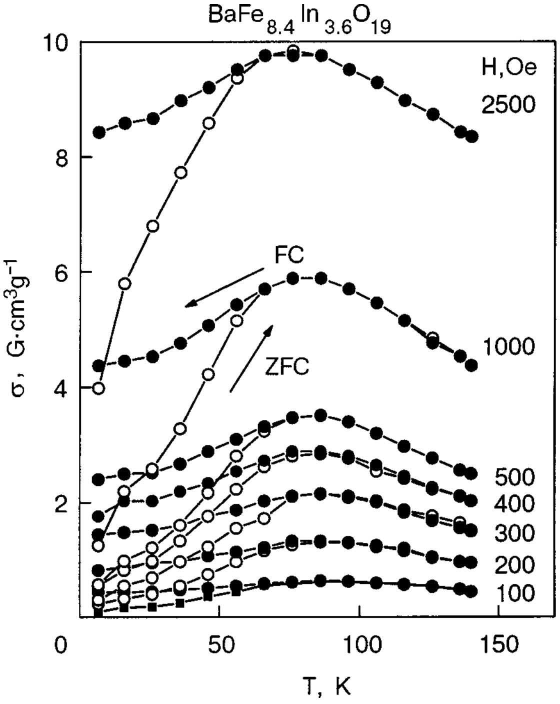

FIG. 2. The magnetization polytherms $\sigma_H(T)$ of a polycrystalline sample of BaFe$_{8.4}$In$_{3.6}$O$_{19}$ and the ZFC and FC regimes (see text).

the high sensitivity of the apparatus (10^{-3} G·cm^3/g) the relative trend of the $\sigma_H(T)$ curves in the ZFC and FC regimes is determined to rather high accuracy, as may be judged by the good reproducibility of the results. Temperature hysteresis has also been observed for the indium-substituted single crystals with $x>3.0$, the experiments having been done in a heating–cooling scheme in the temperature interval 77–300 K in fields up to 17×10^3 Oe.[13] On the whole this behavior is apparently due to a first-order phase transition to helicoidal ordering at a temperature $T\sim120$ K, which was reported in Ref. 9. We note that a third first-order phase transition quite likely exists in reentrant magnets in the temperature region $T_f<T<T_C$, as we observed previously[14,15] in the the spin-glass system $\mathrm{Li_{0.5}Fe_{2.5-\mathit{x}}Ga_{\mathit{x}}O_4}$.

The trend of the magnetization polytherms of the polycrystalline sample with $x=3.6$ (Fig. 2) is in rather good agreement with the results obtained previously for the single crystal.[3] Unlike the case of the single crystal ($x=3.0$), however, the character of the behavior is similar to that which is observed in the vicinity of the multicritical point x_0 of the $x-T$ phase diagram of the aforementioned spin-glass system of Li–Ga spinels.[12] In the concentration region $x\sim x_0$ the character of the trend of the $\sigma_H(T)$ polytherms at low fields (the absence of a sharp spin-glass maximum) is largely determined by the pronounced spatial inhomogeneity of all types of magnetic states, which is due to the presence of regions (clusters) with FiM ordering.[5,12] For the sample with $x=3.6$ the short-range FiM order persists up to $T=300$ K, and it is only at higher temperatures that the temperature dependence of the inverse paramagnetic susceptibility χ^{-1} obeys the characteristic hyperbolic law inherent to ferrimagnetism.[5] Thus the results shown in Figs. 1 and 2 clearly illustrate the difference of the magnetic states realized in the samples with $x=3.0$ and $x=3.6$ at low temperatures.

The temperature dependence of the specific heat of the samples is presented in Fig. 3. Unfortunately, the standard procedure of separating out the magnetic contribution $C_m(T)$ by means of an independent determination of the lattice specific heat of the nonmagnetic analog, as done in Ref. 16, cannot be used in the present case. It is established experimentally[5] that the limiting content of the large $\mathrm{In^{3+}}$ ions ($r=0.92$ Å) in a structure of the magnetoplumbite type is not more than $x=4.0$. For this reason the mathematical processing of the experimental results was done on the basis of the following considerations. Clearly the phonon contribution to the specific heat has about the same value in both samples and in the temperature interval under study is probably proportional to T^3. At low temperatures the magnetic contribution is ordinarily larger than the lattice contribution;[8,14,16] the magnetic contributions in samples with different $\mathrm{In^{3+}}$ concentrations can in principle have not only different values but also different temperature trends. For a qualitative check of this, Fig. 4 shows the experimental $C(T)$ curves plotted in the coordinates C/T versus T. First, it is seen from the data in Fig. 4 that for $4\ \mathrm{K}\leqslant T\leqslant10$ K, where, by assumption, the magnetic contributions to the specific heat should be dominant, the $C/T-T$ plots for the samples with $x=3.0$ and $x=3.6$ are different. It is seen that for neither sample is there a pronounced plateau below 10 K, which would indicate a predominant linear trend of $C(T)$. At the same time, for the sample with $x=3.6$ the extrapolation of this part to $T=0$ K intercepts the horizontal axis at a positive value of $C(T)$, a circumstance that may imply the existence of a linear contribution to the total specific heat. For $T>10$ K the trends of the C/T versus T curves of the two samples are very close, most probably because the dominant contributions to the two curves for $T>10$ K are the practically identical phonon contributions.

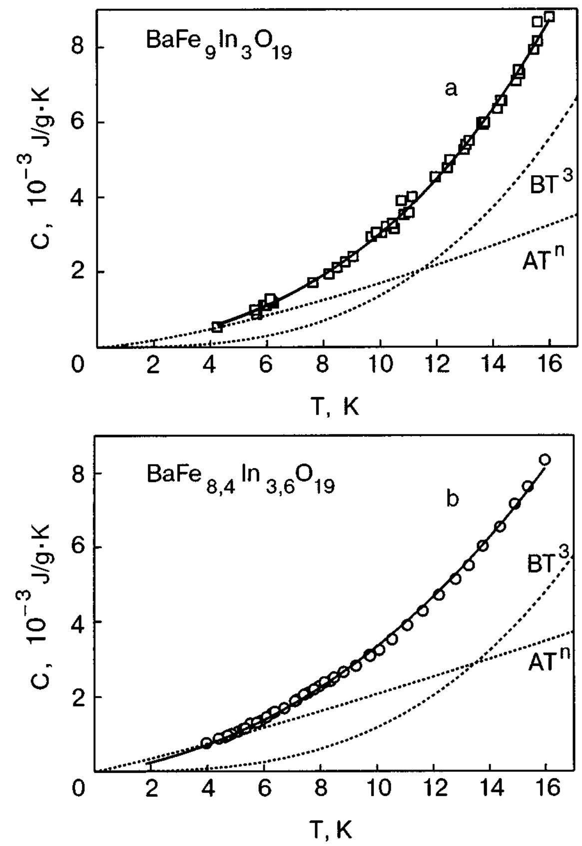

FIG. 3. Temperature dependence of the specific heat of $\mathrm{BaFe_{12-\mathit{x}}In_{\mathit{x}}O_{19}}$ samples. The dotted curves show the decomposition of the experimental $C(T)$ curve into a phonon contribution BT^3 and a magnetic contribution AT^n. (a) $x=3$, $n=1.38\pm0.2$; (b) $x=3.6$, $n=1.11\pm0.05$.

Keeping in mind the qualitative arguments set forth above, we can describe the experimental $C(T)$ curves by approximate expressions of the form

$$C(T)=AT+BT^3, \tag{1}$$

$$C(T)=AT^{3/2}+BT^3, \tag{2}$$

$$C(T)=A_1T+A_2T^{3/2}+BT^3, \tag{3}$$

$$C(T)=AT^n+BT^3. \tag{4}$$

From the standpoint of the concepts developed above, the best agreement with the experimental results was achieved either with the use of relation (4) for both samples, with a simultaneous determination of the three parameters A, B, and n, or with the use of different approximations: Eq. (1) for $x=3.6$ and Eq. (2) for $x=3.0$, in which case only the coefficients A and B are subject to determination. The values of these quantities are given in Table I.

The decomposition of the experimental $C(T)$ curves into magnetic (AT^n) and phonon (BT^3) contributions in accor-

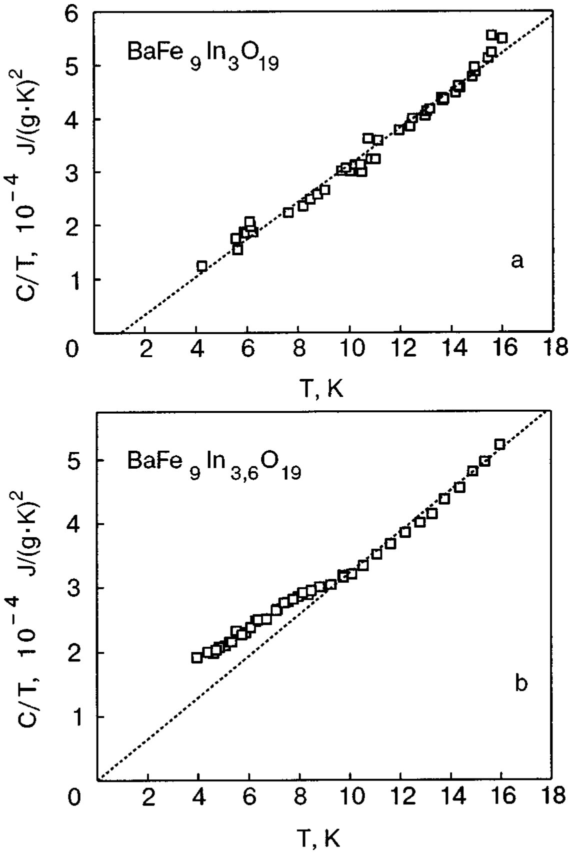

FIG. 4. Experimental curves of $C(T)$ for $BaFe_{12-x}In_xO_{19}$ samples in the coordinates C/T versus T. (a) $x=3$; (b) $x=3.6$.

dance with Eq. (4) is shown by the dotted curves in Fig. 3. The decompositions of the $C(T)$ curves look practically the same when the magnetic contributions are described by the functions $AT^{3/2}$ for $x=3.0$ and AT for $x=3.6$. It is seen that in the approximation used the phonon contribution proportional to BT^3 is indeed close in magnitude for the samples with $x=3.0$ and 3.6 and at low temperatures is less than the magnetic contribution in them, but it becomes predominant starting at temperatures ~ 10 K. A different picture is observed if the same equation, (1), (2), or (3), is used to approximate $C(T)$ for both concentrations of nonmagnetic In^{3+} ions. For example, if the monotonic part $C_m(T)$ has the form $AT^{3/2}$ in both samples, then the photon contribution BT^3 at $T=16$ K is only about half as large as the magnetic contribution and also only half as large as for the sample with $x=3.0$.

TABLE I. Values of the parameters of Eqs. (1), (2), and (4) used for approximation of the experimental $C(T)$ curves in Fig. 3; the correlation coefficient is 0.99.

x	Equation	n	$A\cdot 10^5$ $J\cdot g^{-1}\,K^{(1+n)}$	$B\cdot 10^6$ $J\cdot g^{-1}\,K^{-4}$
3.0	(4)	1.38 ± 0.2	7 ± 2	1.36 ± 0.2
3.6	(4)	1.11 ± 0.05	16 ± 1	1.17 ± 0.05
3.0	(2)	3/2	7 ± 0.2	1.25 ± 0.04
3.6	(1)	1	20 ± 0.2	1.27 ± 0.01

Thus there are sufficient grounds for assuming that for the sample with $x=3.6$ the magnetic part of the specific heat $C_m(T)$ at low temperatures obeys a linear (or quasilinear) law. In accordance with the generally accepted phenomenological indicators,[1,2] including the specific magnetic properties (see Fig. 2 and Refs. 3 and 4) and the behavior of the specific heat (Fig. 3b), it must be concluded that the low-temperature state realized in this sample is a spin-glass state.

For the sample with $x=3.0$ the situation is not so unambiguous, since the temperature dependence of the magnetic part of the specific heat is described by a Bloch law $C_m \propto T^{3/2}$ or, possibly, by some more complicated modification of it.[17–19] This last question requires further study at $T<4$ K, but the very fact that the temperature behavior of the magnetic contributions to the specific heat is different in the spin-glass sample with $x=3.6$ and the sample with $x=3.0$ can be considered as firmly established. This result is of no little importance, since there exists the opinion that in objects whose magnetic properties correspond to the SG state and whose magnetic specific heat $C_m \propto T^{3/2}$, the dependence of this type is due to the predominance of magnetic excitations of spin waves localized in regions of mesoscopic size in which the FiM ordering is preserved.[20] However, the results obtained in the present study do not confirm that hypothesis.

In the objects studied here the formation of a helicoidal structure and its subsequent destruction with a transition to a SG state ($x=3.6$) are due to the selective substitution of the large nonmagnetic ions In^{3+} in the crystal lattice and to the formation of weakly magnetic interlayers in the planes perpendicular to the hexagonal axis **c**. This has been discussed in detail in Ref. 3. We surmise from the data of the magnetic studies (the presence or absence of spontaneous magnetization) that increasing the concentration of In^{3+} ions from $x=3.0$ to $x=3.6$ leads to an increase of the concentration of frustrated bonds to the critical value for the existence of long-range FiM order in the crystal. Meanwhile, this does not noticeably affect the statistics of the distribution of sizes (along the **c** axis) of the regions separated by the weakly magnetic interlayers. For $x=3.0$ the In^{3+} ions occupy $\sim 70\%$ of the pentahedral positions in the lattice, which are of fundamental importance from the standpoint of formation of a macroscopic magnetic structure.[3,9] These positions lie in planes widely separated from each other, by half the lattice period $(c/2)$. It is clear that for destruction of the helicoid it is necessary to increase the concentration of frustrations, either in these weakly magnetic planes or in their nearest neighbors. Consequently, the increase of the concentration of the nonmagnetic In^{3+} ions from $x=3.0$ to $x=3.6$ cannot have an appreciable influence on the character of the mesoscopic inhomogeneities in these samples. It follows that the change in type of the $C_m(T)$ curves when the concentration of In^{3+} ions is increased from $x=3.0$ to $x=3.6$ is due to a change in the exchange in the weakly magnetic interlayers via which the mesoscopic regions interact with each other. The fact that these regions exist is not in itself decisive.

This conclusion is in good agreement with the experimental results obtained in Refs. 1, 2, 12, 14, and 16. For example, in the Li–Ga spinel system, which was mentioned earlier, the pronounced spatial inhomogeneity of the magnetic states in the vicinity of the multicritical point of the $x-T$ diagram, one has $C_m \propto T$ both in the SG and in the FSG states.[14,16] Moreover, in the context of the question under discussion it is appropriate to recall another example (they are not yet numerous)[20,21] in which a dependence $C_m \propto T^{3/2}$ is observed simultaneously with pronounced spin-glass properties. In the dilute spinels $Li_{0.5}Fe_{1.6}Ga_{0.9}O_4$ the linear dependence $C_m \propto (T)$ gives way to a $T^{3/2}$ law if ~ 2 mole% Co^{2+} is added to its composition.[21] There is a simultaneous increase by almost an order of magnitude in the temperature of the phase transition to the state of the FSG type, and for $T = T_f(0)$ the hallmarks of a first-order phase transition appear.[21,22] It cannot be ruled out that in Li–Ga spinels doped with Co^{2+} ions a state similar to the low-temperature state in $BaFe_9In_3O_{19}$ is formed, since, according to Dzyaloshinskii,[23] long-period magnetic structures can form in the presence of anisotropic exchange (the Co^{2+} ions).

In connection with this we can assume that the combination of spin-glass magnetic properties (irreversibility and viscosity) and a temperature dependence of the specific heat of the form $C_m \propto T^{3/2}$ is directly due to the nature of the frustrated state that is realized. It is interesting to note that such behavior can be observed in two fundamentally different situations: i), a large role in the formation of the spectrum of magnetic excitations is played by the structure of the FSG states, and the dependence $C_m \propto T^{3/2}$ is due to the presence of long-range FiM order with helicoidal ordering; ii) magnets with such a combination of properties do not belong to the spin glasses (their ground state is nondegenerate[24]) but form a new variety of frustrated disordered systems. Thus the further theoretical and experimental study of disordered helicoidal structures in different kinds of magnets may give a new impetus to the development of the concepts of frustrated states.

[*] E-mail: Alexander.V.Vankevich@univer.kharkov.ua

---

[1] K. Binder and A. P. Young, Rev. Mod. Phys. **58**, 801 (1986).
[2] I. Ya. Korenblit and E. F. Shender, Usp. Fiz. Nauk **157**, 267 (1989) [Sov. Phys. Usp. **32**, 139 (1989)].
[3] N. N. Efimova, N. V. Tkachenko, and A. V. Borisenko, Fiz. Tverd. Tela (Leningrad) **29**, 1331 (1987) [Sov. Phys. Solid State **29**, 762 (1987)].
[4] N. N. Efimova and N. V. Tkachenko, Fiz. Tverd. Tela (Leningrad) **33**, 1583 (1991) [Sov. Phys. Solid State **33**, 891 (1991)].
[5] N. N. Efimova and Yu. A. Mamalui, in *Physical and Physico-Chemical Properties of Ferrites* [in Russian], Nauka i Tekhnika, Minsk (1975), p. 115.
[6] N. N. Efimova and M. B. Ustimenkova, Zh. Éksp. Teor. Fiz. **114**, 2065 (1998) [JETP **87**, 1122 (1998)].
[7] T. Coto, T. Ando, T. Oku, and M. Furusaka, J. Magn. Magn. Mater. **140–144**, 1785 (1995).
[8] O. Trovarelli, J. G. Sereni, P. Pureur, and J. Shaf, Phys. Rev. B **52**, 15387 (1995).
[9] M. I. Namtalishvili, O. P. Oleshko-Ozhevskiĭ, and I. I. Yamzin, Fiz. Tverd. Tela (Leningrad) **13**, 2543 (1971) [Sov. Phys. Solid State **13**, 2137 (1971)].
[10] A. I. Krivchikov, B. Ya. Gorodilov, and A. Czopnik, ''Adiabatic microcalorimeter,'' in *Proceedings of the International Seminar on Low Temperature Thermometry and Dynamic Temperature Measurement*, Wroclaw (1997), p. 57.
[11] A. V. Alapina, Yu. A. Dushechkin, and B. Ya. Sukharevskiĭ, in *Themophysical Properties of Substances and Materials*, Vol. 9, Izd. Standartov, Moscow (1976), p. 113.
[12] N. N. Efimova, Yu. A. Popkov, and N. V. Tkachenko, Fiz. Nizk. Temp. **15**, 1055 (1989) [Sov. J. Low Temp. Phys. **15**, 584 (1989)]; **16**, 1565, 881 (1990).
[13] N. N. Efimova, Yu. A. Mamalui, and N. V. Tkachenko, Fiz. Tverd. Tela (Leningrad) **26**, 1839 (1984) [Sov. Phys. Solid State **26**, 1112 (1984)].
[14] N. N. Efimova, S. R. Kufterina, A. G. Anders, S. V. Startsev, A. M. Gurevich, and V. N. Eropkin, Fiz. Nizk. Temp. **24**, 1007 (1998) [Low Temp. Phys. **24**, 760 (1998)].
[15] N. N. Efimova, JETP Lett. **67**, 346 (1998).
[16] N. N. Efimova, V. A. Pervakov, V. I. Ovcharenko, and N. Yu. Tyutryumova, Fiz. Tverd. Tela (St. Petersburg) **35**, 2838 (1993) [Phys. Solid State **35**, 1405 (1993)].
[17] Yu. A. Izyumov and R. P. Ozerov, *Magnetic Neutronography* [in Russian], Nauka, Moscow (1966).
[18] U. Krey, J. Phys. Lett. **46** Z, 845 (1985).
[19] N. N. Efimova and S. R. Kufterina, Fiz. Tverd. Tela (St. Petersburg) **40**, 1075 (1998) [Phys. Solid State **40**, 982 (1998)].
[20] J. M. D. Coey, S. Von Molnar, and R. J. Gambino, Solid State Commun. **24**, 167 (1977).
[21] N. N. Efimova and S. R. Kufterina, Fiz. Nizk. Temp. **20**, 338 (1994) [Low Temp. Phys. **20**, 269 (1994)].
[22] N. N. Efimova, Yu. A. Popkov, and S. R. Kufterina, JETP Lett. **64**, 450 (1996).
[23] I. E. Dzyaloshinskiĭ, Zh. Éksp. Teor. Fiz. **46**, 1420 (1964) [Sov. Phys. JETP **19**, 960 (1964)]; **47**, 336 (1964); **20**, 665 (1964).
[24] V. S. Dotsenko, Usp. Fiz. Nauk **163**, 1 (1993) [Phys. Usp. **36**, 455 (1993)].

Translated by Steve Torstveit

LOW TEMPERATURE PHYSICS VOLUME 29, NUMBER 4 APRIL 2003

ELECTRONIC PROPERTIES OF METALS AND ALLOYS

Nonlinear conductivity of a compensated polycrystalline metal in high magnetic field

I. I. Logvinov* and Yu. N. Chiang

B. Verkin Institute for Low Temperature Physics and Engineering, National Academy of Sciences of Ukraine, pr. Lenina 47, 61103 Kharkov, Ukraine

(Submitted October 4, 2002)
Fiz. Nizk. Temp. **29**, 413–417 (April 2003)

The current–voltage (I–V) characteristics in a magnetic field are studied at helium temperatures for thin polycrystalline samples of a metal (pure tin) embedded in a solid-state medium in order to create reproducible experimental conditions. In these samples a nonlinear S-shaped I–V characteristic is obtained for the first time with this type of heat sinking at the surface of the metal. The conditions for the onset of a temperature–electric instability in a metal with an S-shaped I–V characteristic are investigated in relation to the reactive parameters of the circuit. © *2003 American Institute of Physics.* [DOI: 10.1063/1.1542474]

The nonlinear phenomena that can arise in metallic conduction in the case of Joule heating of samples[1] remain little studied because of the specific conditions for their observation, viz., in order for the nonlinear regime to be realized in a given experiment it is necessary to have quasiadiabatic conditions for the electron–phonon system of the metal, for which reason it is necessary to use samples that are not too thick, deliver current densities of the order of 10^5 A/cm^2 to the sample, and at the same time maintain a constant temperature in the thermostat without allowing a boiling crisis for the liquid helium.

In experiments with direct contact of metal samples with a low-temperature liquid coolant, N- and S-shaped I–V characteristics in the case of Joule heating of the sample are due, in the majority of cases, to nonlinearity of the heat removal in these media.

In the case of liquid helium such a regime arises at heat flux densities q through the metal surface in the range from $q \sim 0.1$ W/cm^2 (“bubble” boiling) to $q \geqslant 0.5$ W/cm^2 (“film” boiling characterized by the formation of a gas film around the sample), which correspond to considerable amounts of power delivered to the cryostat (1–10 W) and to a large expenditure of cryogenic liquid.

However, the use of the boiling crisis is not the only way of realizing a nonlinear conduction regime. In our previous studies it became clear that such a possibility also arises in the absence of direct contact of the samples with the liquid.[2,3] Here one eliminates the instability of the heat removal via the liquid coolant, which is due to convective flow and the boiling crisis, making it possible to study the characteristics of a metal in a reproducible nonlinear regime, which includes effects due to the temperature-electric instability. At low temperatures the heat flux through the dielectric heat-removal medium is a monotonically increasing function of temperature, and there exists a region of temperatures in which the rate of growth of the resistivity $\rho(T)$ is higher than the rate of growth of the heat flux $q(T)$ as the temperature is increased.

Indeed, the heat conduction equations at thermal balance between the specific Joule power released in the sample and the specific heat flux from the surface of the sample imply the following expression for the differential conductivity of the metal:[1,4]

$$\frac{dj}{dE}=\frac{\rho(T)[q(T)/\rho(T)]'_T}{[q(T)\rho(T)]'_T}. \tag{1}$$

Thus it follows from Eq. (1) that in order to obtain an N- or S-shaped form of the nonlinear I–V characteristics the behavior of the functions $q(T)$ and $\rho(T)$ should be such as to bring about a change of sign of this expression. It is known[5] that for many heat-removal media the heat flux $q(T)$ from the sample to the thermostat can be approximated by the a function of the form $q(T) \approx \alpha T^{m(T)}$, where α and m are positive numbers. As a result, one can write for a metal the approximate expression $\rho_{H=0}(T)=\rho_0+\beta T^{n(T)}=\rho_0+\rho_T$, where β and n are also positive, $(q\rho)'_T$ is an everywhere positive function, and the sign of expression (1) for different parts of the I–V characteristics can be determined from the relationship of the following parameters:

$$\frac{dj}{dE}=\{m\rho_0+[m-n]\rho_T\}F_1(T), \tag{2}$$

where $F_1(T)$ is a positive function.

It follows from expression (1) that in the case of an inverted temperature dependence of the resistivity, e.g., for $\rho(T) \propto [\rho_T(H=0)]^{-1}$, we obtain for the differential resistivity an expression analogous to Eq. (2):

$$\frac{dE}{dj}=\{m\rho_0+[m-n]\rho_T\}F_2(T), \tag{3}$$

where the function $F_2(T)$ is positive definite.

Thus the I–V characteristic of the sample can assume a nonlinear form characterized by the presence of segments of negative differential conductivity (N- or S-shaped I–V characteristics) only when several conditions hold simultaneously. First, $\rho_T \gg \rho_0$ if $[n-m]\rho_T > m\rho_0$, and, second,

$m-n<0$, which requires that the temperature dependence of $q(T)$ be weaker than that of $\rho(T)$, and that is possible when the electron temperature coincides with the temperature of the crystal lattice. This corresponds to the regime of quasiadiabatic heating of the sample, i.e., when the relaxation time of the electrons is much shorter than the thermal times. As a result, the temperature region in which negative differential conductivity (resistivity) can exist in a metallic sample is bounded both below and above, and that makes for an N- or S-shaped form of the I–V characteristic of such samples.

As follows from Eq. (1), for $\rho(T)\propto\rho_T$, i.e., for temperature dependence of the resistivity like that of the metal in the absence of magnetic field, the differential conductivity decreases with increasing temperature, passes through zero to negative values, and then rises again: such an I–V characteristic has an N-shaped form. The presence of an inverted temperature dependence of the resistivity in comparison with the $\rho(T)$ curve for $H=0$ leads to a lowering of the differential resistivity with increasing temperature, and upon reaching negative values it leads to an S-shaped I–V characteristic. This sort of dependence of $\rho(T)$ can be obtained by applying a strong magnetic field, in which for some (compensated) metals the behavior is close to $\rho_H(T)\propto H^2/\rho_{T(H=0)}$ even at those temperatures where satisfaction of the necessary inequalities $\rho_T\gg\rho_0$ and $[m-n]<0$ takes place under conditions for which $\omega\tau_{(H=0)}$ is not too different from 1. Here ω and $\tau_{(H=0)}$ are the cyclotron frequency and relaxation time.

It is known that for suitable geometric parameters of the metallic samples under the conditions of the nonlinear regimes considered, it is possible for spatially inhomogeneous distributions of the temperature, electric field, and current to arise.[1,4] For N-shaped I–V characteristics the nonuniformity is along the length of the sample, in the form a temperature–electric domain, while for S-shaped I–V characteristics the nonuniformity is over the width of the sample, in the form of a current pinch.

In view of the many restrictions listed above for realization of a nonlinear regime for metallic samples, the phenomena associated with negative differential resistivity in metals remain insufficiently well studied at the present time. In particular, it has not been possible to observe S-type I–V characteristics in thin metallic slabs.

In the present study we have for the first time investigated a nonlinear regime with an S-shaped I–V characteristic, obtained in a polycrystalline metal (tin) in the absence of a boiling crisis on its surface and in the cryogenic system on the whole, and we have observed an instability of the voltage across the sample due to its temperature-electric instability (without the formation of a current pinch). We have investigated the possibility of realizing a stable regime with negative differential resistance through the use of different kinds of heat-removal media—glass-reinforced plastic, a dielectric with high thermal conductivity (Araldite), and a crystalline medium.

The indicated regime was studied in samples of pure polycrystalline tin in the form stripes with dimensions $L\times W\times d\approx 100\times 0.8\times 0.09$ mm. The principle of the measurements and the technique used are analogous to those described in Ref. 3, and they are supplemented by equipment that permits making measurements in an external transverse magnetic field with an induction of up to 5 T. All of the results presented were measured at a dc current through the sample in the range from 0 to 80 A.

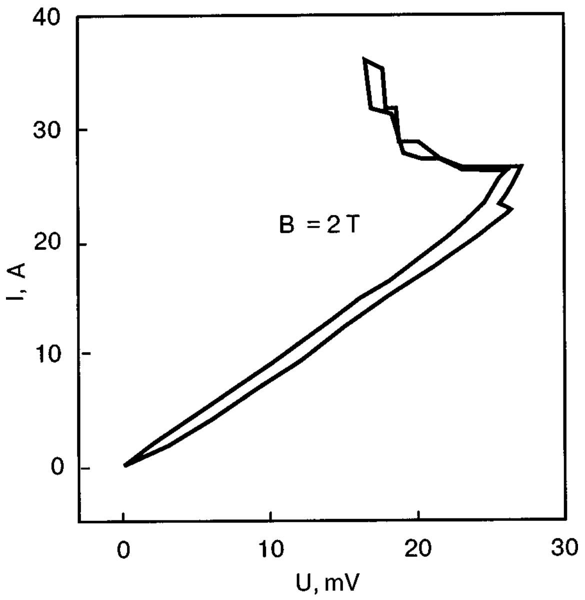

FIG. 1. Current–voltage (I–V) characteristic of a polycrystalline tin slab in a liquid helium medium.

Figure 1 shows the I–V characteristic of a sample directly immersed in liquid helium in a magnetic field of 2 T. It is seen that in thin polycrystalline samples under conditions of comparatively low values of $[\rho(T,H)]'_T\approx 0.3\Omega\cdot\mathrm{m/K}$ ($\omega\tau_{(H=0)}$ just barely greater than 1) at temperatures maintaining a boiling crisis of the helium at their surface, one can observe a regime of negative differential resistance, which previously had not been successfully realized in such samples in the same magnetic fields.[6] However, it can be seen in the figure that the effect is accompanied by hysteresis, as is confirmed by the temperature instability of the nonlinear regime under these conditions. Previously we had encountered instability in a study of the N-shaped regime of the I–V characteristic (in particular, see Ref. 7, where the boiling crisis on the surface of a metallic sample significantly reduced the current necessary for obtaining a temperature–electric domain and also led to hysteresis).

Figures 2–4 show the results of studies of S-shaped I–V characteristics under conditions such that there is no boiling crisis of the liquid at the surface of the samples and in the cryogenic system as a whole. It is seen that under such experimental conditions the S-shaped regime of nonlinearity obtained on heating of a sample with an inverted temperature dependence of $\rho(T,H)$ in comparison with the temperature dependence of $\rho(T,H=0)$ is manifested most distinctly with the use of a crystalline heat-removal medium (Fig. 4). This case corresponds to temperature behavior of the functions $q(T)$ and $R(T,H=5\ \mathrm{T})$ (curves *2* and *3* in Fig. 5) calculated from the data of measurements of the I–V characteristic with the use of the heat balance equation

$$R(T)I^2=q(T)A$$

(where A is the surface area of the sample). The temperature

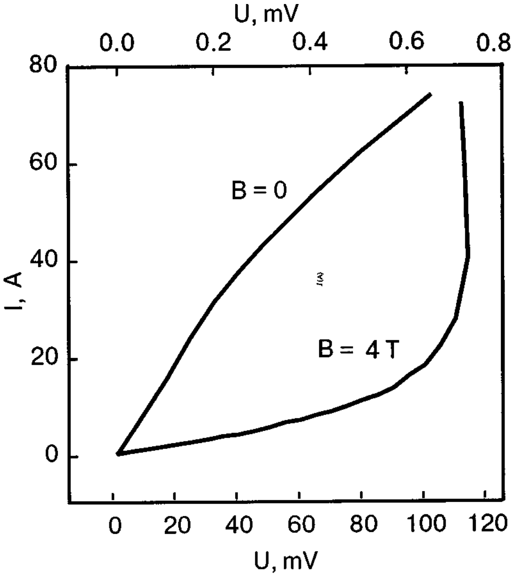

FIG. 2. I–V characteristic of a polycrystalline tin slab with a glass-reinforced plastic heat-removal medium; $T_0=4.2$ K.

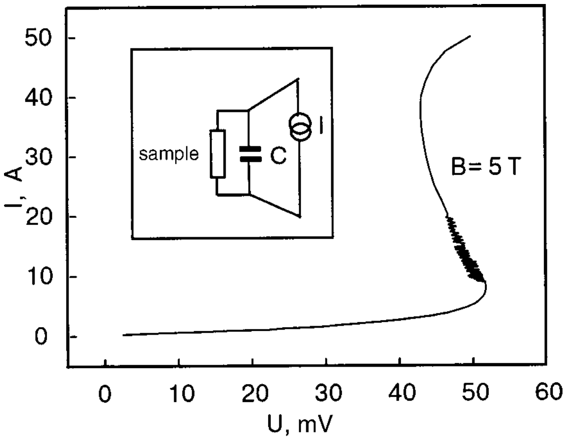

FIG. 4. The I–V characteristic of a polycrystalline tin slab in a crystalline sulfur medium. $T_0=4.2$ K, $B=5$ T. The inset shows a diagram of the connection of the capacitance in the circuit.

dependence of the function $[qR](T)$ (curve *1*) gives an idea of the temperature region of negative differential resistivity of the sample under study.

As is known from the theory of nonlinear circuits, a circuit containing a dc current source, an energy store, and an element with negative differential resistance (NDR) can undergo relaxation self-oscillations. It is known that for samples with an S-shaped I–V characteristic the connection of a sufficiently large capacitance C in parallel with the sample leads to a self-oscillatory instability, which was realized in an experiment on the part of the I–V characteristic having the greatest value of the NDR. When the I–V characteristics were registered using a recording potentiometer the instability was manifested in the appearance of nonmonotonicity at that place, as is seen in Fig. 4. The inset shows a measurement circuit employing a capacitance. Unlike the case of an N-shaped I–V characteristic, when an self-oscillatory process can be excited in a fixed-voltage regime with a suitable inductance in the circuit,[8] in the case of an S-shaped I–V characteristic the self-oscillations can arise in a fixed-current regime and can be described by a system of equations including, in addition to the heat balance equation, the following differential equation of the circuit:

$$C\frac{dU}{dt}+\frac{U}{R(T,H)}=I_0,\quad R(T,H)=\rho(T,H)L/Wd. \tag{4}$$

The period Δt of the oscillations observed for a sample with resistance $R(293\text{ K})\approx 0.16\ \Omega$ equals ≈ 0.1 s, in agreement with the following dependence on the parameters of the system:

$$\Delta t - R(T,H)C + c_V(T)/q(T),$$

where $c_V(T)$ is the specific heat of the sample. The condition for the appearance of oscillations reduces to the requirement

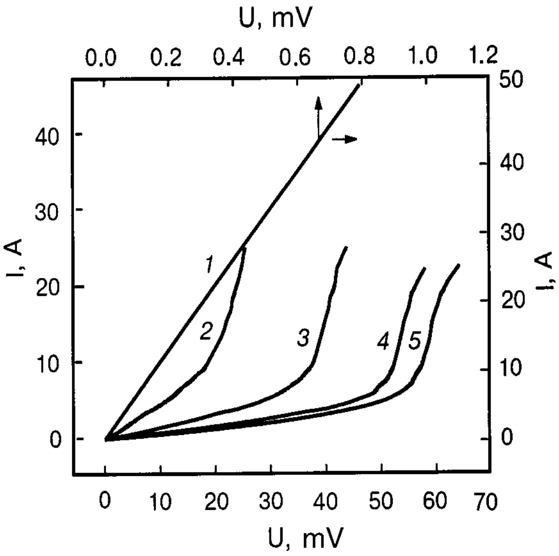

FIG. 3. I–V characteristics of a polycrystalline tin slab in a solid dielectric (Araldite) medium in various magnetic fields B [T]: 0 (*1*), 1 (*2*), 2 (*3*), 3 (*4*), and 4 (*5*); $T_0=4.2$ K.

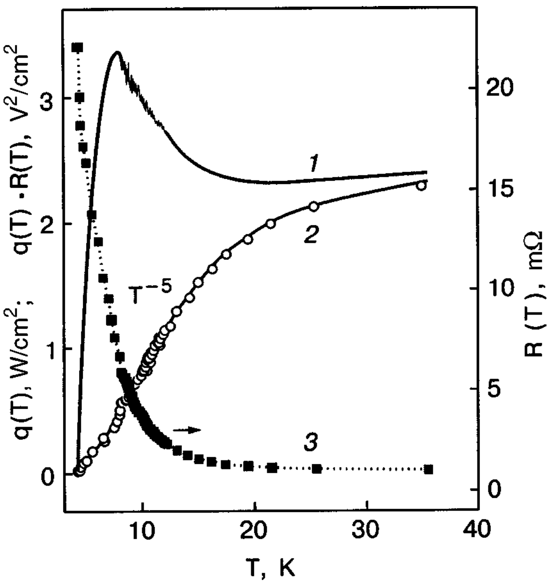

FIG. 5. Temperature dependence of the functions $[qR](T)$ (*1*), $q(T)$ (*2*), and $R(T)$ (*3*) for the I–V characteristic of a polycrystalline tin slab in a medium of crystalline sulfur in a magnetic field of 5 T.

that the relations $R < -dU/dI$ and $RC > [c_V(T)/q(T)]$ be satisfied. The value of $c_V(T)/q(T)$ does not exceed 10^{-3} s.

Let us conclude with a summary of the results of this study. We have for the first time obtained nonlinear current–voltage characteristics of thin polycrystalline samples of a metal (pure tin) in a magnetic field at helium temperatures in the absence of a liquid boiling crisis at the boundary of the sample for different types of heat removal. It was found that the use of a crystalline dielectric as the heat-removal medium makes it possible to realize a nonlinear conduction regime corresponding to an S-shaped I–V characteristic in a pure compensated metal in a magnetic field of up to 5 T. In that regime we studied the dynamics of the observed temperature–electric instability in relation to the reactive parameters of the circuit.

*E-mail: logvinov@ilt.kharkov.ua

---

[1] A. A. Slutskin and A. M. Kadigrobov, JETP Lett. **28**, 201 (1978).

[2] Yu. N. Chiang and A. G. Ordynets, Fiz. Nizk. Temp. **6**, 1279 (1980) [Sov. J. Low Temp. Phys. **6**, 622 (1980)].

[3] I. I. Logvinov and Yu. N. Chiang, Fiz. Nizk. Temp. **21**, 867 (1995) [Low Temp. Phys. **21**, 668 (1995)].

[4] A. M. Kadigrobov, A. A. Slutskin, and I. V. Krivosheĭ, Zh. Éksp. Teor. Fiz. **87**, 1314 (1984) [Sov. Phys. JETP **60**, 754 (1984)].

[5] W. Frost (Ed.), *Heat Transfer at Low Temperatures*, Plenum Press, New York (1975), Mir, Moscow (1977).

[6] V. A. Bondar', A. M. Kadigrobov, V. N. Morgun, and N. N. Chebotaev, Metallofizika **13**, 49 (1991).

[7] Yu. N. Tszyan (Chiang) and I. I. Logvinov, Fiz. Nizk. Temp. **8**, 774 (1982) [Sov. J. Low Temp. Phys. **8**, 388 (1982)].

[8] Yu. N. Tszyan (Chiang), I. I. Logvinov, and A. M. Kadigrobov, Fiz. Nizk. Temp. **12**, 1248 (1986) [Sov. J. Low Temp. Phys. **12**, 702 (1986)].

Translated by Steve Torstveit

LOW TEMPERATURE PHYSICS VOLUME 29, NUMBER 4 APRIL 2003

LOW-DIMENSIONAL AND DISORDERED SYSTEMS

Influence of magnetoelastic coupling on the formation of a spatially inhomogeneous phase in two-dimensional ferromagnets

Yu. A. Fridman,* D. V. Spirin, and Ph. N. Klevets

V. I. Vernadskii Tavricheskii National University, ul. Yaltinskaya 4, 95007 Simferopol, Ukraine

(Submitted June 20, 2002; revised August 5, 2002)
Fiz. Nizk. Temp. **29**, 418–423 (April 2003)

The influence of magnetoelastic coupling on the existence region of a spatially inhomogeneous state in a two-dimensional anisotropic ferromagnet is investigated. The phase transitions to the spatially inhomogeneous state under the influence of magnetic field and upon a change in the single-ion anisotropy constant are examined. It is shown that the magnetoelastic coupling enlarges the existence region of this phase substantially and also increases the domain width. © *2003 American Institute of Physics.* [DOI: 10.1063/1.1542475]

1. INTRODUCTION

The magnetic properties of ultrathin films have been the subject of many papers.[1–12] Such systems are of interest in connection with their possible application in microelectronics, engineering, and laser physics. Because these objects are truly two-dimensional (the films are 1–10 atomic layers thick), their theoretical and experimental study can shed light on some fundamental questions of the physics of magnetism of low-dimensional systems.

Numerous studies have shown that both temperature-induced[1,3–5] and magnetic-field-induced[1] phase transitions can occur in ultrathin magnetic films. Both spatially homogeneous states[1–10] and an inhomogeneous phase[1] can be realized. The inhomogeneous phase appears primarily as a result of dipole–dipole coupling. The role of dipole–dipole coupling in two-dimensional systems is discussed in detail in Ref. 11.

It is well known[5,12,13] that in the vicinity of phase transitions the dynamics of a system is influenced substantially by the magnetoelastic coupling, which leads to both dynamic effects (softening of the corresponding branch of elastic excitations) and static effects (the formation of a striction gap in the spectrum of magnetic excitations). However, in our view the influence of magnetoelastic coupling on the phase transitions mentioned above has not been studied sufficiently.

As the object of study we chose a monolayer magnetic film not bonded to a substrate.[12] The film has single-ion anisotropy of the easy-axis type, with its axis of easy magnetization perpendicular to the film plane. The system is in a uniform external magnetic field applied parallel to the film plane. In addition, we shall take the magnetoelastic coupling into account with the assumption that the strains are planar.[14]

In this paper we consider phase transitions to a spatially inhomogeneous state under the influence of both magnetic field and changes in the material constants. The latter means that phase transitions can occur even in the absence of magnetic field, being induced, for example, by a change in the value of the single-ion anisotropy. Such a change may be brought about by an increase in temperature, for example.

2. PHASE TRANSITIONS IN MAGNETIC FIELD

We assume that the magnetic field is parallel to the OY axis and that the film plane is XOY. We consider a ferromagnet with single-ion anisotropy of the easy-axis type, the easy axis being perpendicular to the film plane. The Hamiltonian of such a system can be written in the form

$$\begin{aligned} H = & -\frac{1}{2}\sum_{\substack{n,n'\\ i,j=x,y,z}} [J(n-n')\delta_{ij}+V^{ij}(n-n')]S_n^i S_{n'}^j, \\ & -H\sum_n S_n^y - \frac{\beta}{2}\sum_n (S_n^z)^2 + \lambda \sum_{\substack{n\\ i,j=x,y}} S_n^i S_n^j u_{ij} \\ & + \frac{E}{2(1-\sigma^2)}\sum [u_{xx}^2+u_{yy}^2+2\sigma u_{xx}u_{yy} \\ & +2(1-\sigma^2)u_{xy}^2], \end{aligned} \tag{1}$$

where S_n^i is the ith component of the spin operator at site n; $J(n-n')$ is the exchange interaction parameter, H is the external magnetic field in energy units, β is the single-ion anisotropy, λ is the magnetoelastic coupling constant, u_{ij} are the components of the elastic strain tensor, E is Young's modulus, σ is Poisson's ratio, and $V^{ij}(n-n')$ are the components of the magnetic dipole interaction tensor, the Fourier transforms of which have the form[11]

$$V^{xx}(k) = \frac{A_0}{3} - k\Omega_0 \cos^2\varphi,$$

$$V^{yy}(k) = \frac{A_0}{3} - k\Omega_0 \sin^2\varphi,$$

$$V^{zz}(k) = -\frac{2A_0}{3} + k\Omega_0,$$

$$V^{xy}(k) = -\frac{k\Omega_0}{2}\sin 2\varphi, \quad V^{xz}(k) = V^{yz}(k) = 0,$$

1063-777X/2003/29(4)/4/$24.00

$$A_0=\frac{2}{3}(g\mu_B)^2\sum R^{-3},\quad \Omega_0=\frac{2\pi(g\mu_B)^2}{a^2}.$$

Here we have introduced the following notation: g is the gyromagnetic ratio, μ_B is the Bohr magneton, a^2 is the "volume" of the two-dimensional unit cell, and φ is the angle between the direction of the wave vector $\mathbf{k}$ and the OX axis. The two-dimensionality of the system is taken into account in the calculation of the components of the magnetic dipole interaction tensor. In addition, the wave vector $\mathbf{k}$ is a two-component vector lying in the film plane.

In the case of low fields $H<\beta$ the system will be found in a canted phase, i.e., the magnetization vector makes an angle θ with the anisotropy axis.

We rotate the coordinate system so as to bring the quantization axis (the OZ axis) into coincidence with the direction of the magnetic moment. The components of the strain tensor are written in the form $u_{ij}=u_{ij}^{(0)}+u_{ij}^{(1)}$, where $u_{ij}^{(0)}$ are the spontaneous strains and $u_{ij}^{(1)}$ is the dynamic part of the strain tensor, which describes the vibrations of the crystal lattice sites.

The spontaneous strains are determined from the condition that the free energy density be minimum and in the present case take the form

$$u_{xx}^{(0)}=\frac{\lambda S^2\sigma}{E}\sin^2\theta,$$

$$u_{yy}^{(0)}=-\frac{\lambda S^2}{E}\sin^2\theta, \tag{2}$$

$$u_{xy}^{(0)}=0,$$

where S is the magnitude of the spin of the magnetic ion.

The components of the tensor $u_{ij}^{(1)}$ are related to the creation operator $b_{k,\nu}^{+}$ and annihilation operator $b_{k,\nu}$ for phonons of polarization ν by the following relation:[15]

$$u_{ij}^{(1)}=\frac{i}{2}\sum_{\mathbf{k},\nu}\frac{1}{\sqrt{2m\omega_\nu(k)}}[b_{\mathbf{k},\nu}e^{i\mathbf{k}\cdot\mathbf{r}}-b_{\mathbf{k},\nu}^{+}e^{-i\mathbf{k}\cdot\mathbf{r}}]\cdot[e_\nu^i k_j+e_\nu^j k_i], \tag{3}$$

where m is the mass of the magnetic ion, $\omega_\nu(k)=c_\nu k$ is the spectrum of noninteracting phonons, and $\mathbf{e}_\nu$ is the polarization unit vector of the phonons. In what follows we will be considering a transversely polarized acoustic wave.

Using the Holstein–Primakoff transformation for the spin operators[16] and the representation (3) for the elastic vibrations, we write the Hamiltonian (1) in terms of the phonon and magnon creation and annihilation operators:

$$\mathcal{H}=\sum_k\Big[A_{1k}a_k^{+}a_k+A_{2k}b_k^{+}b_k+\frac{1}{2}(B_{1k}a_k^{+}a_{-k}^{+}+B_{1k}^{*}a_{-k}a_k)+C_k(b_k^{+}a_{-k}^{+}+b_k^{+}a_k)+C_k^{*}(a_k^{+}b_k+b_{-k}a_k)\Big], \tag{4}$$

where a_k^{+}, a_k, b_k^{+}, and b_k are the Fourier transforms of the magnon and phonon creation and annihilation operators, respectively,

$$A_{1k}=H\sin\theta+\frac{\beta S}{2}(2\cos^2\theta-\sin^2\theta)-\frac{S}{2}\left(\frac{A_0}{3}+\frac{A_0}{3}\cos^2\theta+\frac{4A_0}{3}\cos 2\theta-k\Omega_0\cos 2\theta\right)+\frac{\lambda^2S^3\sin^2\theta}{E}(2\sin^2\theta-\cos^2\theta+\sigma)+\alpha Sk^2,$$

$$A_{2k}=\omega_t(k), \tag{5}$$

$$B_{1k}=B_{1k}^{*}=\frac{\beta S}{2}\sin^2\theta-\frac{S}{2}(A_0\sin^2\theta+k\Omega_0\cos 2\theta)+\frac{\lambda^2S^3\sin^2\theta}{E}(\cos^2\theta+\sigma),$$

$$C_k=-\frac{i\lambda S\sqrt{Sk}\sin\theta}{2\sqrt{mc_t}},$$

$\alpha=J_0R_0^2$, R_0 is the radius of the exchange interaction, and c_t is the velocity of transverse sound.

In the general case the quantities appearing in Eq. (5) depend on the direction of the wave vector, i.e., on the angle φ. However, it can be shown that the lowest value of the field of the phase transition from the canted phase (and the highest value of the field at the transition from the in-plane phase) is obtained for $\varphi=\pi/2$. This is the case that we shall consider below.

In the Hamiltonian (4) we have taken into account that the coefficient of the terms linear in the creation and annihilation operators is equal to zero:

$$H-S(\beta-A_0)\sin\theta+\frac{2\lambda^2S^3}{E}\sin^3\theta=0. \tag{6}$$

The solution of this equation makes it possible to determine the angle θ as a function of the external field and the material constants. Solving this equation by perturbation theory, we obtain

$$\sin\theta=\frac{H}{S(\beta-A_0)}+\frac{b_0H^3}{S^3(\beta-A_0)^4},\quad b_0=\frac{2\lambda^2S^2}{E}. \tag{7}$$

The Hamiltonian (4) is reduced to diagonal form by the standard $u-v$ transformation:[16]

$$H^{(2)}=E_0+\sum_k[\omega_1(k)\alpha_k^{+}\alpha_k+\omega_2(k)\beta_k^{+}\beta_k], \tag{8}$$

where E_0 is the energy of the zero-point vibrations, $\omega_i(k)$ is the energy of the ith branch of coupled magnetoelastic waves, which is determined from the equation

$$\begin{vmatrix} A_{1k}-\omega & B_{1k} & C_k & C_k \\ B_{1k} & A_{1k}+\omega & C_k^{*} & C_k^{*} \\ C_k^{*} & C_k & A_{2k}-\omega & 0 \\ C_k^{*} & C_k & 0 & A_{2k}+\omega \end{vmatrix}=0. \tag{9}$$

Hence

$$\omega_{1,2}^2=\frac{1}{2}\{A_{1k}^2-B_{1k}^2+\omega_t^2 \pm\sqrt{(A_{1k}^2-B_{1k}^2-\omega_t^2)^2+16|C_k|^2\omega_t(A_{1k}+B_{1k})}\}. \tag{10}$$

The plus sign corresponds to the quasimagnon branch of excitations, and the minus sign to the quasiphonon branch. Vanishing of the frequency (10) is a sign of a phase transition. After a number of straightforward manipulations we obtain the equation for the phase transition line:

$$\omega_t(A_{1k}-B_{1k})-4|C_k|^2=0. \tag{11}$$

Making use of the definition of the transverse sound velocity[14]

$$c_t^2=\frac{E}{2m(1+\sigma)}$$

we obtain from Eq. (11)

$$H\sin\theta+S(\beta-A_0)\cos 2\theta-b_0S\sin^2\theta(2\cos^2\theta+\sigma) +k\Omega_0S\cos 2\theta+\alpha Sk^2=0. \tag{12}$$

From Eq. (12) it is easy to find the value of the wave vector that determines the domain width:

$$k_1^*=-\frac{\Omega_0\cos 2\theta}{2\alpha}. \tag{13}$$

The transition from the canted to the inhomogeneous phase occurs at an angle θ close to $\pi/2$, in which case $\cos 2\theta<0$ and $k_1^*>0$. Solving Eq. (12) using perturbation theory, we obtain the field of the transition from the canted to the inhomogeneous phase:

$$H_1=S(\beta-A_0)-\frac{b_0S}{2}(3+\sigma)-\frac{\Omega_0^2S}{8\alpha}. \tag{14}$$

Since we are assuming that the energies of the single-ion anisotropy and external magnetic field are much larger than the magnetic dipole and magnetoelastic coupling parameters, we easily obtain from (10) the following expressions for the quasiphonon spectrum:

$$\omega_1^2(k)=\omega_t^2(k)\left(1-\frac{b_0S(1+\sigma)\sin^2\theta}{H\sin\theta+S(\beta-A_0)\cos 2\theta-b_0S\sin^2\theta\cos 2\theta+k\Omega_0S\cos 2\theta+\alpha Sk^2}\right) \tag{15}$$

and quasimagnon spectrum

$$\omega_2^2(k)=[H\sin\theta+S(\beta-A_0)\cos 2\theta-b_0S\sin^2\theta\cos 2\theta +k\Omega_0S\cos 2\theta+\alpha Sk^2][H+S(\beta-A_0)\cos^2\theta +b_0S\sin^2\theta(\sin^2\theta+\sigma)+\alpha Sk^2]. \tag{16}$$

From $H=H_1$ the quasiphonon spectrum softens:

$$\omega_1^2(k)=\omega_t^2(k)\frac{\alpha k^2}{b_0},$$

while at the same time a magnetoelastic gap appears in the quasimagnon spectrum:

$$\omega_2(0)=S\sqrt{b_0(\beta-A_0)}.$$

It should be noted that taking the magnetoelastic coupling into account leads to a weak renormalization of the magnon velocity. The corresponding terms in Eq. (16) are dropped, since the change in velocity is not more than 0.1%. For the same reason, we have neglected the analogous term in the denominator of Eq. (13).

The value of $1/k_1^*$ determines the domain width.[1] In our case, for typical values of the parameters E, λ, β, A_0, Ω_0, and σ (Refs. 1, 7, and 17), an estimate gives $k_1^*\approx 3\times 10^5$ cm^{-1} and $1/k_1^*\approx 3\times 10^{-6}$ cm.

Let us now consider the case when the external magnetic field is large, and, as a result, the magnetic moment of the system lies along the field direction. We shall call this the "in-plane" phase, since the magnetic moment lies in the film plane. As the magnetic field is decreased, a phase transition will occur. As was shown in Ref. 1, this transition is to a phase with a spatially inhomogeneous distribution of the magnetization.

Since in the in-plane phase the angle $\theta=\pi/2$, the transition field can be found from (12):

$$H_2=S(\beta-A_0)+b_0S\sigma+\frac{\Omega_0^2S}{4\alpha}. \tag{17}$$

Instability arises for

$$k_2^*=\frac{\Omega_0}{2\alpha}. \tag{18}$$

We note that the domain width in this geometry is somewhat smaller than for the transition from the canted phase ($k_1^*\approx 3.5\times 10^5$ cm^{-1}, and $1/k_1^*\approx 2.86\times 10^{-6}$ cm, i.e., for the transition from the easy-plane phase to the inhomogeneous phase its value is 5% less than for the transition from the canted to the inhomogeneous phase).

The quasiparticle spectra are easily obtained by substituting $\theta=\pi/2$ into Eqs. (15) and (16).

The existence region of the spatially inhomogeneous phase can be determined from Eqs. (14) and (17):

$$\Delta H=H_2-H_1=\frac{3}{2}\left[\frac{\Omega_0^2S}{4\alpha}+b_0S(1+\sigma)\right]. \tag{19}$$

3. PHASE TRANSITIONS IN MATERIAL CONSTANTS

Let us examine the phase transitions that occur in a two-dimensional ferromagnet in the absence of external magnetic field. The ferromagnet under consideration is assumed to have single-ion anisotropy of the easy-axis type, with the axis of anisotropy perpendicular to the film plane. Such a system can have phase transitions upon a change in the anisotropy: the presence of a magnetic dipole interaction gives rise to an effective anisotropy of the easy-plane type, which can compete with the easy-axis anisotropy. The value of the latter can vary as a function of temperature, pressure, impurity concentration, etc.[18]

Let us consider the region of values of the anisotropy constant β close to the magnetic dipole interaction parameter A_0. Let the easy-axis anisotropy be such that a phase with magnetization perpendicular to the film plane is realized ($\beta > A_0$). If the OZ axis is chosen along the magnetization vector (XOY is the film plane), the Hamiltonian of the system is the same as (1) if $H=0$.

It is easy to show that there are no spontaneous strains for such a system, and hybridization of the magnetic and elastic excitations does not occur. The value of the anisotropy at which the phase transition from the easy-axis phase occurs is determined from the condition that the gap in the magnon spectrum vanish:

$$\beta_1 = A_0. \tag{20}$$

Let us consider the question of the whether a canted phase exists in such a model. In this case Eq. (6) takes the form

$$-S(\beta - A_0)\sin\theta + \frac{2\lambda^2 S^3}{E}\sin^3\theta = 0. \tag{21}$$

It follows from Eq. (21) that for $\beta < A_0$ there is a single solution $\theta = 0$. Thus a canted phase is not realized in the system (in the absence of magnetic field).

We shall now find the value of the anisotropy at which the phase transition from the in-plane phase to the inhomogeneous state occurs. For this it is clearly sufficient to set $H=0$ in Eq. (17), and then

$$\beta_2 = A_0 - b_0\sigma - \frac{\Omega_0^2}{4\alpha}. \tag{22}$$

The existence region of the inhomogeneous phase is determined from Eqs. (20) and (22):

$$\Delta\beta = b_0\sigma + \frac{\Omega_0^2}{4\alpha}. \tag{23}$$

4. INFLUENCE OF MAGNETOELASTIC COUPLING ON THE FORMATION OF INHOMOGENEOUS STRUCTURES

As a result of the studies done we can state that the magnetoelastic coupling has a substantial influence on the formation of the spatially inhomogeneous phase. This influence is manifested in two ways. First, in enhancement of the mass of the quasimagnons. This effect is reflected in a slight decrease of the domain width (by less than 0.1%).

In addition, hybridization of the magnon and phonon excitations has some substantial effects. It results in a phase transition on the quasiphonon branch of excitations, and the existence region of the spatially inhomogeneous structure is enlarged. Numerical estimates for typical values of the parameters E, λ, β, A_0, Ω_0, and σ (Refs. 1, 7, and 17) give $\Delta\beta \approx 25$ Oe and $\Delta H \approx 40$ Oe. Taking the magnetoelastic coupling into account leads to an increase of $\Delta\beta$ by approximately 4% and of ΔH by 10%. Such a change can be considered unimportant if the value of the magnetoelastic energy H_{me} is negligible compared to the anisotropy energy H_a or dipole energy H_{dd}: we assume that $H_{me} \approx 3$ Oe, while $H_a \approx 100$ kOe and $H_{dd} \approx 14$ kOe. It should be noted that in the geometry considered here the magnetic subsystem interacts actively with the transversely polarized phonon mode and practically not at all with the longitudinally polarized mode (the magnetoelastic coupling only renormalizes the longitudinal sound velocity slightly).

Thus, along with the dipole–dipole interaction, the magnetoelastic coupling plays a substantial role in the formation of magnetic spatially inhomogeneous structures in two-dimensional ferromagnets.

[*] E-mail: frid@tnu.crimea.ua

---

[1] R. P. Erickson and D. L. Mills, Phys. Rev. B **46**, 861 (1992).
[2] Y. Yafet, J. Kwo, and E. M. Gyorgy, Phys. Rev. B **33**, 6519 (1986).
[3] D. P. Pappas, K.-P. Kämper, and H. Horster, Phys. Rev. Lett. **64**, 3179 (1990).
[4] Y. Millev and J. Kirschner, Phys. Rev. B **54**, 4137 (1996).
[5] Yu. A. Fridman, D. V. Spirin, and C. N. Alexeyev, J. Magn. Magn. Mater. **234**, 174 (2001).
[6] D. Pescia, M. Stampanoni, G. L. Bona, A. Vaterlaus, R. F. Willis, and F. Meier, Phys. Rev. Lett. **58**, 2126 (1987).
[7] P. Bruno, Phys. Rev. B **43**, 6015 (1991).
[8] J. J. Krebs, B. T. Jonker, and G. A. Prinz, J. Appl. Phys. **63(8)**, 3467 (1998).
[9] A. Hucht and K. D. Usadel, Phys. Rev. B **55**, 12309 (1997).
[10] A. Moschel and K. D. Usadel, Phys. Rev. B **51**, 16111 (1995).
[11] S. V. Maleev, Zh. Éksp. Teor. Fiz. **70**, 2374 (1976) [Sov. Phys. JETP **43**, 1240 (1976)].
[12] B. A. Ivanov and E. V. Tartakovskaya, JETP Lett. **63**, 835 (1996).
[13] A. I. Akhiezer, V. G. Bar'yakhtar, and S. V. Peletminskii, *Spin Waves*, North-Holland, Amsterdam (1968), Nauka, Moscow (1967).
[14] L. D. Landau and E. M. Lifshitz, *Theory of Elasticity*, Pergamon Press, Oxford (1996), Nauka, Moscow (1987).
[15] L. D. Landau and E. M. Lifshitz, *Statistical Physics*, Pergamon Press, Oxford (1980), Nauka, Moscow (1976).
[16] V. G. Bar'yakhtar, V. N. Krivoruchko, and D. A. Yablonskiĭ, *Green's Functions in the Theory of Magnetism* [in Russian], Naukova Dumka, Kiev (1984).
[17] E. A. Turov, A. A. Lugovoĭ, V. V. Buchel'nikov, Yu. A. Kuzavko, V. G. Shavrov, and O. V. Yan, Fiz. Met. Metalloved. **66**, 12 (1989).
[18] S. Chikazumi, *Physics of Ferromagnetism*, 2nd ed., Clarendon Press, Oxford (1997), Mir, Moscow (1987).

Translated by Steve Torstveit

LOW TEMPERATURE PHYSICS VOLUME 29, NUMBER 4 APRIL 2003

Quantum interferometry and spin–orbit effects in a heterostructure with a 2D hole gas in a $Si_{0.2}Ge_{0.8}$ quantum well

V. V. Andrievskiĭ, A. Yu. Rozheshchenko, and Yu. F. Komnik*

B. Verkin Institute for Low Temperature Physics and Engineering, National Academy of Sciences of Ukraine, pr. Lenina 47, 61103 Kharkov, Ukraine

M. Myronov, O. A. Mironov, and T. E. Whall

Department of Physics, University of Warwick, Coventry CV4 7AL, UK

(Submitted August 2, 2002)
Fiz. Nizk. Temp. **29**, 424–431 (April 2003)

The magnetic-field dependence (up to 110 kOe) of the resistance of $Si_{0.7}Ge_{0.3}/Si_{0.2}Ge_{0.8}/Si_{0.7}Ge_{0.3}$ with a 2D hole gas in a $Si_{0.2}Ge_{0.8}$ quantum well is measured in the temperature range 0.335–10 K and in a range of variation of the currents from 100 nA to 50 μA. Shubnikov–de Haas oscillations are observed in the region of high magnetic fields, and in the low-field region $H \leqslant 1$ kOe a positive magnetoresistance is observed which gives way to a negative magnetoresistance as the field is increased. This peculiarity is explained by effects of weak localization of the 2D charge carriers under conditions when the spin–orbit scattering time τ_{so} is close to the inelastic scattering time τ_φ, and it is evidence of a splitting of the spin states under the influence of a perturbing potential due to the formation of a two-dimensional potential well (the Rashba mechanism). Analysis of the weak localization effects gave the values of the characteristic relaxation times as $\tau_\varphi = 7.2T^{-1} \times 10^{-12}$ s and $\tau_{so} = 1.36 \times 10^{-12}$ s. From these characteristics of the heterostructure studied, a value of $\Delta = 2.97$ meV was obtained for the spin splitting. © *2003 American Institute of Physics.* [DOI: 10.1063/1.1542476]

INTRODUCTION

The study of quantum interference and quantum oscillation effects in heterojunctions yields information about the characteristics of the charge carriers in two-dimensional electron systems. In some cases the behavior of the magnetoresistance of inversion layers in heterostructures in weak magnetic fields[1–4] attests to the existence of appreciable spin–orbit scattering, which has been linked to a lifting of the spin degeneracy in zero magnetic field in the absence of inversion symmetry in the crystal[5] or under the influence of an asymmetric electric field which forms a two-dimensional structure.[6] The lifting of the spin degeneracy in zero magnetic field leads to the formation of two electronic subsystems with nearly the same characteristic parameters. The existence of spin splitting in such objects has been confirmed by the finding of two effective masses for the charge carriers by the cyclotron resonance technique,[7] and also by the observation of beats of the Shubnikov–de Haas oscillations in different heterostructures.[8–13] The concepts of spin splitting have been used successfully to explain the positive magnetoresistance at low magnetic fields in the weak localization effect.[2–4]

In this paper we present the results of a study of weak localization effects and the interaction of charge carriers in a $Si_{0.7}Ge_{0.3}/Si_{0.2}Ge_{0.8}/Si_{0.7}Ge_{0.3}$ heterostructure, which exhibits its spin–orbit effects (unlike the $Si/Si_{1-x}Ge_x/Si$ heterostructures with $x = 0.13$ and 0.36 studied previously,[14,15] for which the spin–orbit effects could be neglected). This study included the investigation and analysis of the variation of the magnetoresistance at low and high magnetic fields (up to 110 kOe) in the temperature range 0.335–10 K for transport currents varying from 100 nA to 50 μA. The results made it possible to determine the following:

— the values of the effective mass m^* and quantum time τ_q of the charge carriers, on the basis of an analysis of the change in amplitude of the Shubnikov–de Haas oscillations upon a change in magnetic field and temperature;

— the temperature dependence of the dephasing time τ_φ and the spin–orbit scattering time τ_{so} by extracting the quantum corrections to the conduction, which are manifested in temperature and magnetic-field dependence of the conductivity;

— the temperature dependence of the electron–phonon relaxation time τ_{eph}, with the use of the electron overheating effect;

— the splitting Δ of the spin states, on the basis of data for the spin–orbit interaction time.

The simultaneous observation of Shubnikov–de Haas oscillations (which are ordinarily manifested only in pure and perfect samples) and quantum interference effects (the observation of which requires a rather high level of elastic scattering) in the same sample turns out to be entirely possible, as was noted in Refs. 14 and 15, since these effects are manifested at different values of the magnetic fields. The weak localization effect and electron interaction effects are manifested at low magnetic fields, where the magnetic length $L_H = (\hbar c/2eH)^{1/2}$ should be larger than the mean free path l. (The length L_H corresponds to the field value for which an area $2\pi L_H^2$ is threaded by one magnetic flux quantum $\Phi_0 = hc/2e$.) As the magnetic field is increased, the inequality $L_H < l$ comes to be satisfied, and magnetic quantization ef-

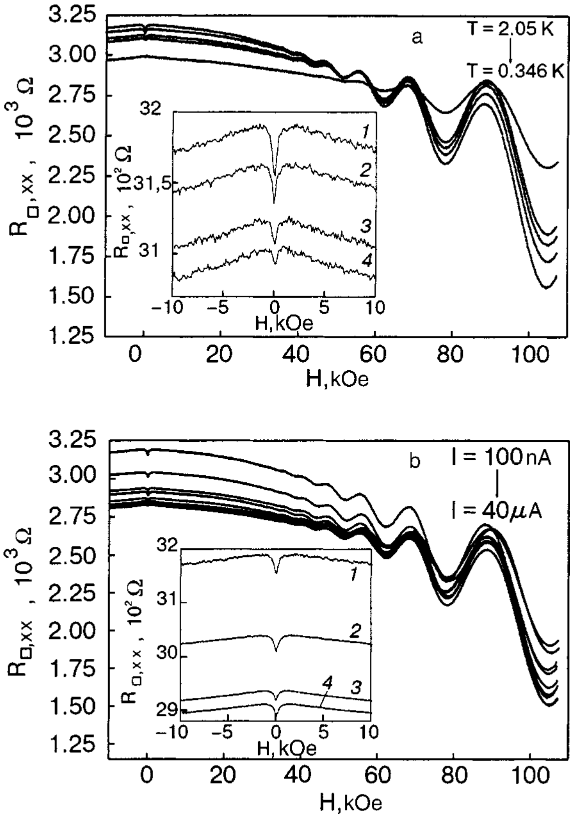

FIG. 1. Magnetic-field curves of the resistance $R_{\square}$ at different temperatures (a) and currents (b). a — $I=100$ nA, T [K]: 205, 1.738, 1.44, 0.754, 0.346. The inset shows the region of low magnetic fields for different T [K]: 0.36 (*1*), 0.754 (*2*), 1.44 (*3*), 1.738 (*4*). b — $T\approx 0.35$ K, currents: 100 nA, 300 nA, 1 μA, 2 μA, 5 μA, 10 μA, 15 μA, 28 μA, 40 μA. In the inset $I=100$ nA (*1*), 300 nA (*2*), 1 μA (*3*), 2 μA (*4*).

fects such as Shubnikov–de Haas oscillations can appear. An estimate of the mean free path in the sample gives a value $l\approx 300$ Å. This value of l and, accordingly, of L_H, corresponds to a magnetic field $H=3.6$ kOe. Analysis of weak localization effects can be carried out at fields less than that value.

1. EXPERIMENTAL RESULTS

The object of study was a $Si_{0.7}Ge_{0.3}/Si_{0.2}Ge_{0.8}/Si_{0.7}Ge_{0.3}$ heterostructure obtained by molecular-beam epitaxy; a quantum well is formed in the $Si_{0.2}Ge_{0.8}$ region, which is 10 nm wide.[1)]

The carriers (holes) appear in the quantum well from a boron-doped layer located a distance ~10 nm from the well. From a crystallographic standpoint such a structure is a stressed pseudomorphic heterostructure. The stressed state is due primarily to the 4% difference in the lattice constants of germanium and silicon (5.65 and 5.43 Å, respectively). The electronic properties of the heterostructure are determined by the two-dimensional electron gas filling the potential well. The conducting region had a "double cross" configuration in the form of a narrow strip ~0.55 mm wide and ~2.25 mm long, with a distance of ~1.22 mm between the two pairs of narrow potential leads.

Figure 1 shows recordings of the magnetic-field-induced variation of the diagonal component of the sheet resistance (resistance per square) of the sample at different temperatures (Fig. 1a) and current values (Fig. 1b). The amplitude of the Shubnikov–de Haas oscillations decreases with increasing temperature and current. In the low-field region positive magnetoresistance is observed (see the inset to Fig. 1), with a characteristic initial segment of steep growth followed by a maximum and then a slow decline down to negative values. This form of the magnetoresistance curves is characteristic for the weak localization effect[16–20] under conditions such that τ_φ and τ_{so} are close in value. It is seen in the insets in Fig. 1 that the height of the maximum (above the zero-field value of the resistance) decreases rapidly with increasing temperature and current growth.

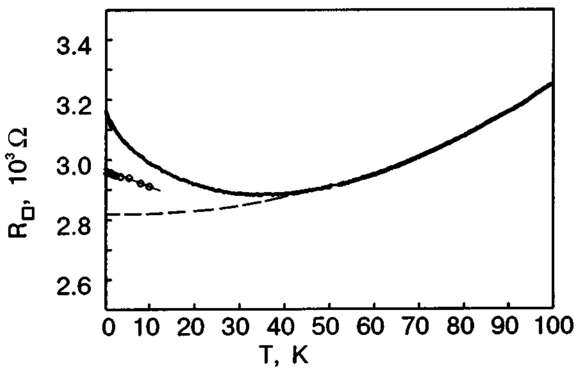

FIG. 2. Temperature dependence of the resistance $R_{\square}$. The solid curve shows the experimental data; the data points are the calculated values of the quantum correction due to the weak localization effect for the values of τ_φ and τ_{so} obtained from an analysis of the magnetoresistance curves. The dashed curve is the assumed temperature dependence of the "classical" resistance.

The temperature variation of the resistance of the sample in zero magnetic field (Fig. 2) confirms the assumption that one is seeing a manifestation of effects of weak localization and quasiparticle interaction: the minimum and the increase of the resistance with decreasing temperature T are due to the contribution of quantum corrections to the conductivity, which grow as the temperature is lowered.[18,21]

2. CALCULATION OF THE CHARACTERISTIC PARAMETERS OF THE CHARGE CARRIERS

The heterostructure under study has a hole type of conductivity, and the structure of its valence band is therefore important. In pure silicon there are two degenerate maxima in the valence band at the point $k=0$, where two bands with different values of the curvature touch; the corresponding values of the effective mass m^* are $0.49m_0$ and $0.16m_0$. The valence bands in germanium have an analogous structure with $m^*=0.28m_0$ and $0.04m_0$.

The form of the Shubnikov–de Haas oscillations (Fig. 1) attests to the fact that they are formed by a single dominant type of charge carrier. The proposed spin splitting of the bands was not in any way reflected in the form of the oscillations. For this reason the analysis of the oscillatory curves can be done in the standard way.

It is known that the Shubnikov–de Haas oscillations are described by the relation

$$\frac{\Delta\rho_{xx}}{\rho_{xx}^{0}} \propto \frac{\psi}{\sinh\psi}\exp\left(-\frac{\pi\alpha}{\omega_c\tau}\right)\cos\left(\frac{2\pi\varepsilon_F}{\hbar\omega_c}-\Phi\right), \qquad (1)$$

where $\psi=2\pi^2kT/(\hbar\omega_c)$, $\omega_c=eH/m^*c$ is the cyclotron frequency, $\alpha=\tau/\tau_q$, τ is the transport time, τ_q is the quantum scattering time, and Φ is the phase. If the Fermi energy for the two-dimensional electron gas is written in the form $\varepsilon_F=\pi\hbar^2n/m^*$ (n is the concentration of electrons (holes)), then, knowing the change in amplitude of the oscillations upon changes of the temperature and magnetic field, we can determine the unknown parameters m^*, n, and τ_q. For example, having constructed the dependence of $\ln([\Delta\rho(T)/\rho(0)][\sinh\psi(T)/\psi(T)])$ on $(\omega_C\tau)^{-1}=(\mu H)^{-1}$ (where μ is the mobility), by fitting the experimental data to a single straight line we can find α and then determine τ_q, and having constructed the dependence of $\ln(\Delta\rho(H)/\rho(0))$ on $\ln(\psi(H)/\sinh\psi(H))-(\pi\alpha/\mu H)$ and plotting all the experimental data on a single straight line, we can find m^*. The resulting value $m^*=0.16m_0$ apparently corresponds to heavy holes in the heterostructure under study. This value will be used in the calculations below.

The carrier concentration p_{SdH} found in an analysis of the Shubnikov–de Haas oscillations equals 1.46×10^{12} cm^{-2}. It is close to the value $p_H=1.36\times10^{12}$ cm^{-2} obtained from measurements of the Hall coefficient.

The values m^* and p_H can be used to find the elastic scattering time from the electrical conductivity of the channel, which gives a value $\tau=0.147\times10^{-12}$ s, and the mean free path of the holes, $l=310$ Å, and also the Fermi velocity v_F, mobility μ, diffusion coefficient D, and Fermi energy ε_F, by making use of the relations for a two-dimensional system: $v_F=(\hbar/m)(2\pi p_2)^{1/2}$, $D=v_F^2\tau/2$, $\varepsilon_F=\pi\hbar^2p_2/m$. The following values are obtained: $v_F=2.11\times10^7$ cm/s, $\mu=1590$ cm^2/(V·s), $D=32.7$ cm^2/s, and $\varepsilon_F=20.35$ meV.

3. ANALYSIS OF THE QUANTUM CORRECTIONS

In a two-dimensional system the contribution of the weak localization effect to the temperature dependence of the conductivity is described by the relation[17,22]

$$\Delta\sigma_T=-\frac{e^2}{2\pi^2\hbar}\left[\frac{3}{2}\ln\frac{\tau_\varphi^*}{\tau}-\frac{1}{2}\ln\frac{\tau_\varphi}{\tau}\right], \tag{2}$$

where τ is the elastic relaxation time of the electrons, $\tau_\varphi^{-1}=\tau_{\varphi0}^{-1}+2\tau_s^{-1}$, $(\tau_\varphi^*)^{-1}=\tau_{\varphi0}^{-1}+{}^4/_3\tau_{so}^{-1}+{}^2/_3\tau_s^{-1}$, $\tau_{\varphi0}$ is the phase relaxation time due to inelastic scattering processes, τ_{so} is the spin–orbit scattering time, and τ_s is the time for spin–spin scattering on magnetic impurities (in the object studied here there is no spin–spin scattering, so the time τ_s can be neglected, and in that case $\tau_{\varphi0}\equiv\tau_\varphi$). One can go from the resistance to the quantum corrections to the conductivity with the aid of the relation $-\Delta\sigma_T(T)=[R(T)R_\square(T_{\min})]^{-1}$, where $R_\square$ is the resistance per square of the two-dimensional system, and $T_{\min}$ is the temperature at which the minimum of the function $R(T)$ is observed and the contribution of the corrections is negligible.

In a two-dimensional system in a perpendicular magnetic field the change of conductivity due to the weak localization effect is described by the relation[23]

$$\Delta\sigma_H^L=\frac{e^2}{2\pi^2\hbar}\left[\frac{3}{2}f_2\left(\frac{4eHD\tau_\varphi^*}{\hbar c}\right)-\frac{1}{2}f_2\left(\frac{4eHD\tau_\varphi}{\hbar c}\right)\right], \tag{3}$$

where $f_2(x)=\ln(x)+\psi(1/2+1/x)$, ψ is the logarithmic derivative of the Γ function, and $D=(1/2)v_F^2\tau$ is the electron (hole) diffusion coefficient. The characteristic field $H_0^L=\hbar c/4eD\tau_\varphi$ corresponds to a change of the form of the function $f_2(x)$ from quadratic to logarithmic. For analysis of the variation of the quantum correction in the magnetic field one can use the relation $-\Delta\sigma_H(H)=[R(H)-R(0)]\times[R(H)R_\square(0)]^{-1}$; here $-\Delta\sigma_H(H)$ reflects the change in the magnetoresistance.

A computer fitting of the theoretical dependence (3), which contains two unknown fitting parameters, τ_φ and τ_φ^*, to the experimental data for the magnetoresistance allows one to find the values of τ_φ and τ_φ^* and then τ_{so}. This sort of fitting has turned out to be the most successful when an additional term proportional to H^2 is introduced. We assume that this term reflects the contribution of a correction due to the hole–hole interaction in the Cooper channel and corresponds to a repulsion between quasiparticles. Such a correction to the conductivity has been identified for $Si_{0.64}Ge_{0.36}$ heterostructures with a quantum channel.[14] The expression for the correction in the Cooper channel is given in Refs. 18, 22, and 23:

$$\Delta\sigma_H^C=-\frac{e^2}{2\pi^2\hbar}\lambda_H^C\varphi_2(\alpha);\quad \alpha=\frac{2eDH}{\pi ckT}, \tag{4}$$

where λ_H^C is the coupling constant. The characteristic field $H_0^C=\pi ckT/2eD$ corresponds to a change in the functional dependence of $\varphi_2(\lambda)$ from quadratic to logarithmic. This allows us to use the quadratic approximation for $\Delta\sigma_H^C$ at low magnetic fields ($H<H_0^C$).

Taking the Cooper correction into account at the lowest temperatures and at low currents can explain the temperature behavior of the maximum that arises on the $\Delta\sigma(H)$ curve in the weak localization effect under conditions when the elastic scattering time τ_φ is close to the spin–orbit scattering time τ_{so}. The magnetic field $H_{\max}$ corresponding to the maximum is somewhat higher than the characteristic field H_0^L and should increase weakly with increasing temperature (as a consequence of the decrease of τ_φ and τ_φ^* with increasing T). The weak decrease of $H_{\max}$ observed in this study (see Fig. 1) is due to fact that the Cooper correction falls off with increasing temperature as $1/T^2$. A rough estimate of the coupling constant λ_H^C at the lowest temperature of the experiment and at low current is 0.023. It follows from the calculations that the temperature dependence $\tau_\varphi(T)$ at $T>3$ K is described by the relation $\tau_\varphi\simeq7.2T^{-1}\times10^{-12}$ s. This is close to the analogous temperature dependence $\tau_\varphi=6.6T^{-1}\times10^{-12}$ s for p-$Si/Si_{1-x}Ge_x/Si$ heterostructures with $x=0.13$ and 0.36.[14] A dependence of the form $\tau_\varphi\propto T^{-1}$ corresponds to the manifestation of electron–electron (in the present case hole–hole) scattering processes in disordered two-dimensional systems.[21,22] For the spin–orbit interaction time an average value of $\tau_{so}=1.36\times10^{-12}$ s is obtained.

Figure 3 shows the values obtained for τ_φ and τ_{so} as functions of temperature. The deviation of τ_φ from the relation $\tau_\varphi=7.2T^{-1}\times10^{-12}$ s at $T<3$ K is apparently due to the influence of spin effects. The positive magnetoresistance on the initial parts of the $R_\square(H)$ curve (Fig. 1) vanishes when the inequality $\tau_{so}<\tau_\varphi$ changes to the opposite, $\tau_{so}>\tau_\varphi$. Using the values found for the diffusion coefficient D and for

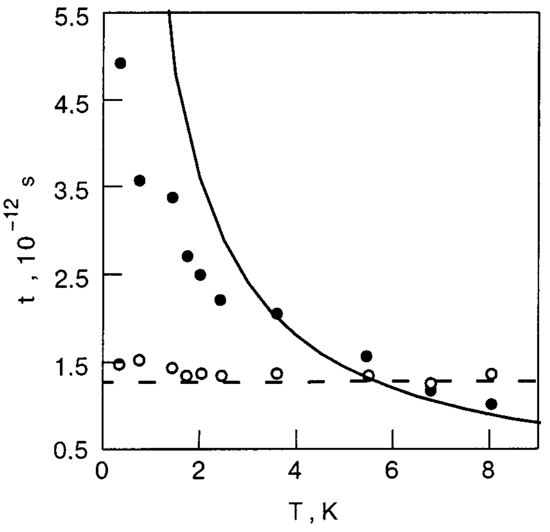

FIG. 3. Values of the dephasing time τ_φ (●) and spin–orbit scattering time τ_{so} (○) at different temperatures. The solid curve is a plot of $\tau_\varphi = 7.2T^{-1} \times 10^{-12}$ s.

$\tau_\varphi(T)$, we can estimate the characteristic fields H_0^L and H_0^C: at a temperature of 1 K they are 0.05 and 0.34 kOe, respectively. At magnetic fields exceeding these values by one or two orders of magnitude, the quantum corrections practically vanish, and the anomalous temperature dependence of the resistance vanishes accordingly.

We have satisfied ourselves that the values found for $\tau_\varphi(T)$ and τ_{s0} give a completely realistic description of the anomalous temperature dependence of the resistance of the sample (Fig. 2). The values calculated according to Eq. (2) for the localized correction $\Delta\sigma_T^L$ are shown by the data points in Fig. 2. The dashed curve reflects the assumed temperature variation of the "classical" resistance of the sample. It was obtained by extrapolating the functional dependence of the resistance on temperature from the region considerably above the minimum of the resistance. It is seen in Fig. 2 that a quantum correction due to the interaction in the Cooper channel is present in addition to the localization correction.

4. TEMPERATURE DEPENDENCE OF THE ELECTRON–PHONON SCATTERING TIME OF THE CHARGE CARRIERS

The electron–phonon interaction time $\tau_{e\mathrm{ph}}$ can be found with the aid of the electron overheating effect.[24] Under conditions of overheating the electron temperature T_e is elevated with respect to the phonon temperature T_{ph} under the influence of an electric field (current), and the transfer of excess energy from the electron to the phonon system is governed by the time $\tau_{e\mathrm{ph}}$. A necessary condition for realization of the electron overheating effect is the unimpeded escape of phonons from the conducting layer into the surrounding crystal. This requirement is clearly met in the sample studied here.

A comparison of the change in amplitude of the Shubnikov–de Haas oscillations upon an increase in temperature and an increase in current (Fig. 4) allows one to find the value of T_e at each specified value of the current (the arrows in Fig. 4).

The time $\tau_{e\mathrm{ph}}$ can be calculated with the aid of the heat balance equation, which implies the relation[25]

$$(kT_e)^2 = (kT_{\mathrm{ph}})^2 + \frac{6}{\pi^2}(eE)^2 D\tau_{e\mathrm{ph}}. \tag{5}$$

The electric field E is easily found from the values of the current I and resistance per square $R_\square$: $E = IR_\square/a$ (where a is the width of the conducting channel). The temperature of the crystal is used for T_{ph}. The values found for $\tau_{e\mathrm{ph}}$ with the use of Eq. (5) are referred to electron–phonon interaction temperatures $T_{e\mathrm{ph}}$ under conditions of electron overheating, where to a first approximation the estimate $T_{e\mathrm{ph}} = (1/2)(T_{\mathrm{ph}} + T_e)$ is valid.[15,26]

The observed temperature dependence observed of $\tau_{e\mathrm{ph}}$ has the form $\tau_{e\mathrm{ph}} = 1.1T^2 \cdot 10^{-8}$ and is close to the analogous dependence for Si/Si$_{0.7}$Ge$_{0.3}$/Si heterostructures.[15] A dependence $\tau_{e\mathrm{ph}}^{-1} \propto T^2$ is characteristic for two-dimensional electron systems[27] and is realized at low temperatures under conditions such that the wave momentum of the thermal phonon is sufficient to change the electron wave vector by the maximum amount $2k_F$.

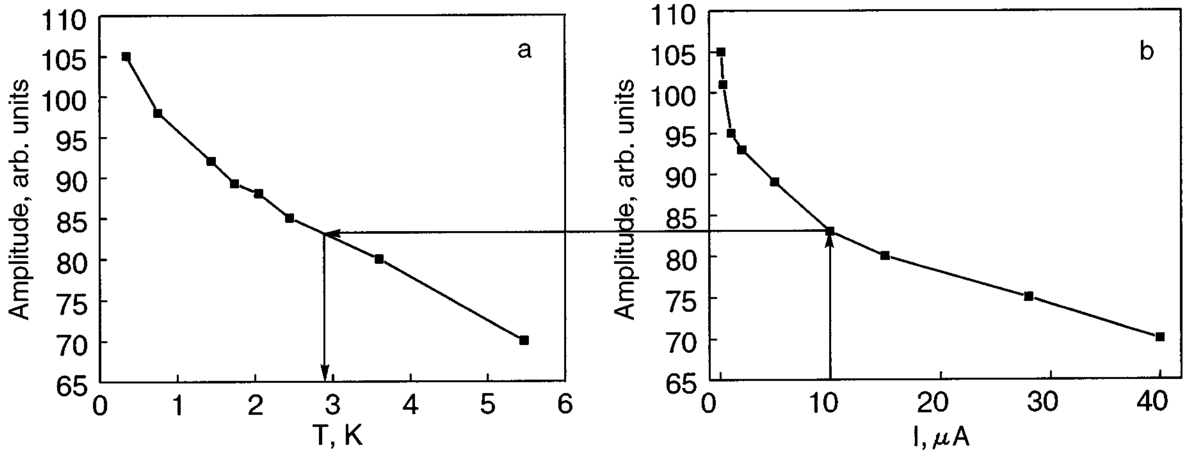

FIG. 4. Variation of the amplitude of the Shubnikov–de Haas oscillations as a function of temperature (a) and current (b).

It should be noted that it remains unclear why the resistance of the sample decreases so noticeably as the current is increased at zero magnetic field (see Fig. 1b): increasing the current from 100 nA to 10 μA leads to a decrease of $R_\square$ from 3150 Ω to 2850 Ω. The resistance remains unchanged as the current is increased further. It is seen in Fig. 4 that at a current of 10 μA the value of the overheating of the electron temperature is 3 K, which, according to Fig. 2, corresponds to a decrease of the resistance only to 3080 Ω. A probable cause of this disagreement might be the direct influence of the electric field on the quantum corrections. We note that the in-plane electric field in the two-dimensional structure was extremely small in these experiments, ranging from 0.066 V/cm at 100 nA to 0.65 V/cm at 10 μA.

The influence of electric field on the quantum localization correction has been considered in a number of theoretical papers.[25,28–32] According to Refs. 25, 31, and 32, a change in the value of the localization correction under the influence of electric field occurs only as a result of a change in the electron temperature (or the electron drift velocity). The absence of a direct influence of the electric field on the localization correction has been established in experiments on films of gold[33] and bismuth.[34] However, as was shown in Ref. 35, an electric field (with a strength of 10–30 V/cm) decreases the quantum correction due to the electron–electron interaction considerably, as a result of a decrease of the coupling constant λ. This decrease in λ is caused by a feature of the scattering in a two-dimensional electron system. In this conceptual framework the observed decrease of the resistance of the sample with increasing current in zero field, which is greater than the expected decrease of the resistance due to the electron overheating effect, is yet another indication of the presence of a contribution to the conductivity from the quantum correction due to the hole–hole interaction.

5. SPIN SPLITTING AND SPIN–ORBIT RELAXATION

Our analysis of the magnetoresistance curves of the $Si_{0.2}Ge_{0.8}$ quantum-well heterostructure has made it possible to determine the value of the spin splitting Δ on the basis of the value obtained for the spin–orbit scattering time τ_{so}.

The possibility of lifting the spin degeneracy in semiconductor crystals was first shown by Dresselhaus.[5] The cause of the lifting of the spin degeneracy in crystals lacking a center of inversion (in structures of the zinc blende, wurtzite, etc., types) is the asymmetric crystalline field. When the spin–orbit interaction is taken into account, the symmetry with respect to time inversion is broken. The value of the spin splitting is proportional to the cube of the wave vector, k^3 (the cubic Dresselhaus term). In Refs. 36–38 it was shown that the formation of a symmetric quantum well in such a crystal leads to additional lowering of its symmetry and to an additive contribution to the spin splitting which has a linear dependence on k (the linear Dresselhaus term). Another cause of lifting of the spin degeneracy was pointed out by Rashba.[6,39,40] In considering the properties of a two-dimensional electron gas, Rashba noticed that the appearance of an asymmetric quantum well in a crystal is due to the presence of a perturbing potential that acts along the normal to the plane of the two-dimensional gas and leads to lifting of the spin degeneracy. Spin splitting of this nature has a linear dependence on the magnitude of the wave vector (the linear Rashba term). We note that in the $Si_{0.2}Ge_{0.8}$ quantum-well heterostructure under study the spin splitting is due to the Rashba mechanism, since germanium and silicon are centrosymmetric crystals.

The spin–orbit scattering of electrons on impurities is the main mechanism for relaxation of the spin state under conditions where the spin degeneracy is lifted, for any type of spin splitting. Elliot[41] considered the spin relaxation mechanism under conditions such that the spin splitting is greater than the elastic scattering energy ($\hbar/\tau<\Delta$) (see also Ref. 42). There is a linear relation between the spin relaxation rate and the elastic scattering rate. D'yakonov and Perel'[43] considered the case when the impurity scattering energy is greater than the spin splitting ($\hbar/\tau>\Delta$). Scattering leads to "randomization" of the spin states, and the spin relaxation rate turns out to be proportional to the elastic scattering time.

From the carrier kinetic characteristics found for the heterostructure under study we can conclude that the main mechanism of spin relaxation is the D'yakonov–Perel' one. The value of τ obtained by us means that the inequality $\hbar/\tau>\Delta$ holds up to $\Delta\approx 4.8$ meV. The spin–orbit relaxation time τ_{so} can be used to determine the value of the spin splitting from the relation[43]

$$\frac{1}{\tau_{so}}\approx\Omega_0^2\tau, \tag{6}$$

where the precession frequency $\Omega_0=\Delta/2\hbar$. The value of the spin splitting Δ calculated from Eq. (6) is 2.97 meV for the heterostructure under study.

Our results show that heterostructures based on the isovalent semiconductors Si and Ge can be of interest for creating electronic devices with controllable spin transport.[44]

[*] E-mail: komnik@ilt.kharkov.ua

[1)] The sample was grown by the advanced Semiconductors Group, University of Warwick, Coventry, UK.

---

[1] G. M. Gusev, Z. D. Kvon, and V. N. Ovsiuk, J. Phys. C **17**, L683 (1984).

[2] G. Dresselhaus, C. M. A. Papavassilion, R. G. Wheeler, and R. N. Sacks, Phys. Rev. Lett. **68**, 106 (1992).

[3] G. L. Chen, J. Han, T. T. Huang, S. Datta, and D. B. Janes, Phys. Rev. B **47**, 4084 (1993).

[4] T. Hassenkam, S. Pedersen, K. Baklanov, A. Kristensen, C. B. Sorensen, and P. E. Lindelof, Phys. Rev. B **55**, 9298 (1997).

[5] G. Dresselhaus, Phys. Rev. **100**, 580 (1955).

[6] Yu. A. Bychkov and É. I. Rashba, JETP Lett. **39**, 78 (1984).

[7] H. L. Stormer, Z. Schlesinger, A. Chang, D. C. Tsui, A. C. Gossard, and W. Wiegmann, Phys. Rev. Lett. **51**, 126 (1983).

[8] J. Luo, H. Munekata, F. F. Fang, and P. J. Stiles, Phys. Rev. B **38**, 10142 (1988).

[9] B. Das, D. C. Miller, S. Datta, R. Reifenberger, W. P. Hong, P. K. Bhattacharya, J. Singh, and M. Jaffe, Phys. Rev. B **39**, 1411 (1989).

[10] B. Das, S. Datta, and R. Reifenberger, Phys. Rev. B **41**, 8278 (1990).

[11] J. Luo, H. Munekata, F. F. Fang, and P. J. Stiles, Phys. Rev. B **41**, 7685 (1990).

[12] J. Nitta, T. Akazaki, H. Takayanagi, and T. Enoki, Phys. Rev. Lett. **78**, 1335 (1997).

[13] T. Koga, J. Nitta, T. Akazaki, and H. Takayanagi, Proc. NGS10, IPAP Conf., Ser. **2**, 227 (2001).

[14] Yu. F. Komnik, V. V. Andrievskiĭ, I. B. Berkutov, S. S. Kryachko, M. Myronov, and T. E. Whall, Fiz. Nizk. Temp. **26**, 829 (2000) [Low Temp. Phys. **26**, 598 (2000)].

[15] V. V. Andrievskiĭ, I. B. Berkutov, Yu. F. Komnik, O. A. Mironov, and T. E. Whall, Fiz. Nizk. Temp. **26**, 1202 (2000) [Low Temp. Phys. **26**, 890 (2000)].

[16] P. W. Anderson, E. Abrahams, and T. V. Ramakrishnan, Phys. Rev. Lett. **43**, 718 (1979).

[17] B. L. Altshuler, D. E. Khmel'nitskii, A. I. Larkin, and P. A. Lee, Phys. Rev. B **22**, 5142 (1980).

[18] B. L. Altshuler, A. G. Aronov, and P. A. Lee, Phys. Rev. Lett. **44**, 1288 (1980).

[19] S. Hikami, A. I. Larkin, and Y. Nagaoka, Prog. Theor. Phys. **63**, 707 (1980).

[20] B. L. Altshuler, A. G. Aronov, and D. E. Khmel'nitskii, J. Phys. C **15**, 7367 (1982).

[21] B. I. Altshuler and A. G. Aronov, in *Electron-Electron Interaction in Disordered Systems*, Vol. 10 of Modern Problems in Condensed Matter Science, A. L. Efros and M. P. Pollak (Eds.), North-Holland, Amsterdam (1985), p. 1.

[22] B. L. Altshuler, A. G. Aronov, M. E. Gershenson, and Yu. V. Sharvin, in *Soviet Science Review A*, Vol. 9, Harwood Academic Publisher, Schur, Switzerland (1987), p. 223.

[23] B. L. Al'tshuler, A. G. Aronov, A. I. Larkin, and D. E. Khmel'nitskiĭ, Zh. Éksp. Teor. Fiz. **81**, 768 (1981) [Sov. Phys. JETP **54**, 411 (1981)].

[24] V. A. Shklovskii, J. Low Temp. Phys. **41**, 375 (1980).

[25] S. Hershfield and V. Ambegaokar, Phys. Rev. B **34**, 2147 (1986).

[26] S. I. Dorozhkin, F. Lell, and W. Schoepe, Solid State Commun. **60**, 245 (1986).

[27] V. Karpus, Fiz. Tekh. Poluprovodn. **20**, 12 (1986) [Sov. Phys. Semicond. **20**, 6 (1986)].

[28] T. Tsuzuki, Physica B & C **107**, 679 (1981).

[29] M. Kaveh and N. F. Mott, J. Phys. C **14**, L177 (1981).

[30] M. J. Uren, R. A. Davies, M. Kaveh, and M. Pepper, J. Phys. C **14**, L413 (1981).

[31] G. V. Hu and R. F. O'Connel, Physica A **153**, 114 (1988).

[32] G. V. Hu and R. F. O'Connel, Solid-State Electron. **32**, 1253 (1989).

[33] G. Bergmann, Z. Phys. **49**, 133 (1982).

[34] V. Yu. Kashirin and Yu. F. Komnik, Fiz. Nizk. Temp. **20**, 1148 (1994) [Low Temp. Phys. **20**, 902 (1994)].

[35] Yu. F. Komnik and V. Yu. Kashirin, Fiz. Nizk. Temp. **20**, 1256 (1994) [Low Temp. Phys. **20**, 983 (1994)].

[36] S. V. Iordanskii, Yu. B. Lyanda-Geller, and G. E. Pikus, JETP Lett. **60**, 206 (1994).

[37] F. G. Pikus and G. E. Pikus, Phys. Rev. B **51**, 16928 (1995).

[38] W. Knap, C. Skierbiszewski, A. Zduniak, E. Litwin-Staszewska, D. Bertho, F. Kobbi, J. L. Robert, G. E. Pikus, F. G. Pikus, S. V. Iordanskii, V. Mösser and K. Zekentes, and Yu. B. Lyanda-Geller, Phys. Rev. B **53**, 3912 (1996).

[39] É. I. Rashba and V. I. Sheka, Fiz. Tverd. Tela (Leningrad) **1**, Sb. stateĭ II, 162 (1959) [Sov. Phys. Solid State **3**, 1257 (1961)].

[40] É. I. Rashba, Fiz. Tverd. Tela (Leningrad) **2**, 1224 (1960) [Sov. Phys. Solid State **2**, 1109 (1960)].

[41] R. J. Elliot, Phys. Rev. **96**, 266 (1954), *ibid.* **96**, 280 (1954).

[42] Y. Yafet, Solid State Phys. **14**, 1 (1963).

[43] M. I. D'yakonov and V. I. Perel', Zh. Éksp. Teor. Fiz. **60**, 1954 (1971) [Sov. Phys. JETP **33**, 1053 (1971)].

[44] S. Datta and B. Das, Appl. Phys. Lett. **56**, 665 (1990).

Translated by Steve Torstveit

LOW TEMPERATURE PHYSICS VOLUME 29, NUMBER 4 APRIL 2003

LATTICE DYNAMICS

Low-temperature thermal expansion of pure and inert-gas-doped fullerite C_{60}

A. N. Aleksandrovskii*, A. V. Dolbin, V. B. Esel'son, V. G. Gavrilko, V. G. Manzhelii, and B. G. Udovidchenko

B. Verkin Institute for Low Temperature Physics and Engineering of the National Academy of Science of Ukraine, 47 Lenin Ave., Kharkov 61103, Ukraine

A. S. Bakai

National Science Center "Kharkov Institute of Physics and Technology," 1 Akademicheskaya Str., Kharkov 61108, Ukraine

G. E. Gadd and S. Moricca

Australian Nuclear Science and Technology Organisation, NSW 2234, Australia

B. Sundqvist

Department of Experimental Physics, Umea University, SE-901 87 Umea, Sweden

(Submitted October 24, 2002)
Fiz. Nizk. Temp. **29**, 432–442 (April 2003)

The low-temperature (2–24 K) thermal expansion of pure (single-crystal and polycrystalline) C_{60} and polycrystalline C_{60} intercalated with He, Ne, Ar, and Kr is investigated using a high-resolution capacitance dilatometer. The investigation of the time dependence of the sample length variations $\Delta L(t)$ on heating by ΔT shows that the thermal expansion is determined by the sum of positive and negative contributions, which have different relaxation times. The negative thermal expansion usually prevails at helium temperatures. The positive expansion is connected with the phonon thermalization of the system. The negative expansion is caused by reorientation of the C_{60} molecules. It is assumed that the reorientation is of a quantum character. The inert gas impurities affect the reorientation of the C_{60} molecules very strongly, especially at liquid-helium temperatures. A temperature hysteresis of the thermal expansion coefficient of Kr– and He–C_{60} solutions is revealed. The hysteresis is attributed to orientational polymorphous transformation in these systems. © *2003 American Institute of Physics.* [DOI: 10.1063/1.1542477]

1. INTRODUCTION

Here we report the results obtained in a series of investigations of the low-temperature (2–24 K) thermal expansion of pure C_{60} and C_{60} doped with inert gases.

Earlier[1,2] we detected a negative and very large coefficient of linear thermal expansion of polycrystalline and single-crystal C_{60} in the region of liquid-helium temperatures. This unusual effect has stimulated our further research.

One of the characteristic features of fullerite C_{60} is the substantial influence of the orientational states of its molecules on the physical properties of the crystal. A molecule of fullerene C_{60} is shaped as a truncated icosahedron whose surface forms 20 hexagons and 12 pentagons. The noncentral interaction between the globular molecules of C_{60} is much weaker than the central one, and fullerene molecules show reorientational motion over a wide temperature range. At condensation, fullerite C_{60} forms a face-centered cubic (fcc) lattice. As is shown by experimental studies (see, for example, Ref. 3), the rotation of molecules in this phase is weakly hindered. On decreasing the temperature to about 260 K, a structural-orientational phase transition occurs into a low-temperature phase of $Pa3$ symmetry. This transition is accompanied by partial orientational ordering of the rotation axes of the C_{60} molecules. The almost free rotation of molecules changes into rotation around the space diagonal $\langle 111\rangle$. On a further decrease in temperature in the $Pa3$ phase, the rotational motion of the molecules around the $\langle 111\rangle$ axes slows down. Near $T\approx 90$ K the rotation of molecules around the $\langle 111\rangle$ axes is hindered almost entirely, and an orientational glass is formed.

Initially, our goal was to clear up the nature of the negative thermal expansion of C_{60}. In this context it was interesting and important to find out how impurities could influence this effect. It seemed natural to start with inert gases as impurities, which, being comparatively simple atoms, would hopefully facilitate the interpretation of the results. By introducing different inert gases (He, Ne, Ar, and Kr) into the fullerite lattice, we intended to find how the sizes of the impurity atoms may influence the negative thermal expansion.

In the course of these investigations of C_{60} doped with inert gases, new effects have been revealed, which appear worthy of special and independent consideration.

2. EXPERIMENTAL ASPECTS

The linear thermal expansion coefficient was measured using a capacitive dilatometer[4] with a resolution of $2 \cdot 10^{-9}$ cm, specially modified for measuring fullerite samples. The dilatometer was constructed so that all elements capable of affecting the measured results on account of their own thermal expansion were in a bath of liquid helium at constant temperature. The scheme of the measuring cell of the dilatometer, the procedure for mounting the sample in the dilatometer, and the measurement procedure have been described elsewhere.[1,2] The thermal expansion of fullerite C_{60} was measured by a step change technique, described as follows. With the sample at a constant temperature T_1, the temperature of the objective table (containing the sample) was then changed to a temperature T_2, which from this moment was kept constant. Changes in temperature and sample length were registered once a minute and processed by a computer in real time. When the temperature drift of the sample was no more than 0.01 K in 10 minutes, we determined the change of its length due to the change in temperature from T_1 to T_2. During the measurements the steps from T_1 to T_2 were 0.1–1 K, depending on the temperature range.

The change in the sample length was determined during both a temperature increase and decrease. The linear thermal expansion coefficient α was obtained by differentiation with respect to T of the temperature dependence of the relative elongation $\Delta L/L$ of the samples.

The low-temperature thermal expansion of C_{60} fullerite should be isotropic because it has a cubic lattice. Thus, in principle, both single-crystal and polycrystalline C_{60} can be used in studies of the thermal expansion.

Our polycrystalline samples were produced by compacting C_{60} powder under a pressure of 0.1 GPa. The stresses thus induced could affect the results of the subsequent dilatometric measurement. Gas molecules adsorbed at grain boundaries could also influence the results. In order to ascertain the presence of such effects, we also investigated C_{60} in the form of a single crystal. In the preparation of the inert-gas–C_{60} sample the single crystal was not subjected to the compression and mechanical treatment as in the polycrystalline samples.

Four samples of pure C_{60} were used—three polycrystals [C_{60}(I),C_{60}(III),C_{60}(IV)], and one single crystal [C_{60}(II)]. In the subsequent experiments the samples C_{60}(III) and C_{60}(IV) were saturated with inert gases. Information pertaining to the pure C_{60} samples is given below.

C_{60}(I). The sublimated C_{60} powder for sample preparation was supplied by Term USA, Berkeley, CA, and had a nominal purity of better than 99.98%. No traces of solvents were found by Raman analysis within its accuracy (0.1% by mass). The room temperature powder x-ray diffraction pattern of the material displayed sharp peaks from the fcc structure ($a = 14.13$ Å). In an atmosphere of dry argon the C_{60} powder was loaded in a small piston-cylinder device used for the sample preparation. After subsequent compacting of the powder at about 0.1 GPa, the sample (pellet 6 mm in diameter and about 2.4 mm in height, with grain sizes of 0.1–0.3 mm) was immediately transferred into a glass tube and dried under dynamic vacuum of 10^{-6} Torr for about 16 hours. The compacting procedure was done in air and did not exceed 15 minutes. Finally, the sample was sealed in a vacuum of 10^{-6}, shielded from light, and kept in that state for 3 months until the beginning of the dilatometric measurements.

C_{60}(II). A very large C_{60} single crystal (≈6.5×4.3×3.1 mm) was obtained from Dr. M. Haluska, Vienna. This crystal was grown by the sublimation method in an ampoule under vacuum from Hoechst "Super Gold Grade" C_{60}. The crystal was never exposed to air or oxygen after growth was completed, and it was transferred from its growth tube while under Ar, into a glass ampoule, which was then evacuated before sealing.

C_{60}(III). The sample was a cylinder 9 mm high and 10 mm in diameter. The sample characteristics and the preparation conditions are similar to those for the sample C_{60}(I).

C_{60}(IV). The C_{60} powder was supplied by the SES research company and had a nominal purity of 99.99%. The conditions of compacting for the sample C_{60}(IV) were similar to those for the sample C_{60}(I). The sample was 6.5 mm in height and 10 mm in diameter. The average grain size was 0.1 mm. The powder and the sample prepared were kept in the air. Immediately prior to measurement of the thermal expansion, the sample was evacuated dynamically for six days.

It is important to note that all of our fullerite samples had a purity better than 99.98%.

The procedure for mounting the samples in the dilatometer were as follows. Prior to sample mounting, the glass ampoule containing the sample was opened in an argon atmosphere at with an overpressure of around 200 Torr. During the process of mounting the sample in the measuring cell of the dilatometer, the sample was exposed to the air for no more than 20 minutes and then was evacuated. During the measurements the vacuum in the dilatometer cell was maintained at a level of 10^{-6} Torr. The measurement procedure was the same for all samples.

3. RESULTS AND DISCUSSION

3.1. Pure C_{60}

The typical time dependence of the change in the C_{60} sample length ΔL after a fast increase in the temperature of

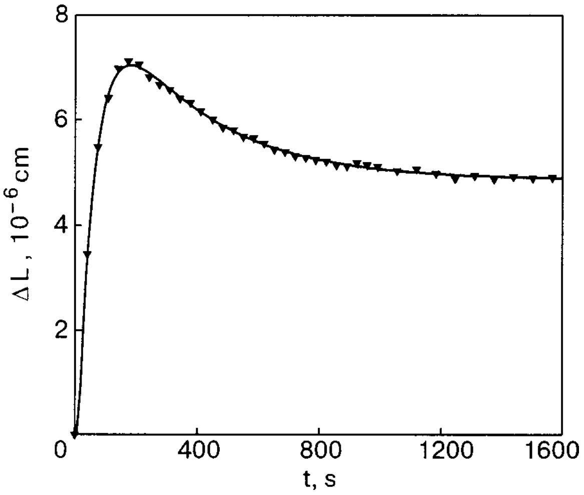

FIG. 1. The characteristic time dependence of the sample length variations $\Delta L(t)$ on heating by ΔT.

the objective table (with the sample) by ΔT is shown in Fig. 1. At each temperature the sign of the total thermal expansion is determined by two competing mechanisms responsible for expansion and contraction of the sample.

The temperature dependence of the thermal expansion coefficient for the four pure C_{60} samples is shown in Fig. 2. In the same figure the open circles show the linear expansion coefficients measured dilatometrically by Gugenberger *et al.*[5] on single-crystal C_{60}. Note that until the studies reported here, the thermal expansion of C_{60} had not been investigated below 5 K.

Above 7 K the results obtained are all in good agreement. However, considerable discordance is observed for the different samples in the region of liquid-helium temperatures. In this region the thermal expansion coefficient for samples I, II, and III have unusually high negative values for such low temperatures, while, that of sample IV, in contrast, always has a positive value. The discrepancy in the α values for different samples will be discussed in the next Section. Here we shall attempt to explain the nontrivial effect of negative thermal expansion of C_{60}.

A possible mechanism responsible for the negative thermal expansion of fullerite C_{60} might be rotational tunneling of molecules. Sheard[6] was the first to call attention to the fact that rotational tunneling of molecules can lead to a negative thermal expansion. This problem was considered in detail by Freiman[7] as applied to the thermal expansion of solid methane.

The large moment of inertia of the C_{60} molecule is a strong objection to the assumption of a rotational tunneling mechanism as producing the negative thermal expansion coefficient of C_{60} fullerite below liquid-helium temperatures. In the orientational glass, which evolves in the fullerite below 90 K, the potential barriers U_ϕ impeding rotation of the molecules can vary over wide limits. The tunneling rotation can be performed only by those molecules for which the U_ϕ barriers are quite low. C_{60} molecules that experience such barriers are referred to as defects. If the U_ϕ barriers grow upon a decrease in the crystal volume, the tunneling rotation leads to a negative thermal expansion of the crystal.[6,7]

In the case of tunneling rotation the absolute values of the Grüneisen coefficient can be very high.[2,8] In Fig. 3 (Ref. 2) the temperature dependence of the Grüneisen coefficient is shown for the samples C_{60}(I) and C_{60}(II).

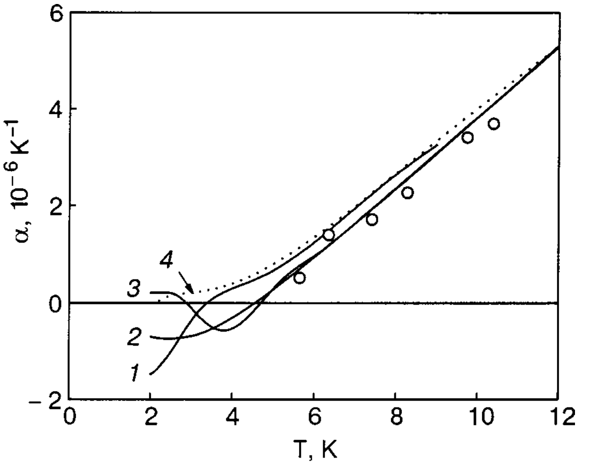

FIG. 2. Temperature dependence of the thermal expansion coefficient of pure fullerite C_{60}: *1*—C_{60}(I); *2*—C_{60}(II); *3*—C_{60}(III); *4*—C_{60}(IV); ○—Gugenberger *et al.*, Phys. Rev. Lett. (1992).

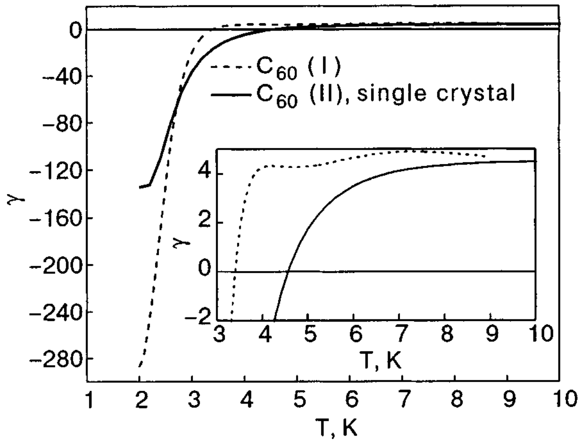

FIG. 3. Grüneisen parameter of fullerite C_{60}.

It should be noted here that the Grüneisen coefficients for the phonon and libron spectra of molecular crystals are usually of the order of one.[9] The unusually large negative values of γ testify in favor of the assumption of the tunneling nature of the negative thermal expansion of fullerite C_{60}.

The different factors that might cause the negative thermal expansion of fullerite C_{60} were analyzed in Refs. 10 and 11. Since the C_{60} molecules have fivefold symmetry axes, they cannot be entirely orientationally ordered; hence, certain defects are inevitable at low temperatures. The negative thermal expansion was explained qualitatively[11] by assuming the coexistence of different orientational domains in the simple cubic lattice of C_{60}. The potential relief is much smoother in the interdomain space (domain walls) than inside the domains, and the U_ϕ barriers impeding rotation of the molecules are noticeably lower in the domain walls. As a result, the molecules in the domain walls (unlike those inside the domains) can overcome the barriers through tunneling down to much lower temperatures.

3.2. C_{60} doped with Ar and Ne

We investigated the thermal expansion coefficient α of C_{60}(III) samples doped with Ar and Ne.[12,13] The penetration of gas atoms into the fullerite lattice was expected to change the U_ϕ barriers and hence effect rotation of the neighboring C_{60} molecules. The impurity atoms could thus influence the probability of rotational tunneling of these molecules and the tunneling-induced contribution to the thermal expansion. If the U_ϕ barrier height and (or) width increase, the total negative thermal expansion $\int \alpha dT$ should decrease and shift towards lower temperatures. Recall that in the low-temperature phase each C_{60} molecule is associated with two tetrahedral and one octahedral interstitial cavities, whose average linear dimensions are about 2.2 and 4.2 Å, respectively.[14,15] According to x-ray and neutron diffraction data,[16–19] the Ne and Ar atoms, with gas-kinetic diameters 2.788 and 3.405 Å,[20] respectively, occupy only the octahedral cavities.

The C_{60}(III) sample was doped with neon and argon at room temperature under atmospheric pressure. The doping lasted for 340 hours for neon and 460 hours for argon. In

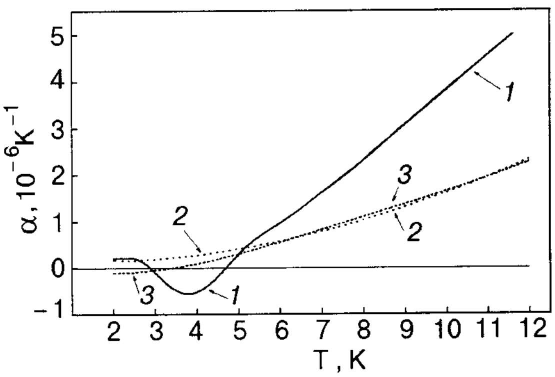

FIG. 4. Linear thermal expansion coefficients: pure fullerite (*1*), fullerite doped with neon (*2*), fullerite doped with argon (*3*).

these experiments we did not measure the Ne and Ar concentrations in the fullerite. According to Ref. 16, on C_{60} saturation with Ne at room temperature under atmospheric pressure, the Ne concentration in C_{60} reaches 20 mole%.

Figure 4 shows the measured thermal expansion coefficients of fullerite before doping (curve *1*) and after doping with neon (curve *2*) and argon (curve *3*). It is seen that the doping has strongly affected the thermal expansion of C_{60}: the introduction of the doping gas has reduced the positive coefficient considerably and has strongly suppressed the effect of negative thermal expansion and shifted it towards lower temperatures. To explain the effects observed, it seems natural to assume that the impurity atoms impede rotation of the C_{60} molecules and thus enhance the noncentral forces acting upon the C_{60} molecules. With the noncentral forces enhanced, the libration frequencies ω_i of the C_{60} molecules should increase, and at $T < \hbar\omega_i/k$ the contribution of librational excitations to the heat capacity and thermal expansion of the crystal should decrease. At $T > 6$ K the tunneling effects are no longer important. In this temperature range the translational lattice vibrations and the molecule librations are responsible for the thermal expansion. In Refs. 21 and 22 the librational excitation contribution to the heat capacity of C_{60} was described using two libration frequencies with energies equivalent to 30 and 58 K. Thus, the inequality $T < \hbar\omega_i/k$ holds for the temperature interval 5–12 K, and the assumption of a decrease in the librational excitation contribution to the thermal expansion at these temperatures seems to be reasonable. As the noncentral forces increase, the U_ϕ barriers impeding rotation of the molecules become higher. This diminishes the probability of rotational C_{60} tunneling and the tunneling splitting of the energy levels. As a result, the negative thermal expansion decreases, and the region of tunnel effects shifts towards lower temperatures.

We should remember that the librational excitation contribution is made by all C_{60} molecules, while the negative contribution is made only by the molecules which we call "defects."

An interesting feature was exhibited by the linear thermal expansion coefficient of Ne- and Ar-doped C_{60} (see Fig. 4). At 6–12 K the $\alpha(T)$ values practically coincide for Ar- and Ne-saturated samples. Let us assume that doping with Ar and Ne increases the libration frequencies of the C_{60} molecules to such an extent that the contribution of librational excitations to the thermal expansion is negligible up to 12 K. Besides, it is natural to expect that the Ar and Ne impurities have negligible effect on the translational vibration of the lattice and their contribution to the thermal expansion. If this is correct, the thermal expansions of the Ne–C_{60} and Ar–C_{60} solutions and the contribution of the translational vibrations to the thermal expansion of pure C_{60} should coincide in the 6–12 K region, where the contributions of librational excitations and tunneling to $\alpha(T)$ are not observable. We tried to describe the contribution of translational vibrations as

$$\Delta\alpha_{\rm trans} = \gamma C(T/\Theta_D)/BV, \qquad (1)$$

where γ is the Grüneisen coefficient, V is the molar volume of C_{60}, B is the bulk modulus of C_{60}, $C(T/\Theta_D)$ is the Debye heat capacity, and Θ_D is the Debye temperature of C_{60}. The calculation was done using $V = 416.7\,\mathrm{cm^3/mole}$ (Ref. 23) and $B = 10.3\,\mathrm{GPa}$.[24] Θ_D and γ were fitting parameters; $\Delta\alpha_{\rm trans}$ can be described well by the above expression (1) taking $\gamma = 2.68$ and $\Theta_D = 54\,\mathrm{K}$. The fitting parameter γ is close to the corresponding values for rare-gas solids.[20] The published data for Θ_D of C_{60} show a large scatter. Analysis of the temperature-heat-capacity dependences yields $\Theta_D = 37$,[22] 50,[25,26] 60,[27] 80,[28] and 188 K.[29] A value $\Theta_D = 100\,\mathrm{K}$ was obtained in studies[30] of elastic properties on single-crystal C_{60}. Even if we disregard the too-high values $\Theta_0 = 188\,\mathrm{K}$[29] and $\Theta_D = 100\,\mathrm{K}$, where the error is quite appreciable,[30] the scatter of Θ_D values is still wide. The Debye temperatures obtained by the calorimetric method are highly sensitive to the impurities present in fullerite and the technique employed to separate the contributions to the heat capacity. The Θ_D results calculated from ultrasound velocities are more reliable, since they are mainly determined by the translational vibrations of the lattice and are not very sensitive to impurities. The ultrasound data for single-crystal C_{60} at $T = 300\,\mathrm{K}$ give $\Theta_D = 66\,\mathrm{K}$.[31] In Ref. 23 previously published data on ultrasound velocities of polycrystalline C_{60} were analyzed and extrapolated to low temperatures. The Debye temperature thus calculated at $T = 0$ is 55.4 K, which is very close to our result.

The above consideration suggests that our γ and Θ_D are quite realistic and thus strengthens the assumption that curves *2* and *3* in Fig. 4 describe the contribution of translational vibrations to the thermal expansion coefficient of pure C_{60}. Proceeding from this assumption, we can take the difference between curve *1* and curves *2, 3* (Fig. 4) at 6–12 K as the contribution of librational excitations $\Delta\alpha_{\rm lib}$ to the thermal expansion coefficient of pure C_{60}; $\Delta\alpha_{\rm lib}$ is well described by the Einstein term with the characteristic Einstein temperature $\Theta_E = 39\,\mathrm{K}$. This value does not conflict with the above results.[22] Note that the idea of the impeding effect of the impurity gas molecules upon the rotational motion of the C_{60} molecules was put forward earlier in Ref. 32. The idea is supported by the fact that at low temperatures ($T = 15\,\mathrm{K}$) the lattice parameter of a saturated Ar_xC_{60} solution is 0.006 Å smaller than that of pure fullerite.[18]

To obtain more information, we studied how the thermal expansion coefficient changed when the doping atoms were removed from the sample. For this purpose, the measuring cell with the sample was warmed to room temperature and evacuated to $1\cdot 10^{-3}$ Torr. The gas evacuation at room temperature lasted for 3 days. The thermal expansion was then

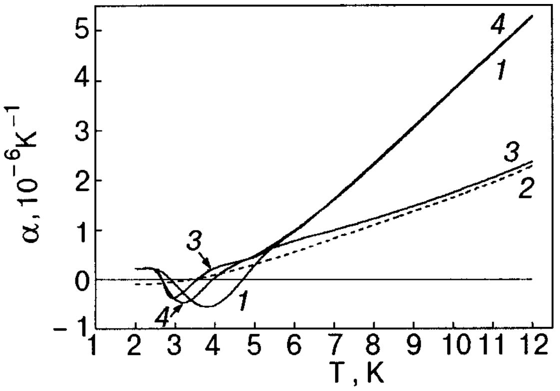

FIG. 5. Temperature dependence of the thermal expansion coefficients: pure fullerite (*1*), Ar-doped fullerite (*2*); fullerite after evacuation of Ar for 3 (*3*) and for 45 (*4*) days.

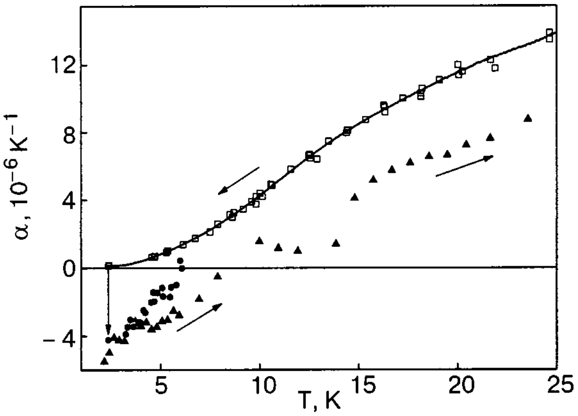

FIG. 6. Temperature dependence of the thermal expansion coefficients of Kr-doped fullerite.

measured at low temperatures. The results are shown in Fig. 5 (curve *3*). It is seen that the thermal expansion coefficient changes only slightly above 5 K, but below 3.5 K the negative thermal expansion now again has the minimum typical for undoped C_{60}. The measuring cell with the sample was warmed again to room temperature, and gas evacuation was continued for 42 days. The thermal expansion coefficients measured thereafter are shown in Fig. 5 (curve *4*). Note that after evacuation of argon for a total of 45 days the "high-temperature" part of the thermal expansion coefficient was restored completely. The negative thermal expansion in the range 2.5–5 K was, however, still different from the value for the initial pure sample. Similar experiments were done on a sample saturated with neon. After a 45 days' exposure of the sample to room temperature and vacuum, the results obtained before and after doping coincided in the whole temperature interval. We can thus conclude that the C_{60} sample was completely free of neon. A desaturation of this duration was not sufficient to remove all argon from the sample.

The changes in $\alpha(T)$ after removal of argon from the sample may be explained as follows. The molecules we called "defects" in Sec. 3.1 become permanently displaced with respect to the lattice sites. As a result, the octahedral voids surrounding such molecules are not identical, and the potential wells that they form for the impurity are different, too—deeper or shallower than the octahedral potential wells adjacent to most of the C_{60} molecules. At the initial stage of evacuation, the Ar atoms first leave the shallow potential wells near the defects, and this causes faster changes in the negative part of $\alpha(T)$. The removal of the Ar atoms from the deeper wells proceeds more slowly than in most of the crystal volume. That is why at the completing stage, the positive part of $\alpha(T)$ is restored faster at $T>5$ K.

This consideration leads us to assume that the distinctions in the behavior of $\alpha(T)$ for different pure C_{60} samples (see Fig. 2) can be attributed to different amounts of "residual" impurity, particles of which are still present in the deep potential wells near the defects. The negative thermal expansion should therefore be particularly sensitive to the pre-history of the sample.

We believe that the absence of the negative contribution to the thermal expansion for pure C_{60} (sample IV) down to 2 K is connected with saturation of the sample with air gases. The results of the TGA analysis are also evidence that appreciable amounts of gas are present in sample.

3.3. C_{60} doped with Kr and He

It was noted above that on doping with Ar the molar volume of C_{60} decreased at $T<60$ K.[18] Like Ar atoms, the introduced Ne atoms occupy only octahedral interstitial positions, but their gas-kinetic diameter is smaller. It is natural to assume that at low temperatures the doping with Ne also leads to a decrease in the average distance between the C_{60} molecules in the lattice. The above discussion agrees with the conclusion that Ar and Ne impurities impede the rotational motion of C_{60} molecules.

Our next goal was to investigate how impurities that increase the volume of fullerite affect its thermal expansion. The impurities chosen were Kr and He. When admixed, the Kr atoms occupy the octahedral interstitial cavities, and because of the rather large gas-kinetic diameter of Kr atoms the volume of the solid C_{60} increases.[18] When He impurity is added,[33] the volume of C_{60} increases presumably because the He atoms occupy not only the octahedral interstitial cavities but the much smaller tetrahedral ones as well.[32,33]

3.3.1. **C_{60}–Kr**. The C_{60}(IV) powder was saturated with Kr at $T=500\,°\mathrm{C}$ and a Kr pressure of 170–200 MPa for 43 hours. The Kr concentration was found from a thermal gravimetric analysis[18] to be 60 mole%. The compaction of the powder, the procedure of mounting the sample in the dilatometer, and the measurement procedure were similar to those applied to C_{60}(I).

The thermal expansion of C_{60} doped with Kr was measured in six experimental runs. The temperature dependence of the thermal expansion coefficient $\alpha(T)$ is illustrated in Fig. 6. The measurement was made on heating (solid circles and triangles) and cooling (open squares and the smoothed solid curve) of the sample. Note two important features in the behavior of the thermal expansion coefficient.

First, there is a hysteresis of the temperature dependence $\alpha(T)$. Let us recall that $\alpha(T)$ hysteresis was not observed for pure C_{60} and C_{60} doped with small amounts of Ne and Ar. The results obtained in different measurement runs on the sample being cooled down from the highest measurement temperature (24 K) exhibit good agreement. The deviation from the smoothed curve is not large. However, the agreement is much worse for the sample being heated from liquid-helium temperatures. The scatter in the data is quite appreciable even within one measurement run. To avoid extra complexity of Fig. 6, the results of only two measurements made on heating the sample are shown in the figure. We emphasize, however, that in all the cases the α values measured on cooling are higher than the α values obtained on heating and exceed the thermal expansion coefficient of the initial C_{60}(IV) sample at $T>10$ K. The excess increases with temperature and reaches 15% at $T=22$ K. Another important point should be noted. To change from α measured on cooling to α measured on heating at the lowest experimental temperature (2 K), we had to keep the sample at $T\approx 2$ K for no less than three hours. Let us detail the procedure as an example. On cooling the sample down from 24 K we reach $T=2.4$ K and start measuring the thermal expansion on heating. The values of the first two measurements are close to the results of extrapolation from the $\alpha(T)$ dependence for the cooling case following $\alpha(T)\sim T^3$. On the subsequent measurement the thermal expansion coefficient changed abruptly to the value indicated by the vertical arrow in Fig. 6.

Now we discuss the other feature in the temperature dependence of the thermal expansion coefficient for the Kr–C_{60}(IV) solution. The α values obtained on heating the sample in the region of liquid-helium temperatures become negative. Their absolute values are several times higher than those for the pure C_{60}(I), C_{60}(II), and C_{60}(III) samples and for C_{60}(III) doped with Ne and Ar. It is interesting that the C_{60}(IV) sample itself (we used it for doping with Kr) has no negative thermal expansion in the whole temperature interval (2–24 K).

No negative contribution to the thermal expansion was detected on cooling the C_{60}(IV)+Kr sample from the highest temperature (24 K) to 2 K. However, if the sample was previously kept at $T=2$ K over three hours and then cycled in the interval 2–5 K, no $\alpha(T)$ hysteresis was observed. The negative contribution to the thermal expansion exists both on cooling and on heating. Let us analyze the behavior of the negative contribution to the thermal expansion of the sample. The characteristic time dependence of the sample length variations $\Delta L(t)$ on heating by ΔT is shown in Fig. 1. We describe this dependence as:

$$\Delta L(t)=A[1-\exp(-t/\tau_1)+B[\exp(-t/\tau_2)-1], \qquad (2)$$

where the first term describes the positive contribution and the second term stands for the negative one; A and B are the absolute values of the corresponding contributions at $t\rightarrow\infty$; τ_1 and τ_2 are the characteristic relaxation times for these contributions.

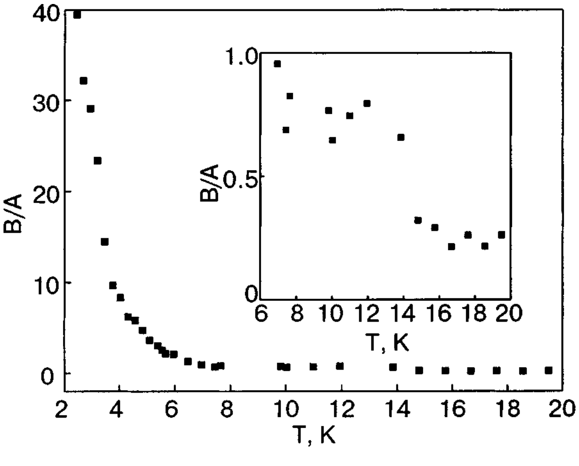

FIG. 7. The relation between negative and positive contributions to the thermal expansion of Kr-doped C_{60}.

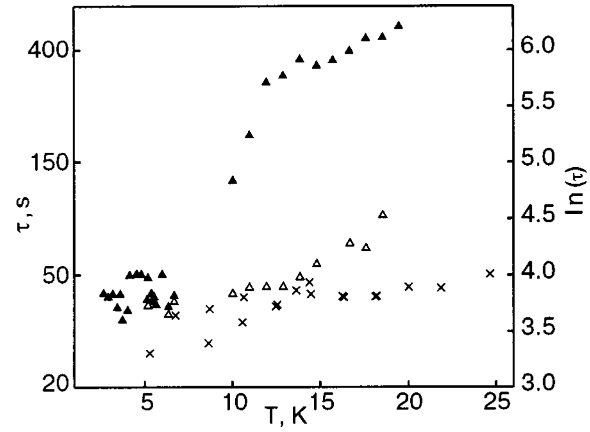

FIG. 8. Characteristic relaxation times of positive τ_1 (△,×) and negative τ_2 (▲) contributions to the thermal expansion of Kr-doped C_{60}.

The B/A value is the ratio between the negative and positive contributions to the thermal expansion. The averaged temperature dependence of the B/A ratio calculated from the data obtained on heating the sample is shown in Fig. 7. The negative contribution prevails at liquid-helium temperatures and remains significant up to 20 K.

The temperature dependences of the relaxation times τ_1 and τ_2 are illustrated in Fig. 8. The τ_1 values were calculated on both heating (△) and cooling (×) of the sample.

We propose the following explanation of the features observed in the thermal expansion of the Kr–C_{60} solution. The hysteresis and the jumplike change in the thermal expansion coefficient of C_{60} doped with Kr show evidence that this orientational glass undergoes polymorphous transformation, and two orientationally disordered phases coexist in the interval 2–24 K. The phenomenon of polymorphism has been known for the case of structural glasses, though it is not completely clear yet. For orientational glasses it seems to be found here for the first time. Below we use the term "polymorphism," which was introduced in analogy with polymorphism in[34] and then was reintroduced by others.[35] Note that when the sample is heated from 2 to 24 K and cooled again to 2 K, its volume decreases by $\Delta V=0.017\%$ because of the thermal expansion hysteresis. ΔV can be treated as the lower limit for the difference between the molar volumes of the glasses mentioned.

For the future we are planning more detailed investigations of polymorphism in this type of orientational glasses.

At the lowest temperatures of the experiment, the glass with the larger molar volume is more advantageous thermodynamically. The thermal expansion of this glass is determined by two contributions (see Fig. 1.) The lattice excitations (phonons and librons) make a positive contribution to the thermal expansion, while the molecular reorientations contribute negatively. Earlier, we attributed the negative thermal expansion of pure C_{60} to the tunnel reorientation of its molecules. The Kr atoms occupying the octahedral interstitial sites of C_{60} increase the volume of the crystal and the degree of disordering in it. This should suppress the barriers impeding the rotation and increase the probability of rotational tunneling. As a result, we can expect that the negative contribution to the thermal expansion would increase and the temperature interval in which this contribution exists would become wider. This is what we observe experimentally.

It is interesting that the difference between the $\alpha(T)$ curves taken on heating and cooling (Fig. 6) coincides, within the experimental error, with the value of the negative contribution to the thermal expansion. Thus the contributions of the lattice excitations to the thermal expansion of the two types of glasses are practically equal. The difference in the thermal expansion of these glasses is due to the processes of molecular reorientation by C_{60}.

The increase in the molar volume of C_{60} on its doping with Kr should suppress to some extent the frequencies of translational and orientational vibrations of the C_{60} lattice. As a result, the contribution of the lattice excitations to the thermal expansion of C_{60} should be larger in the temperature interval studied. We believe that this is the reason why the thermal expansion coefficient measured on cooling of $C_{60}(\mathrm{IV})+\mathrm{Kr}$ exceeds that of the initial $C_{60}(\mathrm{IV})$ sample.

The relaxation times τ_1 and τ_2 introduced in Eq. (2) describe the equalizing of the temperature over the sample (thermalization) and the orientational relaxation, respectively. As can be seen in Fig. 8, the process of orientational relaxation is slower. Commonly, in thermally activated processes τ_2 does not increase with temperature. This is another argument in favor of tunnel reorientation in a portion of the C_{60} molecules.

3.3.2. **C_{60}–He**. The starting sample was $C_{60}(\mathrm{III})$. It was previously used in different experiments and was therefore saturated with Ar, Ne, and D_2. Employing prolonged evacuation of the sample at room temperature, we succeeded in removing Ar and Ne nearly completely. The return of the thermal expansion coefficients of the previously doped sample to the values of pure $C_{60}(\mathrm{III})$ was taken as an indication that desaturation was completed. As to D_2, keeping C_{60}–D_2 in vacuum at room temperature for 180 days was not sufficient to remove all dissolved gas, and we had to prolong the procedure for 48 hours more at $T=250\,^\circ\mathrm{C}$. But even after this vacuum exposure the desaturation was not complete. The thermal expansion of the sample was still positive at liquid-helium temperature. In the investigated interval of temperatures the thermal expansion of this sample practically coincided with that of $C_{60}(\mathrm{IV})$, and no hysteresis was detected. To saturate it with He, the sample was kept in the dilatometric cell for 24 hours at room temperature under a He pressure of 1 atm. The dilatometric cell was then cooled for 7 hours to $T=4.2\,\mathrm{K}$. During cooling the He pressure decreased in the closed volume of the dilatometer, and helium was added at 112 and 45 K to restore the pressure to 1 atm.

At 4.2 K the He gas was evacuated from the dilatometer and during measurement of the thermal expansion the C_{60}–He sample was kept in vacuum. No indications of the sample desaturation were observed during the dilatometric measurements.

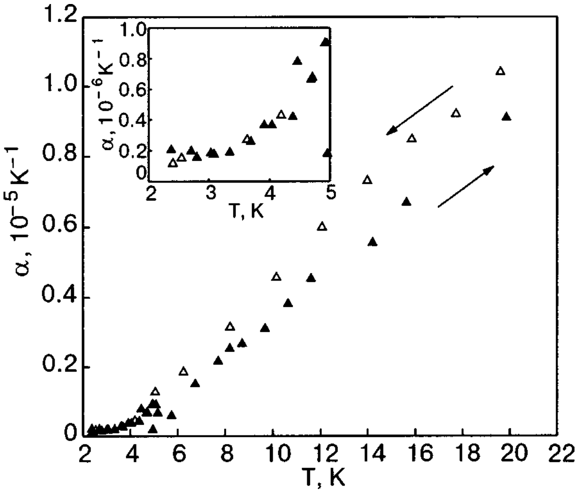

FIG. 9. Temperature dependence of the thermal expansion coefficients of He-doped fullerite.

The temperature dependence of the linear expansion coefficient of $C_{60}+\mathrm{He}$ is shown in Fig. 9 for the heating (solid triangles) and cooling (open triangles) conditions. Along with $C_{60}(\mathrm{IV})+\mathrm{Kr}$, the thermal expansion of $C_{60}+\mathrm{He}$ has some peculiarities, such as (*a*) the hysteresis, (*b*) the negative contribution to the thermal expansion observed on heating, and (*c*) the α values measured on cooling, which exceed the coefficients for the initial C_{60} sample. In contrast to $C_{60}(\mathrm{IV})+\mathrm{Kr}$, for $C_{60}+\mathrm{He}$ the hysteresis is smaller in magnitude and appears only if the temperature range considered lies above 5 K. The negative contribution to the thermal expansion of $C_{60}+\mathrm{He}$ is always smaller in absolute value than the positive one. The heating of the sample to the highest temperature (20 K) and the subsequent cooling to 2 K lead to a $4.6\cdot10^{-3}\%$ decrease in the volume of the sample. For $C_{60}(\mathrm{IV})+\mathrm{Kr}$ the decrease is $17\cdot10^{-3}\%$.

Next the $C_{60}+\mathrm{He}$ sample was partially desaturated. To do this, the sample was heated to 250 K for 11 hours during continuous dynamic evacuation and then cooled to 4.2 K for 7 hours. The thermal expansion coefficients of $C_{60}+\mathrm{He}$ measured after the partial desaturation are shown in Fig. 10

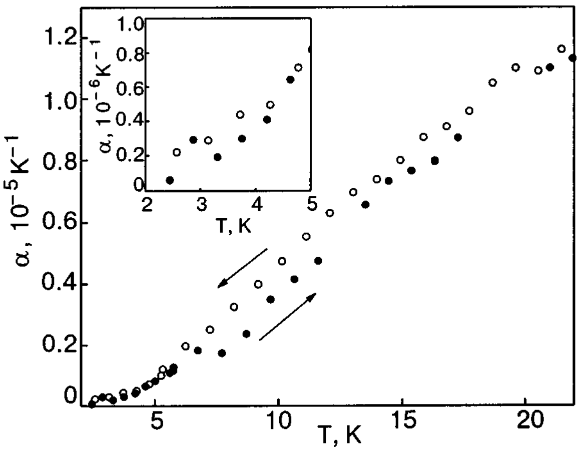

FIG. 10. Temperature dependence of the thermal expansion coefficients of He-doped fullerite after partial desaturation.

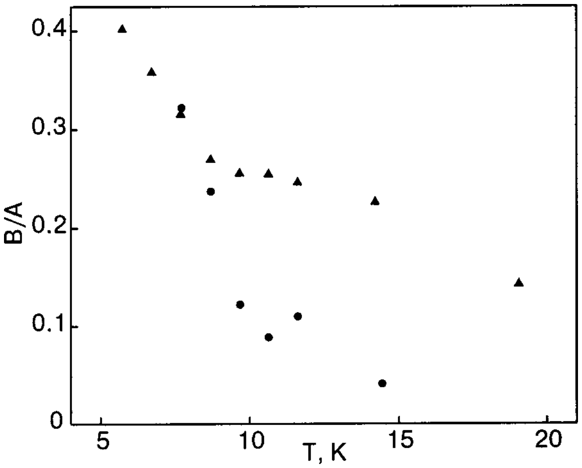

FIG. 11. The ratio between the absolute values of the negative and positive contributions to the thermal expansion of C_{60} doped with He: before partial desaturation (▲); after partial desaturation (●).

(solid circles for heating and open circles for cooling). After the partial desaturation, the hysteresis became narrower, and the relative change in the volume caused by heating the sample to 23 K and subsequent cooling to 2 K decreased to $3.2\cdot 10^{-3}\%$.

The temperature dependence of the absolute value of the ratio between the negative and positive contributions to the thermal expansion coefficient measured on heating the sample is shown in Fig. 11. As might be expected, after the partial desaturation the negative contribution, i.e., the contribution made by reorientation of the C_{60} molecules, becomes weaker.

The temperature dependences of the relaxation times of the positive (τ_1) and negative (τ_2) contributions to the thermal expansion of C_{60} doped with He are shown in Fig. 12. It is seen that the partial desaturation does not have much influence on τ_1 and τ_2. We have found no qualitative distinctions between the temperature dependences of the relaxation times of the C_{60}+He and C_{60}(IV)+Kr solutions. At $T>12$ K the orientational relaxation times τ_2 are larger for C_{60}+He than for C_{60}(IV)+Kr.

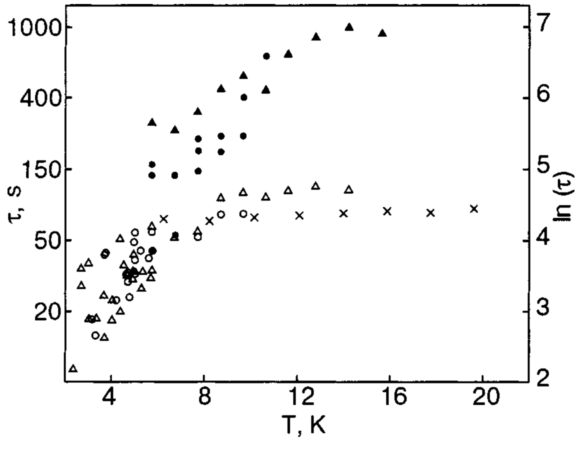

FIG. 12. Characteristic relaxation times τ of the thermal expansion of C_{60} +He: τ_1 (△,×), τ_2 (▲)—before partial desaturation; τ_1 (○), τ_2 (●)—after partial desaturation.

The detected features of the thermal expansion of fullerite C_{60} doped with helium can be explained in the framework of the model that we proposed for C_{60}+Kr.

4. CONCLUSIONS

The low-temperature thermal expansion of the orientational glass of pure C_{60} and C_{60} doped with inert gases is determined by the sum of positive and negative contributions. The analysis of their magnitudes, temperature dependences, and the related relaxation times has permitted us to assume that the positive contribution is made by the lattice excitations (phonons and librational excitations), while the negative contribution results from tunneling reorientation of a portion of the C_{60} molecules.

The implantation of Ar and Ne impurities decreasing the molar volume of fullerite enhances the noncentral interaction between the C_{60} molecules. The change caused by the impurities in the thermal expansion of C_{60} was interpreted as evidence of lower probability of rotational tunneling and higher libration frequency of the C_{60} molecules in the fullerite lattice.

The implantation of Kr and He impurities, increasing the molar volume of C_{60}, makes the noncentral interaction between the C_{60} molecules weaker. This generates two effects. First, the probability of rotational tunneling of the C_{60} molecules becomes higher; hence, the contribution of rotational tunneling to thermal expansion increases and the temperature interval in which this contribution exists becomes wider. Second, there is hysteresis of the thermal expansion of doped fullerite. The hysteresis may be due to the formation and mutual conversion of two phases of this orientational glass: this permits us to extend the phenomenon of polymorphism to orientational glasses as well.

*E-mail: aalex@ilt.kharkov.ua

---

[1] A. N. Aleksandrovskii, V. B. Esel'son, V. G. Manzhelii, A. Soldatov, B. Sundqvist, and B. G. Udovidchenko, Fiz. Nizk. Temp. **23**, 1256 (1997) [Low Temp. Phys. **23**, 943 (1997)].
[2] A. N. Aleksandrovskii, V. B. Esel'son, V. G. Manzhelii, A. Soldatov, B. Sundqvist, and B. G. Udovidchenko, Fiz. Nizk. Temp. **26**, 100 (2000) [Low Temp. Phys. **26**, 75 (2000)].
[3] J. D. Axe, S. C. Moss, and D. A. Neumann, in *Solid State Physics: Advances in Research and Applications*, H. E. Ehrenreich and F. Spaepen (Eds.), Vol. 48, Academic Press, New York (1994), p. 149.
[4] A. M. Tolkachev, A. N. Aleksandrovskii, and V. I. Kuchnev, Cryogenics **15**, 547 (1975).
[5] F. Gugenberger, R. Heid, C. Meingast, P. Adelmann, M. Braun, H. Wuhl, M. Haluska, and H. Kuzmany, Phys. Rev. Lett. **69**, 3774 (1992).
[6] F. W. Sheard, in *AIP Conf. Proc., N3, Thermal Expansion—1971*, M. G. Graham and H. E. Hagy (Eds.), AIP, New York (1972), p. 151.
[7] Yu. A. Freiman, Fiz. Nizk. Temp. **9**, 657 (1983) [Sov. J. Low Temp. Phys. **9**, 335 (1983)].
[8] V. Narayanamurti and R. O. Pohl, Rev. Mod. Phys. **42**, 201 (1970).
[9] V. G. Manzhelii, Yu. A. Freiman, M. I. Klein, and A. A. Maradudin (Eds.), *Physics of Cryocrystals*, AIP Press, Woodbury, New York (1996).
[10] V. M. Loktev, Fiz. Nizk. Temp. **25**, 1099 (1999) [Low Temp. Phys. **25**, 823 (1999)].
[11] V. M. Loktev, Yu. G. Pogorelov, and J. N. Khalack, Fiz. Nizk. Temp. **27**, 539 (2001) [Low Temp. Phys. **27**, 397 (2001)].
[12] A. N. Aleksandrovskii, V. G. Gavrilko, V. B. Esel'son, V. G. Manzhelii, B. Sundqvist, B. G. Udovidchenko, and V. P. Maletskiy, Fiz. Nizk. Temp. **27**, 333 (2001) [Low Temp. Phys. **27**, 245 (2001)].
[13] A. N. Aleksandrovskii, V. G. Gavrilko, V. B. Esel'son, V. G. Manzhelii, B.

Sundqvist, B. G. Udovidchenko, and V. P. Maletskiy, Fiz. Nizk. Temp. **27**, 1401 (2001) [Low Temp. Phys. **27**, 1033 (2001)].

[14] M. J. Rosseinsky, Mater. Chem. **5**, 1497 (1995).

[15] Charles H. Pennington and Victor A. Stenger, Rev. Mod. Phys. **68**, 855 (1996).

[16] B. Morosin, J. D. Jorgenson, Simine Short, G. H. Kwei, and J. E. Schirber, Phys. Rev. B **53**, 1675 (1996).

[17] G. E. Gadd, M. James, S. Moricca, P. J. Evans, and R. L. Davis, Fullerene Sci. Technol. **4**, 853 (1996).

[18] G. E. Gadd, S. J. Kennedy, S. Moricca, C. J. Howard, M. M. Elcombe, P. J. Evans, and M. James, Phys. Rev. B **55**, 14794 (1997).

[19] G. E. Gadd, S. Moricca, S. J. Kennedy, M. M. Elcombe, P. J. Evans, M. Blackford, D. Cassidy, C. J. Howard, P. Prasad, J. V. Hanna, A. Burchwood, and D. Levy, J. Phys. Chem. Solids **58**, 1823 (1997).

[20] *Rare Gas Solids*, M. L. Klein and J. A. Venables (Eds.), Vol. 1 (1977), Vol. 2 (1978), Academic Press, New York.

[21] W. P. Beyermann, M. F. Hundley, J. D. Thompson, F. N. Diederich, and G. Gruner, Phys. Rev. Lett. **68**, 2046 (1992).

[22] W. P. Beyermann, M. F. Hundley, J. D. Thompson, F. N. Diederich, and G. Gruner, Phys. Rev. Lett. **69**, 2737 (1992).

[23] N. A. Aksenova, A. P. Isakina, A. I. Prokhvatilov, and M. A. Strzhemechny, Fiz. Nizk. Temp. **25**, 964 (1999) [Low Temp. Phys. **25**, 724 (1999)].

[24] B. Sundqvist, O. Anderson, A. Lundin, and A. Soldatov, Solid State Commun. **93**, 109 (1995).

[25] T. Atake, T. Tanaka, H. K. Kikuchi, K. Saito, S. Suzuki, I. Ikemoto, and Y. Ashiba, Physica C **185–189**, 427 (1992).

[26] T. Atake, T. Tanaka, H. Kawaji, H. K. Kikuchi, K. Saito, S. Suzuki, Y. Ashiba, and I. Ikemoto, Chem. Phys. Lett. **196**, 321 (1992).

[27] B. Sundqvist, Physica B **265**, 208 (1999).

[28] J. R. Olson, K. A. Topp, and R. O. Pohl, Science **259**, 1145 (1993).

[29] E. Grivei, B. Nysten, M. Gassart, A. Demain, and J.-P. Issi, Solid State Commun. **85**, 73 (1993).

[30] S. Hoen, N. G. Chopra, X. D. Xiang, R. Mostovoy, Jianguo Hou, W. A. Vareka, and A. Zettl, Phys. Rev. B **46**, 12737 (1992).

[31] N. P. Kobelev, R. K. Nikolaev, Ya. M. Soifer, and S. S. Khasanov, Fiz. Tverd. Tela (St. Petersburg) **40**, 173 (1998) [Phys. Solid State **40**, 154 (1998)].

[32] G. A. Samara, L. V. Hansen, R. A. Assink, B. Morosin, J. E. Schirber, and D. Loy, Phys. Rev. B **47**, 4756 (1993).

[33] I. V. Legchenkova, A. I. Prokhvatilov, Yu. E. Stetsenko, M. A. Strzhemechny, K. A. Yagotintsev, A. A. Avdeenko, V. V. Eremenko, P. V. Zinoviev, V. N. Zoryanski, N. B. Silaeva, and R. S. Ruoff, Fiz. Nizk. Temp. **28**, 1320 (2002) [Low Temp. Phys. **28**, 942 (2002)].

[34] L. S. Palatnik, A. A. Nechitailo, and A. A. Koz'ma, Dokl. Akad. Nauk SSSR **36**, 1134 (1981).

[35] C. A. Angell, Science **267**, 1924 (1995).

This article was published in English in the original Russian journal. Reproduced here with stylistic changes by AIP.

LOW TEMPERATURE PHYSICS VOLUME 29, NUMBER 4 APRIL 2003

Dispersion relations for cubic crystals with noncentral interactions. Cryocrystals

E. V. Manzheliĭ*

B. Verkin Institute for Low Temperature Physics and Engineering, National Academy of Sciences of Ukraine, pr. Lenina 47, 61103 Kharkov, Ukraine

(Submitted November 20, 2002; revised December 11, 2002)
Fiz. Nizk. Temp. **29**, 443–450 (April 2003)

A study is made of how the presence of noncentral interactions of molecules with their nearest and next-nearest neighbors in crystals with cubic symmetry affects the dispersion relations. For certain directions in simple cubic (sc) and body-centered cubic (bcc) crystals with nearest-neighbor interactions the vibrational frequency depends only on the value of the noncentral interaction. A relatively small noncentral interaction has an important influence on the dynamic characteristics of a face-centered cubic (fcc) crystal. Quantitative estimates are made for cryocrystals with bcc and fcc lattices.
[DOI: 10.1063/1.1542478]

INTRODUCTION

Many properties of substances with short-range interactions between their particles can be estimated to a sufficient degree of accuracy by taking into account the interaction with the second coordination sphere. The majority of simple molecular crystals fall into this category. Many of their crystals have cubic symmetry; this is characteristic, in particular, for the various phases of cryocrystals.

Dispersion relations for crystals of cubic symmetry with allowance for the central interaction of particles with the nearest and next-nearest neighbors in the crystal lattice were established in Refs. 1 and 2. It was shown that a number of the fundamental features of the dispersion relations in simple cubic (sc) and body-centered cubic (bcc) lattices can be determined by taking into account the central interaction with next-nearest neighbors. For example, in a number of directions the frequency of transverse oscillations depends only on the value of the interaction with next-nearest neighbors. Furthermore, when only the interaction with nearest neighbors is taken into account in sc and bcc lattices, the longitudinal and transverse vibrational branches coincide, something that has never been observed in experiment. Taking the interaction with next-nearest neighbors into account removes this coincidence. For many molecular crystals, even the simplest ones, noncentral interactions have a very substantial influence on the behavior of many lattice characteristics.[3]

The goal of this study was to investigate the influence of noncentral interactions of particles with nearest and next-nearest neighbors in the lattice on the dynamic properties of crystals of cubic symmetry.

SIMPLE CUBIC LATTICE

Consider a simple cubic lattice. Many substances have unit cells of the sc type. Such substances include TlBr, TlI, NH_4Cl, CuPd, and one of the phases of C_{60}. The matrices of force constants of the interactions with the nearest and next-nearest neighbors of the sc lattice[4] have the form

$$\Phi_{ik}(a(1,0,0))=-\begin{pmatrix}\alpha & 0 & 0\\ 0 & \beta & 0\\ 0 & 0 & \beta\end{pmatrix},$$
$$\Phi_{ik}(a(1,1,0))=-\begin{pmatrix}\beta' & \gamma' & 0\\ \gamma' & \beta' & 0\\ 0 & 0 & \alpha'\end{pmatrix}. \qquad (1)$$

Here a is the lattice constant, $a(1,0,0)$ is the radius vector of one of the nearest neighbors, and $a(1,1,0)$ is the radius vector of the one of the next-nearest neighbors. The remaining force-constant matrices are obtained from those given above by a transformation of the group O_h (Ref. 4). In the case of a central interaction one has $\beta=0$, $\beta'=\gamma'$, and $\alpha'=0$ (Ref. 4).

In this paper we consider an interaction to be noncentral if its force constants differ from those for a central interaction. For example, let us give expressions for the force constants of the sc lattice if the interaction between atoms is described by an isotropic pair potential $f(\mathbf{r},\ \mathbf{r}')=f(|\mathbf{r}-\mathbf{r}'|)$. In that case

$$\Phi_{ik}=-f''(l)\,\frac{x_i x_k}{l^2}+f'(l)\,\frac{x_i x_R}{l^3}-\frac{f'(l)}{l}\,\delta_{ik}, \qquad (2)$$

where x_i and x_k are the components of the radius vector of an atom in equilibrium, and l is the distance between neighbors. In the case of a central interaction one has $f'(l)=0$.

To illustrate the influence of a noncentral interaction on the dynamic properties of the sc lattice, let us give and analyze the dispersion relations for the high-symmetry directions of the sc crystal.

1. Along the direction $\mathbf{k}=k(1,0,0)$ the dispersion relations are described by the expressions

$$m\omega_l^2=2\alpha(1-\cos ak)+8\beta'(1-\cos ak),$$
$$m\omega_t^2=2\beta(1-\cos ak)+4\alpha'(1-\cos ak)+4\beta'(1-\cos ak). \qquad (3)$$

Here ω is the angular frequency of the oscillations, $\mathbf{k}$ is the wave vector, and m is the mass of an atom. The subscripts l and t correspond to longitudinal and transverse oscillations, respectively. It is seen from the above expressions that in the case of only a nearest-neighbor interaction it is necessary to take the noncentral interaction between atoms into account, since otherwise $\omega_t \equiv 0$ and the lattice is unstable. It is clear that in the case of a weak noncentral interaction with nearest neighbors stability of the sc lattice is brought about by the interaction with remote neighbors.

2. In the direction $\mathbf{k}=k(1,1,0)$ the dispersion relation has the form

$$\begin{aligned} m\omega_l^2 &= 2\alpha(1-\cos ak)+2\beta(1-\cos ak) \\ &\quad +2\beta'(3-2\cos ak-\cos 2ak)+4\alpha'(1-\cos ak) \\ &\quad +4\gamma'(1-\cos 2ak), \end{aligned} \tag{4}$$

$$\begin{aligned} m\omega_{t_1}^2 &= (2\alpha+2\beta)(1-\cos ak)+2\beta'(3-2\cos ak \\ &\quad -\cos 2ak)+4\alpha'(1-\cos ak) \\ &\quad -2\gamma'(1-\cos 2ak), \end{aligned}$$

$$m\omega_{t_2}^2 = 4\beta(1-\cos ak)+8\beta'(1-\cos ak).$$

In analogy with the direction $\mathbf{k}=k(1,0,0)$, one of the frequencies of transverse oscillations is independent of the value of the central interaction with nearest neighbors. It should be noted that a difference of the longitudinal and transverse branches of oscillations arises only when the interaction with non-nearest neighbors is taken into account.

3. For the direction $\mathbf{k}=k(1,1,1)$ the dispersion curves are described by the expressions

$$\begin{aligned} m\omega_l^2 &= (2\alpha+4\beta)(1-\cos ak)+(4\beta'+4\gamma') \\ &\quad \times(1-\cos 2ak)+2\alpha'(1-\cos 2ak), \\ m\omega_t^2 &= (2\alpha+4\beta)(1-\cos ak)+(2\gamma'-2\alpha') \\ &\quad \times(1-\cos 2ak). \end{aligned} \tag{5}$$

We see that in order for all three branches not to coincide, it is necessary to take into account the interaction with next-nearest neighbors. In the sc lattice there are twice as many next-nearest as nearest neighbors, and the distance to the next-nearest neighbors is larger than the distance to nearest neighbors by a factor of $\sqrt{2}$.

The experimental study of dispersion relations is rather complicated. However, in recent years some new experimental data on the elastic constants of cubic crystals have appeared (see, e.g., Refs. 5 and 6) which can also yield information about the noncentral interaction between atoms or molecules.

The elastic constants can be expressed in terms of the force constants as

$$c_{11}=\frac{\alpha}{a}+\frac{4\beta'}{a},\quad c_{12}=\frac{4\gamma'}{a}-\frac{\beta}{a}-\frac{2\beta'}{a}-\frac{2\alpha'}{a},$$

$$c_{44}=\frac{\beta}{a}+\frac{2\beta'}{a}+\frac{2\alpha'}{a}. \tag{6}$$

If the noncentral interaction with next-nearest neighbors, which is known to be small, is set equal to zero ($\beta=0$, $\beta'=\gamma'$), one can use the system of equations (6) with the experimental data on the elastic constants to determine the values of the three force constants α, β, and β'.

Thus the noncentral interaction of nearest neighbors determines the stability of the sc crystal lattice. For certain crystallographic directions this type of interaction leads to a nonzero dispersion curve corresponding to one of the transverse acoustic modes. If the non-central interaction of nearest neighbors is small, then for stability of the sc lattice it is necessary to take the interaction with non-nearest neighbors into account. Moreover, inclusion of the interaction with next-nearest neighbors removes the coincidence of the longitudinal branch of oscillations with the transverse branches.

BODY-CENTERED CUBIC LATTICE

The bcc lattice is found in a large number of crystals, e.g., ^{3}He, ^{4}He, SF$_6$, Fe, Nb, V, Na, and Cr. The matrices of the force constants of the interaction with nearest and next-nearest neighbors in the bcc lattice have the form[4]

$$\begin{aligned} \Phi_{ik}\left(\frac{a}{2}(1,1,1)\right) &= -\begin{pmatrix} \alpha'' & \gamma'' & \gamma'' \\ \gamma'' & \alpha'' & \gamma'' \\ \gamma'' & \gamma'' & \alpha'' \end{pmatrix}, \\ \Phi_{ik}(a(1,0,0)) &= -\begin{pmatrix} \alpha & 0 & 0 \\ 0 & \beta & 0 \\ 0 & 0 & \beta \end{pmatrix}. \end{aligned} \tag{7}$$

In analogy with Eq. (1), $(a/2)(1,1,1)$ is the radius vector of one of the nearest neighbors, and $a(1,0,0)$ is the radius vector of one of the next-nearest neighbors. The remaining force matrices are obtained from those indicated above by a transformation of the O_h group,[4] and in the case of a central interaction one has $\beta=0$ and $\alpha''=\gamma''$ (Ref. 4).

Let us analyze the influence of a noncentral interaction on the dispersion relations and elastic constants of the bcc lattice.

1. For the direction $\mathbf{k}=k(1,0,0)$ the dispersion relations have the form

$$\begin{aligned} m\omega_l^2 &= 8\alpha''\left(1-\cos\frac{ak}{2}\right)+2\alpha(1-\cos ak), \\ m\omega_t^2 &= 8\alpha''\left(1-\cos\frac{ak}{2}\right)+2\beta(1-\cos ak). \end{aligned} \tag{8}$$

We see that the noncentral interaction with nearest neighbors affects only the shape of the dispersion curves, while the frequency difference between the longitudinal and transverse modes depends on the difference between the force constants of the central and noncentral interaction with next-nearest neighbors.

2. Along the direction $\mathbf{k}=k(1,1,0)$ the dispersion curves are described by the expression

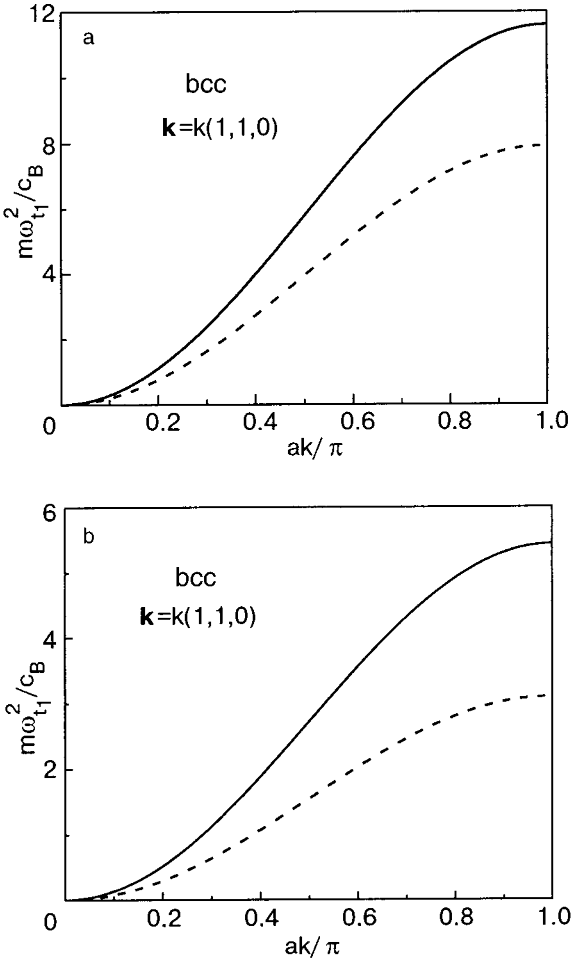

FIG. 1. Transverse vibrational branches $m\omega_{t1}^2/c_B$ of the bcc lattice for the direction $\mathbf{k}=k(1,1,0)$. The dashed lines show the dispersion curves corresponding to the constants $c_B=7.1\times10^2$ dyn/cm, $n_B=1.6\times10^2$ dyn/cm, and $\alpha=2.1\times10^3$ dyn/cm (a) and $c_B=4.6\times10^2$ dyn/cm, $n_B=6\times10^1$ dyn/cm, and $\alpha=6.27\times10^2$ dyn/cm (b). The solid lines are the dispersion curves $m\omega_{t1}^2/c_B$ corresponding to $c_B=7.1\times10^2$ dyn/cm, $n_B=0$, and $\alpha=2.1\times10^3$ dyn/cm (a) and $c_B=4.6\times10^2$ dyn/cm, $n_B=0$, and $\alpha=6.27\times10^2$ dyn/cm (the case of a central interaction) (b). The force constants were obtained from the elastic constants of SF_6 (Ref. 7) at $T=100$ K (a) and 221 K (b).

$$\begin{aligned}
m\omega_l^2&=4\alpha''(1-\cos ak)+4\gamma''(1-\cos ak)\\
&\quad+2\alpha(1-\cos ak)+2\beta(1-\cos ak),\\
m\omega_{t_1}^2&=(4\alpha''-4\gamma'')(1-\cos ak)+2\alpha(1-\cos ak)\\
&\quad+2\beta(1-\cos ak),\\
m\omega_{t_2}^2&=4\alpha''(1-\cos ak)+4\beta(1-\cos ak).
\end{aligned}\tag{9}$$

We see that ω_{t1} depends on the interaction with the nearest neighbors only in the case when this interaction is noncentral, and in the case of a weak noncentral interaction with nearest neighbors the stability of the lattice is determined by the interaction with non-nearest neighbors.

3. For the $\mathbf{k}=k(1,1,1)$ direction the noncentral interaction with nearest neighbors and the interaction with non-nearest neighbors affect only the shape of the dispersion curves. The dispersion relations for this direction have the form

$$\begin{aligned}
m\omega_l^2&=8\alpha''\left(1-\cos^3\frac{ak}{2}\right)+16\gamma''\cos\frac{ak}{2}\sin^2\frac{ak}{2}\\
&\quad+2\alpha(1-\cos ak)+4\beta(1-\cos ak),\\
m\omega_t^2&=8\alpha''\left(1-\cos^3\frac{ak}{2}\right)-8\gamma''\cos\frac{ak}{2}\sin^2\frac{ak}{2}\\
&\quad+2\alpha(1-\cos ak)+4\beta(1-\cos ak).
\end{aligned}\tag{10}$$

The expressions relating the elastic constants with the force constants are

$$\begin{aligned}
&c_{11}=\frac{2\alpha''}{a}+\frac{2\alpha}{a},\quad c_{12}=\frac{4\gamma''}{a}-\frac{2\alpha''}{a}-\frac{2\beta}{a},\\
&c_{44}=\frac{2\alpha''}{a}+\frac{2\beta}{a}.
\end{aligned}\tag{11}$$

As an example of the influence of a noncentral interaction on the dispersion relations of bcc crystals, we give the dispersion curves obtained using the force constants determined from the elastic constants of sulfur hexafluoride at temperatures of 100 and 221 K (Ref. 7) without allowance for the orientational–translational interaction (Fig. 1). The elastic constants of sulfur hexafluoride at 100 K were obtained by a

TABLE I. Deviations from the Cauchy relation for cryocrystals.

Substance	T, K	δ [Refs.]
Ar	10	−0.06 [10,14]
	82	−0.18 [10,14]
	82.3	−0.28 [10,15]
Kr	10	−0.06 [10,16]
	114	−0.23 [10,17]
	115	−0.27 [10,18]
Xe	10	−0.04 [10,19]
	111	−0.12 [10,19]
	159.6	−0.13 [10,19]
	156	−0.22 [10,20]
Ne	5	−0.11 [10,21]
	6	−0.03 [10,22]
	23.7	−0.14 [10,22]
	24.3	−0.18 [10,23]
CD_4	32.5	−0.26 [5,24]
	34.5	−0.38 [5,25]
	85.57	−0.39 [5,26]
	89.2	−0.33 [5,27]
CO_2	95	−0.18 [5,28]
CO	60.9	−0.26 [5,29]
N_2	15	−0.33 [6,30]
CH_4	30	−0.13 [6,31]
	85	−0.4 [6,31]
C_{60}	300	−0.25 [32]
SF_6	187	−0.47 [7]
	221	−0.41 [7]
	100	−0.54*

*Obtained from Ref. 7 by linear extrapolation.

linear extrapolation. For comparison, Fig. 1 shows the curves corresponding to an isotropic pair potential for the interatomic interaction, in which case $\beta''=\gamma''=c_B$. For the case of an isotropic pair potential

$$\frac{1}{3}f''\left(\frac{\sqrt{3}}{2}a\right)=c_B,\quad \frac{4f'\left(\frac{\sqrt{3}}{2}a\right)}{3\sqrt{3}a}=n_B. \tag{12}$$

We see that a noncentral interaction can have a substantial quantitative influence on the dispersion curves.

Thus the noncentral interaction with nearest neighbors and the interaction with next-nearest neighbors in the bcc lattice influence the dynamic properties in a manner analogous to the case of the sc lattice.

FACE-CENTERED CUBIC LATTICE

The fcc lattice is found in solidified rare gases, in one of the phases of N_2, CO, CO_2, N_2O, CH_4, NH_3, and C_{60}, and also in Ag, Ni, and Cu. Unlike the sc and bcc lattices, where taking a noncentral interaction with nearest neighbors into account leads to qualitative changes in the theoretical dispersion curves, for the fcc lattice there are only quantitative changes in the dispersion relations, although those changes can be quite substantial. The value of the noncentral interaction can be inferred, in particular, from experimental data on the deviation from the Cauchy relation $\delta=(-c_{12}+c_{44})/c_{12}$ (see Table I).

With the central and noncentral interactions of the nearest and next-nearest neighbors taken into account, the force-constant matrices of the fcc lattice have the form[4]

$$\Phi_{ik}\left(\frac{a}{2}(1,1,0)\right)=-\begin{pmatrix}\beta' & \gamma' & 0\\ \gamma' & \beta' & 0\\ 0 & 0 & \alpha'\end{pmatrix},$$
$$\Phi_{ik}(a(1,0,0))=-\begin{pmatrix}\alpha & 0 & 0\\ 0 & \beta & 0\\ 0 & 0 & \beta\end{pmatrix}. \tag{13}$$

For a fcc crystal $(a/2)(1,1,0)$ is the radius vector of one of the nearest neighbors, and $a(1,0,0)$ is the radius vector of one of the next-nearest neighbors. The remaining force matrices are obtained from those indicated above by a transformation of the O_h group.[4] For a central interaction one has $\beta'=\gamma'$, $\alpha'=0$, and $\beta=0$.

By analogy with Eq. (12) we introduce the notation

$$\frac{1}{2}f''\left(\frac{\sqrt{2}}{2}a\right)=c_F,\quad \frac{\sqrt{2}}{2}\,\frac{f'\left(\frac{\sqrt{2}}{2}a\right)}{a}=n_F. \tag{14}$$

For certain high-symmetry directions the dispersion relations take the forms:

1) for the $\mathbf{k}=k(1,0,0)$ direction

$$m\omega_l^2=16\beta'\sin^2\frac{ak}{4}+2\alpha(1-\cos ak),$$
$$m\omega_t^2=8\beta'\sin^2\frac{ak}{4}+2\beta(1-\cos ak); \tag{15}$$

2) for the $\mathbf{k}=k(1,1,0)$ direction

$$\begin{aligned}m\omega_l^2={}&8\beta'\sin^2\frac{ak}{4}+4\beta'\sin^2\frac{ak}{2}+8\alpha'\sin^2\frac{ak}{2}\\&+4\gamma'\sin^2\frac{ak}{2}+2\alpha(1-\cos ak)\\&+2\beta(1-\cos ak),\\ m\omega_{t_1}^2={}&8\beta'\sin^2\frac{ak}{4}+4\beta'\sin^2\frac{ak}{2}+8\alpha'\sin^2\frac{ak}{4}\\&-4\gamma'\sin^2\frac{ak}{2}+2\alpha(1-\cos ak)\\&+2\beta(1-\cos ak),\end{aligned} \tag{16}$$

$$m\omega_{t_2}^2=16\beta'\sin^2\frac{ak}{4}+4\alpha'\sin^2\frac{ak}{4}+4\beta(1-\cos ak);$$

3) along the $\mathbf{k}=k(1,1,1)$ direction the dispersion relations are described by the expressions

$$\begin{aligned}m\omega_l^2={}&8\beta'\sin^2\frac{ak}{2}+8\gamma'\sin^2\frac{ak}{2}+4\alpha'\sin^2\frac{ak}{2}\\&+2\alpha(1-\cos ak),\end{aligned} \tag{17}$$

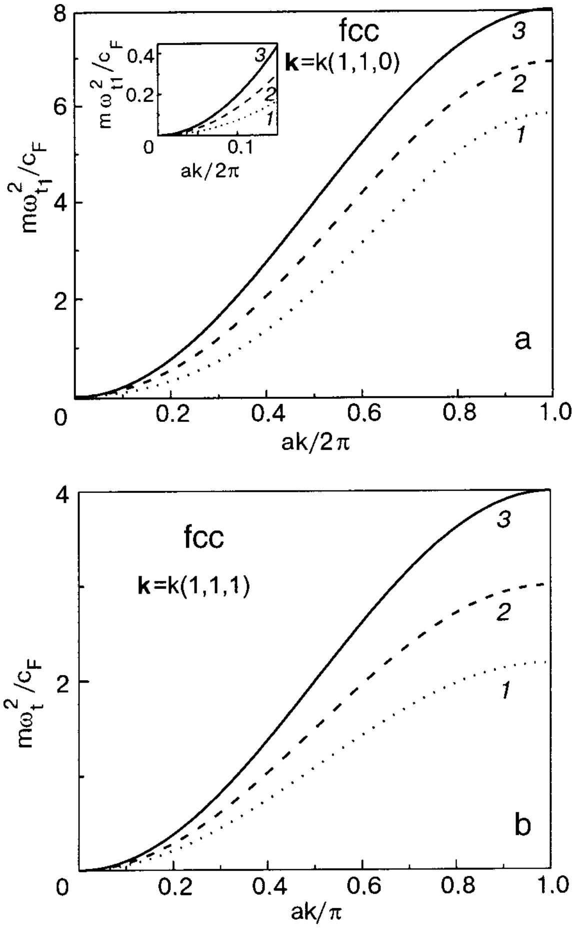

FIG. 2. Transverse vibrational branches $m\omega_{t1}^2/c_F$ of the fcc lattice for the direction $\mathbf{k}=k(1,1,0)$ (a) and $m\omega_t^2/c_F$ for $\mathbf{k}=k(1,1,1)$ (b). For the dispersion curves shown the values of the constants c_f and n_F were obtained for $\delta=-0.5$ (*1*), -0.3 (*2*), and 0 (the case of a central interaction) (*3*).

$$m\omega_t^2 = 8\beta' \sin^2\frac{ak}{2} + 4\alpha' \sin^2\frac{ak}{2} - 4\gamma' \sin^2\frac{ak}{2} + 2\beta(1-\cos ak).$$

For fcc crystals the expressions for the elastic constants as functions of the force constants of the interactions with nearest and next-nearest neighbors are

$$c_{11} = \frac{4\beta'}{a} + \frac{4\alpha}{a}, \quad c_{12} = \frac{4\gamma'}{a} - \frac{2\beta'}{a} - \frac{2\alpha'}{a} - \frac{\beta}{a}, \quad c_{44} = \frac{\beta}{a} + \frac{2\beta' + 2\alpha'}{a}. \tag{18}$$

To illustrate the influence of a noncentral interaction on the dispersion curves of fcc crystals for different values of the deviation from the Cauchy relations, let us give the dispersion curves for $\delta_1 = -0.3$ and $\delta_2 = -0.5$, with only the interaction with nearest neighbors taken into account (Fig. 2). For comparison, Fig. 2 shows the dispersion curves obtained without the noncentral interaction (for $n_F = 0$). We note that the values chosen for δ are close to those obtained experimentally for simple molecular crystals (see Table I). It is seen in Fig. 2 that, even though the contribution of the noncentral interaction to the force constants is small at the chosen values of δ ($n_F/c_F \approx -0.046$ and $n_F/c_F \approx -0.11$, respectively), there exist crystallographic directions for which the contribution of the noncentral interaction to the vibrational frequencies is substantial.

The use of an isotropic pair potential, which, strictly speaking, is unsuitable for a quantitative description of the force constants, nevertheless permits estimation of the contribution of the noncentral interaction to the dispersion relations for the directions chosen. By way of illustration we note that by virtue of the symmetry of the fcc lattice, even a doubling of the force constants would only have a slight influence on the curves shown in Fig. 2.

Thus in fcc crystals the inclusion of a noncentral interaction leads to only quantitative changes of the dispersion relations, although these changes can be significant.

INFLUENCE OF NONCENTRAL INTERACTION ON THE DISPERSION LAWS IN CRYOCRYSTALS

The results obtained in the present study are of interest primarily for the simplest molecular crystals (molecular cryocrystals). First, the majority of these substances have phases with lattices of cubic symmetry.[5,6] Second, as a rule, the forces of interaction in cryocrystals are short-range forces, and it is often sufficient to take only the nearest neighbors into account in estimating the behavior of the lattice properties.[8,9] Third, noncentral interactions play a large role in molecular cryocrystals.[3] It is of interest to calculate the dispersion curves and to estimate the influence of a noncentral interaction on them at values of the force constants close to those realized in cryocrystals. We have already discussed the possibility of calculating the force constants from the values of the elastic constants. Experimental studies of the sound velocities and Brillouin scattering in single-crystal samples of cryocrystals have been reported recently.[6] Table II gives numerical values of the force constants obtained from the elastic constants in the nearest-neighbor approximation for molecules crystals with the fcc lattice.

Table III gives the force constants of sulfur hexafluoride SF_6 (a bcc crystal). The values were obtained from the elastic constants without allowance for the orientational–translational interaction. The role of the noncentral interaction can be judged, in particular, from the deviation of $\delta(T)$ from the Cauchy relation for the elastic constants.[3,4] We re-

TABLE II. Force constants for cryocrystals with the fcc lattice.

Substance	T	Θ_D	c_{11}	c_{12}	c_{44}	β'	γ'	α'	δ
	K		GPa			10^2 dyn/cm		10 dyn/cm	
CO_2	95	152 [5]	13.6±0.6 [5,28]	6.2±1.0 [5,28]	5.1±0.3 [5,28]	19	26	−4.8	−0.18
CO	60.9	103 [5]	2.41±0.05 [5,29]	1.44±0.04 [5,29]	1.06±0.04 [5,29]	3.5	3.6	−4.2	−0.26
N_2	15	81.3 [5]	2.9±0.05 [5,30]	2.0±0.01 [5,30]	1.35±0.05 [5,30]	4.0	4.7	−2.8	−0.33
C_{60}	300	55 [34,35]	14.9±0.9 [32]	8.8±1.0 [32]	6.6±0.18 [32]	53	5.8	−1.8	−0.25
CD_4	32.5	138 [5]	3.08±0.2 [5,24]	2.14±0.24 [5,24]	1.58±0.6 [5,24]	4.5	5.5	1.2	−0.26
	34.5		3.28±0.16 [5,25]	2.39±0.16 [5,25]	1.49±0.1 [5,25]	4.8 4.98±0.25*	5.7 5.89±0.28*	−4.0 8.3±0.29*	−0.38
CH_4	32.5	141 [5]	2.92±0.06 [6,31]	1.89±0.05 [6,31]	1.62±0.05 [6,31]	4.3	5.2	4.5	−0.15
	34.5		2.89±0.06 [6,31]	1.88±0.05 [6,31]	1.59±0.05 [6,31]	4.3	5.1	4.2	−0.15
	30		2.96±0.06 [6,31]	1.9±0.05 [6,31]	1.65±0.05 [6,31]	4.4	5.2	4.8	−0.13

*The values of the force constants were obtained from the experimental dispersion curves with the use of the Born–von Kárman model.[24] Θ_D is the Debye temperature, and c_{11}, c_{12}, and c_{44} are elastic constants.

TABLE III. Force constants for cryocrystals with the bcc lattice.

Substance	T	Θ_D	c_{11}	c_{12}	c_{44}	α''	γ''	α	δ
	K		GPa			10^2 dyn/cm			
SF_6	187	48.3 [35]	4.997 [7]	2.776 [7]	1.483 [7]	4.1	5.6	7.3	−0.47
	100		9.0*	4.48*	1.89*	5.5	8.8	21	−0.54

*Obtained from Ref. 7 by linear extrapolation. Θ_D is the Debye temperature, and c_{11}, c_{12}, and c_{44} are elastic constants.

call that this relation, which applies to cubic crystals, should hold for harmonic crystals with a central interaction. Anharmonic effects are substantial for quantum crystals at all temperatures in their existence region and for classical crystals at high temperatures. Table I gives the values of δ for classical atomic crystals (Ar, Kr, Xe) at $T=10$ K, where the temperature dependence of the elastic constants can be ignored, and at high temperatures. Even for these fcc crystals with a central interaction, in which case one would expect the best conformity with the Cauchy relation, δ has rather large values at high temperatures. At 10 K the values of δ are close to zero, within the experimental error. The data in Table I indicate that to estimate the contribution to the force constants of cryocrystals from the noncentral interaction of their molecules, one should use experimental values of the elastic constants which have been obtained at sufficiently low temperatures. It should be remembered that the choice of these temperatures depends substantially on the substance. In particular, for solid CH_4, CD_4, CO, and N_2 a temperature of 50 K is already high in this sense, while for solid CO_2 or N_2O it can be considered low, and in the case of fullerite C_{60} the anharmonicity can be neglected even at 300 K.

When the elastic constants obtained from ultrasonic studies are used in calculations, one should be mindful of the renormalization of the sound velocities due to the interaction between the translational and orientational branches of the spectrum. As far as we know, order-of-magnitude theoretical estimates of this renormalization have been made only for the sc lattice with molecules of cubic symmetry.[11,12] In a number of cases, however, analysis of experimental data on the sound velocities in cryocrystals permits drawing the conclusion that this renormalization is small and, to a first approximation, may be neglected. As an example, we note that the $\alpha\rightarrow\beta$ transition in solid nitrogen is accompanied by a decrease in the velocity of longitudinal and transverse sound by 8% and 3%, respectively.[5,13] At the same time, the interaction between the translational and orientational motion of the molecules in the crystal should be affected considerably by the vanishing of the long-range orientational order at this transition. This suggests that the sound velocity in solid nitrogen has only a weak dependence on this interaction. It is important to note the following circumstance: in Ref. 24 the force constants for solid CD_4 were calculated from the experimental dispersion curves with the use of the Born–von Kármán model. The values of β' and γ' reported in Ref. 24 agree with our values to within the error limits. The discrepancy in the values of α' is comparatively large. However, this constant is the least accurately determined. In view of what we have said above, the estimates made in the present study can be regarded as giving a realistic idea of the influence of a noncentral interaction on the dispersion curves of cryocrystals.

In closing the author thanks E. S. Syrkin and V. G. Manzhelii for posing the problem and for a discussion of the results.

[*] E-mail: emanzhelii@ilt.kharkov.ua

---

[1] E. V. Manzhelii and E. S. Syrkin, Physica B **263–264**, 439 (1999).
[2] E. V. Manzheliĭ and E. S. Syrkin, Fiz. Nizk. Temp. **25**, 1224 (1999) [Low Temp. Phys. **25**, 917 (1999)].
[3] V. G. Manzhelii and Yu. A. Freiman (Eds.), *Physics of Cryocrystals*, AIP Press, Woodbury, New York (1996).
[4] G. Leibfried, in *Handbuch der Physik*, Vol. 7, Part 1, S. Flügge (Ed.), Springer-Verlag, Berlin (1955), p. 105, *Mikroskopicheskaya Teoriya Mekhanicheskikh i Teplovyk Svoĭstv Kristallov*, Gos. Izd-vo Fiz-Mat. Lit., Moscow (1963).
[5] V. G. Manzhelii, A. I. Prokhvatilov, V. G. Gavrilko, and A. P. Isakina, *Structure and Thermodynamic Properties of Cryocrystals*, Handbook, Begell House, New York, Wallingford, UK (1999).
[6] A. I. Prokhvatilov, *Plasticity and Elasticity of Cryocrystals*, Handbook, Begell House, New York, Wallingford, UK (2001).
[7] H. Kiefte, R. Penney, and M. J. Clouter, J. Chem. Phys. **88**, 5846 (1988).
[8] M. L. Klein and J. A. Venables (Eds.), *Rare Gas Solids*, Academic Press, London–New York–San Francisco, Vol. I (1976), Vol. II (1977).
[9] I. G. Kaplan, *Theory of Intermolecular Interactions*, Elsevier, New York (1986), Nauka, Moscow (1982).
[10] P. Corpiun and E. Luscher, Thermal and Elastic Properties at Low Pressure in: Rare Gas Solids, M. L. Klein and J. A. Venables (Eds.), Academic Press, London, New York, San Francisko, Vol. II (1977).
[11] Yu. A. Freiman and A. I. Erenburg, Elementary Excitation Spectrum and Thermodynamic Properties of Low-Pressure Phases in: Physics of Cryocristals, V. G. Manzhelii and Yu. A. Freiman (Eds.), AIP Publisher, New York (1996).
[12] V. A. Slyusarev and Yu. A. Freĭman, Fiz. Tverd. Tela (Leningrad) **13**, 646 (1971) [Sov. Phys. Solid State **13**, 534 (1971)].
[13] P. A. Bezugli, L. M. Tarasenko, and Yu. C. Ivanov, Fiz. Tverd. Tela (Leningrad) **10**, 2119 (1968) [Sov. Phys. Solid State **10**, 1660 (1968)].
[14] Y. Fujii, N. A. Lurie, R. Pynn, and G. Shirane, J. Phys. Chem. Solids **36**, 145 (1975).
[15] S. Gerwutz and B. P. Stocheff, Phys. Rev. B **10**, 3487 (1974).
[16] J. Skalyo Jr. and Y. Endoh, Phys. Rev. B **9**, 1797 (1974).
[17] J. Skalyo Jr., Y. Endoh, and G. Shirane, Phys. Rev. B **7**, 4670 (1973).
[18] D. Landheer, H. E. Jacson, R. A. McLaren, and B. P. Stoicheff, Phys. Rev. B **13**, 888 (1976).
[19] N. A. Lurie, G. Shirane, and J. Skalyo Jr., Phys. Rev. B **9**, 2661 (1974).
[20] W. S. Gornal and B. P. Stoicheff, Phys. Rev. B **4**, 4518 (1971).
[21] J. Skalyo Jr., V. J. Minkievicz, and G. Shirane, Phys. Rev. B **6**, 4766 (1972).
[22] Y. Endoh, G. Shirane, and J. Skalyo Jr., Phys. Rev. B **11**, 1681 (1975).
[23] R. A. McLaren, H. Kiefte, D. Landheer, and B. P. Stoicheff, Phys. Rev. B **11**, 1705 (1975).
[24] W. G. Stirling, W. Press, and H. H. Stiller, J. Phys. C **10**, 3959 (1977).
[25] W. Press, B. Borner, and H. H. Stiller, Solid State Commun. **9**, 1113 (1971).
[26] S. V. Marx and R. O. Simmons, J. Chem. Phys. **81**, 944 (1984).
[27] S. C. Rand and B. P. Stoicheff, Can. J. Phys. **60**, 287 (1982).
[28] B. M. Powell, G. Dolling, G. Piseri, and P. Martel, in *Proceedings of the Symposium on Neutron Scattering, Grenoble 1972*, p. 207.
[29] V. Askarpour, H. Kiefte, and M. J. Clouter, Can. J. Chem. **66**, 541 (1988).
[30] J. K. Kjems and G. Dolling, Phys. Rev. B **11**, 1639 (1975).
[31] E. Grigoriantz and M. J. Clouter, J. Low Temp. Phys. **111**, 717 (1998).
[32] N. P. Kobelev, R. K. Nikolaev, Ya. M. Soĭfer, and S. S. Khasanov, Fiz.

Tverd. Tela (St. Petersburg) **40**, 173 (1998) [Phys. Solid State **40**, 1254 (1998)].

[33] A. N. Aleksandrovskii, V. G. Gavrilko, V. B. Esel'son, V. G. Manzhelii, B. G. Udovidchenko, V. P. Maletskiy, and B. Sundkvist, Fiz. Nizk. Temp. **27**, 1401 (2001) [Low Temp. Phys. **27**, 1033 (2001)].

[34] N. A. Aksenova, A. P. Isakina, A. I. Prokhvatilov, and M. A. Strzhemechny, Fiz. Nizk. Temp. **25**, 964 (1999) [Low Temp. Phys. **25**, 724 (1999)].

[35] A. P. Isakina and A. I. Prokhvatilov, Fiz. Nizk. Temp. **19**, 201 (1993) [Low Temp. Phys. **19**, 142 (1993)].

Translated by Steve Torstveit

LOW TEMPERATURE PHYSICS VOLUME 29, NUMBER 4 APRIL 2003

LOW-TEMPERATURE PHYSICS OF PLASTICITY AND STRENGTH

Quantitative analysis of the creep deformation jump stimulated by the superconducting transition in β-tin

V. D. Natsik,* V. P. Soldatov, G. I. Kirichenko, and L. G. Ivanchenko

B. Verkin Institute for Low Temperature Physics and Engineering, National Academy of Sciences of Ukraine, pr. Lenina 47, 61103 Kharkov, Ukraine

(Submitted July 23, 2002)
Fiz. Nizk. Temp. **29**, 451–468 (April 2003)

The detailed study begun earlier (V. P. Soldatov *et al.*, Fiz. Nizk. Temp. **27**, 1421 (2001) [Low Temp. Phys. **27**, 1048 (2001)]) on the kinetics of transient creep stimulated by the $n-s$ superconducting transition in single crystals of pure β-Sn is continued. The samples are oriented for slip in the (100)⟨010⟩ system. In that case the kinetics of creep is governed by the motion of dislocations through the barriers of the Peierls potential relief. Experiments are carried out at temperatures of $T_1 = 1.6$ K and $T_2 = 3.2$ K, which are lower than the critical temperature of tin, $T_c = 3.72$ K; the $n-s$ and $s-n$ transitions are brought about by turning a magnetic field off and on. The staged character of the creep curves $\delta\varepsilon_{ns}(t)$ after an $n-s$ transition is confirmed: at $T_1 = 1.6$ K one can distinguish a transient, a dynamic, and a fluctuation stage, and at $T_2 = 3.2$ K, a transient and a fluctuation stage. The quantitative characteristics of each stage are investigated as functions of the creep rate at the time of the $n-s$ transition and the total prestrain of the sample. The method of small loads is used to construct the macroscopic stress–strain diagram of β-Sn for the temperatures indicated and the work-hardening coefficients characterizing the intensity of the hardening on a macroscopic scale are determined. In the Appendix a theory of low-temperature creep in metals is set forth which involves the quantum (tunneling), dynamic, and thermally activated motion of dislocations in the Peierls potential relief. The features and characteristics of the dynamic and fluctuation stages of the experimental creep curves $\delta\varepsilon_{ns}(t)$ of tin are compared with the theory. It is established that the fluctuation stage of creep in tin is of a quantum character in the temperature interval studied. An analysis of the creep curves allows estimation of the work-hardening coefficient on the macro- and microscopic scales. It is found that the transient creep of β-Sn at temperatures in the liquid-helium region is due to low-energy dislocation processes involving a tunneling through effective potential barriers of the order of 10^{-3} eV in height. [DOI: 10.1063/1.1542479]

INTRODUCTION

The transition of a metallic superconductor from the normal to the superconducting state ($n-s$ transition) during its deformation in a creep regime substantially alters the kinetics of the process: the strain rate increases sharply and an additional amount of creep deformation appears.[1,2] Such a reaction to a change of the electronic state is a manifestation of the plastification effect, the disordering of a metal by a superconducting transition.[3,4] It has been established that the first cause of this effect is the sharp decrease of the electron drag on dislocations owing to the Cooper condensation of the conduction electrons,[4–6] and its study therefore provides a unique opportunity to elucidate the role of the conduction electrons in various processes of low-temperature plasticity of metals. In addition, experiment shows that the quantitative characteristics of the plastification effect are extremely sensitive to the type, magnitude, height, and concentration of the barriers governing the mobility of dislocations in a deformable superconductor.[7–11] This circumstance allows one to use a study of the plastification effect to solve a number of more general problems of the dislocation physics of plasticity. One such problem is to elucidate the relative role of thermal and quantum fluctuations and also the role of phonon and electron viscosities in the processes by which the dislocations overcome local and extended barriers of various types which are impeding their slip.

In Ref. 12 we studied the kinetics of the increment of creep deformation induced by the $n-s$ transition in single-crystal samples of pure β-tin during their deformation along the slip system (100)⟨010⟩. The experiment was done at a temperature of 1.6 K, which is below the critical temperature $T_c = 3.72$ K of the superconducting transition, and the direct $n-s$ and inverse $s-n$ transitions are brought about by turning off and on an external magnetic field $H > H_c$ (H_c is the critical field of the transition). The variation of the strain increment $\delta\varepsilon_{ns}(t)$ after the $n-s$ transition in the case of coarse measurements has a jumplike character: a significant increase in the value of the strain is observed over short time intervals (Fig. 1a). However, with the aid of a fast sweep system it was established that this ‘‘jump’’ consists of several

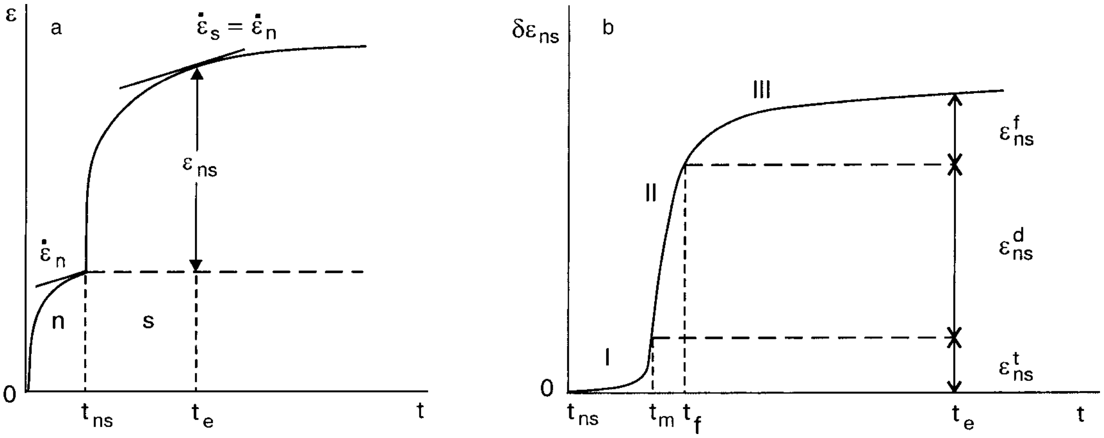

FIG. 1. Characteristic form of the creep curve of single crystals of β-tin at the transition from the normal to the superconducting state, for slow (a) and fast (b) recording of the strain.

stages (Fig. 1b). In the first stage the creep rate $\dot{\varepsilon}_s(t)$ in the superconducting state increases from its value $\dot{\varepsilon}_n(t_{ns})$ in the normal state at the time t_{ns} of the transition, to a maximum value $\dot{\varepsilon}_s(t_m)$ at some time t_m. Subsequently, for $t>t_m$ the creep rate $\dot{\varepsilon}_s(t)$ decreases monotonically, but in a number of cases this process can be divided into a stage t_f-t_m of fast change and a stage $t>t_f$ of slow change of $\dot{\varepsilon}_s(t)$. The durations of the stages, t_m-t_{ns} and t_f-t_m, turn out to depend on both the value of the creep rate $\dot{\varepsilon}_n(t_{ns})$ at the time of the $n-s$ transition and on the value of the total plastic deformation ε of the sample over the time preceding the transition; in some cases the second stage vanishes, i.e., $t_f \to t_m$.

We have shown in a series of papers[13–15] that the low-temperature plastic flow of pure β-tin in the slip system $(100)\langle 010\rangle$ is governed by the thermal-fluctuational or quantum-fluctuational (tunneling) motion of dislocations in the Peierls potential relief. On the basis of these ideas one can offer a quantitative interpretation of the staged nature of the growth of the creep deformation $\delta\varepsilon_{ns}(t)$ with allowance for the specifics of the motion of the dislocations through the Peierls barriers at temperatures of the order of 1 K and the values of the effective stress $\tau^* \simeq \tau_P$ (τ_P is the Peierls stress). Under such conditions the sharp decrease of the electron viscosity coefficient of the dislocations B at the $n-s$ transition ($B_s \ll B_n$) not only leads to a change of the fluctuation regime of the the motion of dislocations through the Peierls barriers but can, over time, transfer a portion of the dislocation flow into regime of dynamic above-barrier motion. In the final analysis this leads to a staged character of the creep "jump" $\delta\varepsilon_{ns}(t)$.[12]

The experiments of Ref. 12 and their interpretation there on the basis of the concepts set forth above have only permitted us to obtain a qualitative description of the staged character of the creep jump at the $n-s$ transition. In this paper we make a more detailed experimental study of the effect of the staged character for samples of pure β-Sn; in particular, we study its appearance at two substantially different temperatures, $T_1 = 1.6$ K and $T_2 = 3.2$ K. A quantitative analysis of the experimental data is also given, which permits obtaining additional estimates for the parameters of the dislocation flow that governs the creep and to refine the mechanism by which the dislocations move through the Peierls barriers under conditions of deep cooling.

As we know, for $\tau^* < \tau_P$ the overcoming of the Peierls barriers takes place as a result of the nucleation and moving apart of pairs of kinks of a critical size. When τ^* is close to τ_P the value of the effective energy barrier preventing the nucleation of kinks is extremely small, and for $T \leqslant 1$ K this process occurs by quantum tunneling, the probability of which depends substantially on the electron drag coefficient B of the dislocations.[15,16] The decrease of B at the $n-s$ transition not only exceeds the quantum-fluctuation (tunneling) mobility of the dislocations but also promotes the appearance of dynamic (inertial) effects. Increasing the temperature leads to an increased role of thermal activation in the process of nucleation of dislocation kinks. One of the tasks of the present study is to estimate the relative influence of quantum fluctuations, thermal activation, and inertial effects on the kinetics of creep which is governed by the motion of dislocations through barriers of very low height.

To interpret the experimental results obtained in a study of the influence of the $n-s$ transition on the creep of tin, we attempted to further refine the theory of the low-temperature creep of metals, according to which the process of plastic flow is governed by thermally activated, quantum, or dynamic motion of dislocations in the Peierls relief. The solution of this problem by the one of the authors (Natsik) is presented in the Appendix.

In this paper we also consider an important topic in the physics of plasticity: problems of work hardening of crystals. An increase of the plastic strain of a crystalline sample is ordinarily accompanied by the accumulation of defects in it and the growth of internal stresses which impede the slip of dislocations. Two levels of manifestation of this effect can be distinguished: in the recording of macroscopic stress–strain diagrams of the crystal (the macroscopic scale) the result of hardening is a monotonic growth of the deforming stress corresponding to a constant strain rate; in the initiation of an individual creep curve by an incremental load, a rapid change of the temperature or of the electronic state of the crystal (the microscopic scale), hardening leads to a decrease in the creep rate with time. In this connection there two ways of empirical determination of the parameters characterizing the hardening: analysis of the macroscopic stress–strain diagrams, and analysis of individual curves of transient creep. However, strictly speaking, there are no grounds for assuming that the values of the hardening parameters under the different conditions of deformation will be the same. This question is another topic of this paper.

1. EXPERIMENTAL TECHNIQUES AND RESULTS

1.1. Samples, means of deformation, and recording of the deformation

Single crystals of β-Sn were grown for this study from a 99.9995% pure stock by a modified Bridgman method in batches of 10 samples from a single seed.[17] They had a double-lobed shape in the jaws of the testing machine, with a working part of rectangular cross section with dimensions of $25\times5\times1.5$ mm. The longitudinal axis of the samples coincided with the $\langle110\rangle$ direction, which ensured the most favorable conditions for slip in the system $(100)\langle010\rangle$.

The samples were placed inside a superconducting solenoid and were drawn in the creep regime at temperatures of 1.6 K and 3.2 K, which are below the critical temperature of β-tin, $T_c=3.72$ K. The state of the electronic subsystem in the sample was measured by turning on (normal state) or off (superconducting state) the longitudinal magnetic field of a solenoid with field strength $H>H_c=309$ G.

The deforming stress on the sample was increased in small increments $\Delta\tau=0.1$–0.4 MPa. Up until the yield point τ_0 ($\Sigma\Delta\tau<\tau_0$) the sample was deformed in the normal state; here the strain increments corresponding to the applied load increments led to elastic straining of the sample, and the creep curves had a characteristic Γ-shaped form. After the yield point was reached ($\Sigma\Delta\tau>\tau_0$) the creep curves corresponding to each successive load increment manifested a pronounced stage of plastic flow with a decaying strain rate. In the normal state at the time when the strain rate reached some specified value $\dot\varepsilon_n$ on the stress–strain diagram (the time t_{ns}) the sample underwent a transition to the superconducting state, and the increment of creep deformation $\delta\varepsilon_{ns}(t)=\varepsilon_s(t)-\varepsilon_n(t_{ns})$ was recorded. Then the normal state was restored in the sample, and the measurement was repeated at a higher degree of deformation of the sample.

The deformation increments $\Delta\varepsilon(t)$ corresponding to each stress increment $\Delta\tau$ were registered by a highly sensitive pickup and were recorded automatically on a KSP-4 recording potentiometer; here the relative deformation of the sample was measured to an accuracy of 5×10^{-5}. At the same time, the signal from the pickup was sent to an N307/1 fast plotter, which provided a higher resolution in terms of the strain (by a factor of 2–16) and time (0.06 s). The deformation $\delta\varepsilon_{ns}(t)$ accompanying each $n-s$ transition was recorded on both a "coarse" and a sensitive plotter. Examples of the recordings corresponding to a single $n-s$ transition are shown in Fig. 1.

The experiments were carried out at temperatures of $T_1=1.6$ K and $T_2=3.2$ K. We studied how the value of the total strain ε of the sample and the value of the starting rate $\dot\varepsilon_n(t_{ns})$ affect the characteristics of the creep jump at the $n-s$ transition. Multiple $n-s$ transitions were brought about as the strain was varied in the range $2\%<\varepsilon<9\%$ for four reference values of the starting creep rate $\dot\varepsilon_n$ $[10^{-5}\ \mathrm{s}^{-1}]$: 0.6, 1.3, 2.5, and 7. These values practically spanned the entire range of transient creep rates for which correct measurements could be made.

1.2. Measurement of the creep jump at the *n–s* transition and its division into stages

The transient creep induced by the $n-s$ transition continues for quite a long time, and it is hard to establish the time at which it stops. Therefore, as an integral characteristic of the plastification effect it is convenient to consider the increase of the strain ε_{ns} in the time interval t_e-t_{ns} over which the creep rate $\dot\varepsilon_s(t)$ in the superconducting state reaches the starting value $\dot\varepsilon_n(t_{ns})$ (see Fig. 1):

$$\dot\varepsilon_s(t_e)=\dot\varepsilon_n(t_{ns}),$$
$$\varepsilon_{ns}=\varepsilon_s(t_e)-\varepsilon_n(t_{ns})\equiv\delta\varepsilon_{ns}(t_e). \tag{1}$$

Here and below it is assumed that the growth increment $\delta\varepsilon_{ns}(t)$ is measured in relation to the strain at the starting time t_{ns}. It is seen in Fig. 1a that the graphical determination of ε_{ns} by the method of tangents does not present any particular difficulties.

One of the important tasks in the processing of experimental data is to divide up the creep curves $\delta\varepsilon_{ns}(t)$ registered in experiments into stages. A procedure for precise division into stages and the justification for this procedure are described in Ref. 12. This procedure reduces to a graphical

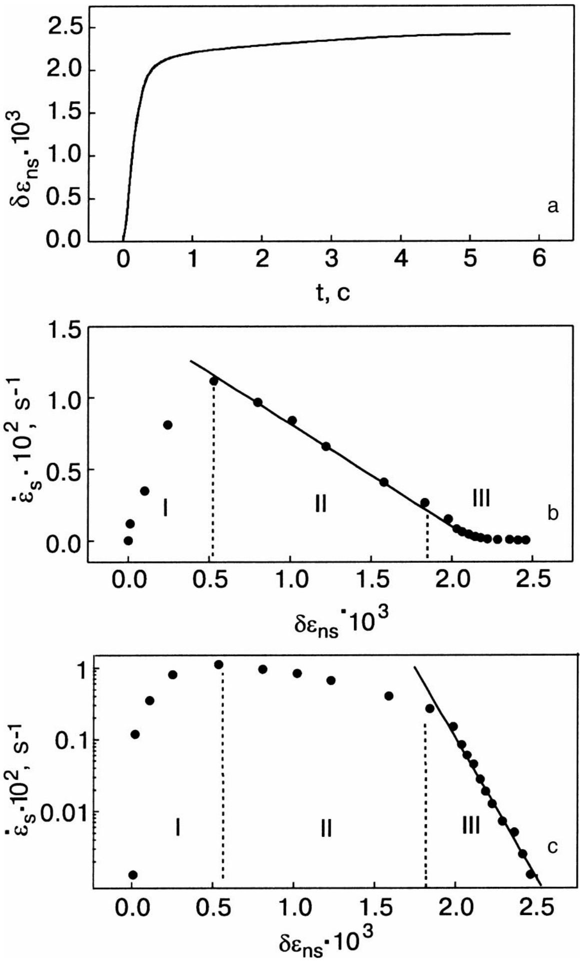

FIG. 2. Kinetics of the creep of β-tin after the $n-s$ transition at $T_1=1.6$ K for a total strain $\varepsilon=0.06$ and a starting creep rate $\dot\varepsilon_n=1.3\times10^{-5}$ s^{-1}: the time dependence of the strain increment $\delta\varepsilon_{ns}$ (a); the dependence of the creep rate $\dot\varepsilon_s$ in the superconducting state on the strain increment $\delta\varepsilon_{ns}$ in the coordinates $\dot\varepsilon_s$ versus $\delta\varepsilon_{ns}$ (b) and in the coordinates $\ln\dot\varepsilon_s$ versus $\delta\varepsilon_{ns}$ (c).

differentiation of the creep jumps $\partial/\partial t[\delta\varepsilon_{ns}(t)]\equiv\dot{\varepsilon}_s(t)$ and construction of the creep curves in the coordinates $\dot{\varepsilon}_s$ versus $\delta\varepsilon_{ns}$ and $\ln\dot{\varepsilon}_s$ versus $\delta\varepsilon_{ns}$. Figures 2 and 3 show examples of the implementation of this procedure for the temperature values used in the experiment, $T_1=1.6$ K and $T_2=3.2$ K, but at the same starting values of the creep rate $\dot{\varepsilon}_n(t_{ns})=1.3\times10^{-5}$ s^{-1}.

It is shown in Ref. 12 that a protracted transient creep can in general be the result of two modes of plastic flow or regimes of motion of the dislocations: dynamic (above-barrier) and fluctuational (occurring by quantum or thermal activation). These regimes (modes) correspond to different creep equations, which relate small increments of the strain $\delta\varepsilon(t)$ and the strain rate $\partial/\partial t[\delta\varepsilon(t)]=\dot{\varepsilon}(t)$:

for the dynamic regime

$$\dot{\varepsilon}(t)=\dot{\varepsilon}(t_0)-C_d\delta\varepsilon(t); \tag{2}$$

and for the fluctuation regime

$$\ln\dot{\varepsilon}(t)=\ln\dot{\varepsilon}(t_0)-C_f\delta\varepsilon(t). \tag{3}$$

Here t_0 is the time at which the corresponding regime of creep begins, and C_d and C_f are constants whose values are determined by the characteristics of the dislocations and the barriers they must overcome, the temperature of the crystal, etc.

The experimental creep curves $\delta\varepsilon_{ns}(t)$ or fragments of them (stages) should also be described by Eqs. (2) and (3) (this question is discussed in more detail in the Appendix; see formulas [(A14) and (A19)]). In addition, the strain increment after the $n-s$ transition should have a certain transient stage I, over the course of which which the dynamic equilibrium in the motion of dislocations, which had been disrupted by the sharp change in the electron viscosity at the time t_{ns}, is restored (a detailed discussion of this stage can be found in Ref. 12).

We see in Fig. 2 that for $T_1=1.6$ K the creep curve $\delta\varepsilon_{ns}(t)$ exhibits all three stages: the transient stage I, the dynamic stage II, and the fluctuation stage III. At the higher temperature $T_2=3.2$ K the dynamic stage is absent, and only the transient stage I and fluctuation stage III remain (see Fig. 3). From these figures it is easy to determine the maximum value of the creep rate $\dot{\varepsilon}_s(t_m)$ and the strain increment ε_{ns}^i $(i=t,d,f)$, corresponding to the three different stages (i.e., individual components of the total jump):

$$\varepsilon_{ns}^t=\varepsilon_s(t_m)-\varepsilon_s(t_{ns}),\quad \varepsilon_{ns}^d=\varepsilon_s(t_f)-\varepsilon_s(t_m),$$

$$\varepsilon_{ns}^f=\varepsilon_s(t_e)-\varepsilon_s(t_f). \tag{4}$$

Since the items of main interest from the standpoint of the problems stated in the Introduction are the dynamic ε_{ns}^d and fluctuational ε_{ns}^f components of the jump, the analysis below is restricted to an analysis of only these stages and their relative contribution to the total value of the jump in ε_{ns}.

1.3. Kinetics of the jump $\delta\varepsilon_{ns}(t)$ at temperature 1.6 K

In experiments at the temperature $T_1=1.6$ K the samples were deformed in the creep regime under multiple incremental loads $\Delta\tau$ until their destruction. Multiple $n-s$ transitions were brought about at different degrees of total strain $\varepsilon=\Sigma\Delta\varepsilon$ and for different values of the starting strain rate $\dot{\varepsilon}_n$. The whole set of recorded creep curves $\delta\varepsilon_{n,s}(t)$ was processed in accordance with the procedure described in Sec. 1.2. To reveal the dependence on ε of the total value of the jump ε_{ns} and its constituents ε_{mn}^i, these quantities have been divided into groups pertaining to four comparatively narrow intervals of $\dot{\varepsilon}_n$ values, with a spread of a factor of 1.5–2. To reveal how the characteristics of the jump depend on $\dot{\varepsilon}_n$, the values obtained were averaged over intervals $\Delta\varepsilon\sim1\%$.

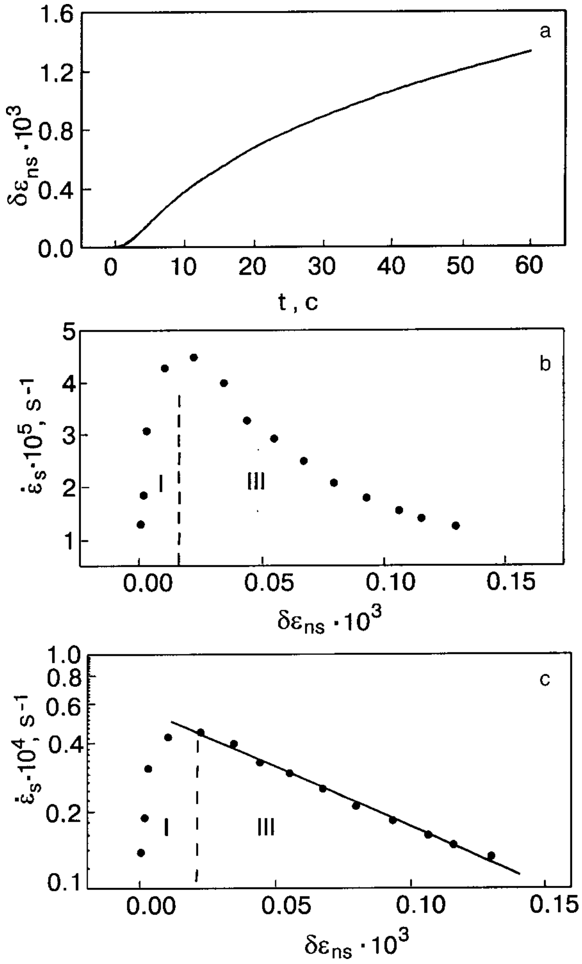

FIG. 3. Kinetics of the creep of β-tin after the $n-s$ transition at $T_2=3.2$ K for a total strain $\varepsilon=0.06$ and a starting creep rate $\dot{\varepsilon}_n=1.3\times10^{-5}$ s^{-1}: the time dependence of the strain increment $\delta\varepsilon_{ns}$ (a); the dependence of the creep rate after the $n-s$ transition on the strain increment $\delta\varepsilon_{ns}$ in the coordinates $\dot{\varepsilon}_s$ versus $\delta\varepsilon_{ns}$ (b) and in the coordinates $\ln\dot{\varepsilon}_s$ versus $\delta\varepsilon_{ns}$ (c).

Figure 4 shows the total jump ε_{ns} and its constituents ε_{ns}^d and ε_{ns}^f as functions of the total plastic deformation ε of the samples prior to the $n-s$ transition for several narrow intervals of values of the starting strain rate $\dot{\varepsilon}_n$. One notices the following details of those curves:

—the characteristics of the effect are monotonically decreasing functions of the strain ε with maximum values near the strain corresponding to the yield point of the sample, and for $\varepsilon>6-7\%$ these curves go to saturation;

—the total jump and its constituents retain finite values throughout the strain interval, up until destruction of the crystal;

—in slightly deformed crystals ($\varepsilon<5\%$) the dynamic mode of the jump is predominant at all values of $\dot{\varepsilon}_n$;

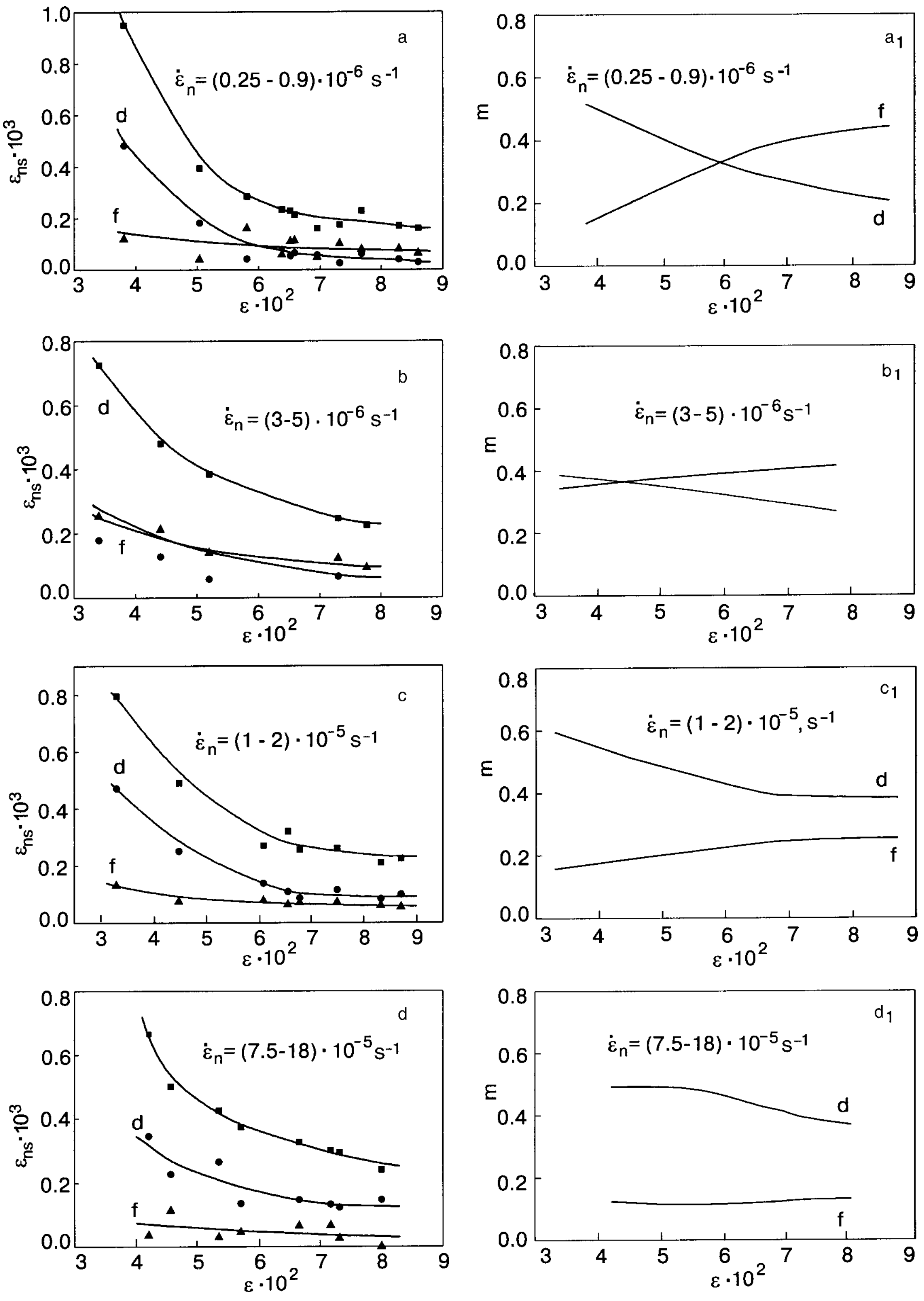

FIG. 4. Dependence of the total jump ε_{ns} (■) and its constituents ε_{ns}^d (●) and ε_{ns}^f (▲) on the value of the total strain ε prior to the $n-s$ transition and on the value of the starting creep rate $\dot{\varepsilon}_n$ for $T_1=1.6$ K; panels a$_1$, b$_1$, c$_1$, and d_1 show the relative values of the dynamic m^d and fluctuation m^f constituents of the modes.

— the fluctuation mode of the jump is less sensitive than the dynamic mode to deformational distortions of the crystal, and at high rates $\dot{\varepsilon}_n$ it becomes practically insensitive to them.

A clear picture of the relationship of the dynamic and fluctuation modes in the jump $\delta\varepsilon_{ns}(t)$ at different values of the total strain of the crystal gives the curves presented in Fig. 4a$_1$–d$_1$. A quantitative characteristic of this relationship is the "specific weight" m^i of the corresponding mode, which is equal to the ratio of the absolute increments of the strain of each mode to the total jump in the strain:

$$m^d=\frac{\varepsilon_{ns}^d}{\varepsilon_{ns}},\quad m^f=\frac{\varepsilon_{ns}^f}{\varepsilon_{ns}}.$$

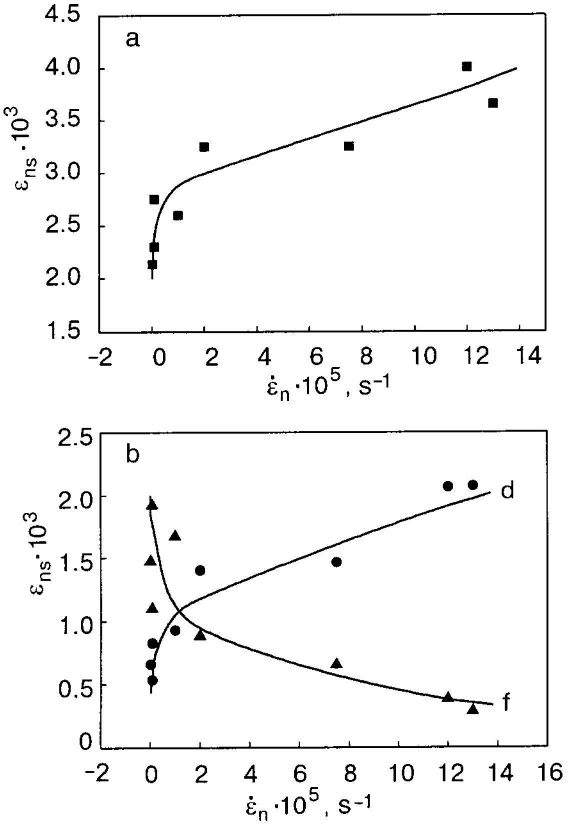

FIG. 5. Dependence of the total jump ε_{ns} (■) (a) and its dynamic ε_{ns}^d (●) and fluctuation ε_{ns}^f (▲) constituents (b) on the value of the starting creep rate $\dot\varepsilon_n$ at $T_1=1.6$ K.

The values of the parameters m^i were calculated from the averaged values of ε_{ns}^f, ε_{ns}^d, and ε_{ns}, which are shown in Fig. 4a–d. It is seen in Fig. 4a$_1$–d$_1$ that for small values of the starting rate ($\dot\varepsilon_n<10^{-5}$ s^{-1}) the contributions of the two modes to the total jump of the creep ε_{ns} are comparable in size; here the dynamic mode is prevalent in the initial stage of the deformation, while the fluctuation mode is predominant before destruction of the sample. For relatively large values $\dot\varepsilon_n>10^{-5}$ s^{-1} the main role in the development of the jump is played by the dynamic mode of plastic flow, but its contribution is diminished somewhat at high degrees of deformation.

More-detailed information about the influence of the starting rate $\dot\varepsilon_n$ on the kinetics of the jump at $T_1=1.6$ is given in Fig. 5, which shows the data for degrees of deformation $\varepsilon>6\%$, where the total jump ε_{ns} is practically independent of ε. A principal feature of the curves obtained is the presence of two intervals along the axis of strain rates $\dot\varepsilon_n$: a comparatively narrow interval of high rate sensitivity and a wide interval of low rate sensitivity of the jump. The second important result that can be extracted from the data presented is that the dynamic and fluctuation modes of the jump have opposite tendencies in response to changes in the rate $\dot\varepsilon_n$: the contribution of the dynamic mode to the disordering effect increases with increasing $\dot\varepsilon_n$, while the fluctuation contribution falls off (Fig. 5b).

1.4. Features of the kinetics of the creep jump $\delta\varepsilon_{ns}(t)$ at 3.2 K

The parameters characterizing the plastification effect at $T_2=3.2$ K are determined at several strictly fixed values of the starting creep rate $\dot\varepsilon_n$ [10^{-5} s^{-1}]: 0.6, 1.3, 2.5, and 7. For these measurements a simple methodological device was used which permitted a rather accurate determination of the point along the creep curve at which the strain rate reached a given value. For this purpose a dense network of parallel straight lines, corresponding to the chosen strain rate, was drawn on the tape of the N307/1 chart recorder. The given value of $\dot\varepsilon_n$ was reached when the creep curve touched one of these lines, and that served as a signal for turning off the magnetic field of the solenoid in which the sample was being strained (this determined the time t_{ns} at which the sample went from the normal to the superconducting state). In the given series of experiments the starting creep rates were chosen so as to partially overlap the range of $\dot\varepsilon_n$ values used in the measurements for $T_1=1.6$ K.

Analysis of the creep curves $\delta\varepsilon_{ns}(t)$ recorded at $T_2=3.2$ K showed that at all values of the starting rate $\dot\varepsilon_n$ the dynamic stage is absent from the curves, and the value of the

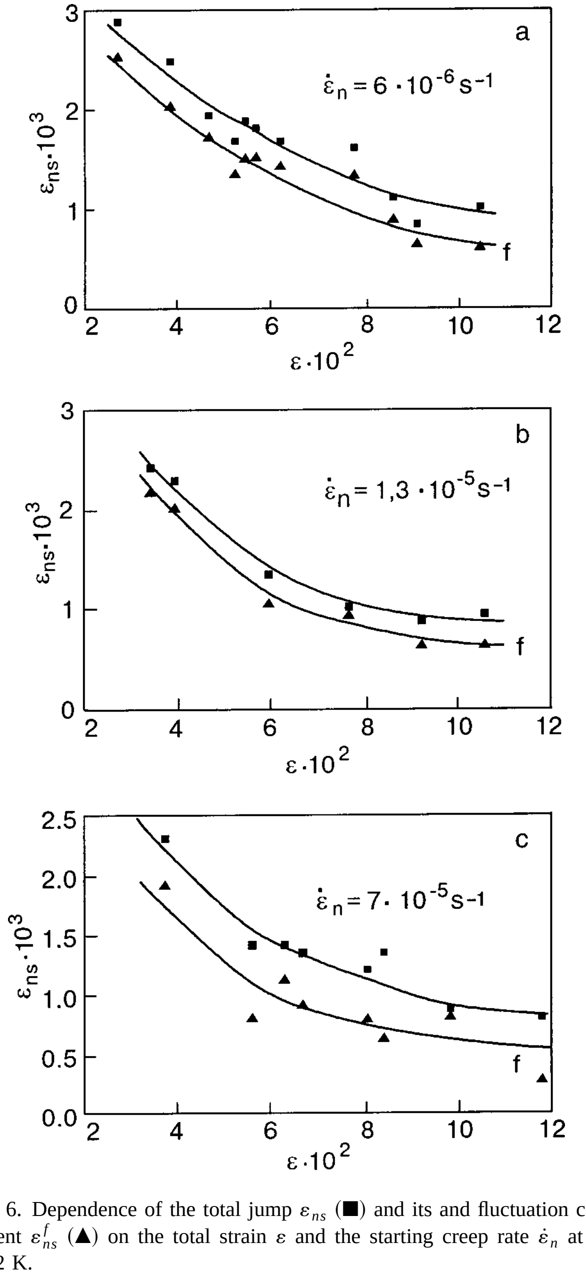

FIG. 6. Dependence of the total jump ε_{ns} (■) and its and fluctuation constituent ε_{ns}^f (▲) on the total strain ε and the starting creep rate $\dot\varepsilon_n$ at $T_2=3.2$ K.

TABLE I. Dependence of $\ln[\dot{\varepsilon}_s(t_f)/\dot{\varepsilon}_n(t_{ns})]$ on ε at $T=3.2$ K for $\dot{\varepsilon}_n=1.3\times10^{-5}$ s^{-1}.

$\varepsilon\cdot10^2$	$\ln[\dot{\varepsilon}_s(t_f)/\dot{\varepsilon}_n(t_{ns})]$
3.4	1.348
4.0	1.407
6.0	1.17
7.7	1.167
9.2	0.753
10.6	1.030

jump in creep is determined solely by the transient and fluctuation stages. The main results of these experiments are given in Fig. 6. On a qualitative level these results reduce to the following:

— increasing the temperature of the experiment to 3.2 K, which is close to the critical temperature of the superconducting transition T_c, does not alter the character of the strain dependence of the total jump and its constituents but leads only to an increase in its absolute values;

— the influence of the value of the starting rate of creep on the value of the jump near T_c persists, but it is very weak;

— with increasing temperature the relative contribution of the fluctuation mode to the disordering effect increases, while the dynamic mode vanishes.

The quantitative characteristics of the results of the experiment described are the values of the ratios of the rates, $\dot{\varepsilon}_s(t_f)/\dot{\varepsilon}_n(t_{ns})$. Table I gives the dependence of this parameter on ε for one of the intermediate values of the starting rate $\dot{\varepsilon}_n=1.3\times10^{-5}$ s^{-1}, and Table II gives the dependence on $\dot{\varepsilon}_n$ for $\varepsilon=6\times10^{-2}$.

1.5. Stress–strain diagrams and work-hardening coefficient obtained by the creep method in β-Sn single crystals

One of the most important parameters of the dislocation theory of plastic flow is the work-hardening coefficient κ. This parameter characterizes the growth of the internal stresses τ_i in the investigated slip planes of a crystal as the total plastic deformation ε increases; this growth of the internal stresses is due to the accumulation of defects in the course of the process. It is usually assumed that the effective stress $\tau^*=\tau-\tau_i(\varepsilon)$ acting on a dislocation increases by an amount τ_i as a result of a small strain increment $\delta\varepsilon$:

$$\delta\tau_i=\kappa\delta\varepsilon. \tag{5}$$

TABLE II. Dependence of $\ln[\dot{\varepsilon}_s(t_f)/\dot{\varepsilon}_n(t_{ns})]$ on $\dot{\varepsilon}_n$ at $T=3.2$ K for $\varepsilon=0.06$.

$\dot{\varepsilon}_n\cdot10^5$ s^{-1}	$\ln[\dot{\varepsilon}_s(t_f)/\dot{\varepsilon}_n(t_{ns})]$
0.6	1.35
0.87	1.30
1.3	1.17
2.5	1.12
4.5	1.02
7.0	1.04

We note that the existing dislocation theories of creep do not consider the microscopic mechanisms of work hardening—the coefficient κ is introduced as a phenomenological parameter of the theory. Therefore the theoretical interpretation of the experimental data on the dependence of the creep parameters on the temperature T, strain ε, etc. requires additional effort to obtain experimental measurements of the corresponding dependences for $\kappa=\kappa(T,\varepsilon,\dots)$.

Most often for measuring κ one employs experiments in which the stress–strain diagram $\tau(\varepsilon,\dot{\varepsilon})$ is recorded at a fixed constant strain rate $\dot{\varepsilon}=$const. In terms of dislocation physics this condition corresponds to a constant value of the effective stress along the strain curve, $\tau^*=$const, if it is assumed that the plastic deformation does not affect the value and density of the localized potential barriers impeding the slip of the dislocations but that only the magnitude of the long-range internal stresses changes. In these cases one can obtain the value of κ by graphical differentiation of the diagram $\tau(\varepsilon,\dot{\varepsilon})$: $\kappa(\varepsilon,\dot{\varepsilon})=[d\tau(\varepsilon,\dot{\varepsilon})/d\varepsilon]_{\dot{\varepsilon}}$.

However, it was found recently[18] that in the low-temperature region the work hardening of the majority of crystals depends weakly on the strain rate. This makes it possible to use the method of additional incremental loading for recording the stress–strain diagrams and determining the work-hardening coefficient: one constructs a smoothed curve representing the relationship between the total strain $\varepsilon=\Sigma\Delta\varepsilon$ and the total load $\tau=\sigma\Delta\tau$ applied to the sample in small increments $\Delta\tau$. Experience shows that in low-temperature straining the $\tau(\varepsilon)$ diagram obtained in this way is quite insensitive to both the value and the frequency with which the incremental loads $\Delta\tau$ are applied over a wide range of their values.

The stress–strain diagrams of pure β-Sn in the slip system $(100)\langle010\rangle$ in the normal state at $T_1=1.6$ K and $T_2=3.2$ K are shown in Fig. 7a, while Fig. 7b shows the $\kappa(\varepsilon,T)$ curves obtained from them. One notices a rather high sensitivity of κ to both growth of the strain ε and to a change of temperature.

It was mentioned in the Introduction that there also exists a possibility of determining the work-hardening coefficient κ by analysis of individual transient creep curves. This is the subject of the next Section.

2. DISCUSSION OF THE RESULTS

In this Section we propose a theoretical interpretation of the experimental results presented above on the kinetics of the creep jumps $\delta\varepsilon_{ns}(t)$ caused by the $n-s$ transition: the experimental results are compared with the conclusions of the theory set forth in the Appendix. Empirical estimates for the parameters of the theory are also obtained which supplement and refine the results of Refs. 12 and 15.

Empirical estimates for a number of parameters of the Peierls relief and of the dislocations in the investigated slip

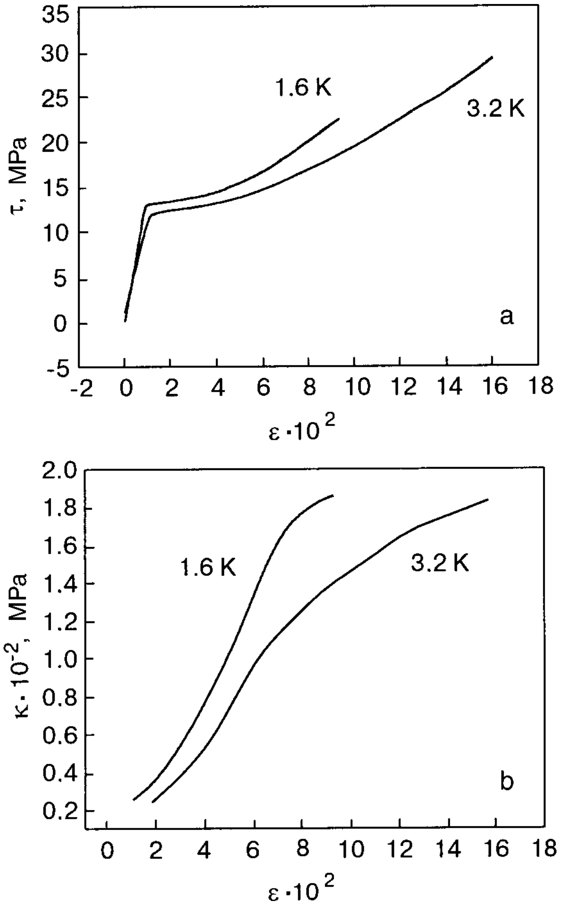

FIG. 7. Macroscopic stress–strain diagram of β-tin single crystals in the normal state, constructed by the method of incremental loading (a), and the strain dependence of the hardening coefficient $\kappa(\varepsilon)$ (b) at 1.6 K and 3.2 K.

system of β-tin were obtained earlier in Ref. 15 on the basis of an analysis of the temperature and velocity dependence of the yield stress:

$$\begin{gathered}\tau_P=1.2\cdot 10^7\ \text{Pa},\quad H_c=2\cdot 10^{-20}\ \text{J}\kappa,\\ B_n=2\cdot 10^{-5}\ \text{Pa}\cdot\text{s},\quad Q_0=5\cdot 10^2,\\ \Theta_P=3.3\ \text{K},\quad \Theta_{Bn}=0.4\ \text{K},\\ \nu_0\simeq 5\cdot 10^{11}\ \text{s}^{-1},\ a=3.2\ \ 10^{-10}\ \text{m},\ b=5.8\cdot 10^{10}\ \text{m}.\end{gathered}\tag{6}$$

The values of the energy gap $\Delta(T)$ for β-tin at the two temperatures used were taken from Refs. 19 and 20:

$$\left[\frac{\Delta(T)}{kT}\right]_{1.6-\text{K}}=4.26,\quad \left[\frac{\Delta(T)}{kT}\right]_{3.2-\text{K}}=1.32.\tag{7}$$

2.1. Jump in the creep deformation at 1.6 K

At the temperature $T_1=1.6$ K the increase ("jump") in the strain after the sample is brought to the superconducting state, $\delta\varepsilon_{ns}(t)$, has pronounced stages: after the transient stage I comes a dynamic stage II, which is followed by a stage III (see Fig. 2). The durations of the stages, t_m-t_{ns}, t_f-t_m, and t_e-t_f, and also the corresponding increases in the strain, ε_{ns}^t, ε_{ns}^d, and ε_{ns}^f, depend on the strain rate $\dot{\varepsilon}_n$ at the time of the transition t_{ns} and on the value of the total strain preceding the transition (see Fig. 4). It is seen from Fig. 4 that the parameters of the jump depend only weakly on the strain at values $\varepsilon\geqslant 6\times 10^{-2}$, and we shall therefore discuss the results obtained for this value of the strain and a starting value of the strain rate $\dot{\varepsilon}_n=1.3\times 10^{-5}\ \text{s}^{-1}$.

According to the concepts set forth in the Appendix, the transient stage I and the dynamic stage II involve changes of the regimes of dynamic motion of the dislocations, and on the time interval t_f-t_{ns} the value of the internal stress τ_i can be assumed constant. Since the external stress τ also remains unchanged at the $n-s$ transition, the force parameter δ_τ on this time interval retains the value that it had at the time t_{ns}, i.e., $\delta_\tau=\delta_{\tau n}$. Adopting this assumption, let us compare the experimental data shown in Fig. 2 with the theoretical expressions (A19) and (A14), the first of which describes the kinetics of creep in stage II, and the second, in stage III. From Fig. 2 we obtain the following empirical values of the parameters appearing in the kinetic relations (A14) and (A19):

$$\begin{gathered}\dot{\varepsilon}_s(t_m)=1.2\cdot 10^{-2}\ \ \text{s}^{-1},\ \ \dot{\varepsilon}_s(t_f)=1.3\cdot 10^{-3}\ \ \text{s}^{-1},\\ C_d=8.2\ \ \text{s}^{-1},\ \ C_f=8.0\cdot 10^3.\end{gathered}\tag{8}$$

Using formulas (A3) and (A19) and also the numerical values given above for the parameters of the theory, we obtain the following empirical estimates for the parameters q and ρ_{d0} which characterize the dynamic creep regime:

$$q=6.8\cdot 10^2,\ \ \rho_{d0}=1.5\cdot 10^3\ \ \text{m}^{-2}.\tag{9}$$

Let us now consider the fluctuational creep stage III at $T_1=1.6$ K, a temperature considerably lower than the characteristic temperature Θ_P separating the regions of quantum-activated and thermally activated motion of the dislocations. In this case stage II is described by formulas (A12a), (A14), and (A16a). Using formula (A12a) and the numerical values of the parameters in (6)–(8), we can obtain an empirical estimate of the force parameter $\delta_{\tau n}$ characterizing the effective stress acting on the dislocation at the time t_{ns} of the superconducting transition:

$$\delta_{\tau n}\simeq 4\cdot 10^{-2}.\tag{10}$$

Substituting this value of the parameter $\delta_{\tau n}$ into formula (A1), we obtain an estimate for the value of the effective potential barrier E_c that the dislocations must overcome in order to become mobile in the Peierls relief:

$$E_c(\tau_n^*)=H_c\delta_{\tau n}^{5/4}\simeq 2\cdot 10^{-3}\ \ \text{eV}.\tag{11}$$

The analysis given above suggests that at temperatures of the order of 1–2 K the fluctuational creep of β-tin is determined by the tunneling motion of dislocations through effective potential barriers of very low height. Essentially, we are talking about a tunneling transition of small parts of a dislocation line through an individual barrier of the Peierls relief, i.e., about the nucleation of a pair of kinks on the dislocation. The probability of tunneling depends on the electron drag coefficient of the dislocations and increases substantially as a result of its change from B_n to B_s, and this is ultimately the microscopic mechanism for the creep jump at the $n-s$ transition.

Knowing the value of the spin parameter $\delta\tau_n$, we can estimate the characteristic value of the density of mobile dislocations ρ, the motion of which determines the fluctuational creep of β-tin under the given conditions. Formulas (A5a) and (A9) imply the relation

$$\rho = \frac{\dot{\varepsilon}(t_{ns})}{a^2 b \nu_0 v_{kn}^{1/2}} \exp\left(\frac{Q_0 \delta_{\tau n}}{2 s_0}\right). \tag{12}$$

At low values of the spin parameter $\delta_{\tau n}$ (10) the width of a dislocation kink $l \simeq a$, and the kink velocity $v_{kn} \simeq 7 \times 10^3$ m/s [see formula (A11)]. Using the numerical values of the other parameters from (6), we obtain the estimate

$$\rho \simeq 10^7 \ \mathrm{m}^{-2}. \tag{13}$$

We see that this value is much greater than the dislocation density ρ_{d0} (9) that governs the dynamic stage of creep.

2.2. Jump of the creep deformation at 3.2 K

At 3.2 K the strain increase $\delta\varepsilon_{ns}(t)$ after the $n-s$ transition has only the transient stage I and the fluctuation stage III (see Fig. 3). The dependence of the main parameters of stage III on the total strain ε and on the value of the starting rate $\dot{\varepsilon}_n(t_{ns})$ can be obtained by using Fig. 6 and Tables I and II. In addition, Fig. 3c permits estimation of the values of two more parameters, corresponding to the values of the starting rate $\dot{\varepsilon}_n = 1.3 \times 10^{-5}$ s^{-1} and total strain $\varepsilon = 6 \times 10^{-2}$:

$$\dot{\varepsilon}_s(t_f) = 4.5 \cdot 10^{-5} \ \mathrm{s}^{-1}, \quad C_f = 1.2 \cdot 10^3. \tag{14}$$

The temperature $T_2 = 3.2$ K falls in an intermediate temperature interval separating the regions of tunneling and thermally activated motion of dislocations, and this to some degree complicates the interpretation of the experimental data. Using the numerical values of the parameters from (6), (7), and (14), one can establish a discrepancy between the activational formula (A12b) and the experimental data. Indeed, by substituting the data obtained into (A12b), one obtains an equation for the force parameter $\delta_{\tau n}$ which does not have solutions: $\delta_{\tau n} < 1$. At the same time, those values agree qualitatively with the tunneling asymptotics (A12a) for reasonable values of the force parameter $\delta_{\tau n}$ and of the corresponding barrier height E_c:

$$\delta_{\tau n} \simeq 1.4 \cdot 10^{-2}, \quad E_c(\tau^*) \simeq 0.6 \cdot 10^{-3} \ \mathrm{eV}. \tag{15}$$

We note that even such small values of the force parameter $\delta_{\tau n}$ and effective barrier do not violate the condition of quasiclassicality of the tunneling process, $Q_0 \delta_{\tau n} \gg 1$, which was assumed to be satisfied in the calculation of the argument of the exponential function in formula (A4) in the quantum limit.[15]

Another test of the applicability of the quantum asymptotics for describing the experimental results obtained at 3.2 K can be proposed. It is based on analysis of the dependence of the creep rate $\dot{\varepsilon}_s(t_f)$ at the start of stage III on the value of the starting rate $\dot{\varepsilon}_n(t_{ns})$ (see Table II). In the quantum limit, equations (A5a), (A9) and (A12a) imply the relation

$$g^{4/3}(T) = g_0^{4/3}(T)[\ln \dot{\varepsilon}_{0n} - \ln \dot{\varepsilon}_n(t_{ns})], \tag{16}$$

in which we have used the notation

$$g(T) = \ln\left[\left(\frac{2}{1 + \exp\dfrac{\Delta(T)}{kT}}\right)^{1/2} \frac{\dot{\varepsilon}_s(t_f)}{\dot{\varepsilon}_n(t_{ns})}\right], \tag{17}$$

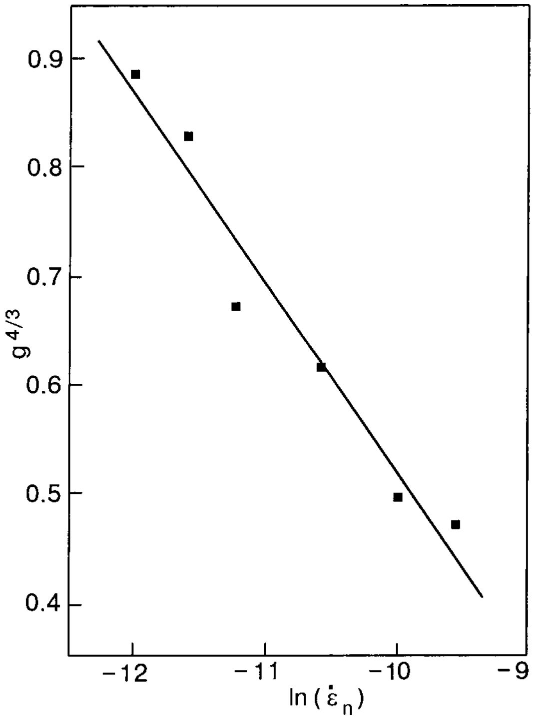

FIG. 8. Dependence of g in Eq. (16) on the starting creep rate $\dot{\varepsilon}_n$ in the coordinates $g^{4/3}$ versus $\ln \dot{\varepsilon}_n$ at a temperature of 3.2 K and the value of the total strain $\varepsilon = 0.06$: ■—experimental values; solid curve—a rectilinear extrapolation according to the equation $a^{4/3} = A_1 - A_2 \ln \dot{\varepsilon}_n$ with the coefficients $A_1 = -1.22$ and $A_2 = 0.17$.

$$g_0(T) = \left(\frac{Q_0}{2 s_0}\right)^{1/4} \frac{\Theta_{Bn}}{\Theta_P} \tanh \frac{\Delta(T)}{2kT}, \tag{18}$$

$$\dot{\varepsilon}_{0n} = (a^2 b \nu_0 v_{ku})^{1/2} \rho. \tag{19}$$

The data of Table II on the dependence of $\dot{\varepsilon}_s(t_f)$ on $\dot{\varepsilon}_n(t_{ns})$ are plotted in Fig. 8 in the coordinates $g^{4/3}$ versus $\ln \dot{\varepsilon}_n$. It is seen that in these coordinates this relation is approximated rather well by a straight line $g^{4/3} = A_1 - A_2 \ln \dot{\varepsilon}_n$, which agrees with Eq. (16) if we introduce the notation

$$A_1 = g_0^{4/3} \ln \dot{\varepsilon}_{0n}, \quad A_2 = g_0^{4/3}(T). \tag{20}$$

Calculating $g_0(T)$ at 3.2 K using formula (18), we get the value $A_2 = g_0^{4/3}(3.2\,\mathrm{K}) \cong 0.2$, which is close to the slope of the straight line in Fig. 8.

Thus we arrive at the conclusion that the transient creep of β-tin at the characteristic rates $\dot{\varepsilon} = 10^{-5}$–$10^{-4}$ cm^{-1} at $\varepsilon = 6 \times 10^{-2}$ is governed by the quantum motion of dislocations at all temperatures $T < \Theta_P = 3.3$ K. This creep process differs from the active deformation process near the yield point, for which, at strain rates $\dot{\varepsilon}$ of the order of 7×10^{-5} s^{-1}, quantum plasticity is observed at lower temperatures $T < 0.5\Theta_P \simeq 1.6$ K.[15] It must be said, however, that the samples studied here and in Ref. 15 were single crystals grown at different times from different seeds, and we have no assurance that the initial defect structure of the samples was identical (for example, they could have substantially different levels of internal stress).

2.3. Intensity of work hardening during low-temperature creep

The macroscopic stress–strain diagrams of β-tin shown in Fig. 7, which were obtained in the normal state by the method of successive incremental loads, give the following values of the work-hardening coefficient $\kappa(T,\varepsilon)$ at values $\varepsilon=0.06$:

$$\begin{aligned}&\kappa(T=1.6\ \text{K};\ \ \varepsilon=0.06)=1.3\cdot 10^8\ \ \text{Pa},\\ &\kappa(T=3.2\ \text{K};\ \ \varepsilon=0.06)=0.9\cdot 10^8\ \ \text{Pa}.\end{aligned}\tag{21}$$

As was mentioned above, analysis of the transient creep curves also enables one to obtain empirical estimates for the hardening coefficient. In the case of quantum creep this dependence is obtained by the use of formula (A16a), which determines the logarithmic creep coefficient $\alpha_f=C_f^{-1}$:

$$\kappa_f=\frac{2s_0\tau_P}{Q_0}C_f.\tag{22}$$

The experimental values of C_f from (8) and (14) give the following values for the coefficient κ_{fs} which characterizes the hardening in the process of quantum creep in the superconducting state of β-tin at the two temperatures used:

$$\begin{aligned}&\kappa_{fs}(T_1=1.6\ \text{K};\ \ \varepsilon=0.06)\simeq 3.4\cdot 10^8\ \ \text{Pa},\\ &\kappa_{fs}(T_2=3.2\ \text{K};\ \ \varepsilon=0.06)\simeq 0.6\cdot 10^8\ \ \text{Pa}.\end{aligned}\tag{23}$$

Comparing (21) and (23), we arrive at the conclusion that, generally speaking, the work-hardening processes on the macroscopic and microscopic scales take place with different intensities.

The causes of such a difference are not completely clear at present. In particular, we are not sure whether the incremental loads $\Delta\tau$ used in constructing the $\tau(\varepsilon)$ diagram were small enough and that the creep curves caused by these loads at $T_1=1.6$ K did not contain rather prolonged transient and dynamic stages in addition to the fluctuation state. It might also be that the intensity of the hardening in the final fluctuation stage III of the creep curve $\delta\varepsilon_{ns}(t)$ depends on the presence and significance of the dynamic stage II.

We note that the conclusion stated above is of a preliminary nature, and a more detailed study of this question will come later. We propose to take one more circumstance into account—the presence of random inhomogeneities of the defect structure and the resulting statistical scatter of the plasticity and hardening parameters. Therefore the parameters obtained in the analysis of the individual concrete creep curves shown in Figs. 2 and 3 are in need of some statistical processing.

APPENDIX. THEORY OF LOW-TEMPERATURE CREEP OF A METAL DUE TO THE MOTION OF DISLOCATIONS IN THE PEIERLS RELIEF (V. D. Natsik)

1. PREMISES AND BASIC RELATIONS

The rate of low-temperature plastic deformation of a number of pure, impurity-free single crystals is controlled by the Peierls potential relief.[21] In particular, this is the case for single crystals of β-tin oriented for predominant slip in the system $(100)\langle 010\rangle$.

At comparatively low values of the effective stress $\tau^*=\tau-\tau_i(\varepsilon)<\tau_P$ (τ_P is the Peierls stress, τ is the external deforming stress, and τ_i is the internal stress) the plastic deformation in these cases occurs as a result of processes of nucleation, dynamic expansion, and annihilation of kink pairs on the dislocations. The kink mechanism brings about the motion of dislocations from one trough of the Peierls relief to another under the influence of the effective stress τ^*. This regime of plastic flow will be called fluctuational. At higher values of $\tau^*>\tau_P$ the dislocations move in the above-barrier regime, and the plastic flow takes on a dynamic character.

The general regularities of the motion of dislocation strings in the Peierls relief at low and very low temperatures are described in Refs. 15 and 16. The theory is based on taking into account the combined influence exerted on this process by quantum tunneling, thermal activation, and electron viscosity. In Ref. 15 this theory is applied to the description of the plastic flow of metals under conditions of deformation at a constant rate (active deformation), and expressions are obtained for the jump in the deforming stress at the $n-s$ transition under those conditions. Here the general concepts and relations of the theory will be used for describing the plasticity of a metal under conditions of creep. A detailed analysis of the influence of an $n-s$ transition on creep will also be carried out.

The kink mechanism of dislocation motion involves overcoming an effective potential barrier equal to the energy of a critical kink pair $E_c(\tau^*)$. For $\tau^*-\tau_P\ll\tau_P$ the value of the barrier is described by the expression

$$E_c(\tau^*)=H_c\delta_\tau^{5/4},\quad \delta_\tau=1-\frac{\tau^*}{\tau_P},\tag{A1}$$

where H_c is a characteristic energy whose value is determined by the parameters of the Peierls relief and the linear tension of the dislocations (empirical estimates for β-Sn give a value $H_c\simeq 0.13$ eV; Refs. 13 and 15). At temperatures of the order of 1 K and the creep rates $\dot{\varepsilon}\leqslant 10^{-5}\ \text{s}^{-1}$ observed in experiment, extremely small values of the parameter δ_τ ($\delta_\tau\ll 1\ \text{s}^{-1}$) are realized, and the effective energy barriers that have to be overcome by the dislocations is extremely small, $E_c(\tau^*)\ll H_c$. Under these conditions the mobility of dislocations is largely determined by the combined action and competition of thermal activation, quantum fluctuations, viscous drag, and inertial effects.

As a set of dislocations of the same type moves in the Peierls relief in an established fluctuation or dynamic regime, the average velocity $V(\tau^*,T,B)$ of an individual dislocation or sufficiently long segment of a dislocation line depends on the effectively stress τ^*, the temperature T, and electron drag coefficient B. The plastic deformation rate $\dot{\varepsilon}$ corresponding to such motion is given by the equation

$$\dot{\varepsilon}=\rho bV(\tau^*,T,B),\tag{A2}$$

where ρ is the density of mobile dislocations, and b is the value of their Burgers vector. The cause of the plastification effect at the $n-s$ transition is a sharp change of the coefficient B from the value B_n to the value B_s (Ref. 4):

$$B_s=\frac{2B_n}{1+\exp[\Delta(T)/kT]},\tag{A3}$$

where $\Delta(T)$ is the energy gap of the superconductor, and k is Boltzmann's constant.

The use of Eq. (A2) for describing the creep process and the influence of the $n-s$ transition on the creep is possible only in those cases when the explicit form of $V(\tau^*,T,B)$ as a function of its arguments is known. It was shown in Ref. 15 that the velocity V_f of fluctuational motion of dislocations for $\tau_P-\tau^*\ll\tau_P$ and at low temperatures is given by the formula

$$V_f(\tau^*,T,B)=\left(\frac{a^2\nu_0 v_k}{b}\right)^{1/2}\exp\left[-\frac{H_c\delta_\tau^{5/4}}{2kT^*(\delta_\tau,T,B)}\right]. \tag{A4}$$

The argument of the exponential function in Eq. (A4) contains the effective temperature $T^*(\delta_\tau,T,B)$, for which one can write the following asymptotic expressions:

$$T^*\simeq s_0(\Theta_P\delta_\tau^{1/4}-\Theta_B),\quad T\ll\Theta_P; \tag{A5a}$$

$$T^*\simeq T\left(1+\frac{s_1}{Q_0\delta_\tau}\ln\frac{\Theta_S}{T}\right)-\frac{s_1\Theta_B}{Q_0\delta_\tau},\quad T\gg\Theta_P. \tag{A5b}$$

In formulas (A4) and (A5) we have used the following notation: a is the period of the Peierls relief, ν_0 is the characteristic vibrational frequency of a dislocation in a trough of the Peierls relief, Θ_P and Θ_B are, respectively, the characteristic temperatures associated with the zero-point vibrations of the dislocation string in a trough of the Peierls relief and with the damping of these vibrations by electron drag, $Q_0=H_c/k\Theta_P$ is the quasiclassicality parameter for the process of tunnel nucleation of a kink pair, Θ_S is the characteristic temperature of a free dislocation string, v_k is the velocity of kinks along the dislocation line, and $s_0\cong0.9$ and $s_1\simeq5.4$ are numerical parameters.

We note that the effective temperature T^* in formula (A4) describes the intensity of the quantum motion of a dislocation string in the Peierls relief in the limit $T\to0$ and the intensity of its thermal motion in the classical limit $T\gg\Theta_P$ and $Q_0\to\infty$. The influence of electron drag on the fluctuational motion of a dislocation is determined by the dependence on B of both the effective temperature T^* and the kink velocity v_k in the pre-exponential factor in (A4).

The motion of kinks along a dislocation occurs in the dynamic regime, and their velocity v_k is determined by the relation $ab\tau^*=\beta v_k$, where on the left-hand side is the force due to the stress τ^* (Ref. 22) and on the right is the electron drag force. The electron drag coefficient β for a kink is proportional to the drag coefficient B of a rectilinear dislocation: $\beta=a^2B/l$, where l is the width of the kink.[4] As a result, we have

$$v_k(\tau^*,\ B)=\frac{lb\tau^*}{aB}. \tag{A6}$$

In individual cases where the external stress τ acting on a crystal or the internal state of the crystal (temperature T, drag coefficient B, etc.) are rapidly changing for all of the dislocations or for sufficiently long individual segments of dislocation lines, a steady-state regime of dynamic motion can be realized which is described by a formula analogous to (A6):

$$V_d(\tau^*,B)=\frac{b\tau^*}{B}. \tag{A7}$$

Temperature can influence the dynamic plasticity only through temperature dependence of B. Here it is especially easy to understand the cause of the plastification effect at the $n-s$ transition: a sharp decrease of B [see formula (A3)] leads to a sharp increase in the dislocation velocity (A7) and in the plastic deformation rate (A2) at constant values of the effective stress τ^* and dislocation density ρ.

Our proposed dislocation description of the kinetics of the creep jump at the $n-s$ transition relies on several premises:

—on an individual creep curve $\delta\varepsilon_{ns}(t)$ the internal stress increment τ_i is proportional to the strain increment [see formula (5)], and therefore the change of the effective stress is described by the formula

$$\tau^*(t)=\tau_n^*-\kappa(\varepsilon)\delta\varepsilon_{ns}(t), \tag{A8}$$

where ε and $\tau_n^*=\tau-\tau_i(\varepsilon)$ are, respectively, the value of the total deformation and the value of the effective stress in the normal state prior to the $n-s$ transition;

—before the time t_{ns} of the superconducting transition the plastic deformation in the normal state takes place in a fluctuation regime at values $\tau^*\simeq\tau_P$ (Refs. 12 and 15) and is described by formulas (A2) and (A4) with $\tau^*=\tau_n^*$, $B=B_n$, $\delta_\tau=\delta_{\tau n}=1-\tau_n^*/\tau_P\ll1$;

—in the course of the transient stage I, i.e., in the time interval t_m-t_{ns}, a transition occurs from the regime of dislocation motion corresponding to the value $B=B_n$ to a new regime with $B=B_s$, but the value of the effective stress does not change substantially at this transition, i.e., $\tau^*(t_m)\simeq\tau^*(t_{ns})\equiv\tau_n^*$.

2. FLUCTUATION CONSTITUENT OF THE CREEP JUMP AT THE $n-s$ TRANSITION

Turning to a theoretical description of the kinetics of the creep jump $\delta\varepsilon_{ns}(t)$, let us first consider the simpler case in which the fluctuation regime of dislocation motion prior to the $n-s$ transition persists after the transition as well, i.e., the dynamic stage is absent, and $t_m=t_f$. In that case the starting creep rate $\dot\varepsilon(t_{ns})$ and the maximum rate $\dot\varepsilon(t_f)$ corresponding to the time at which the fluctuation stage begins, $t_f=t_m$, will be given by the expressions

$$\dot\varepsilon_n(t_{ns})=\rho(a^2b\nu_0v_{kn})^{1/2}\exp\left[-\frac{H_c\delta_{\tau n}^{5/4}}{2kT^*(\delta_{\tau n},T,B_n)}\right], \tag{A9}$$

$$\dot\varepsilon_s(t_{ns})=\rho(a^2b\nu_0v_{ks})^{1/2}\exp\left[-\frac{H_c\delta_{\tau n}^{5/4}}{2kT^*(\delta_{\tau n},T,B_s)}\right], \tag{A10}$$

where v_{kn} and v_{ks} are the velocities of the dynamic motion of dislocation kinks under the influence of the effective stress $\tau^*\simeq\tau_P$ in the normal and superconducting states, respectively. According to formulas (A3) and (A6) we have

$$v_{kn}\simeq\frac{lb\tau_p}{aB_n},\quad v_{ks}\simeq\frac{v_{kn}}{2}\left[1+\exp\frac{\Delta(T)}{kT}\right]. \tag{A11}$$

Using formulas (A9)–(A11), it is easy to obtain an expression for the ratio of creep rates $\dot{\varepsilon}_s(t_m)/\dot{\varepsilon}_n(t_{ns})$. In writing this expression we make use of the smallness of the parameter $\Theta_B/\Theta_P \leqslant 10^{-1}$ (Ref. 15), which describes the influence of the electron drag on the quantum tunneling of dislocations through the Peierls barriers, and we restrict consideration to the linear approximation in this parameter. In the quantum limit $T \ll \Theta_P$ we obtain

$$\ln\frac{\dot{\varepsilon}_s(t_f)}{\dot{\varepsilon}_n(t_{ns})} \simeq \frac{1}{2}\ln\frac{1+\exp\dfrac{\Delta(T)}{kT}}{2} + \frac{Q_0}{2s_0}\left(\frac{V_{Bn}}{\Theta_P}\right)\delta_{\tau n}^{3/4}\tanh\frac{\Delta(T)}{2kT}. \qquad \text{(A12a)}$$

The expression which is valid in the region of intermediate and high temperatures $T \geqslant \Theta_P$ is

$$\ln\frac{\dot{\varepsilon}_s(t_f)}{\dot{\varepsilon}_n(t_{ns})} \simeq \frac{1}{2}\ln\frac{1+\exp\dfrac{\Delta(T)}{kT}}{2} + \frac{s_1}{2}\left(\frac{\Theta_{Bn}}{\Theta_p}\right)\left(\frac{\Theta_P}{T}\right)^2\delta_{\tau n}^{9/4} \times\left(\delta_{\tau n}+\frac{s_1}{Q_0}\ln\frac{\Theta_s}{T}\right)^{-2}\tanh\frac{\Delta(T)}{2kT}. \qquad \text{(A12b)}$$

The temporal variation of the strain increment $\delta\varepsilon_{ns}(t)$ can be described by assuming that on an individual creep curve the variation of the parameter δ_τ, in accordance with (A8), is proportional to $\delta\varepsilon_{ns}(t)$:

$$\delta_\tau = \delta_{\tau n} + \frac{\kappa}{\tau_p}\delta\varepsilon_{ns}(t). \qquad \text{(A13)}$$

Calculating the argument of the exponential function in (A4) in the linear approximation in the strain increment $\delta\varepsilon_{ns}(t)$, we can write the equation of plastic flow (A2) in a form corresponding to the empirical relation (3):

$$\ln\left[\frac{d}{dt}\delta\varepsilon_{ns}(t)\right] = \ln\dot{\varepsilon}_s(t_f) - C_f\delta\varepsilon_{ns}(t). \qquad \text{(A14)}$$

The creep curve determined by this equation is described by the logarithmic expression

$$\delta\varepsilon_{ns}(t) = \alpha_f\ln\left[\frac{\dot{\varepsilon}_s(t_f)}{\alpha_f}t+1\right]. \qquad \text{(A15)}$$

The value of the coefficient of logarithmic creep $\alpha_f = C_f^{-1}$ depends, generally speaking, on the temperature T, the parameter $\delta_{\tau n}$, and the drag coefficient B_s or the temperature Θ_{Bs} proportional to it. However, this last dependence can be neglected in view of the small value of the ratio $\Theta_{Bs}/\Theta_P < 10^{-1}$. As a result, for the coefficient α_f in the quantum limit ($T \ll \Theta_P$) we obtain the expression

$$\alpha_f \simeq \frac{2s_0\tau_P}{\kappa Q_0}. \qquad \text{(A16a)}$$

In the region of intermediate and high temperature ($T \geqslant \Theta_P$) the value of this coefficient depends in a complicated way on the parameter $\delta_{\tau n}$ and temperature T:

$$\alpha_f = \frac{8\tau_p}{5\kappa Q_0}\left(\frac{T}{\Theta_p}\right)\left(\delta_{\tau n}+\frac{s_1}{Q_0}\ln\frac{\Theta_s}{T}\right)^2 \times\left(\delta_{\tau n}+\frac{9s_1}{5Q_0}\ln\frac{\Theta_s}{T}\right)^{-1}\delta_{\tau n}^{-5/4}. \qquad \text{(A16b)}$$

We note that the empirical values of the coefficient α_f can be obtained in two ways, by plotting the experimentally recorded curves of the creep $\delta\varepsilon_{ns}(t)$ initiated by the $n-s$ transition in the coordinates $\dot{\varepsilon}_s$ versus $\delta\varepsilon_{ns}$ or in the coordinates $\ln\dot{\varepsilon}_s$ versus $\delta\varepsilon_{ns}$.

3. DYNAMIC CONSTITUENT OF THE CREEP JUMP AT THE *n–s* TRANSITION

It can be expected that the case described above, in which the fluctuational creep regime persists after the $n-s$ transition, will be realized at temperatures close to the critical temperature T_c, where the transition-induced jump of the drag coefficient B is not too large. At lower temperatures the appreciable decrease of B at the $n-s$ transition under conditions where τ^* is close to the Peierls stress τ_P can lead to the transition of individual segments of the dislocation strings to the dynamic regime of motion.

This possibility, which was analyzed in Ref. 23, is due to the inertial properties of a dislocation string, the role of which increases in the superconducting state as a consequence of the small value of the electron drag coefficient B_s. After completion of the transient stage I, these dislocation segments acquire a velocity V_d determined by the relation

$$B_sV_d \simeq b\tau_p. \qquad \text{(A17)}$$

In describing the contribution of such segments to the increment of the creep deformation one should, of course, take into account the decrease of their total number with time (the "exhaustion" process) due to the linear tension of the dislocation strings and the presence of regions in the crystal with locally high values of the internal stress, $\tau_i > \tau - \tau_P$. We note that the influence of the "exhaustion" of the density of fast dislocations (moving in the dynamic regime) on the creep kinetics is qualitatively equivalent to the influence of work hardening on the dislocations moving in the fluctuation regime: both of these factors lead to a decay of the creep rate with time.

The process of "exhaustion" of the fast dislocations can be taken into account in the equations of the theory of creep by analogy with the incorporation of the work hardening. We denote by the symbol ρ_d the total length of dislocation segments moving in the above-barrier regime per unit volume of the crystal (the density of fast dislocations). If ρ_{d0} is the initial density of such dislocations, its decrease on an individual creep curve can be assumed to be proportional to the strain increment $\delta\varepsilon(t)$:

$$\rho_d = \rho_{d0}[1-q\,\delta\varepsilon(t)], \qquad \text{(A18)}$$

where q is the exhaustion coefficient. The role played by the phenomenological parameters of the theory, ρ_{d0} and q, in the description of dynamic creep is the same as the role of the parameters ρ and κ in the description of fluctuational creep.

Their values for each particular situation that can be realized in an experiment can be obtained from an analysis of the experimental data.

Using formulas (A2), (A17), and (A18), it is easy to obtain an equation describing the contribution of the dynamic mode of plastic flow to the creep deformation increment $\delta\varepsilon(t)$ initiated by the $n-s$ transition. This equation has the form corresponding to the empirical relation (2)

$$\frac{d}{dt}[\delta\varepsilon_{ns}(t)]=\dot{\varepsilon}(t_m)-C_d\delta\varepsilon_{ns}(t); \tag{A19}$$

$$\dot{\varepsilon}_s(t_m)=\frac{\rho_{d0}b^2\tau_P}{B_s},\quad C_d=q\dot{\varepsilon}_s(t_m).$$

The strain increment $\delta\varepsilon_{ns}(t)$ in the dynamic creep regime is described by the solution of equation (A19), which has the form

$$\delta\varepsilon_{ns}(t)=q^{-1}[1-\exp(-q\dot{\varepsilon}_s(t_m)t)]. \tag{A20}$$

Under conditions of a specific experiment, even at a low density of fast dislocations ($\rho_{d0}\ll\rho$) the contribution of the dynamic mode (A20) to the increment of the creep deformation $\delta\varepsilon(t)$ can turn out to be considerably larger than the fluctuation contribution (A15).

In those cases when a sufficiently long fragment of the creep curve $\delta\varepsilon(t)$ becomes a straight line in the coordinates $\dot{\varepsilon}$ versus $\delta\varepsilon$ (see, e.g., Fig. 2b), it becomes possible to obtain empirical estimates of the parameters ρ_{d0} and q. It must be taken into account, however, that the values of these parameters depend very substantially on the details of the particular experimental situation at the time of the $n-s$ transition: on the values of the parameter δ_τ, the ratio B_n/B_s, the total dislocation density ρ, the characteristic magnitude and distribution of the internal stresses, etc. For this reason the empirical values of ρ_{d0} and q have a large scatter.

We note one more important circumstance that should be taken into account in an interpretation of the creep curves recorded in experiments. The dynamic creep stage II, if present, is governed, as a rule, by the dynamic motion of a comparatively small number of dislocation segments ($\rho_{d0}\ll\rho$) and should not be accompanied by any significant change of the total dislocation density ρ and the internal stresses τ_i due to the dislocations. It can therefore be assumed that at the end of this stage and the start of the fluctuational creep stage III, the value of τ_i and the related parameter δ_τ still have the values which they had at the time of the $n-s$ transition. This assumption makes it possible to use formulas (A14) and (A15) for the description of stage II both in those cases when it arises immediately after the transient stage I and in the presence of a dynamic stage II between those stages.

This study was supported by the Target Program of the Department of Physics and Astronomy of the National Academy of Sciences of Ukraine, subject 1.4.10.1.8.

*E-mail: natsik@ilt.kharkov.ua

---

[1] I. A. Gindin, B. G. Lazarev, Ya. D. Starodubov, and V. P. Lebedev, Dokl. Akad. Nauk SSSR **188**, 803 (1969) [Sov. Phys. Dokl. **14**, 1011 (1970)].

[2] V. P. Soldatov, V. I. Startsev, and T. I. Vainblat, Phys. Status Solidi B **37**, 47 (1970).

[3] V. I. Startsev, V. Ya. Il'ichev, and V. V. Pustovalov, *Plasticity and Strength of Metals and Alloys at Low Temperatures* [in Russian], Metallurgiya, Moscow (1975).

[4] M. I. Kaganov, V. Ya. Kravchenko, and V. D. Natsik, Usp. Fiz. Nauk **111**, 656 (1973) [Sov. Phys. Usp. **16**, 878 (1974)].

[5] M. I. Kaganov and V. D. Natsik, JETP Lett. **11**, 379 (1970).

[6] G. P. Huffman and N. Louat, Phys. Rev. Lett. **24**, 1055 (1970).

[7] M. Suenaga and J. M. Galligan, Scr. Metall. **4**, 697 (1970).

[8] A. V. Granato, Phys. Rev. Lett. **27**, 660 (1971).

[9] V. D. Natsik, Zh. Éksp. Teor. Fiz. **61**, 2540 (1971) [Sov. Phys. JETP **34**, 1359 (1972)].

[10] G. Kostorz, Phys. Status Solidi B **58**, 9 (1973).

[11] V. L. Indenbom and Yu. Z. Éstrin, JETP Lett. **17**, 568 (1973).

[12] V. P. Soldatov, V. D. Natsik, and G. I. Kirichenko, Fiz. Nizk. Temp. **27**, 1421 (2001) [Low Temp. Phys. **27**, 1048 (2001)].

[13] G. I. Kirichenko, V. D. Natsik, and V. P. Soldatov, Fiz. Met. Metalloved. **63**, 386 (1987).

[14] G. I. Kirichenko, V. V. Pustovalov, V. P. Soldatov, and S. É. Shumilin, Fiz. Nizk. Temp. **11**, 1206 (1985) [Sov. J. Low Temp. Phys. **11**, 666 (1985)].

[15] V. D. Natsik, G. I. Kirichenko, V. V. Pustovalov, V. P. Soldatov, and S. É. Shumilin, Fiz. Nizk. Temp. **22**, 965 (1996) [Low Temp. Phys. **22**, 740 (1996)].

[16] B. V. Petukhov, Fiz. Nizk. Temp. **11**, 1090 (1985) [Sov. J. Low Temp. Phys. **11**, 601 (1985)].

[17] Yu. G. Kazarov, in *Physics of the Condensed State* [in Russian], Kharkov (1973), issue 11, p. 100.

[18] R. Berner and G. Kronmüller, *Plastische Verfomung von Einkristallen*, Springer-Verlag, Berlin (1969), Mir, Moscow (1969).

[19] P. A. Bezuglyĭ, A. A. Galkin, and A. P. Korolyuk, Zh. Éksp. Teor. Fiz. **39**, 7 (1960) [Sov. Phys. JETP **12**, 4 (1961)].

[20] G. Giaever and K. Megerle, Phys. Rev. **122**, 110 (1961).

[21] V. V. Pustovalov, Fiz. Nizk. Temp. **15**, 901 (1989) [Sov. J. Low Temp. Phys. **15**, 497 (1989)].

[22] A. Seeger and P. Schiller, in *Physical Acoustics*, edited by W. P. Mason, Vol. III, Part A, Academic Press, New York (1966), Mir, Moscow (1969).

[23] T. Suzuki and H. Koizumi, Philos. Mag. A **67**, 1153 (1993).

Translated by Steve Torstveit

SHORT NOTES

Electron diffraction study of the rms displacements of the atoms in free clusters of krypton

V. V. Eremenko, S. I. Kovalenko, and D. D. Solnyshkin

*B. Verkin Institute for Low Temperature Physics and Engineering, National Academy of Sciences of Ukraine, pr. Lenina 47, 61103 Kharkov, Ukraine**

(Submitted October 3, 2002; revised November 4, 2002)
Fiz. Nizk. Temp. **29**, 469–472 (April 2003)

The size dependence of the rms amplitude $\langle u^2\rangle^{1/2}$ of the atoms in free clusters of krypton is determined for the first time, by an electron diffraction technique. The mean size $\bar{N}$ of the clusters formed in supersonic jets of krypton varied from 1×10^3 to 2×10^4 atoms/cluster. It is found that $\langle u^2\rangle^{1/2}$ increases with decreasing cluster size. A comparison of the dependence observed in experiment with that calculated with allowance for the fractional contribution of surface atoms shows that for clusters with $\bar{N}\geqslant4\times10^3$ atoms/cluster the increase of $\langle u^2\rangle^{1/2}$ with decreasing $\bar{N}$ is due solely to the growth of the relative number of surface atoms. The correlation between the calculation and experiment vanishes when $\bar{N}\leqslant4\times10^3$ atoms/cluster. In that case the experimental values are considerably higher than the calculated value, a circumstance which indicates that in small aggregations there are other factors besides the surface which contribute to the growth of $\langle u^2\rangle^{1/2}$. [DOI: 10.1063/1.1542480]

Clusters, which are small complexes of microparticles, occupy a middle ground between isolated atoms (or molecules) and bulk samples. This makes for distinctive properties of nanocomplexes, which are of interest both for basic physics and for technical applications. Of particular scientific significance is the study of rare-gas clusters. This is because of the relatively simple character of the forces of intermolecular interaction in these objects, which makes them an extremely convenient tool for the critical verification of the different theoretical models describing the properties of clusters.

In this paper we present the results of an electron diffraction study of the size dependence of the rms displacements $\langle u^2\rangle^{1/2}$ of the atoms in krypton clusters which are free of substrates. Such studies have been done previously for argon clusters.[1] The studies on krypton will yield more-complete information about the size dependence of $\langle u^2\rangle^{1/2}$ for rare-gas clusters, will expand the size region of atomic complexes that can be investigated and will shed some light on the features that have been observed on the size dependence of $\langle u^2\rangle^{1/2}$ in argon and which are characteristic for clusters of heavier rare gases. Another important goal of this study is to establish the contribution of the cluster surface to the experimental value of the rms amplitude of the atoms.

EXPERIMENTAL TECHNIQUES AND RESULTS

Observations were made by the electron diffraction technique on an apparatus with the following basic components: an ultrasonic cluster beam generator, a liquid-hydrogen-cooled cryogenic condensation pump for removing the gas jet, and a standard ÉMR-100M electron diffraction unit. A detailed description of the apparatus is presented in Ref. 1. The generator of the ultrasonic cluster beam is described in detail in Ref. 2. The mean size $\bar{N}$ of the clusters (i.e., the average number of atoms in a cluster) was varied by varying the gas pressure P_0 at the entrance to the nozzle, which was held at a constant temperature T_0. The average characteristic linear dimensions δ [Å] of the crystalline clusters was determined from the broadening of the diffraction peaks by the well-known Serlyakov–Sherrer relation with allowance for the additional smearing of the peaks on account of the presence of stacking faults. A statistical processing of the results of the observations showed that δ was determined to a relative error of $\pm10\%$.

For finding the lattice parameter a_{Kr} of the crystalline clusters we made photographic recordings of the diffraction patterns. The relative error in a_{Kr} was $\pm(0.1-0.3)\%$, depending on the degree of smearing of the diffraction peaks on account of the cluster size. We determined the temperature of the clusters with the aid of data on the lattice parameter and its temperature dependence which were obtained in Ref. 3 for Kr island films with a coherent scattering region with a characteristic linear dimension of 40–60 Å.

The intensity I of the diffraction peaks was established by processing diffraction patterns that had been obtained using electrometric registration. The relative error of determination of the intensity was usually not more than $\pm3\%$.

The techniques used to determine the device constant $2L\lambda$ (L is the distance from the diffraction region to the recording device, and λ is the electron wavelength) and the instrumental width of the diffraction peaks are described in Ref. 1.

For finding the value of the rms displacements of the atoms of the cluster we used the dependence of the tempera-

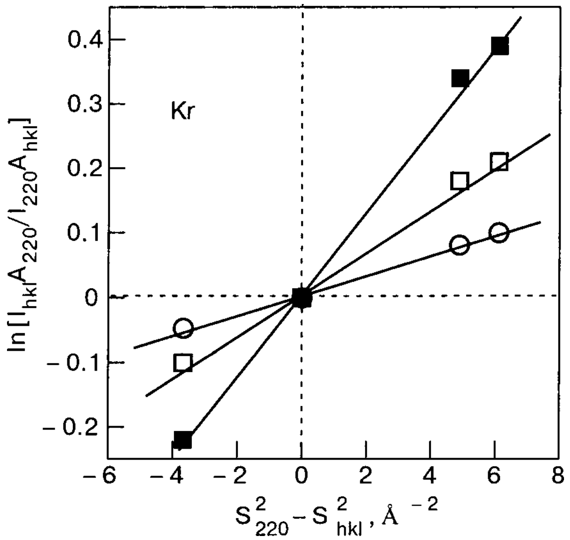

FIG. 1. Logarithm of the normalized intensity of the diffraction peaks versus the difference of the squares of the diffraction vectors, $S^2_{220}-W^2_{hkl}$, in the case of clusters with mean sizes $\overline{N}$ [atoms/cluster]: 1450 (■); 2900 (□) 12500 (○). The following reflections were used in constructing the graphs: (111), (200), (220), and (311).

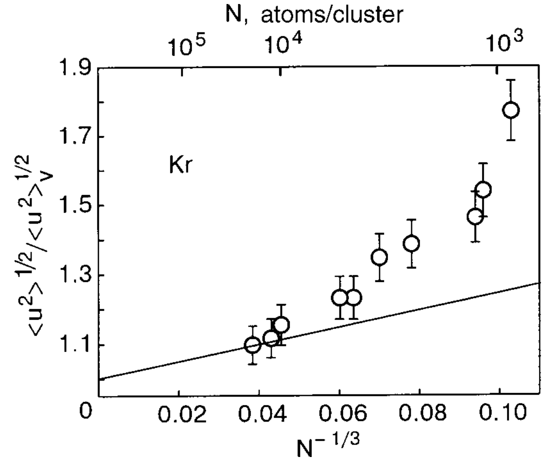

FIG. 2. Size dependence of the rms displacements of the atoms, normalized to the value in the volume. The solid line corresponds to a calculation taking the fractional contribution of the surface into account; the results of the observations are denoted by circlets (○).

ture factor of the intensity of the diffracted rays $\exp(-2M)$ on the diffraction angle θ. In the case of the fcc lattice[4] one has $M=8\pi^2\langle u^2\rangle\sin^2\theta/3\lambda^2$, where $\langle u^2\rangle$ is the mean square value of the total displacement of an atom from its equilibrium position.

Thus the integrated intensity of the diffracted rays reflected by the system of planes $\{hkl\}$ can be written in the form

$$I_{hkl}=I_0A_{hkl}\exp\left(-\frac{16\pi^2\sin^2\theta}{\lambda^2}\frac{\langle u^2\rangle}{3}\right), \tag{1}$$

or

$$I_{hkl}=I_0A_{hkl}\exp\left(-\frac{S^2_{hkl}\langle u^2\rangle}{3}\right), \tag{2}$$

where $S_{hkl}=4\pi\sin\theta/\lambda$ is the magnitude of the diffraction vector, A_{hkl} is the product of all the intensity factors (which are constant for the given system of reflecting planes) except the temperature factor, and I_0 is the intensity of the primary electron beam. Since I_0 can vary noticeably from run to run, it is advisable to normalize the intensity of the diffraction peaks by one of the prominant peaks, e.g., the (220) peak. Thus we determined $\langle u\rangle^2$ using the relation

$$\ln\left(\frac{I_{hkl}}{I_{220}}\frac{A_{220}}{A_{hkl}}\right)=\frac{\langle u^2\rangle}{3}(S^2_{220}-S^2_{hkl}), \tag{3}$$

which establishes the connection between the logarithm of the normalized intensity of the diffraction peak and the difference of the diffraction vectors.

As we see in Fig. 1, the slope of the experimental straight lines increases with increasing mean cluster size. Since the slope is proportional to the mean square amplitude of the atoms [see Eq. (3)], the observed behavior attests to an increase in $\langle u^2\rangle$ as the cluster size decreases. The size dependence of the rms displacements of the atoms is shown in Fig. 2. Here the values of $\overline{N}^{-1/3}\propto 1/\delta$ are plotted on the horizontal axis ($\overline{N}=Vm/v$, where V is the volume of a cluster, v is the volume of the unit cell, and m is the number of atoms in the unit cell; for the fcc lattice we have $m=4$ and $\overline{N}=2\pi\delta^3/3a^3$, where a is the lattice parameter), and along the vertical axis are the values of $\langle u^2\rangle^{1/2}$, normalized to the rms displacement of the atoms in the volume. The values of $\langle u^2\rangle^{1/2}$ obtained from experiment are denoted by circlets. The solid line corresponds to a calculation taking the surface contribution into account and which was done as follows. We assume that the clusters have a spherical shape. In the case of free clusters formed under conditions of isentropic expansion of a gas jet, this assumption is completely correct. We let r be the radius of the spherical cluster, and then $\delta=2r$. We denote the thickness of the surface layer as Δr. In this case the volume of a cluster is $V=(4/3)\pi r^3$, and the volume of the surface layer is $v=4\pi r^2\Delta r$. The relative fraction of atoms in the surface layer is equal to

$$n=\frac{v}{V}=\frac{3\Delta r}{r}. \tag{4}$$

The mean square amplitude of the atomic vibrations measured in experiment is given by the relation

$$\langle u^2\rangle=n\langle u^2\rangle_s+(1-n)\langle u^2\rangle_V, \tag{5}$$

where $\langle u^2\rangle_V$ and $\langle u^2\rangle_s$ are the mean square amplitudes of the atoms in the volume and in the surface layer, respectively.

If we consider only the surface layer, assuming that it is monoatomic, and ignore the much weaker contribution of the next two subsurface layers, then in accordance with the theory of Refs. 5 and 6 we can write $\langle u^2\rangle_s=2\langle u^2\rangle_V$. Substituting this value of $\langle u^2\rangle_s$ into Eq. (5) and taking Eq. (4) into account, we obtain

$$\langle u^2\rangle=\langle u^2\rangle_V\left(1+\frac{3\Delta r}{r}\right). \tag{6}$$

The thickness Δr of a monoatomic surface layer is taken equal to the distance between the centers of two nearest-neighbor atoms. Then in the case of crystalline clusters with the fcc lattice we have

$$\Delta r=\frac{a\sqrt{2}}{2}, \tag{7}$$

where a is the lattice parameter. According to our data, the lattice parameter of krypton clusters is $a_{\mathrm{Kr}}=5.683\pm0.005$ Å and, consequently, $\Delta r=4.18\pm0.005$ Å.

From the value of the parameter a_{Kr} and its temperature dependence we determined the temperature of the clusters, which is needed in order to find $\langle u^2\rangle_V^{1/2}$. It was found to be 55 ± 3 K. The mean square atomic amplitude for the volume of the cluster was calculated using the relation[4]

$$\langle u^2\rangle_V=\frac{9h^2}{4\pi^2mk\theta_D}\,\frac{T}{\theta_D}\left[\frac{1}{4}\,\frac{\theta_D}{T}+\varphi\left(\frac{\theta_D}{T}\right)\right], \tag{8}$$

where h and k are Planck's and Boltzmann's constants, m is the mass of an atom, T is the temperature of the cluster, θ_D is the Debye temperature for a bulk crystal, and $\varphi(\theta_D/T)$ is the Debye function.

If M_a is the atomic mass in a.m.u. and the amplitude of the atomic vibrations is expressed in ångstroms, then Eq. (8) takes the following numerical form:

$$\langle u^2\rangle_V=\frac{424}{M_a\theta_D}\,\frac{T}{\theta_D}\left[\frac{1}{4}\,\frac{\theta_D}{T}+\varphi\left(\frac{\theta_D}{T}\right)\right]. \tag{9}$$

In accordance with the x-ray data, a Debye temperature $\theta_D=65$ K was used in the calculations. The value of the factors in square brackets has been tabulated as a function of θ_D/T in the monograph by Guineir.[4]

From the discussion above we were able to find the dependence of $\langle u^2\rangle^{1/2}$ on $\overline{N}^{-1/3}$ with allowance for the contribution of surface atoms. As we see in Fig. 2, in the case of large clusters the experimental points are in rather good agreement with the results of the calculation. It follows that for clusters with a mean size greater than 4×10^3 atoms/cluster, the increase of $\langle u^2\rangle^{1/2}$ with decreasing $\overline{N}$ is due solely to growth of the relative number of surface atoms. However, the correlation between the calculation and experiment vanishes when $\overline{N}\leqslant3\times10^3$ atoms/cluster. In this case the values of $\langle u^2\rangle^{1/2}$ determined from experiment are substantially larger than the calculated values. Thus the observed effect indicates that in small aggregations there are other significant factors acting besides the growth of the fractional surface contribution whose identification will require additional theoretical analysis. Such an analysis will be done in the future.

We should mention in closing that the experimental size dependence of $\langle u^2\rangle^{1/2}$ for krypton turned out to be qualitatively similar to that observed previously for argon.[1] The quantitative difference lies only in the fact that for small clusters the amount by which the experimentally observed mean square amplitude exceeds the calculated value is somewhat less for krypton than for argon.

The authors thank É. T. Verkhovtseva and V. N. Samovarov for a helpful discussion of the results of this study.

*E-mail: verkhovtsev@ilt.kharkov.ua

---

[1] S. I. Kovalenko, D. D. Solnyshkin, E. T. Verkhovtseva, and V. V. Eremenko, Fiz. Nizk. Temp. **20**, 961 (1994) [Low Temp. Phys. **20**, 758 (1994)].

[2] E. A. Katrunova, A. P. Voĭtenko, G. V. Dobrovol'skaya, V. I. Yaremenko, and É. T. Verkhovtseva, Prib. Tekh. Eksp. **3**, 208 (1977).

[3] S. I. Kovalenko and N. N. Bagrov, Trudy Fiziko-Tekhnicheskogo Instituta Nizkikh Temperatur AN USSR, Fizika Kondensirovannogo Sostoyaniya, issue **11**, 33 (1971).

[4] A. Guinier, *Theorie et Technique de la Radiocristallographie*, Dunod, Paris (1956), Fizmatgiz, Moscow (1961).

[5] A. Maradudin, Solid State Phys. **18**, 273 (1966); **19**, 1 (1966), *Defekty i Kolebatel'nyĭ Spektr Kristallov*, Mir, Moscow (1968).

[6] V. I. Peresada and E. S. Syrkin, Surf. Sci. **54**, 293 (1976).

Translated by Steve Torstveit

Anomalous diamagnetism in the intermetallic compounds $CaPb_3$ and $YbPb_3$

A. E. Baranovskiy,* G. E. Grechnev, G. P. Mikitik, and I. V. Svechakarev

B. Verkin Institute for Low Temperature Physics and Engineering, National Academy of Sciences of Ukraine, pr. Lenina 47, 61103 Kharkov, Ukraine

(Submitted September 16, 2002)
Fiz. Nizk. Temp. **29**, 473–476 (April 2003)

A theoretical study is made of the features of the band structure and orbital magnetic susceptibility χ of the intermetallic compounds $CaPb_3$ and $YbPb_3$. It is shown that the anomalous, strongly temperature-dependent diamagnetism observed earlier in experiments on these compounds is of an interband origin and is due to the presence of degenerate electronic states in the immediate vicinity of the Fermi level. The characteristics of the degenerate states for the two compounds are determined by reconciling the calculated $\chi(T)$ dependence with experiment in the temperature range $5\ \mathrm{K} \leqslant T \leqslant 300\ \mathrm{K}$. © *2003 American Institute of Physics.* [DOI: 10.1063/1.1572412]

Electronic topological phase transitions upon passage of the Fermi level E_F through critical points of the spectrum[1] in a system of slightly split bands are usually accompanied by sharp features in the behavior of the orbital components of the magnetic susceptibility χ of the electrons.[2,3] In some cases of degeneracy of the bands the theory gives a formally divergent result for the orbital magnetism at $T=0$ if the Fermi level coincides with the energy at the point of degeneracy.[4–6] It has been shown[6,7] that the divergence in χ is due to the interband contribution to the orbital magnetic susceptibility. In real systems, in the presence of impurity scattering and at finite temperatures, such a situation corresponds to the "giant" diamagnetic anomaly (so called because of the ratio of the scale of the effect to the volume of the states participating in it). It has been observed in graphite,[4] beryllium,[5] certain bismuth-based alloys,[7,8] and aluminum.[9]

Band degeneracy and the susceptibility anomalies associated with it occur not only in simple metals and semimetals of the sp type but also in intermetallic compounds of transition and rare-earth metals. For example, there is reason to assume[10] that the diamagnetic anomalies in the quasibinary alloys $LaIn_{3-x}Sn_x$ with a cubic lattice of the $AuCu_3$ type[11] is of just such a nature. The amplitude of the anomalies which are observed at concentrations $x \simeq 0.3$ and $x \simeq 2$ exceeds the total spin paramagnetism of the sp- and d-electron bands.[10] Of particular interest in this connection are the structurally analogous isoelectronic compounds $CaPb_3$ and $YbPb_3$, where Yb is found in the same divalent state as Ca. The total number of valence electrons in the unit cell of these compounds and in that of the alloy $LaIn_{3-x}Sn_x$ is the same precisely at $x=2$, and they should also have anomalous diamagnetism at low temperatures; this has indeed been observed in experiment.[12,13] However, unlike the $LaIn_{3-x}Sn_x$ system, this diamagnetism is not smoothed out by the disorder in the lattice of the concentrated alloy and is not masked by the spin paramagnetism, since the contribution of the d electrons to the density of states at the Fermi level in the these compounds is small. It remains to check whether the anomalous diamagnetism and its temperature dependence in the compounds $CaPb_3$ and $YbPb_3$ correspond to the presence of band degeneracy near the Fermi level and to the theory of orbital susceptibility. That is the subject of this paper.

The electronic structure of the compound $CaPb_3$ is calculated from first principles with the use of the method of linearized MT orbitals with the total potential.[14] The exchange–correlation potential is examined in the framework of the local approximation to the theory of the electron density functional.[14] Scalar relativistic effects and the spin–orbit coupling is taken into account at every variational step of a self-consistent calculation of the crystalline potential and band structure.

Figure 1 shows the energy spectrum obtained for $CaPb_3$ in the vicinity of the Fermi level for the XR direction in the Brillouin zone of the simple cubic lattice. It is seen that even with a strong spin–orbit coupling, the crossing of the branches of the spectrum on the XR line is preserved because of the presence of the heavy element lead. The point of degeneracy of the bands is indeed very close to the Fermi level, and the structure of the spectrum in the vicinity of the Fermi level can be approximated by the expression

$$E(k)=\varepsilon_d+ak_3\pm\sqrt{b_{11}k_1^2+b_{22}k_2^2+b_{33}k_3^2}, \tag{1}$$

where ε_d is the energy of the degeneracy point, k_i are the components of the wave vector drawn from the point of degeneracy in the directions parallel to [100], [1−11], and [011], respectively. The values of the coefficients a, b_{11}, b_{22}, and b_{33} and of the local chemical potential level $\zeta=E_F-\varepsilon_d$ for $CaPb_3$ are given in Table I.

Because of the tendency for Yb to change its valence state, a band structure calculation for the compound $YbPb_3$ is a separate, rather complicated problem and will not be carried out here. As an initial approximation for the analysis of the susceptibility of $YbPb_3$ we have used the calculated band spectrum parameters of $CaPb_3$.

The magnetic susceptibility of crystals having a point of degeneracy of the bands near E_F can be written in the form of a sum $\chi=\chi_d+\chi_g$, where χ_d is the main contribution, due to the band degeneracy, and χ_g is the background susceptibility of the sample, which includes all the remaining contri-

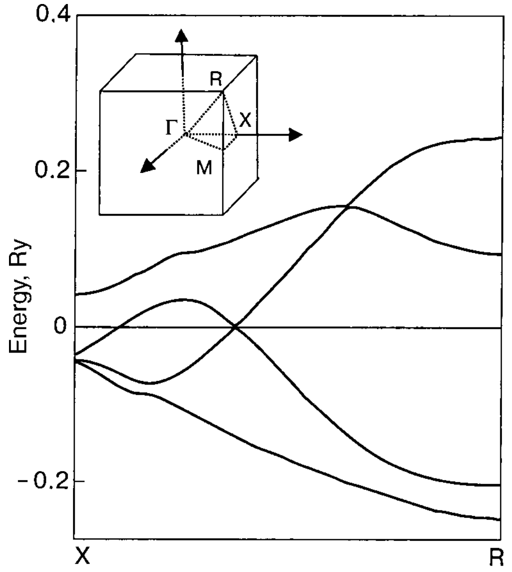

FIG. 1. Electronic spectrum of the compound $CaPb_3$ in the vicinity of a point of degeneracy of the bands. The inset shows the Brillouin zone of a simple cubic lattice.

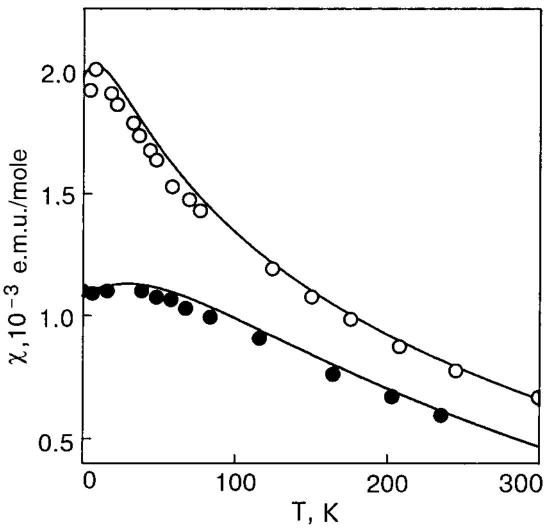

FIG. 2. Temperature dependence of the magnetic susceptibility of the compounds CaP_3 (●; Ref. 13) and $YbPb_3$ (○; Ref. 13). The solid curves are the results of the theoretical calculation.

butions and is assumed to be independent of temperature. In Ref. 6, on the basis of the general theory of orbital susceptibility,[15] the appearance of different types of band degeneracy in the susceptibility was analyzed, and a unified model of the spectrum was found which is consistent with the giant anomalies of χ. The spectrum (1) is a particular case of it. The corresponding expression for the bulk susceptibility[6] with allowance for the symmetry of the Brillouin zone (Fig. 1) has the form

$$\chi_d = AF(\zeta, T), \tag{2}$$

where

$$A = \frac{1}{6\pi^2}\left(\frac{e}{\hbar c}\right)^2 \frac{4}{\sqrt{b_{11}b_{22}b_{33}}} \times [b_{11}b_{22} + b_{11}b_{33} + b_{22}b_{33} - a^2(b_{11} + b_{22})], \tag{3}$$

$$F(\zeta, T) = \int_0^{\zeta_0} \frac{d\varepsilon}{\varepsilon}\left[\frac{1}{1+\exp\left(\frac{-\varepsilon-\zeta}{T}\right)} - \frac{1}{1+\exp\left(\frac{\varepsilon-\zeta}{T}\right)}\right]. \tag{4}$$

Here ζ_0 is the so-called "cutoff parameter," which restricts the domain of application of the model spectrum and which satisfies the condition $\zeta_0 \gg T, |\zeta|$. The scale coefficient A for $CaPb_3$ is found from the data in Table I is given there as well.

For calculating the susceptibility, formulas (2) and (4) were supplemented by the temperature dependence of the chemical potential $\zeta = \zeta(T)$, which is determined by a numerical method from the density of states curve found with allowance for the Fermi distribution function. To avoid manifestations of mechanisms other than single-particle thermal excitations for the influence of temperature on the electronic states and susceptibility (see, e.g., Ref. 5), we restricted the analysis of the function $\chi(T)$ to the temperature range 0–300 K (Fig. 2). The only exception to this was the choice of the cutoff parameter ζ_0, which has practically no effect on the character of the function $\chi(T)$ but regulates the background part χ_d. For the sake of definiteness a value $\zeta_0 \simeq 10$ mRy was taken, which, with allowance for the calculated Pauli spin susceptibility, equal to 4×10^{-5} e.m.u./mole, produces agreement with the experimental value of $\chi(T)$ near the melting temperature.

In a calculation of the susceptibility a defining role is played by the band parameters A and $\zeta(0)$. The accuracy of determination of $\zeta(0)$ in a band calculation from first principles is usually a few millirydbergs, and this parameter is the first to be refined in reconciling the calculated and measured susceptibilities. Furthermore, the features of χ are substantially influenced by the scattering of conduction electrons on different kinds of imperfections of the crystal lattice. The influence of defects on the magnetic susceptibility was taken into account as in the calculations of the orbital susceptibility of alloys,[9,16,17] through the introduction of an additional parameter: the effective scattering temperature T_{sc}. It is analogous to the Dingle temperature T_D in the quantum oscillations of the susceptibility ($T_{sc} \simeq \pi T_D$; Ref. 17) and serves as

TABLE I. Parameters of the energy spectrum for the compounds $CaPb_3$ and $YbPb_3$.

Compound	a^*, erg·cm	b_{11}^*, erg²·cm²	b_{22}^*, erg²·cm²	b_{33}^*, erg²·cm²	A, e.m.u./cm⁻³	ζ, mRy	T_{sc}, K
$CaPb_3$	$8.74 \cdot 10^{-21}$	$2.65 \cdot 10^{-41}$	$1.02 \cdot 10^{-39}$	$1.39 \cdot 10^{-38}$	$1.15 \cdot 10^{-5*}$	1.1	50
$YbPb_3$	–	–	–	–	$1 \cdot 10^{-5}$	0.4	16

Note: An asterisk (∗) denotes parameters obtained by a calculation from first principles.

a second adjustable parameter for reconciling the calculation with experiment.

The results of a calculation of the temperature dependence of χ for the compounds $CaPb_3$ and $YbPb_3$, presented in Fig. 2, corresponds to the optimal choice of parameters ζ and T_{sc} (and also A in the case of $YbPb_3$) given in Table I. As can be seen in Fig. 2, the calculated $\chi(T)$ curves for both compounds achieve good agreement with the experimental data[13] for a minimal correction of the band parameters obtained from first principles. For example, the difference of the parameter A in these compounds is not more than 15%, even though the ions Ca and Yb belong to different classes of metals, and the corrections to the calculated value of ζ amount to fractions of a millirydberg. The values found for the scattering temperature (see Table I) are quite realistic for ordinary samples prepared without special care for their perfection.[13]

Thus we have obtained proof that the anomalous diamagnetism in the compounds $CaPb_3$ and $YbPb_3$ is linked to band degeneracy in the vicinity of E_F and to the corresponding singularity of the orbital susceptibility. It can be assumed that analogous points of band degeneracy near the Fermi level exist in other related compounds and pseudobinary systems RM_3 having structures of the $AuCu_3$ type (definitely including $LaInSn_2$ alloys). The diamagnetic anomalies can be used to monitor the position of the Fermi level relative to these energy benchmarks with an accuracy to a fraction of a millirydberg and can yield valuable information about the reaction of the bands in these systems to different perturbing influences.

*E-mail: baranovskiy@ilt.kharkov.ua

---

[1] I. M. Lifshits, Zh. Éksp. Teor. Fiz. **38**, 1569 (1960) [Sov. Phys. JETP **11**, 1130 (1960)].

[2] B. I. Verkin and I. V. Svechkarev, Usp. Fiz. Nauk **128**, 363 (1979).

[3] S. S. Nedorezov, Fiz. Nizk. Temp. **2**, 1047 (1976) [Sov. J. Low Temp. Phys. **2**, 515 (1976)].

[4] M. P. Sharma, L. G. Johnson, and J. W. McClure, Phys. Rev. B **9**, 2467 (1974).

[5] G. E. Grechnev, I. V. Svechkarev, and Yu. P. Sereda, Zh. Éksp. Teor. Fiz. **75**, 993 (1978) [Sov. Phys. JETP **48**, 502 (1978)].

[6] G. P. Mikitik and I. V. Svechkarev, Fiz. Nizk. Temp. **15**, 295 (1989) [Sov. J. Low Temp. Phys. **15**, 165 (1989)].

[7] G. P. Mikitik and Yu. V. Sharlaĭ, Fiz. Nizk. Temp. **26**, 54 (2000) [Low Temp. Phys. **26**, 39 (2000)].

[8] N. B. Brandt and M. V. Semenov, Zh. Éksp. Teor. Fiz. **69**, 1072 (1975) [Sov. Phys. JETP **42**, 546 (1975)].

[9] S. A. Vorontsov and I. V. Svechkarev, Fiz. Nizk. Temp. **13**, 274 (1987) [Sov. J. Low Temp. Phys. **13**, 155 (1987)].

[10] G. E. Grechnev, A. S. Panfilov, I. V. Svechkarev, A. Czopnik, W. Suski, and A. Hackemer, J. Phys.: Condens. Matter **9**, 6921 (1997).

[11] A. M. Toxen, R. J. Gambino, and L. B. Welsh, Phys. Rev. B **8**, 90 (1973); J. Lawrence, *ibid.* **20**, 3770 (1979).

[12] B. Stalinski, A. Czopnik, N. Iliew, and T. Mydlarz, in *Proceedings of the International Conference of Magnetism, Nauka, Moscow 1973*, p. 349.

[13] J. C. P. Klaasse, F. R. de Boer, and P. F. de Chatel, Physica B **106**, 178 (1981).

[14] O. Eriksson and J. M. Wills, in *Electronic Structure and Physical Properties of Solids*, Hugues Dreysse (ed.) Springer, Berlin (2000), p. 247.

[15] H. Fukuyama, Prog. Theor. Phys. **45**, 704 (1971).

[16] G. E. Grechnev, I. V. Svechkarev, and J. W. McClure, Fiz. Nizk. Temp. **6**, 324 (1980) [Sov. J. Low Temp. Phys. **6**, 154 (1980)].

[17] S. A. Vorontsov and D. G. Dolgopolov, Fiz. Nizk. Temp. **4**, 639 (1978) [Sov. J. Low Temp. Phys. **4**, 308 (1978)].

Translated by Steve Torstveit